Patrick Büker

**Vom Fachbereich VI
(Geographie/Geowissenschaften)
der Universität Trier
zur Erlangung des akademischen Grades
Doktor der Naturwissenschaften
(Dr. rer. nat.)
genehmigte Dissertation**

Development of a stomatal conductance model for white clover and its application for ozone flux predictions

**Betreuer:
Prof. Dr. Willy Werner**

**Berichterstatter:
Prof. Dr. Willy Werner
Prof. Dr. Joachim Hill**

Datum der wissenschaftlichen Aussprache: 14.12.2007

Trier, 2007

S. Philipps

Acknowledgements

When I decided to accept a PhD position at the Geobotany Department of the University of Trier some years ago, I could not have dreamt what impact this decision would have on both my professional as well as my private life. The combination of bio-monitoring and flux modelling methods presented in this thesis has over the course of the years opened various doors for me and has led me from Trier via Wales to England, where I currently work for the Stockholm Environment Institute. On this long and sometimes winding path I have met numerous people, some of which have become close colleagues and even friends.

There is no doubt that this thesis would have been impossible without the kind and self-sacrificing help of some of these lovely people who in one or another way have contributed to make this thesis a success story. I am deeply indebted to these people for their comments, support and general commitment and would like to individually thank them in the following:

First of all, I owe my deepest thanks to Prof. Dr. Willy Werner who has supervised my work throughout the entire period of this PhD thesis. It was he who initiated my interest in bio-monitoring methods and eco-physiology in general during my university years in Trier and I cannot thank him enough for it. His genuine enthusiasm, continuous support, sharp and constructive comments as well as the practical help during measuring campaigns have always been very welcomed.

Further thanks go to Professor Dr. Joachim Hill, who kindly agreed to co-supervise this thesis, a timely and not insignificant task I certainly do not take for granted. His time spent on this task is very much appreciated.

I would also like to express my deep gratitude to Dr. Lisa Emberson for her endless support, the lively discussions about the pros and cons of various flux models and for the introduction to the exciting world of air pollution impact modelling in developed and developing countries in general.

During my 10-month stay at the ICP Vegetation Coordination Centre in Bangor, Wales, Dr. Gina Mills and Dr. Harry Harmens have been my local hosts, a task they fulfilled with

Contents

List of Figures

List of Tables

1. Introduction

Over the last two decades, ozone (O_3) has become the most discussed air pollutant among scientists, politicians and the general public. Its widespread occurrence in the stratosphere and troposphere, its direct participation in some of the severest environmental problems mankind has to deal with at present, such as the depletion of the so called stratospheric ozone-layer, the decline of forests and reduced harvests of staple crops due to increasing tropospheric O_3 concentrations, the difficulties in predicting future atmospheric O_3 concentrations and the unknown dependence of these predictions on suggested climate change scenarios and vice versa, has put this air pollutant in the focus of many research projects.

Most of the atmospheric O_3 molecules are found in the stratosphere (altitude of approx. 10-15 km up to 45 km), where the breaking down of molecular oxygen (O_2) into free oxygen atoms (O) by short-wave radiation and the subsequent reaction of these atoms with oxygen leads to the formation of O_3. The O_3 concentrations in the stratosphere have declined substantially over the last decades, an effect which is believed to be linked to an increase in persistent atmospheric air pollutants such as chlorofluorocarbons. This effect influences life on earth since the stratospheric O_3 is needed to filter the UV-radiation, which is known to damage human, animal and plant cuticles.

In contrast, the O_3 concentrations in the troposphere, i.e. the lower part of the atmosphere up to a height of approx. 10-15 km, have increased during the last decades due to biogenic and anthropogenic emissions. Ground level O_3 directly affects organisms on earth, because it is taken up by human beings, animals and plants via respiration. The impact of O_3 on plants and in particular on white clover will be the focus of this thesis.

The evidence of impacts of O_3 on plants in general has become increasingly important for high-level political negotiations (e.g. within the UNECE, UNEP, GAP Forum etc.) on strategies for the abatement of transboundary air pollutants, such as O_3. As a consequence, an effect-based approach using experimentally derived critical levels for O_3 has been developed to reduce O_3 concentrations and their impacts on vegetation across Europe. While impacts of O_3 on plants, such as visible foliar injury or reductions

of biomass, were traditionally related to O_3 exposure metrics, e.g. the AOT40 index (accumulated exposure over a threshold of 40 ppb), there is now general agreement that these ozone-induced impacts are more closely related to the O_3 dose absorbed through the stomata (Ashmore et al., 2004a,b). This led to an increasing interest in the development of appropriate O_3 flux models mainly based on stomatal conductance (g_s).

This thesis will present a new approach for modelling g_s based on artificial neural networks (ANNs), as well as the application of the developed g_s models to meteorological time-series data for the predictions of O_3 fluxes.

1.1 Formation, distribution and trends of tropospheric ozone

1.1.1 Formation of tropospheric ozone

Until the 1970s the main source of tropospheric O_3 was believed to be the stratosphere, from where the O_3 had directly been transported into the troposphere. Only in highly polluted urban areas, such as Los Angeles, where some of the first adverse effects of air pollution on plants were observed in the 1940s (Middleton et al., 1950), the photochemical production of O_3 was considered as being important. However, Crutzen (1973), Fishman et al. (1979) and others showed first evidence that the photochemical production of O_3 from precursors such as nitrogen oxides (NOx) and organic compounds (VOC) forms the major source of O_3 in the troposphere. In fact, Fowler et al. (1998) recently stressed the importance of oxidised nitrogen, which today accounts for approximately 70% of the total global emissions (Kasibhatla et al., 1993) for O_3 formation.

This clearly defines O_3 as a secondary air pollutant directly connected with anthropogenic activity. Apart from biogenic VOC emissions such as terpenes and isoprene (Simpson et al., 1995), which in comparison with anthropogenic emissions are believed to be a minor source of O_3 precursors, the main sources for the above mentioned precursors are transport, domestic heating, industry, and energy production, all of which are related to fossil fuel combustion (Warneck, 1988; Fuchs, 1994).

Given the high reactivity and oxidation potential of O_3 (Schröter et al., 1991), an equilibrium, called the "NO-photostationary state equation" (Stockwell et al., 1997),

between O_3 production and O_3 destruction would exist in the absence of air pollutants. On the one side, the photolysis of NO_2 by radiation (exactly: photon energy h·v) of wavelength smaller than 420 nm forms the basis for the O_3 formation (Finlayson-Pitts & Pitts, 2000):

$$NO_2 + h·v \ (\lambda < 420 \ nm) \ \rightarrow \ NO + O \quad (1.1)$$
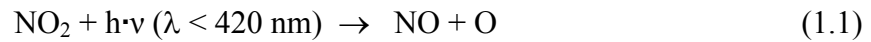
Subsequently, the single oxygen atom reacts with an oxygen molecule to form an O_3 molecule (M is either a nitrogen or oxygen molecule):

$$O + O_2 + M \ \rightarrow \ O_3 + M \quad (1.2)$$

On the other side, O_3 is destroyed by reacting with NO to reproduce NO_2 (Finlayson-Pitts & Pitts, 2000):

$$O_3 + NO \ \rightarrow \ NO_2 + O_2 \quad (1.3)$$

Generally, this reaction takes place in the absence of light, i.e. during night-time hours. However, this equilibrium collapses in the presence of VOCs and carbon monoxide, all of which react with radicals produced by the photolysis of O_3. In a first step, one of the O_3 photolysis reactions produces an excited oxygen atom, $O(^1D)$ (Stockwell et al., 1997):

$$O_3 + h·v \ \rightarrow \ O(^1D) + O_2 \quad (1.4)$$

A fraction of the excited oxygen atoms reacts with water to produce the hydroxyl radical, HO•:

$$O(^1D) + H_2O \rightarrow \ 2HO• \quad (1.5)$$

The hydroxyl radicals react with VOCs (in the following expressed as RH = organic compounds) and carbon monoxide to produce organo-peroxy (RO_2•) and hydro-peroxy (HO_2•) radicals (Stockwell et al., 1997):

$$RH + HO• \rightarrow \ R• + H_2O \quad (1.6)$$

$$R\bullet + O_2 + M \rightarrow \quad RO_2\bullet + M \tag{1.7}$$

$$CO + HO\bullet(+O_2) \rightarrow \quad CO_2 + HO_2\bullet \tag{1.8}$$
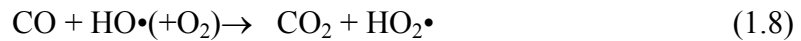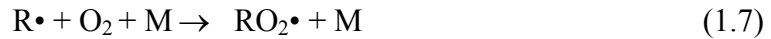
These peroxy radicals oxidise NO to NO_2 without any consumption of O_3, which leads to an increase of the tropospheric O_3 concentration (Stockwell et al., 1997):

$$RO_2\bullet + NO \rightarrow \quad RO\bullet + NO_2\bullet \tag{1.9}$$

$$HO_2\bullet + NO \rightarrow \quad HO\bullet + NO_2\bullet \tag{1.10}$$
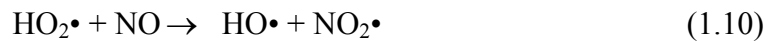
1.1.2 Distribution of tropospheric ozone

On a local scale, the distribution of O_3 is somewhat untypical for an air pollutant because of its usually higher concentrations in sub-urban and rural compared to urban areas. However, the source of rural O_3 concentrations are generally urban agglomerations, from where the O_3 is transported by winds to surrounding areas.
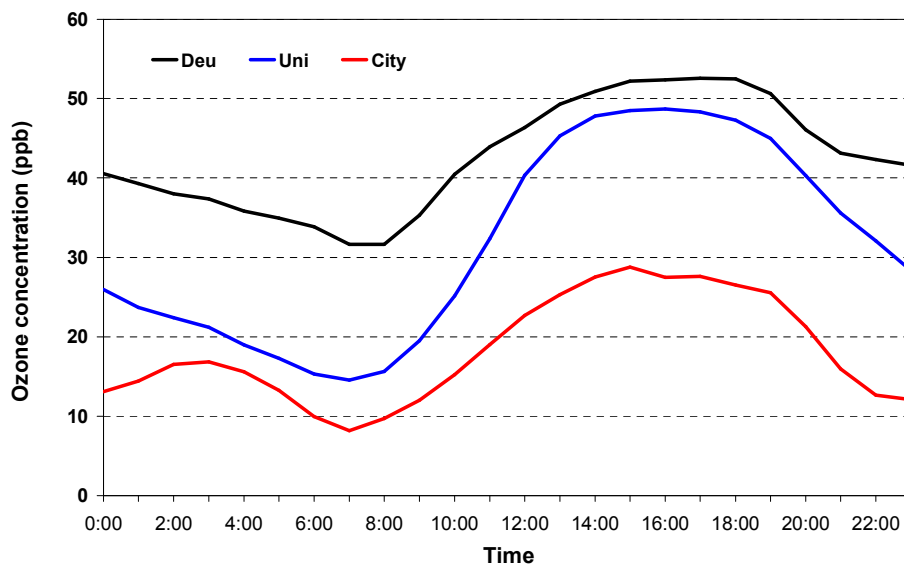
Figure 1.1   Average hourly O_3 concentrations at the urban, suburban and rural site Trier-City, Trier-University and Deuselbach, respectively. Shown are the means of half-hourly measurements carried out in July and August 1997 (62 days).

A typical diurnal course of tropospheric O_3 concentrations for an urban, suburban and rural site in the Trier region is presented in Figure 1.1. During the early morning hours, O_3 concentrations are at a minimum due to surface deposition and nitric oxide emissions. With increasing commuter traffic later in the morning, NO-emissions rise.

The oxidisation of NO to NO_2 and the high solar radiation form the basis for an increase in O_3 concentrations with a relative maximum in the early afternoon. In the early evening hours, O_3 concentrations decrease again due to the decreasing solar radiation and increased NO-emissions from commuter traffic.

Although this pattern is valid for all sites, the curves for the urban, suburban and rural site (Trier-City, Trier-University and Deuselbach, respectively) shown in Figure 1.1 differ in their O_3 concentration level and in their daily amplitude. A typical diurnal time-course of urban and suburban O_3 concentrations is characterised by a high concentration amplitude (Alexander & Drüeke, 1992; Fuchs, 1994), which is in particular the case for the site Trier-University in Figure 1.1.

In contrast, in rural areas such as Deuselbach the amplitude of the diurnal course of the O_3 concentration is less pronounced due to less traffic and therefore less NO emissions. O_3 and its precursors are typically transported from urban to rural areas. Especially during stable high-pressure weather periods in the summertime, O_3 concentrations in rural areas can therefore substantially exceed urban O_3 concentrations (Figure 1.1) because of a diminished O_3 destruction during night-time due to the lack of traffic-related NO-emissions, which deplete O_3 in the absence of sunlight (cf. 1.1.1, reaction 3). Accordingly, O_3 concentrations accumulate over several days in rural areas during long-term high-pressure weather periods, often leading to the exceedance of O_3 concentration thresholds in these areas (Fellenberg, 1990; Alexander & Drüeke, 1992).

Furthermore, there is evidence that O_3 concentrations increase with increasing altitude (PORG, 1993; UBA, 1994) due to higher NO_2 concentrations at the expense of NO concentrations in uplands. Because of the lack of NO emissions, the diurnal amplitude of the O_3 concentration is very low in high altitudes (e.g. alpine areas) (PORG, 1993).

On a European scale, the annual distribution of O_3 concentrations usually shows a maximum during the summer months, which was also reported from the site Deuselbach (Figure 1.2). Furthermore, the annual variation of O_3 concentrations increases from the Northwest to the Southeast of Europe (Toupance & Aranda, 1993). This effect is mainly related to the spatial distribution of O_3 precursors and the prevailing meteorological conditions, which especially favours the O_3 formation in

Southeast Europe (Davies et al., 1992; Beck & Grennfelt, 1994). Thus, peak O_3 concentrations and the frequency of summertime O_3 episodes are higher in Central and Southern than in Northern Europe.
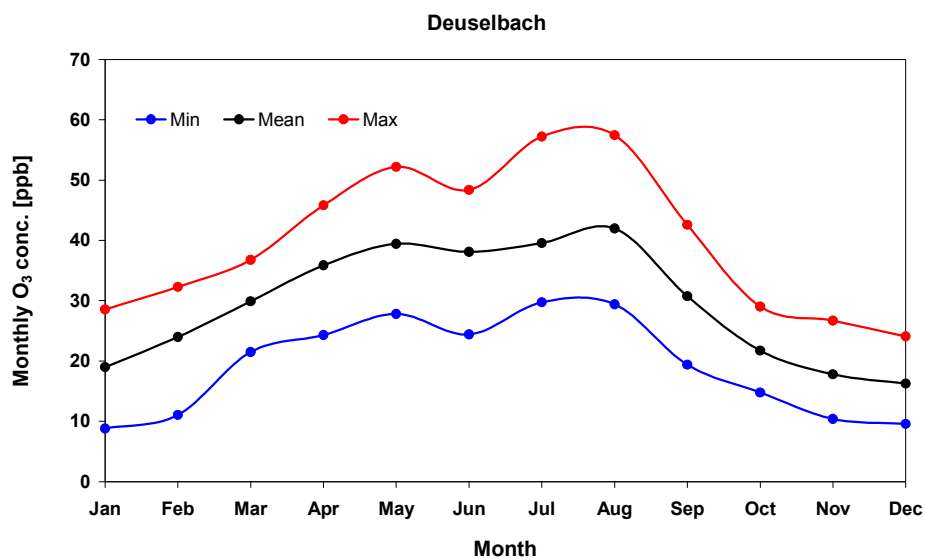
Deuselbach

Figure 1.2   Annual time-course of O_3 concentrations measured at the site Deuselbach (Hunsrück, Rhineland-Palatinate) between 1980 and 2003. Shown are the monthly minimum, mean and maximum O_3 concentrations based on half-hourly measurements (UBA, pers. communication).

On a global scale, there is more O_3 in the troposphere of the northern hemisphere than in the troposphere of the southern hemisphere on an annual basis (Oltmans & Levy, 1994). Accordingly, Müller & Brasseur (1995) showed that approximately 80 % of the NOx emitted on a global basis is due to anthropogenic activity in the northern hemisphere. However, for both hemispheres O_3 annual distributions exhibit maxima between April and July (Logan, 1985; Oltmans and Levy, 1994). For the northern atmosphere, the annual course of the O_3 distribution might be related to the seasonality of the stratosphere-troposphere exchange. Danielsen (1968) and Reiter (1975) have shown that the stratospheric O_3 intrusion rate during spring is much higher than during the autumn. However, springtime photochemical O_3 production in remote areas and summer photochemical O_3 production in less remote areas (e.g. cities) might indicate the anthropogenic influence on the diurnal northern hemisphere O_3 distribution (Penkett & Brice, 1986).

1.1.3 Trends of tropospheric ozone

Over the course of the 20th century, the background surface concentrations of O_3 in Europe have increased by a factor of two to three from their pre-industrial levels (Borrell, 1997). Globally, background tropospheric O_3 levels have risen by approximately 36% since pre-industrial times (IPCC, 2001). Volz & Kley (1988), Anfossi et al. (1991) and Marenco et al. (1994) analysed historical datasets of O_3 concentrations measured in the late 19th/early 20th century in France and northern Italy and found O_3 background concentrations of 5 ppb (autumn and winter) to 15 ppb (spring and autumn). These results match well with model calculations of Crutzen & Zimmermann (1991).
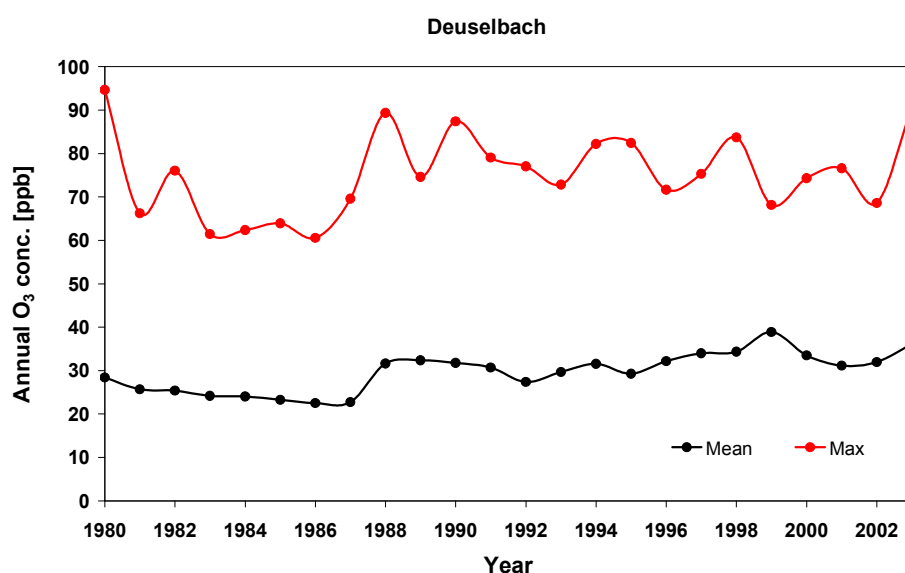
Figure 1.3   Change of annual mean and maximum O_3 concentration (based on half-hourly measurements) at the site Deuselbach (Hunsrück, Rhineland-Palatinate) between 1980 and 2003 (UBA, pers. communication).

Today, tropospheric O_3 background concentrations in central Europe (and elsewhere) are usually in the range of 20 to 40 ppb (the top end during the summer months), with peak O_3 concentrations above 100 ppb (Volz & Kley, 1988; Anfossi et al., 1991; Staehelin et al., 1994; PORG, 1997). The O_3 concentrations trends in Germany are representative for almost all industrialised nations: On the one hand an increase in O_3 background concentrations, on the other hand a stagnation or decline of summer peak concentrations (UBA, 2002), leading to a slight increase in annual mean O_3 concentrations. This trend has also been reported in Deuselbach, one of the experimental sites used in this thesis (Figure 1.3). For the future, these trends are

believed to maintain (Coyle et al., 2003; Vingarzan, 2004), leading to increased daytime mean O_3 concentrations (Ashmore et al, 2002).

Since similar trends have been recognised all over the globe (Emberson et al., 2003), elevated O_3 concentrations are nowadays rated as a hemispherical problem rather than a local or regional one as in the past. This fact results in new challenges for environmental policy, because multi-lateral approaches are needed to protect human beings, animals and plants from adverse O_3 effects. In order to be able to predict future pollutant climates on a local, regional and especially global scale, precise models simulating the atmospheric chemistry, transport and deposition of pollutants such as O_3 are crucial. A comprehensive review of available photochemical oxidant models was published by Fowler et al. (1999b), with special focus on challenges these models will have to face in the future.

Just recently, the scientific community addressed the question of the interaction of air pollutants, in particular O_3, and expected global climate change. There is general agreement that climate change and regional air pollution should not be investigated separately, since both phenomena are closely related aspects of a changing atmosphere with severe effects on ecosystems (Fuhrer, 2003). In fact, Fuhrer (2003) suggests that beneficial effects of elevated CO_2 concentrations, such as increased O_3 tolerance of plants, might be reduced or even lost with increasing global temperatures.

Furthermore, tropospheric O_3 contributes to global warming by absorbing radiant energy (Graedel & Crutzen, 1993) and is considered to be the third largest driver of the anthropogenic "greenhouse effect" (Prather et al., 2001). In return, global warming is expected to favour the O_3 formation through increased emissions of VOCs from the vegetation (Kellomäki et al., 2001), whereas the direct role of the expected climate change was predicted to be a negative feedback on the increase on O_3 concentrations (Johnson et al., 2001). However, many questions about the interactions between increased CO_2 concentrations, increased temperature and the occurrence of secondary air pollutants (e.g. O_3) still remain unsolved to date.

1.2   Effects of ozone on plants

Toxic effects of tropospheric O_3 on plants have been known for approximately five decades now (Richards et al., 1958). However, not until the 1980's the outstanding role of ground-level O_3 for plant health had been recognized (Krupa & Manning, 1988; Ashmore & Bell, 1991). With increasing background levels of O_3 (Borrell, 1997; Ashmore et al, 2002), its widespread occurrence (Simini et al., 1992) and the decline of other air pollutants (e.g. SO_2), it has become evident that O_3 currently is and will continue to be the main threat to vegetation in the near future, both in developed and in developing countries (cf. Stockwell et al., 1997; Fowler et al., 1999a; Turcsányi et al., 1999; Emberson et al., 2003; Wang & Mauzerall, 2004).

Generally, plant response mechanisms to air pollutants, such as O_3, can be defined as either exclusion, tolerance, compensation or repair (Levitt, 1989). The response depends upon the concentration, duration and exposure of the pollutant, environmental conditions, the developmental and metabolic state as well as the detoxification potential of the plant (Guzy & Heath, 1993; Long & Naidu, 2002). The latter is believed to be either genetically predefined or/and dependent on the O_3 history at the site of origin (reflecting a potential adaptation and therefore resistance of the plant to O_3), which is particularly pronounced for short-living semi-natural species (cf. Lyons et al., 1997). Any response of a plant to a single air pollutant or – more realistically – to a mixture of air pollutants requires a change in its "usual behaviour", i.e. the plant is forced to spend energy on the reaction to a stressor attack. To a certain extent, this energy is used to compensate for the attack, for example by stomatal closure, production of antioxidants etc. These mechanisms help to maintain all life-dependant plant-physiological processes and to prevent any form of injury. However, the necessity to spent energy on defence mechanisms can reduce the rate of photosynthesis and/or might alter the photosynthate allocation. Nevertheless, usually only after the detoxification threshold - which defines the point above which the plant is not able to compensate for detrimental effects of toxic stressors anymore - is reached, plants will start to show injury symptoms.

The most obvious air pollutant-induced injury symptom is visible foliar injury. Yet over the last decades, further forms of injury has been described, such as reduced plant productivity, shifts in metabolic pathways, decreased ability to compensate for

secondary stresses (e.g. pathogen attack, cf. Matyssek & Innes (1999)) and accelerated senescence.

On a wider scale, these phytotoxic effects of O_3 potentially have the power to pose a critical threat to present and future world food, fibre and timber production (Krupa et al., 2001), as well as to the conservation of natural plant communities, including their species diversity (Ashmore et al., 1995; Davison & Barnes, 1998; Barnes et al., 1999; Krupa et al., 2001).

In order to determine plant injury specifically caused by exposure to O_3, many laboratory, field-chamber and - more recently - open air experiments have been carried out (e.g. Heagle et al., 1973; Volk et al., 2003; Karnosky et al., 2003; Erbs & Fangmeier, 2005). These experiments have shown that exposure of trees, crops and semi-natural vegetation to O_3 can induce the above mentioned negative impacts on plant health and production, such as visible foliar injury (Sanders & Benton, 1995; Flagler, 1998), premature ageing/senescence (Grandjean & Fuhrer, 1989; Heath & Taylor, 1997), reduction in plant growth and production (Heagle, 1989; Broadmeadow, 1998; Chappelka & Samuelson, 1998; Bortier et al., 2000a), changes in crop quality (Pleijel et al., 1997) and/or a decline in the generative reproductive performance, i.e. amount and dry weight of flowers (Lyons & Barnes, 1998; Gimeno et al., 2004).

1.2.1 Effects of ozone at cellular, biochemical and physiological level

As a strong oxidant, O_3 affects both external and internal surfaces of plants. While external surfaces, i.e. mainly cuticles, are believed to react with O_3 (e.g. Jetter et al. (1996) and Percy et al. (2002) showed degradation of wax tubules in conifer needles and changes in production and structure of cuticular waxes, respectively) and therefore function as O_3 sinks, there is clear general agreement today that the most harmful effects of O_3 are related to O_3 uptake via the leaf stomata rather than O_3 concentrations in the surrounding air (Musselman & Massman, 1999). Since the cuticle is an effective barrier for O_3 uptake (Kerstiens & Lendzian, 1989), O_3 is entering the plant mainly via the stomata, as had been proved for the first time by Rich et al. (1970).

Interestingly, Laisk et al. (1989) measured internal O_3 concentrations close to zero, which is a clear evidence for the quick reaction of O_3 with molecules in the cell wall and plasma membrane due to ozone's extreme reactivity potential (Heath & Taylor, 1997). In other words, the free path of O_3 in the plant is very short, thus only its oxidative products can diffuse into the cell and react with metabolites and biochemicals in the thylakoid membrane and chloroplast (Heath & Taylor, 1997; Long & Naidu, 2002). The reaction of O_3 with the plasma membrane (the initial site of O_3 injury) or – more precisely – with water-soluble organic molecules in the apoplast leads to the formation of various reactive oxygen species (ROS) which induce radical chain reactions (Grimes et al., 1983; Mehlhorn et al., 1990; Kangasjärvi et al., 1994).

The main ROS which are believed to initiate metabolic changes and subsequently productivity losses are hydrogen peroxide (H_2O_2), the hydroxyl radical ($HO^{\cdot}$) and superoxide (O_2^-) (Tingey & Taylor, 1981). Furthermore, there is clear evidence that the production of the plant hormone ethylene (C_2H_4) is highly correlated with O_3 effects, more precisely visible injury (Mehlhorn et al., 1991; Long & Naidu, 2002), or – in other words – ethylene release is stimulated by O_3 exposure (Tingey et al., 1976). Ethylene is known to be responsible for an increased expression of senescence-associated genes and a decreased expression of genes coding for photosynthetic proteins (Miller et al., 1999). There are two main theories about the mechanism of the interaction between O_3, ethylene and damage: a) An increased ethylene production in response to O_3 exposure induces damage via a signal transduction pathway with ethylene being the signal molecule (Sandermann et al., 1998), and b) ozonolysis of the ethylene molecule may produce ROS (Heath & Taylor, 1997). Thus, the question whether ethylene induces damage directly or via production of ROS is still unanswered. However, there is general agreement that O_3 stress, mechanical wounding and pathogen attack all induce ethylene production in the same way (Heath & Taylor, 1997).

To a certain extent plants are able to detoxify ROS, because the aqueous matrix of the cell wall is known to contain many compounds which can act as antioxidants (Larson, 1988; Moldau, 1998; Turcsányi et al., 2000), including ascorbate (Castillo & Greppin, 1988; Takahama & Oniki, 1992; Luwe et al., 1993; Deutsch, 1998), polyamines and phenolics (Langebartels et al., 1991; Eckey-Kaltenbach et al., 1994), and glutathione (Polle et al., 1990; Jamaï et al., 1996), as well as enzymes protecting against ROS, such

as (Cu/Zn) superoxide dismutase (Streller & Wingsle, 1994; Ogawa et al., 1996; Lyons et al., 1999) and peroxidases (Castillo et al., 1984, 1987; Castillo & Greppin, 1986; Takahama & Oniki, 1992; Polle et al., 1994; Ranieri et al., 1996; Torsethaugen et al., 1997). The concentration of these antioxidants and enzymes varies with plant species and the leaf's developmental stage and can be enhanced by an O_3 attack, as has been shown for peroxidases (Castillo et al., 1984; Torsethaugen et al., 1997; Elvira et al., 1998; Calzada et al., 2001), superoxide dismutase (Matters & Scandalios, 1987), glutathione (Madamanchi et al., 1991) and ascorbate (Castillo et al., 1987; Calzada et al., 2001; Van Hove et al., 2001). In contrast, Polle et al. (1993) found a significant decrease in superoxide dismutase activity for Picea abies. Foyer & Mullineaux (1994), Kangasjärvi et al. (1994) and Heath & Taylor (1997) published excellent reviews on detoxification processes in plants.

If the plant is not able to detoxify the different reactive species, the plasma membrane loses its functions, such as permeability, membrane fluidity, K^+-exchange etc., which leads to a loss of transport ability of chemical substances and a loss of ionic homeostasis (Heath & Taylor, 1997; Skärby et al., 1998). Furthermore, dissolution products of O_3 entering the cell might initiate a decline in RUBISCO levels with negative effects for the rate of photosynthesis and productivity (the maximum assimilation rate is proportional to the amount of available RUBISCO linked to the energy produced by electron transport (v. Caemmerer & Farquhar, 1981; Heath & Taylor, 1997)). In fact, an ozone-induced decline of photosynthesis has been proved experimentally for instance by Wallin et al. (1990) for Norway spruce, McKee et al. (1995) for wheat, Farage & Long (1995) for pea, oak and wheat and Kellomäki & Wang (1997a,b) for Scots pine. Farage et al. (1991) and Farage & Long (1999) furthermore stress that often a decline in photosynthesis is an early symptom of an O_3 effect, even before visual damage occurs. Good reviews on changes in photosynthesis and related physiological processes due to air pollution have been published by Darrall (1989) and Saxe (1991).

In addition, there is evidence that exposure to O_3 is able to induce (partial) stomatal closure (e.g. Moldau et al., 1990; Grandjean Grimm & Fuhrer, 1992; McKee et al., 1995; Kellomäki & Wang, 1997; Van Hove et al., 2001), probably by directly affecting the guard cells or the mesophyll (Martin et al., 2000), which might as well reduce the plant's productivity (A/Ci-curves precisely indicate the relationship between

assimilation rate and g_s). A positive relationship between (decreased) net photosynthesis and (decreased) g_s after O_3 exposure was found for example by Hill & Littlefield (1969) for oats, Wallin et al. (1990) for young shoots of Norway spruce, Farage & Long (1995) for pea, oak and wheat, Mikkelsen (1995) for beech, Torsethaugen et al. (1997) for tobacco, Anderson et al. (1997) for Ponderosa pine and Elvira et al. (1998) for Aleppo pine.

These findings are the basis of several widely used models (e.g. Ball et al. 1987; Leuning, 1995; Martin et al., 2000), which predict g_s from the net photosynthetic rate.

However, there are concerns about this procedure which have to be addressed: Firstly, several authors stress that although there is a similar behaviour of g_s and net photosynthetic rate after exposure to O_3, this doesn't necessarily mean that there is a strong mechanistic relationship between these two parameters. Mikkelsen (1995), Farage & Long (1995) and Kellomäki & Wang (1997a) for instance found - based on the analysis of A/C_i curves - that a decrease in net photosynthetic rate was not due to a lower g_s, but to a decrease in biochemical processes of photosynthesis independent of g_s. Secondly, there is evidence that a decline in CO_2 fixation is not necessarily linked to a simultaneous reduction of g_s and vice versa. In fact, a decoupling of g_s and photosynthesis has been shown for Douglas fir by Van Hove & Bossen (1994) (exposure to O_3 reduced net CO_2 assimilation but increased g_s), for aspen clones by Yun & Laurence (1999a) (exposure to O_3 significantly reduced net photosynthesis but not g_s) and for wheat by Müller et al. (2005). The reason for this observation might be the more pronounced light saturation for net photosynthesis in comparison to g_s at certain developmental stages of the plant (Müller et al., 2005). A comprehensive overview of the mechanistic relationship between g_s and photosynthesis can be found in Farquhar & Sharkey (1982).

1.2.2   Ozone-induced visible injury

Several types of visible injury after O_3 exposure have been reported (cf. reviews by Heath, 1980 and Chappelka & Samuelson, 1998). The injury varies widely in its appearance between species (Table 1.1) and with the developmental stage of plants (cf. Heath, 1994; Pääkkönen et al., 1995). However, the most common injury symptoms have been describes as bronzing (mainly on the adaxial leaf surface), chlorosis (from flecking up to large-scale inter-veinal chlorosis), necrosis (mostly flecking) and formation of anthocyanin (Koukol & Dugger, 1967; Jacobsen & Hill, 1970; Sanders & Benton, 1995, Flagler, 1998). Guderian et al. (1985) suppose that visible symptoms can be classified according to chronic or acute O_3 exposure, which causes different forms of damage reflecting different defence strategies of the plants: While leaf necrosis often occurs after short-term exposure to very high O_3 concentrations, chlorosis and bronzing is usually associated with chronic O_3 stress of much lower O_3 concentrations. Disbalances in the redox-status, ROS-production in the chloroplast stroma and a decrease of the chlorophyll-concentration (which leads to a discolouration of the leaf) causes a typical chlorosis (Schraudner et al., 1997), whereas a necrosis appears due to extracellular production of ROS and the destruction of the chlorophyll-rich palisade cells (Guderian et al., 1985; Borriss & Libbert, 1985). There is evidence that chlorosis caused by chronic exposure is reversible, whereas plants cannot recover from necrotic injury (Heath, 1987).

There is a vast variety of papers dealing with ozone-induced visible injury on crops, trees and semi-natural vegetation. Table 1.1 gives an overview of some of these papers without claiming to be complete. In summary, some agricultural crops usually react fastest to O_3 exposure, which makes them ideal indicators for active biomonitoring studies.

However, although visible injury has been established as a parameter for the identification of O_3 sensitivity, its assessment is highly dependant on the knowledge of the evaluator. In fact, chlorosis and necrosis are usually associated with many different types of stresses, and it requires coloured pictorial atlases (Sanders & Benton, 1995; Flagler, 1998) and comprehensive biomonitoring experience to distinguish leaf injury caused by O_3 exposure from injury caused by other stresses. Furthermore, different environmental conditions may alter the development of ozone-induced injury.

Table 1.1   Selection of crop, tree and semi-natural vegetation species that exhibited ozone-induced visible injury. The table includes information on the type of experiment, the reported visible injury symptoms and the source.

Species	Field-grown (f)/ Potted (p)	Chamber study (yes/ no)	Type of reported visible injury	Source
Agricultural crops				
Citrullus lanatus (Watermelon)	f	n	From chlorotic mottle to necrotic brown-red spots (adaxial)	Decoteau et al. (1986)
	p	y & n	Purple stippling and necrosis	Gimeno et al. (1999)
Glycine max (Soybean)	p	n	Necrosis and bronzing on upper leaf surface	Benton et al. (2000)
Lycopersicon esculentum (Tomato)	f	y	Light tan upper surface flecking and premature senescence	Temple (1990)
	p	y	Chlorotic flecking followed by necrotic patches	Hassan et al. (1999)
Nicotiana tabacum (Tobacco)	p & f	?	Dark lesions tending to bleach after exposure to sun	Heggestad (1991)
	p	y	White dots	Günthardt-Goerg (1996)
	p	n	Large-scale bronzing (mostly adaxial)	Ritter (1996)
Phaseolus vulgaris (French Bean)	p	y	Adaxial stippling	Miller & Davis (1981)
	p	n	Dark brown blemishes, mainly adaxial	Tonneijck (1983), Tonneijck & Van Dijk (1997a)
	p	y	Bronze mottling symptoms	Sanders et al. (1992a)
	f	y	Interveinal brown spots on upper leaf surface	Schenone et al. (1992)
	p & f	n	Necrotic stippling	Vandermeiren et al. (1995)
	p	n	Large-scale bronzing (mostly adaxial)	Büker (1997)
Solanum tuberosum (Potato)	f	y & n	Necrotic lesions on adaxial surface of leaves	Donnelly et al. (2001)
Spinacea oleracea (Spinach)	p & f	n	Oily areas, upward bent leaves, white spots in glazed areas	Ashmore (1984), Skärby (1984)
Zea mays (Maize, Corn)	p	y	Not specified	Deveau et al. (1987)

Trees and shrubs				
Alnus glutinosa (Alder)	p	y	Brownish discolouration between 2nd order veins	Günthardt-Goerg (1996)
Betula pendula (Europ. White Birch)	p	y	Light-green dots or bronze discolouration	Günthardt-Goerg (1996)
Betula pendula (Europ. White Birch)	p	y	Small brown necrotic flecks (stippling), adaxial	Pääkkönen et al. (1998)
	p	y & n	Chlorotic spotting, adaxial pigmented stippling, reddening	Vanderheyden et al. (2001), Zhang et al. (2001)
Carpinus betulus (Hornbeam)	p	y	Dots and leaf discolouration	Günthardt-Goerg et al. (2000)
Crataegus monogyna (Hawthorn)	p	y	Dark-coloured stipple or discoloration (reddening or bronzening)	Novak et al. (2003)
Fagus sylvatica (European Beech)	p & f	y & n	Yellowish-brown leaves with small brown necrotic spots	Baumgarten et al. (2000)
	p	y	Slight stippling to large necrotic areas	Clark et al. (2000)
	p	y	Dots and leaf discolouration	Günthardt-Goerg et al. (2000)
Fraxinus excelsior (European Ash)	p	y & n	Chlorotic spotting, adaxial pigmented stippling, reddening	Vanderheyden et al. (2001), Zhang et al. (2001)
	p	y	Dark-coloured stipple or discoloration (reddening or bronzening)	Novak et al. (2003), Novak et al. (2005)
Picea abies (Norway Spruce)	p	y	Increased chlorosis after 3yrs. of fumigation	Braun & Flückiger (1995)
Populus nigra/*Populus* x *euamericana* (Black Poplar (hybrids))	p	y	Light-green leaf tip or leaf rim	Günthardt-Goerg (1996)
	p	n	Yellowish stippling with subsequent large-scale chlorosis	Ritter (1996)
	p	y	Yellow discolouration and necrotic spots	Bortier et al. (2000b)
	p	y	Dark-coloured stipple or discoloration (reddening or bronzening)	Novak et al. (2003), Novak et al. (2005)
Populus tremuloides (Aspen)	p	y	Bifacial black necrosis, followed by leaf abscission	Yun & Laurence (1999b)
Prunus serotina (Black Cherry)	p	y	Dots and leaf discolouration	Günthardt-Goerg et al. (2000)
	p	y & n	Chlorotic spotting, adaxial pigmented stippling, reddening	Vanderheyden et al. (2001), Zhang et al. (2001)
Rhamnus cathartica (Buckthorn)	p	y & n	Chlorotic spotting, adaxial pigmented stippling, reddening	Vanderheyden et al. (2001), Zhang et al. (2001)
Salix alba (White Willow)	p	y	Dark-coloured stipple or discoloration (reddening or bronzening)	Novak et al. (2003)
Salix viminalis (Silky Osier)	p	y & n	Chlorotic spotting, adaxial pigmented stippling, reddening	Vanderheyden et al. (2001)
Tilia platyphyllos (Linden)	p	y	Dark-coloured stipple or discoloration (reddening or bronzening)	Novak et al. (2003)

Viburnum lantana (Wayfaring Tree)	p	y & n	Chlorotic spotting, adaxial pigmented stippling, reddening	Vanderheyden et al. (2001), Zhang et al. (2001)
	p	y	Dark-coloured stipple or discoloration (reddening or bronzening)	Novak et al. (2003), Novak et al. (2005)

Semi-natural vegetation				
Phleum pratense and alpinum (??)	p	y	Necrotic lesions	Danielsson et al. (1999)
Trifolium pratense (Red Clover)	p	y	White-brown necrotic spots	Lüthy-Krause et al. (1989)
	p	y & n	Small discoloured spots, partly necrotic	Pihl Karlsson et al. (1995a)
Trifolium repens (White Clover)	p	y & n	Small necrotic flecks on the upper leaf surface	Becker et al. (1989)
	p	y	Chlorosis and/or necrosis	Heagle et al. (1993)
	p	y & n	Small discoloured spots, partly necrotic	Pihl Karlsson et al. (1995a)
	p	n	Necrotic, point-shape yellow-whitish flecking	Büker (1997)
Trifolium subterraneum (Subterranean Clover)	p	y & n	Small discoloured spots, partly necrotic	Pihl Karlsson et al. (1995a)
	p	n	Chlorotic and bifacial necrotic spots	Pihl Karlsson et al. (1995b)
	p	y & n	Chlorotic and necrotic lesions on leaf surface	Pihl Karlsson et al. (2003)
27 Swedish native herbs and grasses	p	y	Necrotic or reddish flecks on 3 grasses	Pleijel & Danielsson (1997)
24 grassland species of Swiss Arrhenatheretalia plant communities	p	y	Small white-yellow flecks, dark necrotic flecks, leaf discolouration from dark-brown to reddish	Bungener et al. (1999a)
25 herbaceous plant species of arable field margins or disturbed habitats	p	y	Small whitish stipples, whitish flecking, necrotic spots	Bergmann et al. (1999)

1.2.3   Growth and yield reduction

Not all plants respond with characteristic visible injury after being exposed to O_3, as has been shown for instance for some cereals (Hill & Littlefield, 1969; Pleijel, 1999). Instead, they might age more rapidly (also known as premature senescence) which has a negative effect on growth and yield.

The determination of growth and yield reductions is considered a more objective method to quantify the effects of O_3 on plants in comparison with the assessment of visible injury. This method directly measures the loss of plant material after the plant's exposure to O_3. In addition, this response parameter has been proved valuable for deriving dose-response functions, provided that data on O_3 concentration is available. In combination with market prices, dose-response functions enable the calculation of economic losses, which makes this response parameter interesting as a basis for policy measures (Rosendahl & Hansen, 2000).

Often - but not always (see above) - growth and yield reductions are associated with leaf foliar injury, i.e. leaf necrosis might indicate oxidative cell damage, which leads to a reduced photosynthesis, followed by a growth reduction and finally a yield reduction. In other words, yield reductions are usually the result of a reduced plant growth, caused by a decrease of foliar chlorophyll content, reduced photosynthetic activity, altered photosynthate allocation and/or accelerated leaf senescence (Zelitch, I., 1982; Reich & Amundson, 1985).

Growth and yield reductions have been reported for several crops, tree and semi-natural vegetation species. Table 1.2 gives an overview of some growth and yield related experiments without claiming to be complete. Suitable parameters indicating growth and yield reductions vary from species to species, but the most common ones are relative growth rate (Evans, 1972), (total) biomass, fresh and dry weight, 1000 grain weight (cereals) and root to shoot biomass ratio. The latter is a good indicator for ozone-induced alterations in the carbon allocation of a plant, as has been shown by Reiling and Davison (1992) for several native herbaceous species, by Matyssek et al. (1992, 1993) for birch and poplar, by Paludan-Müller et al. (1999) for beech and Landolt et al. (2000) for beech and ash (however, Landolt et al. (2000) did not find changes in the root/shoot ratio for Norway spruce and Scots pine).

In contrast, some studies have shown no or very little effect of O_3 on some of the above mentioned growth parameters (e.g. Samuelson et al. (1996) → biomass of mature *Quercus rubra*; Novak et al. (2003) → no visible injury on Clematis ssp.; Pihl Karlsson et al. (submitted) → relative growth rate of *Trifolium pratense*) or even a yield stimulation following the plant's exposure to lower (ambient) concentrations of O_3. For instance, Sanders et al. (1992b) found a higher yield for *Phaseolus vulgaris* exposed to 7 h mean O_3 concentrations of 32 ppb relative to the control treatment, Bungener et al. (1999) reported a significant ozone-induced stimulation of relative growth rate for *Centaurea jacea* and *Lychnis flos-cuculi* after the first season and a significant biomass increase for *Silene dioïca* after the second growing season, Pleijel & Danielsson (1997) found a significant growth stimulation after exposure to O_3 for *Festuca ovina*, and Karlsson et al. (1997) proved a biomass stimulation for a slow-growing clone of Picea abies after exposure to non-filtered air plus 30 ppb O_3 for approx. 6 weeks.

Despite these examples of ozone-induced growth stimulations, it has to be stressed that the usual effects of O_3 on plants are detrimental.

Table 1.2   Selection of crop, tree and semi-natural vegetation species that showed growth and/or yield reductions following O_3 exposure (AA = ambient air; NF = non-filtered air; RGR = relative growth rate, EDU = ethylenediurea, GP = growth periods).

Species	Field-grown (f)/ Potted (p)	Chamber study (yes/ no)	Reported growth and/or yield reduction after plant's exposure to ozone	Source
Agricultural crops				
Brassica napus ssp. oleifera (Winter Ooilseed Rape)	f	n	8% decrease in plant dry weight and reduced root growth after exposure to daily mean O_3 concentration of 77 ppb for 32 days	Ollerenshaw et al. (1999)
Citrullus lanatus (Watermelon)	p	y & n	Yield loss of up to 39% after exposure to ozone	Gimeno et al. (1999)
Glycine max (Soybean)	f	y	Growth reduction up to 37%	Reich & Amundson (1985)
	p	y	1.5 × ambient O_3 concentration reduced seed yield by 41%	Fiscus et al. (1997)
Lycopersicon esculentum (Tomato)	f	y	Reduced yield by 17 to 54% for different cultivars after exposure to 1.5 times ambient O_3 concentration	Temple (1990)
	p	y	Final yield reduction of 31% for 80ppb O_3 treatment (13 weeks)	Reinert et al. (1997)
	p	y	Yield reduction of 48% for 68 ppb O_3 treatment (75 days)	Hassan et al. (1999)
Nicotiana tabacum (Tobacco)	p	y	Significantly reduced dry weight of leaves & roots after exposure to O_3 (150ppb, 4 h per day) for 2 weeks	Faensen-Thiebes (1983)
Phaseolus vulgaris (French Bean)	p	y	41% reduction in plant dry weight in NF + 20ppb O_3 treatment	Sanders et al. (1992a)
	p	y	26-42% yield reduction in high O_3 treatments (38, 45 & 50 ppb)	Sanders et al. (1992b)
	f	y	Significant reductions in yield after exposure to NF air	Schenone et al. (1992)
	p & f	n	14% pod yield reduction after exposure to ambient O_3 conc.	Vandermeiren et al. (1995)
	p	n	Enhanced dry pod yield by use of EDU → O_3 effect	Tonneijck & Van Dijk (1997a)
	p	y	Biomass and pod yield decreased with increase of O_3 conc.	Tonneijck & Van Dijk (1998)

Solanum tuberosum (Potato)	f	y	Reduced stomatal conductance and yield as well as premature senescence after elevated O_3 exposure in OTCs	Pleijel et al. (2002)
	f	y & n	Reduced above-ground biomass and tuber dry weight after elevated O_3 exposure in OTCs or in FACE faclities	Craigon et al. (2002)
	f	y	Reduced above-ground dry weight by 8.4% after O_3 exposure	Lawson et al. (2001)
Triticum aestivum (Wheat)	f	y	Growth reduction up to 60%	Reich & Amundson (1985)
	f	y	Grain yield decreased with increasing seasonal mean O_3 conc.	Fuhrer et al. (1992)
	f	y	Smaller kernels, decreased 1000-grain weight after O_3 exposure	Ojanperä et al. (1998)
	f	n	Decreased above ground biomass after exposure to 80ppb O_3	Ollerenshaw & Lyons (1999)
	f	y	Relative yield as low as 0.7	Pleijel et al. (2000)
	p	y	Significant reduction in 1000-grain weight after O_3 exposure	Meyer et al. (2000)
Vitis vinifera (Grape)	p	y	Reduction of 90% in grape and sugar yield after 3 yrs exposure	Soja et al. (2004)
Zea mays (Maize, Corn)	p	y	Reduced dry weight in 150 ppb O_3 treatment	Deveau et al. (1987)
Trees				
Acer saccharum (Sugar maple)	p	y	Root dry mass reduced by 10% in shaded plants	Tjoelker et al. (1993)
Alnus glutinosa (Alder)				
Betula pendula (Europ. White Birch)				Matyssek et al. (1992)
	p	y	Reduced growth rate of sensitive clone after O_3 exposure	Pääkkönen et al. (1998)
Fagus sylvatica (European Beech)	p	y	O_3 exposure (46.3 ppm h) reduced new growth by 17 %	Pearson & Mansfield (1994)
	p	y	Signific. reduction in mean biomass for 50% AA + 30 ppb O_3	Clark et al. (2000)
	p	y	Significant decrease in biomass with increasing AOT40	Landolt et al. (2000)
Fraxinus excelsior (European Ash)	p	y	O_3-drought interaction caused decrease in RGR of 32.8%	Reiner et al. (1996)
	p	y	Significant decrease in biomass with increasing AOT40	Landolt et al. (2000)
Picea abies (Norway Spruce)	p	y	Reduced rate of biomass increase in fast growing clone	Karlsson et al. (1997)
	p	y	8% biomass decrease after 4 growing seasons	Karlsson et al. (2002)

	p	y	5% biomass decrease after 4 growing seasons	Ottosson et al. (2003)
Pinus sylvestris (Scots pine)	p	y	Significant decrease in biomass with increasing AOT40	Landolt et al. (2000)
	p	n	Slight decrease in current-year shoot growth	Utriainen & Holopainen (2000)
Populus nigra (Black Poplar)	p	y	Signific. reduction in growth rate after O_3exposure (NF + 30 ppb O_3)	Bortier et al. (2000b)
Populus tremuloides (American Aspen)	p	y	Plants smaller and with lower RGR for elevated O_3 treatment	Volin et al. (1998)
Quercus rubra (Red Oak)	p	y	Plants smaller and with lower RGR for elevated O_3 treatment	Volin et al. (1998)
Semi-natural vegetation				
Calluna vulgaris (Heather)	p	y	Reduced root dry weight by 22.5% in winter (not in summer)	Foot et al. (1996)
Phleum pratense and alpinum (??)	p	y	Significant reduction of biomass after exposure to elevated O_3	Danielsson et al. (1999)
Plantago major (Greater Plantain)	p	y	Reduction in total weight after exposure to O_3	Pearson et al. (1996)
	p	y	Total dry weight reduced by 35% after O_3 exposure for 56 days	Lyons & Barnes (1998)
	p	y	Reduction in biomass & no. of seeds per plant for O_3 treatment	Zheng et al. (2000)
Trifolium pratense (Red Clover)	f	y	Increasing O_3-induced yield loss with time (2 yrs, 9 GP)	Fuhrer et al. (1994)
Trifolium repens (White Clover)	p	y	O_3 significantly decreased total weight of ozone-sensitive clone	Heagle et al. (1993), Heagle & Miller (1996)
	f	y	Increasing O_3-induced yield loss with time (2 yrs, 9 GP)	Fuhrer et al. (1994)
	f	n	Significant effect of ozone on yield	Wilbourn et al. (1995)
	p	n	Dry matter production significantly lower in sensitive clone	Postiglione et al. (2000)
	p	y & n	O_3 significantly decreased biomass of ozone-sensitive clone	Bermejo et al. (2002)
	p	y	Significant decrease in RGR after exposure to O_3	Pihl Karlsson et al. (submitted)
Trifolium subterraneum (Subterranean Clover)	p	n	Increased leaf biomass production by use of EDU $\rightarrow$ O_3 effect	Tonneijck & Van Dijk (1997b)
	p	y	O_3-induced biomass reduction for limited period of plant's life-span	Sild et al. (1999)
	p	y	Significant decrease in RGR after exposure to O_3	Pihl Karlsson et al. (submitted)
24 grassland species of Swiss Arrhenatheretalia plant communities	p	y	Decrease in biomass (partly significant) of 9 species	Bungener et al. (1999b)

1.3   The use of white clover (*Trifolium repens*) as an active bioindicator

In order to get an overview of the status quo and future trends of the emission and deposition of gaseous air pollutants in Germany (as in most industrialised countries), different national and local authorities (Umweltbundesamt, Landesumweltämter, Deutscher Wetterdienst) run monitoring networks at selected sites representing different landscapes, climates, altitudes and political regions.

Usually the equipment of the sites only allows for chemo-physical measurements of pollutants, which help to define pollutant climates over time. Although these concentration measurements have reached a high level of accuracy, they fail to give an indication of potential negative effects of air pollutants on plants. Therefore, the networks are from time to time complemented by bio-monitoring techniques, which are often run by universities or local authorities. By using living organisms, so-called bioindicators, these experiments aim to define the phytotoxicity of the prevailing pollution climate. Dependent on the target pollutant, the bioindicators are divided into accumulation and reaction bioindicators, with O_3 requiring the latter type. Furthermore, there is a distinction between passive and active bioindicators, reflecting the use of plants growing in their natural environment or plants that were cultivated in the greenhouse and then exposed to prevailing air pollutants according to a standardised protocol, respectively (Arndt et al., 1987; Arndt, 1992). Accordingly, the experiment carried out for this thesis has to be classified as an active reaction bio-monitoring.

Most of the recent German bio-monitoring experiments were embedded in large-scale, international research projects, such as the ICP Vegetation[1] (cf. ICP Vegetation, 2004; WGE, 2004) and the EuroBionet (Klumpp et al., 2002). The former has been using white clover clones for its Pan-European O_3 bio-monitoring experiment since 1996 (cf. chapter 4.2).

---

[1] ICP Vegetation: International Cooperative Programme on Effects of Air Pollution on Natural Vegetation and Crops

The history of using white clover for O_3 bio-monitoring experiments both in the USA and Europe goes back to 1989, when Becker et al. for the first time described typical ozone-induced foliar injury as necrotic lesions on white clover. Ever since, several research teams have used this plant to assess the phytotoxic capacity of O_3, including Heagle et al. (1991, 1993, 1994, 1995, 1996), Fuhrer et al. (1993), Ashenden et al. (1995), Pihl Karlsson et al. (1995a), Wilbourn et al. (1995), Heagle & Miller (1996), Büker (1997), Chevone et al. (1998), Schulze (1999), Tang et al. (1999), Heagle & Stefanski (2000), Bermejo et al. (2002) and Pihl Karlsson (2003).

1.4   Regulation of stomatal conductance

The cuticles of most higher plants build an effective barrier for gases to leave or enter the plant, which leads to the stomata being the prime site for gas exchange. In fact, the amount, distribution, size and shape of the stomata, all of which are species-specific, define the rate of incoming and leaving CO_2 as well as water vapour. One of the main challenges of plant life is the regulation of the stomata, which is critical for the balance between carbon gain and water loss, i.e. the balance between sufficient CO_2 uptake for photosynthetic processes and optimal rates of water vapour exchange to prevent life-threatening excessive transpirational losses (cf. Larcher, 1994).

The stomata are in constant movement, because they sensitively react to changes of the leaf-surrounding microclimate. The stomatal function, mediated by the difference in turgor pressure between highly specialised stomatal guard cells and their surrounding cells, is mainly dependent on environmental variables such as light (usually expressed as photosynthetic active radiation (PAR) when referring to plant physiological processes), external CO_2 concentration, air temperature, vapour pressure deficit (VPD), soil water status and wind (Jones, 1992).

There is an exponential increase in the stomatal diffusive resistance (r_s) with decreasing width of the stomatal pores (cf. Jones, 1992). The inverse of r_s is the stomatal conductance ($g_s = 1/r_s$), which is linearly proportional to the pore aperture. The g_s – whose prediction is the main scope of this study - provides an accurate quantification of gas fluxes, including gaseous pollutants, into the plant.

Since g_s is mainly driven by the above listed environmental variables, the rate of g_s varies over the course of a day (diurnal variation) as well as over the course of a growing season (seasonal variation). During the night, stomata are traditionally believed to be mostly shut, although significant rates of night-time g_s have been reported (e.g. Snyder et al., 2003). However, the maximum g_s is definitely achieved during day-time light-saturated growing conditions of plants with non-limiting (low) rates of VPD and soil moisture deficit (SMD). These optimal conditions are rarely met, but close-to-maximum g_s rates of C_3 plants grown in Central Europe are usually reported at fairly warm and humid summer days.

In this thesis, g_s will be mainly predicted from the meteorological variables air temperature, VPD and PAR. The soil water status was not considered to be a main driver for g_s of the white clover clones used in this thesis, because the potted clover plants were kept well-watered throughout the growing season.

1.5 Aims and hypothesis

The aim of the work presented in this thesis was to develop a g_s model for white clover (*Trifolium repens*) based on measured climate, pollution and gas exchange data with the help of artificial neural networks (ANNs), and to use this model for the derivation of flux-response relationships for this species. The framework of the study is depicted in the flow-chart in Figure 1.4.

The following hypotheses were tested in this thesis:

- artificial neural networks (ANNs) are a useful tool for the development of a g_s model for white clover based on measured environmental data;
- the developed models predict realistic diurnal and seasonal rates of g_s for white clover when being applied to measured environmental time-series data;
- realistic diurnal and seasonal rates of O_3 fluxes to white clover can be predicted with the help of the developed g_s models;
- the use of the flux-based AFstX index leads to better dose-response relationships for white clover when compared with the concentration-based AOT40 index;
- the different sensitivity of the ozone-resistant and ozone-sensitive white clover clone can be explained by the higher g_s of the latter;

-   the white clover clone bio-indicator system is a useful tool for the assessment and quantification of effects of ambient O_3 on crops and semi-natural vegetation.
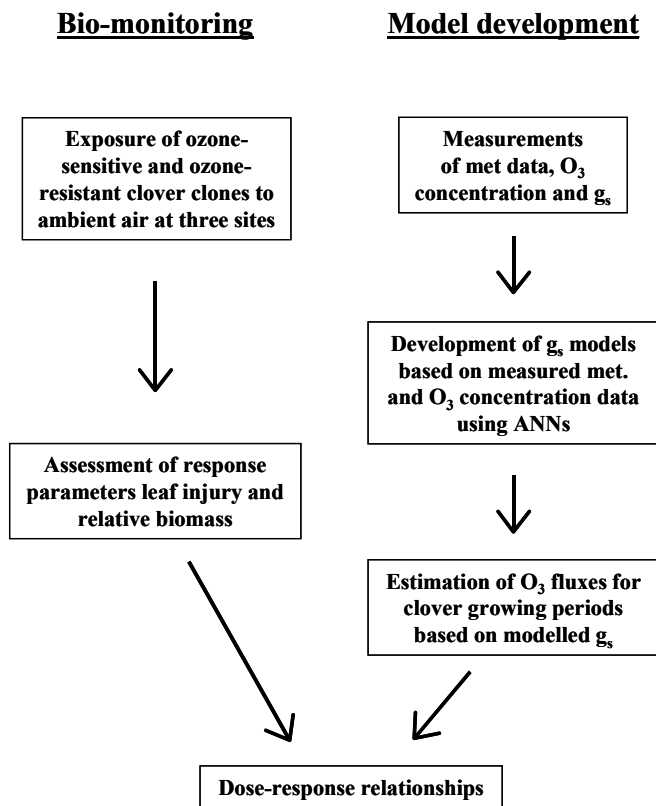
Figure 1.4   Flow-chart of framework of this thesis.

2   Past and present applications of artificial neural networks in natural sciences – an overview

There is a general agreement among scientists that ideal models for predicting plant-atmosphere relationships should be mechanistic (explanatory) rather than (semi-) empirical models. However, such ideal models do not exist. In fact, mechanistic models predicting for instance the gas exchange between the plant interior and its direct environment would be extremely complex as well as time-intensive to develop and to run and therefore remain wishful thinking up-to-date and for the near future.

We have to realize that for many ecological phenomena – most of them are systematically based on highly non-linear relationships between several biotic and/or abiotic parameters – explanations in a mechanistic form are not (yet) available and probably not even necessary. The plant's function addressed in this thesis – i.e. the O_3 uptake via the stomata – is a good example for a very complex phenomenon for which a truly mechanistic explanation does not exist so far. Consequently, we are still dependent on empirical modelling approaches predicting the O_3 uptake of plants.

Traditionally, several statistic techniques, such as multiple linear regression and discriminant analysis, have been used for the quantification and prediction of plant-environment relationships. However, most plant-atmosphere relationships show a highly non-linear behaviour, which makes the use of techniques based on correlation coefficients often inappropriate. This is the main reason, why in recent years Artificial Neural Networks (ANN) have become a very popular tool for environmental modellers. It has been shown that ANNs are suitable in situations where the underlying relationships are non-linear (Lek et al., 1996b; Olden & Jackson, 2002) or even poorly known at all (Lek & Guégan, 1999).

In this chapter a brief history of ANNs will be given, followed by a review of recent ANN-applications in the environmental sciences, a detailed description of a typical feed-forward ANN trained by backpropagation (the most frequently and in this thesis used type of ANNs) and a list of methods to potentially invalidate the "black box" criticism. The development, interpretation and validation of the ANN's used in this thesis are described separately in Chapter 6.

2.1 History of artificial neural networks

When computers were initially developed, they were only able to cope with serial problems, i.e. problems that could be solved step by step in a logical sequence. However, the need for understanding and predicting non-linear phenomena made a further development of computers necessary. The idea was that computers should have the skills to solve parallel problems analogous to the function of the human brain that is able to cope with highly complex tasks such as recognition of faces or wise reactions to threats.

First attempts to simulate the human brain in computer technology are known from the 1940s. For instance, McCulloch and Pitts (1943) developed simple artificial neurons, which in retrospect have to be recognised as initial steps in the history of artificial intelligence (AI). In the following, these neurons were connected with each other, which for the first time created artificial neural networks (ANNs). Early applications of ANNs aimed at analysing biological phenomena such as the mammalian brain function (Lek & Guégan, 1999; Olden et al., 2004).

The main criticisms/disadvantages of the early networks were that they required very complex algorithms and that there was no possibility to weigh the links between input and output. The psychologist Frank Rosenblatt started in the 1950's to overcome this problem by developing the so-called "perceptron model" which consisted of two layers of neurons connected by a single layer of weighted links (Rosenblatt, 1962). The calculations of the output values of this network were based on the weights of the interconnecting neurons. Though this model of weighted networks was further developed in the 1960's (Minsky & Papert, 1969), its main drawback, i.e. the inability to alter the weights during the training process, remained which resulted in limited use of the perceptron model.

The subsequent period of stagnation in the development of ANNs was overcome in the late 1970's/early 1980's when several research groups realised that much more complex, multi-dimensional problems could be tackled using ANNs by introducing multiple layers of perceptrons. Typically, these multiple layer perceptrons consisted of three layers of neurons with adjustable weights of the interconnecting neurons (Rumelhart & McClelland, 1986).

One of the major remaining problems for multilayer networks was to find an adequate algorithm to account for global minima in the error function. Although already developed in the late 1970's, it was not until the mid 1980's that Rumelhart and colleagues (1986) presented the backpropagation training algorithm to a wider research public. Since then, this is the most frequently – and as well in this thesis - used training algorithm.

Beside the multi-layer backpropagation ANNs, various other types of neural networks have been developed, such as the Hopfield network (Hopfield, 1982), Kohonen network (Kohonen, 1982, 1984) and the Boltzmann machine (Ackley et al. 1985). The choice of the network depends on the nature of the problem to be solved. Today, ANNs are able to give satisfactorily answers to questions of auto-associative memory, generalisation, optimisation and data reduction, control and prediction. The latter mentioned ability is the main reason for using ANNs in this thesis.

2.2 Application of artificial neural networks in ecological and environmental sciences

The obvious improvements of ANNs since the late 1980s/early 1990s on the one hand and the further software development and the availability of suitable hardware (e.g. parallel computers and analogue/digital neural cards for personal computers) on the other hand led to an exponentially grown interest in ANNs. In 1992, the world market for the commercial use of ANNs had expanded to be in the order of tens of million dollars and was at that time predicted to be in the range of approximately $5 billion by 2000 (Hubick, 1992).

Scientists from various research fields, such as graphology, psychology, economy, medicine, physics, ecology etc. considered the use of ANNs for different reasons. Successful applications have been reported for replicate tasks like handwritten character recognition (Yeung & Fong, 1994), speech recognition (Rahim et al., 1993; Chu & Bose, 1998), texture recognition (Tirakis et al., 1990; Rangarajan et al., 1991), face recognition (Cottrell & Fleming, 1990), image recognition (Dekruger & Hunt, 1994; Cosatto & Graf, 1995; Kung & Taur, 1995), spectral recognition (Wythoff et al., 1990),

cell classification (Bazoon et al., 1994), chromosome classification (Lerner, 1994) and two-dimensional shape classification (Khotanzad & Lu, 1991).

Furthermore, the predictive ability of ANNs convinced many scientists to favour this tool over standard statistical techniques. Examples of successful predictions with the aid of ANNs have been published in the field of medicine (Burke et al., 1995; Lo et al., 1995; Orr, 1995), economics (Schöneburg, 1990; Refenes et al., 1993; Hoptroff, 1993; Tan et al., 1995) and physics (Chakraborty et al., 1992).

Some early applications of ANNs in ecological and environmental sciences were reported at the beginning of the 1990s (e.g. Colasanti, 1991). Since then, a steadily increasing number of scientists in these fields, especially environmental modellers, focussed on testing the ability of ANNs as a tool for analysing and predicting complex non-linear ecological phenomena.

ANNs are known for being very powerful in dealing with non-linear relationships (Lek et al., 1996b), which makes them an ideal tool for bringing light into the usually very complex relationships between ecological variables. In fact, in direct comparison with traditional statistical model approaches based on regression analyses, ANNs have shown a higher prediction ability (e.g. Baran et al., 1996; Paruelo & Tomasel, 1997; Ramos-Nino et al., 1997; Starett & Adams, 1997; Manel et al., 1999; Özesmi & Özesmi, 1999).

Since the early 1990s, an increasing number of scientists have shown the strengths and advantages of ANNs in very different fields in applied ecology and environmental science. For instance, De Silets et al. (1992) predicted sea water salinity with the help of ANNs, Daniell & Wundke (1993) used ANNs to estimate water nutrient concentrations, Seginer et al. (1994) modelled the greenhouse effect, Edwards and Morse (1995) stressed the potential of ANNs in biodiversity research, Smith and Eli (1995) assessed the rainfall-runoff, Lek et al. (1996 a,b) and Baran et al. (1996) predicted various parameters in brown trout management, Brey et al. (1996) modelled the production/biomass ratio of animal populations, Poff et al. (1996) assessed the effect of climate change on river hydrology and ecology, Roadknight et al. (1997) and Pastor-Bárcenas et al. (2005) predicted surface O_3 concentrations, Tangang et al. (1997)

modelled sea surface temperatures, Goswami & Srividya (1996) and Zhang et al. (1997) used ANNs to estimate rainfall, Van Wijk & Bouten (1999) modelled water and carbon fluxes above European coniferous forests and Karul et al. (2000) modelled eutrophication processes of large water bodies in Turkey.

In plant sciences, ANNs have increasingly been used since the mid 1990s. Hirafuji & Kuboti (1994) determined effects of various stresses on photosynthesis, Scardi (1996), Recknagel et al. (1997) and Whitehead et al. (1997) modelled algal concentrations, Balls (1996), Ball et al. (1998, 2000) and Mills et al. (2000) identified factors which influenced the effects of ambient O_3 on white clover, Maier & Dandy (1997) assessed the incidences of blue-green algae, Barciela et al. (1999) predicted phytoplankton production and Bungener et al. (1999) used ANNs to analyse the injury response of nine grassland species to O_3.

In this thesis ANNs will be used to predict O_3 fluxes to white clover plants in dependence on the environmental parameters air temperature, photosynthetic active radiation (PAR) and vapour pressure deficit (VPD).

The ANN software used in this thesis is NeuroShell 2 (Ward Systems Group Inc., USA). It has been successfully applied to identify non-linear relationships of ecological phenomena for instance by Balls (1996), Roadknight et al. (1997), Ball et al. (1998, 2000), Ryan et al. (2004) etc. The features of this software package and the development of the model will be presented in Chapter 6.

2.3   Backpropagation artificial neural networks

Multi-layer feed-forward artificial neural networks trained by backpropagation algorithm, also known as backpropagation neural networks or single/multi-layer perceptron, is the most commonly used type of networks today, because it has proved to be a powerful method for modelling complex relationships between variables. This was the reason for also applying it in this thesis.

The purpose of these networks is to capture the relationship between a set of model inputs and corresponding outputs. This procedure is called supervised learning. In other words, backpropagation networks develop models only from the data presented, which

together are assumed to implicitly contain the information necessary to establish relations between different input and output parameters by determining the weighted connections between them. Therefore, backpropagation neural networks allow the prediction of output variables for given input variables.

The architecture of a backpropagation neural network consists of three different layers called input, hidden and output layer (Figure 2.1). There can be more than one hidden layer and hidden layers can also be split up into different parallel functioning sub-layers in order to apply different activation functions (see Chapter 6.1) in parallel during model runs. The three types of layers contain one or more interconnected non-linear processing elements, called neurons (Hecht-Nielsen, 1990). The number of neurons in the input layer matches the number of input (independent) variables, whereas the number of neurons in the hidden layer is usually varied – using the trial and error method - during the model training process in order to find the optimal predictive performance of the model. The output layer comprises as many neurons as there are target (dependent) variables.

During the training of the neural network, the internal information or signal "flows" from the input through the hidden layer to the output layer. This happens by connecting all input neurons to all hidden neurons by weighted links, i.e. each input neuron is multiplied by the weight of the connection (Figure 2.1). This weight can be positive or negative. Negative connection weights represent inhibitory effects on neurons (i.e. reducing the intensity of the incoming signal) and decrease the value of the predicted response, whereas positive connection weights represent excitatory effects on neurons (i.e. increasing the intensity of the incoming signal) and increase the value of the predicted response.

Typically a non-linear activation function, e.g. Gaussian, logistic or hyperbolic tangent, is then fed with the sum of the weighted inputs. This process creates a value that is compared with the actual output value. The resulting error value, which is based on the difference between these two values, is in the following returned (or backpropagated, which explains the name of this type of ANNs) in a loop to the hidden neurons and multiplied by an adjusted weighting factor.
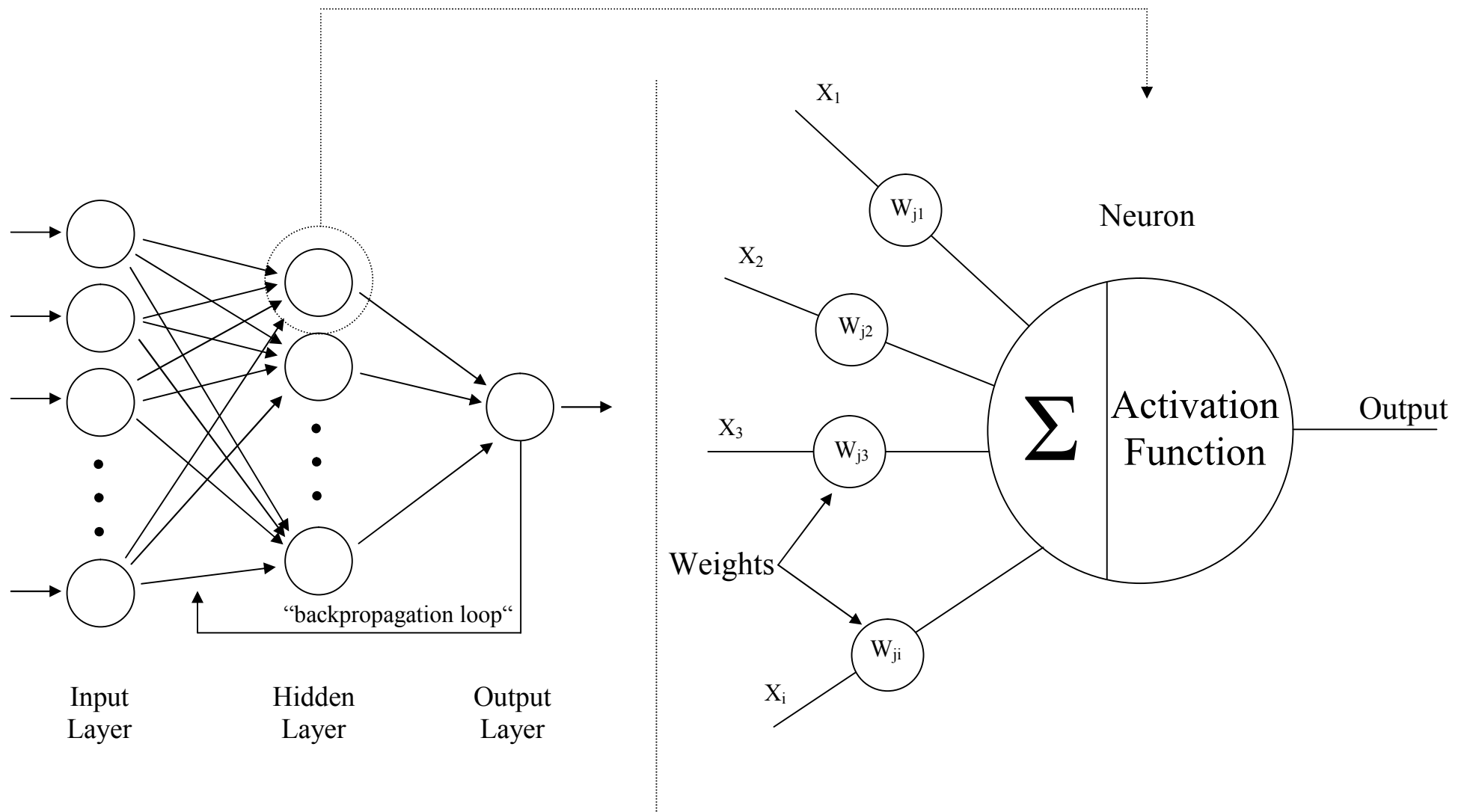
Figure 2.1   Architecture and operation of a typical backpropagation neural network with one hidden layer (after Maier & Dandy, 1998); X_i = output from previous layer, W_{ji} = weight of interconnection j between neuron i and current neuron.

In general, the neurons of the hidden and output layer are stimulated by the neurons of the previous layer according to the following relationship:

$$a_j = \sum_{i=1}^{1} X_i W_{ji},$$
(2.1)

where a_j is the activation of the jth neuron, X_i the output value of the ith neuron of the previous layer and W_{ji} the synaptic weight of the connection between the ith neuron of the previous layer and the jth neuron of the current layer.

The adjustment of the interconnections of the neurons is done repeatedly in order to minimize the output error. The amount by which each connection weight is adjusted depends on the learning rate (η) and the momentum value (μ). These two parameters serve to accelerate the training while preventing the network from falling into local minima (Baran et al., 1996).

The momentum term has the effect of adding a proportion of the previous weight change to the current weight change during the training process. The proportion of the previous weight change added is equal to the momentum, μ. The momentum ensures that general trends are reinforced and oscillatory behaviour is suppressed. The momentum value must be less than 1.0 for convergence (Dai & Macbeth, 1997). Generally, high momentum values are suggested for noisy datasets.

The learning rate η is proportional to the amount a particular connection weight is changed during one epoch (i.e. a complete pass through the network) of the training procedure (cf. Viotti et al., 2002). It is multiplied by the error of the network and its value can vary in the range of 0 to 1. Usually it is set close to zero, because high values (i.e. close to 1) might lead to large oscillations during the training process or – in the worst case – might suppress convergence of the network at all. However, very small learning rates slow down the learning of the network.
This shows the problem of finding the optimal learning rate and momentum for the network. Similar to the decision on the optimal number of used hidden neurons, this problem is usually solved by trial and error.

The above mentioned output error is calculated by the so-called error or performance function. Usually, the output error is defined by either the sum or the mean of the squared differences between the predicted and given (typically measured) output values. Maier and Dandy (1998) have shown that the use of the sum of squared errors, also called the quadratic error function, resulted in a faster learning speed and better generalisation ability of the network in comparison with other error functions. In fact, the ANN software used in this thesis (NeuroShell 2) uses by default the sum of squared errors (SSE) to determine the output error:

$$SSE = 1/2 \sum_{i=1}^{N} (Y_i - \hat{Y}_i)^2 \qquad (2.2)$$

where N is the number of elements, i is the index of elements, Y_i is the desired (measured) value for the ith element and $\hat{Y}_i$ is the calculated or predicted value for the ith element. In theory, one could run the training until the output error does not decrease further. However, this procedure would almost certainly lead to an over-trained network.

Symptomatic for an over-trained (or over-fitted) network is its poor generalisation ability, i.e. the network predicts the output very well when using the dataset it was trained with, but very badly when using a new dataset. This shows that one of the biggest problems in creating a good prediction model is the decision when to stop the training procedure. If the training is stopped too early, the network might not have learned the data patterns properly which might result in a low predictive ability of the network. In contrast, if the training is stopped too late (or if too many hidden neurons have been used), neural networks tend to learn the noise in the data and memorise training patterns instead of interpolating between them, which limits the generalisation with new patterns (like mentioned above).

To overcome this problem, the network should be constantly compared to an initially extracted subset of the data during the training. This subset, in the following called test set, is randomly excluded from the training dataset before the start of the training. It is therefore not used for the computation of the connection weights but for calibrating the network and eventually stopping the training at a certain point. This happens by reading in the test set at intervals the modeller defines and comparing the predicted output value

of the training set with the output values of the test set using the sum of the squared errors like described above. The training should be stopped, when this sum of squared errors is at its minimum.

Once this minimum value is reached, the connection weights remain fixed and the neural network can be used for predictions. Provided the training data was fully representative of the entire data range of each input variable, the network will then be able to accurately predict the output for random data combinations of input variables. In order to test this, a second subset of the training set can be extracted before the start of the training, the so-called (cross-)validation set. This set contains data the network has never "seen" before and therefore gives an insight in the real generalisation and prediction ability of the network.

Finally, it has to be stressed that any data ANNs are applied to should always be in the same range like the data with which the network was trained with to assure satisfactory prediction results, because ANNs have very limited extrapolation abilities.

2.4 Illuminating the "black box"

As mentioned above, ANNs have been successfully used in various different research fields and there is little contradiction that they are an attractive, non-linear alternative to traditional statistical methods. Although it is obvious that ANNs are well suited for developing prediction models (e.g. Baran et al., 1996; Paruelo & Tomasel, 1997; Ramos-Nino et al., 1997; Starett & Adams, 1997; Manel et al., 1999; Özesmi & Özesmi, 1999), there has always been a lot of criticism about the explanatory ability of ANNs. In fact, they have often been considered as being a "black box" approach to modelling ecological phenomena (e.g. Lek & Guégan, 1999; Özesmi & Özesmi, 1999). The reason for this is based on the fact that the contribution of each input variable in predicting the output is difficult to identify, an effect that is increasing with increasing numbers of hidden neurons. Especially in ecological sciences, where the aim of most studies is gaining insight into causal relationships of ecological phenomena, this fact is considered as a big drawback. Furthermore, it is - with the exception of very trivial networks - usually not possible to give the equation of the network code because of the complexity of the internal structure of ANNs.

Unfortunately, this lack of clear, easily understandable relationships between input and output variables make ANN-based models often unpopular among stakeholders, politicians and even researchers. Hence, this fact has to be seen as the major disadvantage of ANNs in comparison with traditional statistical methods.

However, quite a few papers have been published recently giving overviews and performance rankings of methods to enlighten the relationships between input and output variables and general internal processes of ANNs (e.g. Özesmi & Özesmi, 1999; Olden & Jackson, 2002; Gevrey et al., 2003; Olden et al., 2004). Among these methods the most common are:

i)   Pruning algorithms for eliminating irrelevant input (e.g. Bishop, 1995; Maier et al., 1998; van Wijk & Bouten, 1999); this method excludes variables and/or neuron interconnections that are below a pre-defined threshold. By doing this, the network is reduced to a potentially more interpretable size.

ii)   Partial derivatives method (e.g. Dimopoulos et al., 1995, 1999); this method computes the partial derivatives of the ANN output with respect to the input variables. As a result, a profile of the output variations for small changes of each input variable and a classification of the relative contributions of each variable to the network output are obtained.

iii)   Sensitivity analysis (e.g. Lek et al., 1996 a, b; Özesmi & Özesmi, 1999; Olden et al., 2002); traditionally, this method varies each input variable across its entire range while holding all other input variable constant. It gives a good indication of the relative importance of single variables on the dependent variable.

iv)   Garson's algorithm (e.g. Garson, 1991; Goh, 1995; Gevrey et al., 2003; Olden & Jackson, 2002); this method partitions the hidden-output connection weights into components associated with each input neuron using absolute values of connection weights in order to determine the relative importance of the various inputs in the network.

v)   Connection weight approach (e.g. Olden & Jackson, 2002; Olden et al., 2004); this method calculates the product of the raw input-hidden and hidden-output connection weights between each input neuron and output neuron and sums the product across all hidden neurons.

In this thesis, the sensitivity analysis, the connection weight approach and an internal NeuroShell 2 weighting analysis tool have been used (cf. Chapter 6.2), all of them for different reasons: the sensitivity analysis gives a good visual indication of the importance of each input variable on the output variable (which is only a qualitative tool, though), the connection weight approach showed very good results in several studies and proved to be better than Garson's algorithm (e.g. Olden & Jackson, 2002; Olden et al., 2004), while the NeuroShell 2 analysis weighting tool was just practical to use since it was always quickly available. The connection weight approach is basically also a kind of manual pruning tool as it clearly identifies those variables that only marginally contribute to the prediction of the output.

In summary, these different methods can help "illuminating the black box" (Olden & Jackson, 2002). By using a combination of quantitative approaches, such as the connection weight approach, and qualitative/visual approaches, such as neural interpretation diagrams (cf. Özesmi & Özesmi, 1999) and sensitivity analysis, it is now possible to identify and interpret individual and interacting contributions of the input variables in neural networks. Therefore, Olden and Jackson (2002) argue that because of the variety of above mentioned methods to enlighten the internal working of neural networks it is not appropriate anymore to call ANNs "black boxes".

3   Material and methods

3.1   Geographical classification of the natural landscapes of the Trier region and location of experimental sites

The ambient air bio-monitoring experiment of this thesis was conducted at three sites in the Trier region. The West German city of Trier (population approx. 108.000) is located in the German federal state of Rhineland-Palatinate (SW-Germany). The city centre has been built in the valley of the river Mosel, whereas many suburbs, including Tarforst with its University campus, are located on former river terraces north and south of the current river valley floor. The Trier region is a typical German midrange mountain area with several plateaus separated by river and creek valleys. The plateaus are used for forestry (mainly coniferous plantations) and agriculture (cultivation of cereals, dairy farming), whereas the slopes of the valleys are characterized by either little woods or groves (often deciduous trees) or viticulture. The main river, Mosel, separates the low mountain ranges of the "Eifel" and "Hunsrück", both part of the "Mittel-Rheinisches Schiefergebirge".
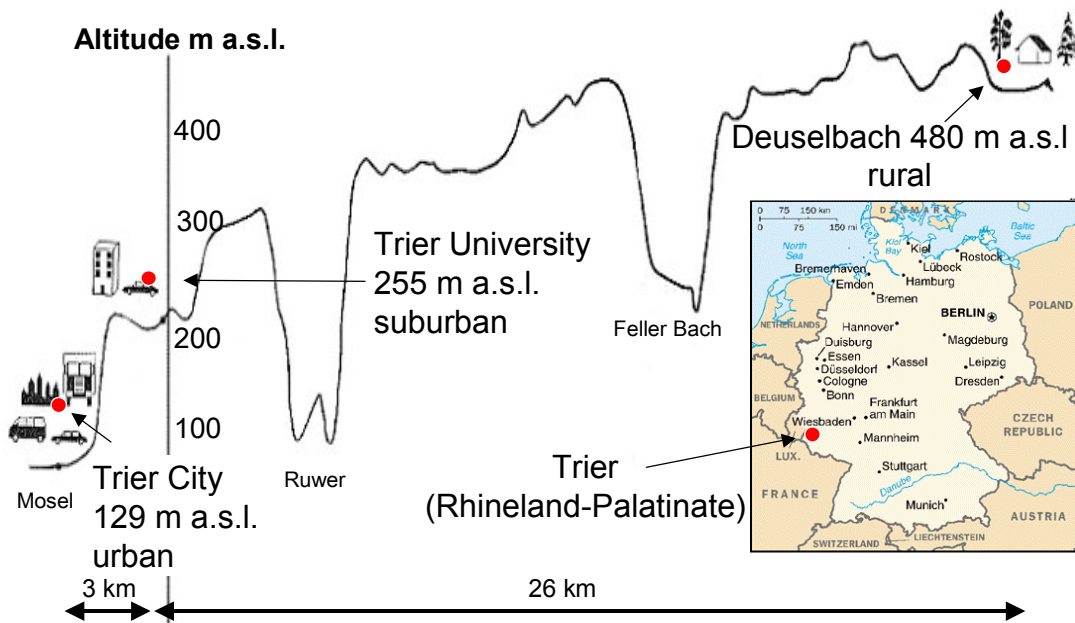
Figure 3.1   Transect showing the location of the field sites Trier-City, Trier-University and Deuselbach, and a map indicating the position of Trier in relation to Germany's national territory.

Due to Trier's vicinity to the Atlantic Ocean, the climate of the region has to be considered predominantly as oceanic with relatively humid, cool summers and mild winters (Closs, 1979). Mostly westerly winds bring an average yearly rainfall of approx. 750mm. The heterogeneous distribution of precipitation in the region is dependent on the high relief energy, which separates the landscape in windward and leeward areas with highly differing precipitation amounts.

The three experimental sites selected for the bio-monitoring were named "Trier-City", "Trier-University" and "Deuselbach". The urban site Trier-City was located on the premises of the "Städtisches Gartenbauamt" (49°45'26"N, 06°38'38"E; 129 m a.s.l.), the sub-urban site Trier-University on the premises of the University of Trier (1997 to 1999: Floristic garden of the Department of Geobotany, 49°44'56"N, 06°41'10"E; 255 m a.s.l. – after that (2000 and 2001) relocation to a new campus approx. 500 meters north of the initial location: 49°44'55"N, 06°40'29"E; 259 m a.s.l.) and the rural site Deuselbach on the premises of the "Messstelle Deuselbach" (49°45'47"N, 07°03'18"E; 480 m a.s.l.) of the Umweltbundesamt (Figure 3.1).

3.2   Plant material and its propagation

Two clones of white clover (*Trifolium repens* L. cv. Regal) with different sensitivity to O3 were selected for this experiment: the ozone-sensitive NC-S clone and the ozone-resistant NC-R clone (Figure 3.2). Each clone is genetically uniform and was originally cultivated by Al Heagle (cf. Heagle et al., 1991, 1995) in North Carolina (therefore the abbreviation **NC**-S and **NC**-R) in the 1980's. His research team collected field-grown white clover for duplication/multiplication and reproduced it vegetatively (asexual) in the greenhouse to maintain the genetic information of the initial "mother plant". The new plants, grown from cuttings of the "mother plant", were then exposed to high concentrations of O_3 in open top chambers (OTCs) in order to identify the most and least ozone-sensitive plants. Subsequently, these most and least ozone-sensitive individuals were again reproduced as described above and again exposed to O_3. This step was repeated several times and finally resulted in the establishment of the ozone-sensitive NC-S and ozone-resistant NC-R clones of identical genetics each.

Figure 3.2   Photos of typically round-shaped and oval-shaped leaves of the ozone-resistant (NC-R, left) and ozone-sensitive (NC-S, right) white clover clones (*Trifolium repens* L. cv. Regal), respectively.

Over the last 20 years, these clover clones (Figure 3.2) have been frequently used for O_3 bio-monitoring experiments both in the USA and Europe (cf. Chapter 2.2.4). The satisfactory results of the clover clone system was a main reason for the ICP Vegetation[1] to introduce this bio-indicator system for its Pan-European O_3 bio-monitoring experiment in 1996, which has been performed during all growing seasons ever since.

Another reason for selecting *Trifolium repens* as a bioindicator for a Pan-European survey was the wide spatial distribution of this species in Europe, ranging from Scandinavia to the Mediterranean and from the Atlantic to the Ural Mountains (the distribution map of the genus *Trifolium* (Figure 3.3) gives an indication of the vast circumpolar presence of species of this genus). In fact, white clover is an important and often dominant species in several grassland communities in Europe, which therefore is of high economical interest, too. Furthermore, the regenerative growth of white clover after a harvest is very quick, which is an important precondition for the experimental approach used in the ICP Vegetation.

The Department of Geobotany of the University of Trier joined the ICP Vegetation in 1996 and used the above described clover clones for the first time in 1997 and in the

---

[1] ICP Vegetation: International cooperative programme on effects of air pollution on natural vegetation and crops

following years until present. The participation in this bio-monitoring network offered the opportunity to use the clover clone plants for additional, more detailed experiments, which form the basis of this thesis.
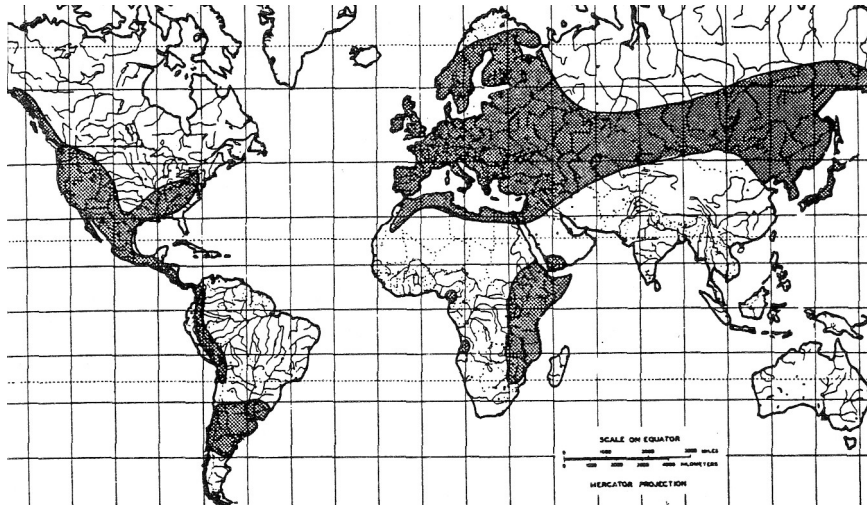
Figure 3.3   Terrestrial spatial distribution of the genus *Trifolium* (Gillet, 1985)

The plant material was always supplied by the Coordination Centre of the ICP Vegetation at CEH Bangor (Centre for Ecology and Hydrology). Virus-free white clover clone cuttings of 7-10 cm length with 3-4 leaf nodes were sent via express delivery from Bangor to Trier. After arrival, cutting were immediately planted into a 1-litre pots in a non-filtered air greenhouse. The pots contained a fertilized peat substrate (TKS 2) and were positioned under mercury-vapour lamps, which supplemented the natural light throughout the daylight hours (i.e. between approx. 7 a.m. and 8 p.m.). All plants were watered regularly, depending on weather conditions. At day 10, 20 ml of a rhizobium-water slurry was added as a soil drench to all plants to initiate the mycorrhizal symbiosis, which is beneficial for the nitrogen fixation in Fabaceae (such as *Trifolium*). In addition, on day 21 after planting all plants were fertilised with 150 ml of a water solution containing 1 g/litre of Peters 5-11-26 (N-P-K) nutrient solution.

At day 28 after planting, all cuttings were transplanted into bigger pots with a volume of 15 litres and a diameter of approx. 30 cm (Figure 3.4). The used substrate was a 1:1:1 mixture of local sterilised soil, peat (TKS 2) and sand, enriched with approx. 60 g of slow release (5 months) fertilizer Osmocote[®] (N:P:K → 14:13:14) per pot. In order to maintain a constant water supply and to prevent water stress, all pots were equipped

with five fibre-glass wicks leaving the bottom of each pot via five holes. This system allowed a capillary water transport whenever the plants were in need of water from water reservoirs (buckets) positioned under the planting pots (Figure 3.4).
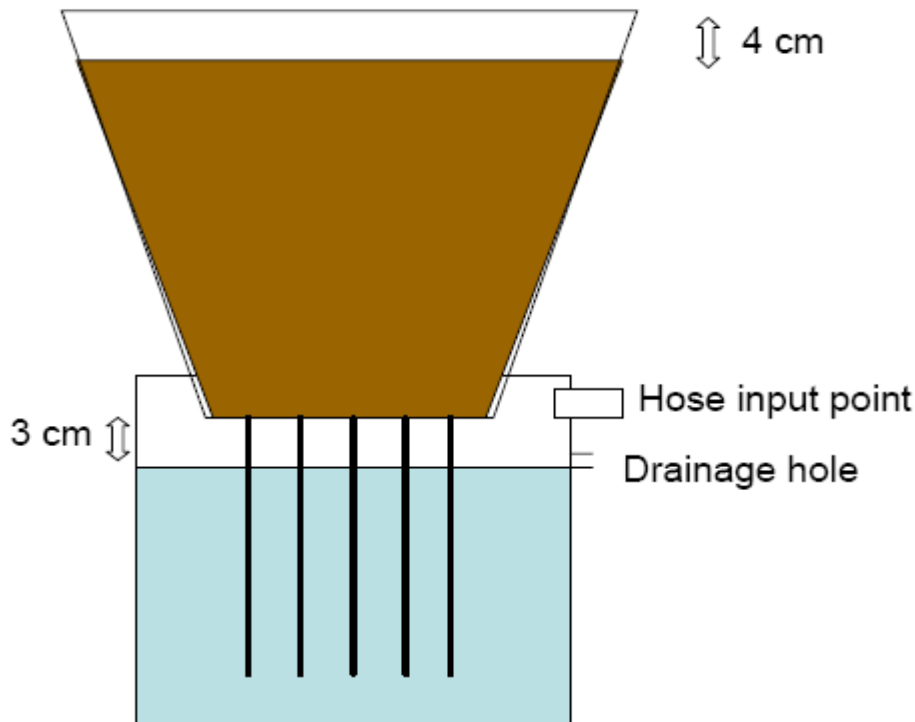
Figure 3.4   Schematic illustration of a typical plant pot and its water reservoir underneath used in this study. The five black lines depict the glass-fibre wicks, which allowed a capillary water transport into the soil/plant.

3.3   Experimental design, meteorological recording and assessment methods

3.3.1   *Experimental design*

The above described potted white clover clones were exposed to ambient air at the sites Trier-City, Trier-University and Deuselbach for 140 days (20 weeks) during the vegetation period of the years 1997 (pilot study), 1998, 1999, 2000 and 2001. Each year, 20 plants of each clone were exposed according to the experimental protocol of the ICP Vegetation (e.g. ICP Vegetation, 1998), which resulted in an experimental design of four rows containing ten pots. The NC-S and NC-R plants were arranged alternately as shown in Figure 3.5. In order to prevent the black planting pots and reservoirs from over-heating, aluminised bubble-wrap was placed around them.

Furthermore, the experimental site was kept free from weed by initially covering it with a black plastic, woven planting foil. Figure 3.6 shows a typical site set-up (shown site: Deuselbach).

During the exposure time, a careful observation for insect pests was required. Especially aphids – though rarely - tended to attack the plants and were therefore treated with the insecticide/pesticide 'Spruzit' (4 % Pyrethrine, 16 % Piperonylbutoxid; Neudorff Chemicals). This was especially necessary in 1998 and 1999. In addition, slugs had to be controlled using slug pellets (Mesurol, Bayer Chemicals), whereas herbivore (e.g. rabbits) attacks were prevented by erecting a rabbit-proof fence around the experimental site.

S	R	S	R	S	R	S	R	S	R
R	S	R	S	R	S	R	S	R	S
S	R	S	R	S	R	S	R	S	R
R	S	R	S	R	S	R	S	R	S
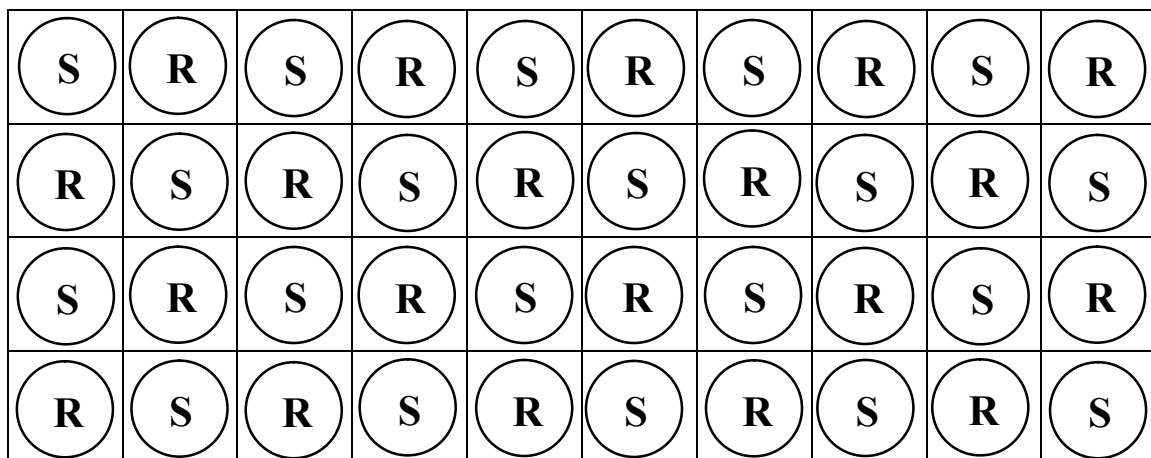
Figure 3.5   Experimental design of the clover bio-monitoring experiment (S = NC-S clone, R = NC-R clone).

Figure 3.6   Typical site set-up showing four rows of potted clover plants in Deuselbach in 1998.

Another potential source of disturbance of the experiment were infections by viruses. Especially the resistant clover clone sometimes showed after weeks of exposure a large yellowish/whitish flecking on the leaves. Unfortunately, there are no chemicals to protect plants from viruses. Hence, plants showing virus infections even after cutting back the infected leaves were excluded from the experiment. However, this was only necessary in September 1998 (removal of two NC-R plants).

3.3.2 Meteorological recordings

In all years, meteorological parameters and the ambient O_3 concentrations were recorded in direct vicinity of the exposed plants at a standardised height of three meters above ground. The meteorological and O_3 concentration data for the site Trier-City were recorded at the weather station "Ostallee", which is run by the federal state of Rhineland-Palatinate. All parameters were recorded half-hourly, but all data were transformed to hourly means prior to their use in this thesis.

At the site Trier-University, air temperature [°C], global radiation [$W*m^{-2}$], relative humidity [%], wind speed [m/s], wind direction [°] and rainfall [mm] were measured in 1997, 1998 and 1999 with the own meteorological station (EcoTech, Messsysteme, Bonn, Germany) of the Department of Geobotany, which was positioned in the floristic garden of the department. The measuring system was always calibrated in springtime prior to its use from May on. O_3 [$\mu g*m^3$] was simultaneously recorded using a Horiba O_3 analyser, which was calibrated annually in spring by cross-validating it with O_3 concentrations measured at the weather station "Deuselbach" of the Bundesumweltamt, as well as on a daily basis with the help of an on-site O_3 generator. All above-mentioned parameters were measured every 10 seconds, saved on a computer located nearby in the glasshouse and manually averaged for 60 minute intervals.

In the years 2000 and 2001, the same meteorological parameters were measured by the weather station of the Department of Climatology of the University of Trier, which was located next to the experimental site of the clover clone experiment. The O_3 concentration [ppb] was measured by the ZIMEN[2] measuring station, also located next to the experimental site. Again, hourly means were calculated for all parameters.

---

[2] ZIMEN = Zentrales Immissionsmessnetz des Landes Rheinland-Pfalz (Landesamt für Umweltschutz und Gewerbeaufsicht, 1978-2001).

The meteorological and O_3 concentration data for the site Deuselbach were recorded in the immediate vicinity of the bio-monitoring experiment on the premises of the weather station Deuselbach of the "Umweltbundesamt". All parameters were recorded half-hourly, but as for the other sites, all data were transformed to hourly means prior to their use in this thesis.

For the model approach, the parameters photosynthetic active radiation (PAR), vapour pressure deficit (VPD) and AOT40 (accumulated concentrations above a threshold of 40 ppb) were required. These parameters could be easily derived from the measured parameters mentioned above by using the following equations (v. Willert et al., 1995):

$$VPD \ [hPa] = e^o - e \tag{3.1}$$

where e^o is the saturation water vapour pressure and e is the water vapour partial pressure. According to Campbell & Norman (1998), the saturation water vapour pressure can be calculated with the following equation:

$$e^o = \exp(52.57633 - 6790.4985/(273.15+T) - 5.02808*\ln(273.15+T)) \tag{3.2}$$

where T is the air temperature [°C]. Subsequently, e can be calculated as followed:

$$e = RH * e^o /100 \tag{3.3}$$

where RH is the relative humidity [%].

PAR was derived from measured global radiation (GR) data based on an empirical relationship detected prior to the main experiment (comparison of global radiation measuring device with PAR sensor of gas exchange measuring system) according to the following equation:

$$PAR \ [\mu mol*m^{-2}*s^{-1}] = 1.941 * GR \ [W \ m^{-2}] \tag{3.4}$$

The AOT40 was calculated according to the following equation:

AOT40 [ppb.h] =

$$\Sigma \ ((O_3 \ \text{concentrations} > 40 \ \text{ppb for GR} > 50 \ \text{W m}^{-2}) - 40) \tag{3.5}$$

3.3.3   Assessment and harvest methods

Visible injury was assessed at least once a week. The first occurrence of O_3 injury on the sensitive and resistant clone (usually white small flecking on leaves) after transplanting and each harvest (see below) was recorded. A more detailed visible injury assessment was done prior to the destructive harvest on each harvest day, i.e. five times per growing season (Table 3.1). First, each plant was graded as either healthy or abnormal, with the cause of the abnormality scored as 1 (slight), 2 (moderate) or 3 (severe) using the following classification:

Table 3.1   Classification of visible injury (ICP Vegetation, 1998)

Abbreviation	Type of abnormality
O	Ozone injury
S	Stunted
D	Diseased
I	Insect damage
Sl	Slug damage
A	Animal (rabbits, deer, birds etc.)
V	Virus

Subsequently, a scoring system - presented in Table 3.2 - developed by the ICP Vegetation (cf. ICP Vegetation, 1998) was used for the detailed visible O_3 injury assessment. Figure 3.7 shows two photos of a NC-S clover clone with an O_3 injury score of 1 and 4.

Table 3.2   Scoring system of visible O_3 injury assessment (ICP Vegetation, 1998)

Score	Extent of visible injury	Definition
0	No injury	No symptoms
1	Very slight injury	Occurrence of first symptoms
2	Slight injury	1-5 % of leaves with slight injury
3	Moderate injury	5-25% of leaves with injury
4	Heavy injury	25 - 90% of leaves with injury
5	Total injury	90-100 % of leaves with injury

Figure 3.7   Visible injury on the sensitive white clover clone (NC-S) after exposure to ambient air. Typical first injury symptoms expressed as white spots at the edge of the leaf (left) and heavy ozone-induced foliar injury (right) would correspond with injury class 1 and 4, respectively (cf. Table 3.2).

After the detailed visible injury assessment, a destructive harvest was carried out. The first harvest always took place four weeks after the plant transplantation and was repeated four times each year (Table 3.3 – 3.5). The forage (leaves, flowers and stolons) was harvested 7 cm above the soil surface by using long-blade scissors. Runners that grew outside the pot perimeter were harvested, too. Injured leaves that remained after cutting the above mentioned top 7 cm of the forage were removed in order to prevent confusion with new injury occurrence at subsequent observations. Furthermore, alcohol was used for disinfection of the scissors to prevent virus spread from plant to plant.

Table 3.3   Clover clone transplantation and harvest dates at the site Trier-City for the
              growing seasons 1997 to 2001.

	1997	**1998**	**1999**	**2000**	**2001**
Transplantation	21/05	19/05	04/05	17/05	21/05
Harvest 1	12/06	16/06	01/06	14/06	18/06
Harvest 2	10/07	14/07	29/06	11/07	16/07
Harvest 3	06/08	11/08	27/07	08/08	13/08
Harvest 4	03/09	08/09	24/08	05/09	10/09
Harvest 5	01/10	06/10	21/09	04/10	08/10

Table 3.4   Clover clone transplantation and harvest dates at the site Trier-University for
              the growing seasons 1997 to 2001.

	1997	**1998**	**1999**	**2000**	**2001**
Transplantation	22/05	20/05	05/05	17/05	22/05
Harvest 1	13/06	17/06	02/06	15/06	19/06
Harvest 2	11/07	15/07	30/06	12/07	17/07
Harvest 3	07/08	12/08	28/07	09/08	14/08
Harvest 4	04/09	09/09	25/08	06/09	11/09
Harvest 5	02/10	07/10	22/09	05/10	09/10

Table 3.5   Clover clone transplantation and harvest dates at the site Deuselbach for the
              growing seasons 1997 to 2001.

	1997	**1998**	**1999**	**2000**	**2001**
Transplantation	20/05	18/05	03/05	16/05	21/05
Harvest 1	11/06	15/06	31/05	13/06	18/06
Harvest 2	09/07	13/07	28/06	10/07	16/07
Harvest 3	05/08	10/08	26/07	07/08	13/08
Harvest 4	02/09	07/09	23/08	04/09	10/09
Harvest 5	30/09	05/10	20/09	02/10	08/10

The plant material was separated in leaves, flowers and stolons, before putting it in
separate labelled paper bags. These bags were dried for 24 hours at 105° Celsius in an
oven.

After drying, the dry weight of leaves, flowers and stolons was determined with a high precision scale. In order to get an indication about the impact of O_3 on plant health and plant productivity, the relationship of the biomass of the ozone-sensitive and the ozone-resistant clover clones was calculated (NC-S/NC-R-ratio). The idea behind this concept is that the ozone-induced growth inhibition due to a diminished photosynthesis is reflected by the difference between the biomass of the ozone-sensitive and ozone-resistant clover clone.

3.4   Stomatal conductance measurements

3.4.1   Description of the gas exchange measuring system

The aim of this thesis was to develop a stomatal conductance model (g_s-model) based on meteorological, phenological and air pollution data in order to quantify the O_3 flux into leaves of clover clone plants. Therefore, measuring stomatal conductance (g_s) was the key activity of the experimental part of this thesis.

Diurnal leaf gas exchange measurements were made using the portable photosynthesis system HCM-1000 (Heinz Walz GmbH, Effeltrich, Germany). The HCM-1000 is an "open system", i.e. the ambient air is absorbed continuously. It consists of the central unit with an input buffer and an intake antenna, a climatised measuring cuvette, a CO_2 dosing unit (optional, not used for field measurements), a lighting unit (optional, not used for field measurements) and a palmtop computer (HP-200/H). The key part of the central unit builds an infrared gas analyser (IRGA, here: BINOS-100/4PS), which calculates the CO_2 and H_2O concentration of the incoming airflow. The concentrations of these two gases are necessary to assess the net photosynthesis and transpiration rate. Apart from the gas analyser, the central unit consists of a manually operated valve for the H_2O regulation, a pump, a small buffer vessel, a mass flow meter, two gas valves and a barometric air pressure sensor. Figure 3.8 shows the pneumatic components along the gas path of the HCM-1000.

Despite the fact that this machine uses a closed cuvette to measure the gas exchange of a defined leaf area of a leaf fixed in the cuvette, it is able to perform measurements under natural conditions by simulating the environmental conditions of the prevailing ambient air as precisely as possible in the climatised measuring cuvette.

Air input antenna

Input
buffer

Filter

Humidity mixing valve

Drier/Humidifier
(H2O-Absorber)

Filter

Pump

Internal
buffer

Filter

Mass
flow
meter

H_2O
meas. side

CO_2
meas. side

Measuring
cuvette

H_2O
meas. side

CO_2
meas. side

Flow meter
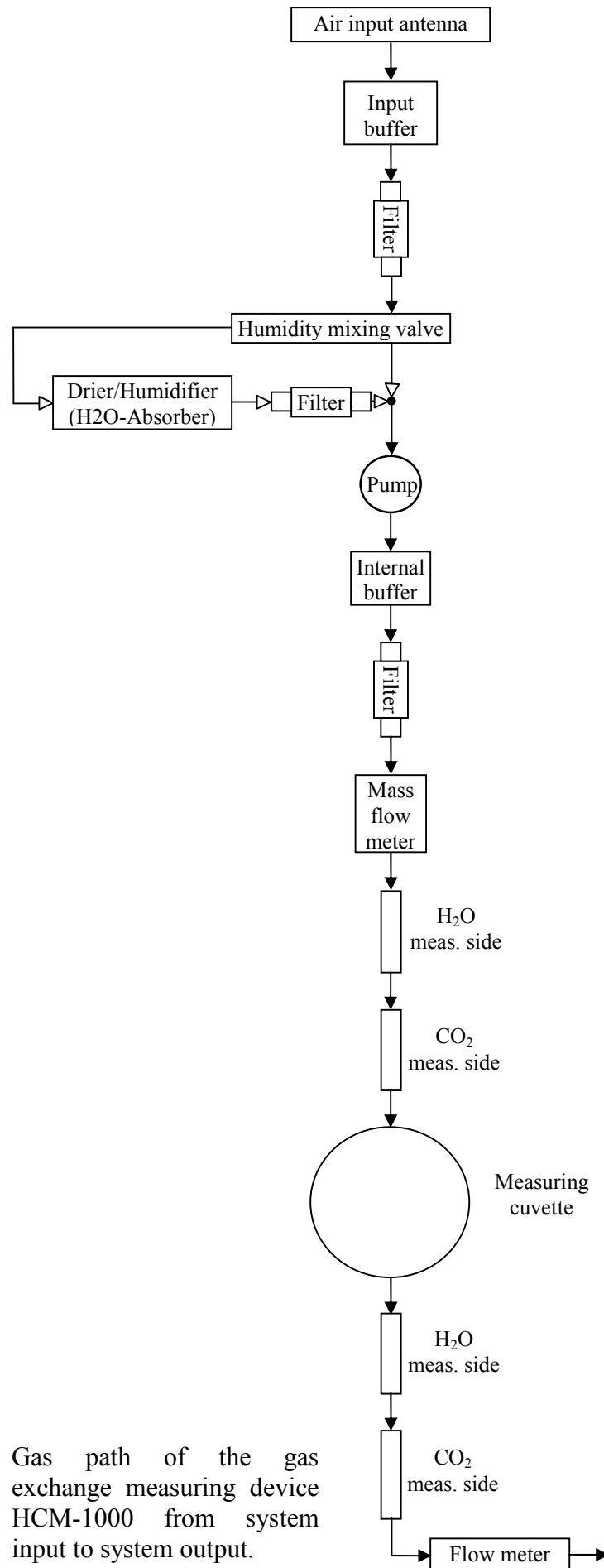
Figure 3.8   Gas   path   of   the   gas
exchange measuring device
HCM-1000   from   system
input to system output.

In fact, the temperature and relative humidity in the cuvette can track ambient air conditions. Furthermore, since the cuvette is transparent, the light conditions in it are similar to the ambient light conditions.

The measuring cuvette comprises several sensors for different meteorological parameters such as the photosynthetically active radiation, air temperature inside the cuvette, relative humidity inside the cuvette, leaf temperature and air temperature outside the cuvette.

The HCM-1000 was directly connected to a palmtop computer (HP-200/H) equipped with a 512kB EPROM card and a software ("DA-1000") for recording and saving all measurements as well as calibrating the system. At the end of each measuring campaign, the measured data points were transferred from the palmtop to a personal computer.

3.4.2   Gas exchange measurements and the determination of stomatal conductance

The above described gas exchange system (as well as all its competitors) is not able to measure the g_s and net photosynthetic rate directly. Instead, these two parameters have to be calculated from the directly measured difference of the H_2O and CO_2 concentration of the incoming airflow before and after streaming through a measuring object (leaf). The operation mode of the gas exchange measurements and the subsequent determination of g_s (which is the key parameter for modelling O_3 fluxes) will be briefly described in the following.

The BINOS 100/4PS gas analyser has two analyser cuvettes, one each for the above mentioned gases. Both cuvettes are separated in two halves, the measuring and the reference side. In order to assess a CO_2 and H_2O measuring point (MP), the air flow is directed through the measuring side of the two analyser cuvettes first, before streaming through the measuring cuvette containing the enclosed measuring object (leaf) and subsequently streaming through the reference side of the analyser cuvette. This procedure is shown schematically in Figure 3.8. The measuring point taken represents the relative difference between the CO_2 and H_2O concentrations of the airflow before and after streaming through the leaf enclosed in the measuring cuvette. However, for the

calculation of the rates of net photosynthesis and transpiration (and subsequently the g_s to water vapour), the absolute differences of these two gases before and after having streamed through the leaf (ΔCO_2 and ΔH_2O, respectively) are needed. This requires - according to the following equation - the assessment of CO_2 and H_2O zero points (ZP) and the base concentrations of the respective gas (C):

$$\Delta CO_2 = (MP_{CO_2} - ZP_{CO_2})/C_{CO_2} \qquad (3.6)$$

and

$$\Delta H_2O = (MP_{H_2O} - ZP_{H_2O})/C_{H_2O} \qquad (3.7)$$

The assessment of a zero point can be done by either leaving the measuring cuvette empty (no enclosed leaf) and progressing in the above mentioned manner (zero cuvette mode) or by changing the order of the analyser cuvettes (zero bypass mode), i.e. directing the air flow through both the measuring and reference sides of the analyser cuvettes first before entering the measuring cuvette. The latter method has the advantage that the enclosed leaf does not have to be removed from the measuring cuvette during the assessment of the zero point which predestines this method to be used during long-lasting (e.g. for several hours) measuring periods.

The stomatal conductance to water vapour (g_{H_2O}) is calculated according to the following equation by v. Caemmerer and Farquhar (1981):

$$g_{H_2O} = E/ALVPD \qquad (3.8)$$

where E is the transpiration rate and ALVPD the water vapour gradient between leaf and air.

The ALVPD is a function of the H_2O mole fraction within and outside the leaf with these two mole fractions being dependent on the total pressure in the measurement cuvette at a measurement point and on the saturated water vapour pressure at the leaf temperature and at the cuvette, respectively (for details see v. Caemmerer & Farquhar,

1981 and v. Willert et al., 1995). The saturated water vapour pressure again is temperature dependant and can be derived from tables (e.g. Walz, 1996).

According to v. Caemmerer & Farquhar (1981), the transpiration rate E [mmol*m^{-2}*s^{-1}] can be calculated using the following formula:

$$E = \frac{u_e * (w_o - w_e)}{LA * (1 - w_o)} \tag{3.9}$$

where u_e is the molar flow at the inlet of the measuring cuvette (at a measuring point MP [mmol s^{-1}]), w_o is the H_2O mole fraction at the outlet of the measuring cuvette [ppm], w_e is the H_2O mole fraction at the inlet of the measuring cuvette [ppm] and LA is the reference variable (here the leaf area in cm²). For calculating the two different mole fractions, see Jones (1992) or Walz (1996).

The term $(w_o - w_e)$ represents the pressure dependant difference between a measurement point and a zero point:

$$(w_o - w_e) = (MP_{H_2O} - ZP_{H_2O}) * 1/h * P_{norm}/P_{reference} \tag{3.10}$$

where P_{norm} is the pressure on which the infrared gas analyser is normalised during the calibration (= 1013 hPa), $P_{reference}$ is the total pressure inside the H_2O reference side of the gas analyser during a measuring point, and h is a sensitivity factor of the H_2O differential measurement, which is dependent on the H_2O basic concentration (dimensionless; for the derivation of h see Walz, 1996).

3.4.3   Description of the measuring programme

Prior to starting a measuring period, some parameters affecting the measurements had to be set and controlled. First of all, the use of an antenna guaranteed the intake of air masses at a height of three meters. This height was chosen because it corresponded with the height at which O_3 concentrations were measured by the nearby ZIMEN-station (cf. Chapter 3.3.2). This height also ensured that the measurements were not disturbed by the respiration of the gas exchange system user. Furthermore, a 10L input buffer was

installed in order to prevent short-term and small fluctuations of the CO_2 concentration of the absorbed ambient air. Then the cuvette temperature, relative humidity and CO_2 concentration were set to track the conditions of the ambient air. Furthermore, the flow rate was always set to 800ml/min, a value recommended by the manufacturer of the gas exchange system. Lastly, the reference measuring area had to be defined. It was constant at 2.5 cm² for all measurements since the enclosed leaf always covered the entire measuring area (PLA = Projected Leaf Area) of 2.5 cm².

At the start of a measuring day of usually several consecutive day-light hours, the gas exchange system was run for at least 20-30 minutes to give the gas analyser the required time to reach operating temperature and to give the entire system time to adapt to the prevailing ambient meteorological conditions. The measurements were started only after the signals for the CO_2 and H_2O zero point remained constant in the measuring mode zero bypass.

First of all, measurements of the CO_2 and H_2O base concentration had to be executed in order to provide real measured values for the subsequent measurements of the CO_2 and H_2O zero points and the CO_2 absolute concentration, all of which were part of the following automated measuring series typically executed over the course of a day (only daylight hours, though). These series followed a predetermined format/pattern:

$$CA,5*(10*MP,ZB),CA,5*….$$

This means that a series always started with a CO_2 absolute measurement (CA), followed by a measuring cycle (10-times a measuring point (MP) before setting a new bypass zero point (ZB)) that was repeated 5-times before starting the loop again with a CO_2 absolute measurement. The measuring signal for each measurement was averaged for 60 seconds, which resulted in one measuring point per minute or approximately 40 measurements per hour (the detection of bypass zero points and a CO_2 absolute measurement took approx. 20 minutes per hour).

All measurements were always carried out on the third or fourth leaf of a white clover plant, counted from the tip of the stolon. This not only minimised the variation in the

dataset by always using leaves of the same age, but was also believed to best represent the average gas exchange of the entire plant.

3.4.4 Restrictions of the measurements

In the early morning hours after sunrise, in the late evening hours before sunset and directly after rainfall events, the air is often highly water-saturated, which can cause problems for the detection of transpiration using gas exchange measuring systems like the HCM-1000. Precisely, absorbed humid air might lead to water vapour condensation inside the measuring cuvette, which affects the transpiration measurements for a longer time. This made measurements during above-mentioned climatic conditions impossible. Furthermore, since it is not possible to use the gas exchange systems during rainfall events, all measurements were carried out either during bright, partly cloudy or fully overcast weather conditions.

3.5 Calculation of ozone fluxes to clover leaves

In order to quantify the potential risk of O_3 to plants, the O_3 uptake rate of a plant, defined as the O_3 flux entering the plant per defined area and time, is calculated and accumulated over the course of the plant's exposure period. This accumulated O_3 uptake rate is then related to effect criteria such as biomass reduction and visible injury.

The stomatal flux algorithm used in this thesis is identical to the one suggested by the UNECE Mapping Manual (UNECE, 2004). It is based on the electrical analogue principle derived from Ohm's law (cf. Monteith and Unsworth, 1990). Assuming that the O_3 concentration at the top of a canopy is a reasonable estimate of the O_3 concentration at the boundary layer of a sunlit upper canopy leaf, the flux (Fst, nmol m^{-2} projected leaf area) can be calculated according to the following formula:

$$Fst = (O_{3(can)} - O_{3(int)}) * g_s * \frac{r_c}{r_b + r_c} \tag{3.11}$$

where $O_{3(can)}$ and $O_{3(int)}$ are the O_3 concentrations at the top of the canopy and in the intercellular spaces of the leaves respectively, r_b the quasi-laminar resistance and r_c the leaf surface resistance.

$O_{3(can)}$ was calculated from the O_3 concentration measured at three meter at all experimental sites according to the neutral stability profile method described in detail in the Mapping Manual (UNECE, 2004). This method is dependant on wind speed measurements and requires the estimation of the deposition velocity (V_g) as well as the aerodynamic (R_a), canopy boundary layer (R_b) and canopy (R_c) resistance, all of which could be calculated from the available meteorological data. For details, see Mapping Manual (UNECE, 2004).

Laisk et al. (1989) have empirically shown that it is justifiable to assume that $O_{3(int)}$ is usually close to zero due to reactive sinks within a leaf, leading to the omission of this term in equation 3.11. r_c is given by

$$r_c = 1/(g_s + g_{ext}) \tag{3.12}$$

where g_{ext} is the cuticular (external) resistance. The Mapping Manual (UNECE, 2004) suggests a constant for the cuticular resistance of

$$g_{ext} = 1/2500 \ [\text{m s}^{-1}] \tag{3.13}$$

whereas the quasi-laminar resistance is derived according to the cross-wind leaf (L) dimension and the wind speed at the canopy height ($u_{(can)}$):

$$r_b = 1.3 * 150 * (L/\ u_{(can)})^{0.5} \ [\text{s m}^{-1}] \tag{3.14}$$

The factor 1.3 accounts for the difference in diffusivity between heat and O_3. To account for the well-fertilised white clover clone plants used in this thesis, L was set to 5 cm.

The central term of the flux algorithm is the g_s, which was modelled using artificial neural networks, the core task of this thesis. The models predict g_s for water vapour

(g_{H_2O}), which has to be converted into g_s for O_3 (g_{O_3}) for the flux calculations under consideration of the differences in molecular diffusivity between water and O_3 ($D_{O_3}/D_{H_2O} = 0.61$):

$$g_{O_3} = g_{H_2O} * D_{O_3}/D_{H_2O} \tag{3.15}$$

In the following, the term g_s is used when stomatal conductance in general is concerned, whereas specific references to g_s of water vapour or O_3 are denoted as "g_s (mmol H_2O m^{-2} PLA s^{-1})" and "g_s (mmol O_3 m^{-2} PLA s^{-1})", respectively. PLA refers to the projected leaf area, the common scaling basis for g_s measurements.

3.6   Dose-response relationships

The clover dose-response relationships using flux- and concentration-based O_3 indices are based on biomass and injury assessment data recorded at three sites at the end of each of four (growth periods 2 to 5) 28-day growth periods of the years 1997 to 2001 (cf. Chapter 3.3.3). The data of the first growth period were always omitted for this analysis, because they represent the usually hugely variable establishing period of the clover plants.

The biomass ratio of the two white clover clones (NC-S/NC-R) determined at each harvest was related to the respective 28-day i) AOT40 value calculated for single as well as combined growth periods and sites, ii) modelled accumulated fluxes with thresholds varying from 0 to 10 nmol m^{-2} s^{-1} (AFst0-10) using the NC-S and NC-SR model and iii) ratio between modelled accumulated fluxes with various thresholds using the NC-S and NC-R ANN-based g_s model. Furthermore, the recorded biomass of both clones (as opposed to the ratio) was related to the respective AOT40 as well as the accumulated fluxes with various thresholds using the NC-S and NC-R model (i.e. biomass of NC-S and NC-R clones vs. AFstX predicted with the NC-S and NC-R models, respectively).

Linear regressions analyses (see chapter 3.7) were applied for the derivation of dose-response functions. These analyses were performed for each individual site and growth period, as well as for combined growth periods and sites.

3.7   Statistics

Common descriptive statistics were applied for the characterisation of the meteorological, O_3 and g_s dataset. In order to analyse potential inter-correlations between different input parameters, a Spearman's rank-order correlation test (a non parametric test had to be used, because the g_s datasets of both genotypes were not normally distributed – see below) was carried out.

It was of high interest in this study whether or not it would be necessary and desirable to develop separate ANN-based flux models for each of the two white clover clones, which was decided upon the results of a test of statistical difference between the g_s data of both clones. The choice of the appropriate test was dependent on the outcome of the Kolmogorov-Smirnov test (K-S test) for normal distribution, which was applied to both NC-S and NC-R g_s-datasets prior to the test of difference. Due to the rejection of the hypothesis of normally distributed data, the nonparametric Mann-Whitney U-test had to be applied.

Furthermore, prior to the development of the ANN-based flux models for both clover clones, a stepwise (multiple) regression analysis of both g_s datasets was carried out to gain a first impression of the suitability of the chosen seven input parameters in explaining the variation in the observations of the output parameter g_s.

To analyse the performance of the ANN-based g_s models by comparing predicted with observed g_s rates, linear regressions were applied. The same statistical method was also used for the determination of dose-response relationships between response (i.e. clover biomass and visible leaf injury) and O_3 exposure (accumulated AOT40) as well as O_3 uptake (AFstX). All statistics were carried out using SPSS 10.

4 Climate of growing seasons 1997 to 2001 in the Trier region

The bio-monitoring experiment using white clover clones was carried out during 5-month growing periods from May to October in five consecutive years 1997 until 2001 at three field sites Trier-City, Trier-University and Deuselbach. The flux model developed in this study was applied to datasets consisting of hourly physical and pollution climate data, covering the complete five growing seasons of the clover bio-monitoring experiment.

In the following sections, each of these five growing seasons is described using i) time courses of the climate and O_3 concentrations of the five growing seasons expressed as daily means for air temperature [°C] and O_3 concentrations [ppb], daily minimum for air temperature and VPD [kPa] as well as daily maximum for air temperature, VPD and PAR [μmol m^{-2} s^{-1}] (Figure 4.1 to 4.5), and ii) bar charts presenting the mean (+ 1 S.D.) of the meteorological parameters air temperature, VPD, PAR and wind speed [m s^{-1}] as well as the mean annual O_3 concentration (Figure 4.6). More detailed figures and tables showing the variation of the climate between single growth periods and years can be found in Appendix A.

The clover plants were always kept well watered in order to prevent any water stress-induced limitations of g_s. This meant there was no need to include a soil water parameter (e.g. soil water potential, soil moisture deficit etc.) as input for the flux model, and hence it was not necessary to include rainfall in Figures 4.1 to 4.6.

4.1 Seasonal differences in physical and pollution climate

In general, the seasonal time courses of air temperature are quite noisy, with some distinct peaks in excess of 25° C during almost all months between June and September in all five years. However, the general trend was an increase in temperature from May until July and August, when all sites experienced the highest (actual and average) air temperatures of up to 35 to 38 °C, followed by a decline towards the end of GP 5, i.e. end of September/beginning of October (Figures 4.1 to 4.5 and Appendix A). Minimum night temperatures were never below 1 °C, i.e. the plants never experienced any frost.

Since VPD is dependent on air temperature, the highest VPD-values were found also during GP 3 or GP 4, i.e. in July and/or August of each year (Figures 4.1 to 4.5, Appendix A). Maximum values of up to 5.5 kPa were recorded, but mean values for 28 days GPs were typically well below 1 kPa.

The same seasonal pattern was not reported for PAR, which showed an almost uniform − if rather scattered - distribution over the GP 1 to 4, with a decline starting during GP 5 (Figures 4.1 to 4.5). Maximum values of up to almost 2000 μmol m^{-2} s^{-1} were usually reported during June (Appendix A), around solstice time. However, apart from during GP 5 in 2000 and 2001, there were no longer periods with PAR values below light saturation (approx. 1200 μmol m^{-2} s^{-1}, cf. van Willert et al., 1995) during any of the GPs of all years (Figure 4.1 to 4.5).

Wind speed (Appendix A), which was included because of its influence in scaling down O_3 concentrations from its measuring height to the plant canopy height, shows a relatively even distribution over the course of the growing season. Maximum values of up to 16 m s^{-1} were reported for different months of the growing seasons. However, depending on the field site, average 28 days values of wind speed never exceeded 5 m s^{-1} (maximum mean value of 4.71 m s^{-1} for GP 5 in Deuselbach, 2001; Appendix A).

The seasonal time courses of the O_3 concentration are − similar to the time courses of air temperature − quite scattered (Figures 4.1 to 4.5), with growing season (i.e. 5 consecutive GPs) hourly maximum values of between 65 and 110 ppb reached at different months in the years 1997 to 2001 (Appendix A). However, concentrations tended to decline towards the end of GP 5 (Figures 4.1 to 4.5, Appendix A). It should be pointed out that episodes of high O_3 concentration normally lasted for two to three days.
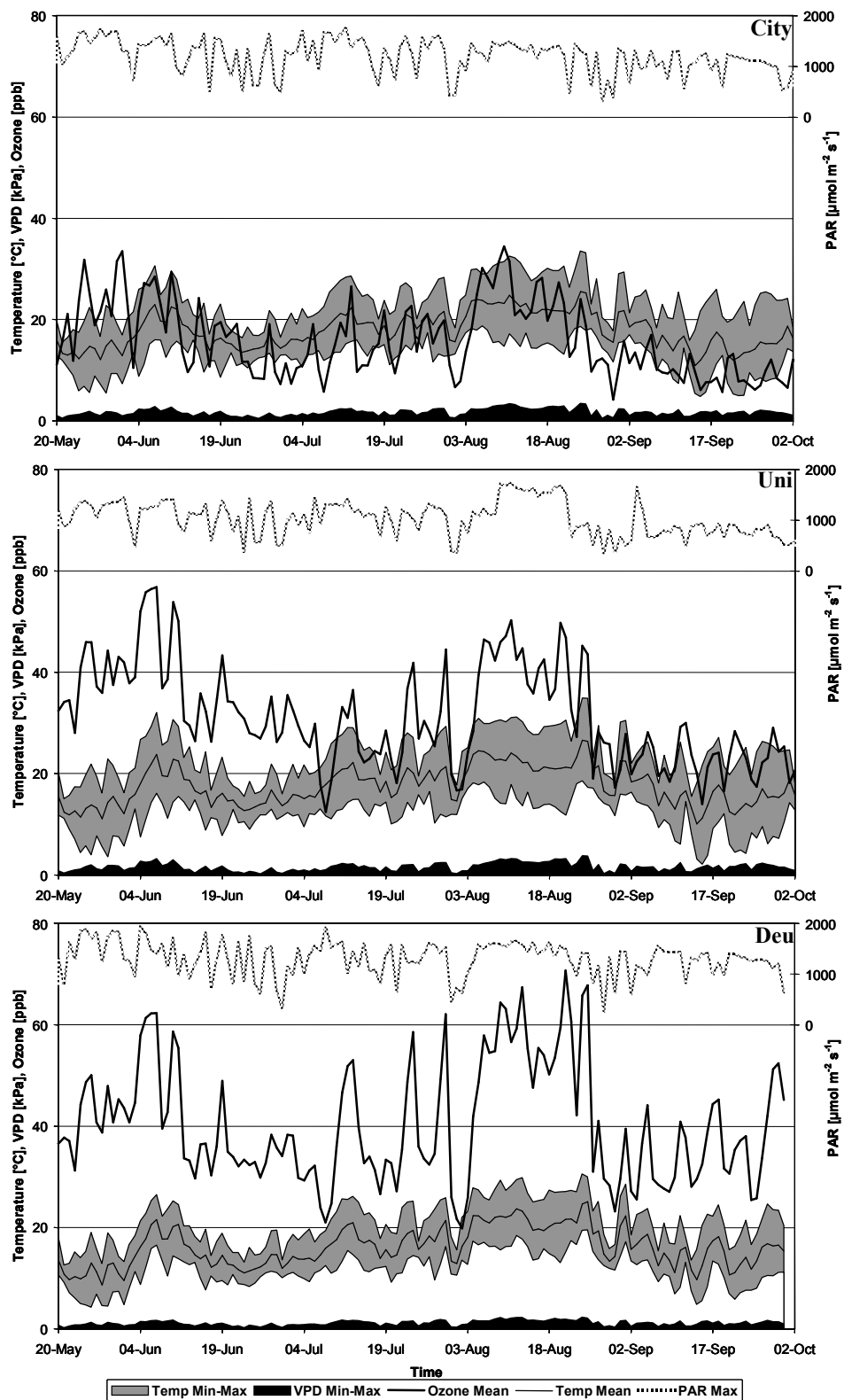
Figure 4.1   Time course of the climate and O_3 concentration at the sites Trier-City (top), Trier-University (middle) and Deuselbach (bottom) during the 1997 growing season, expressed as daily mean (air temperature, O_3 concentration), daily minimum (air temperature, VPD) and daily maximum (air temperature, VPD, PAR).
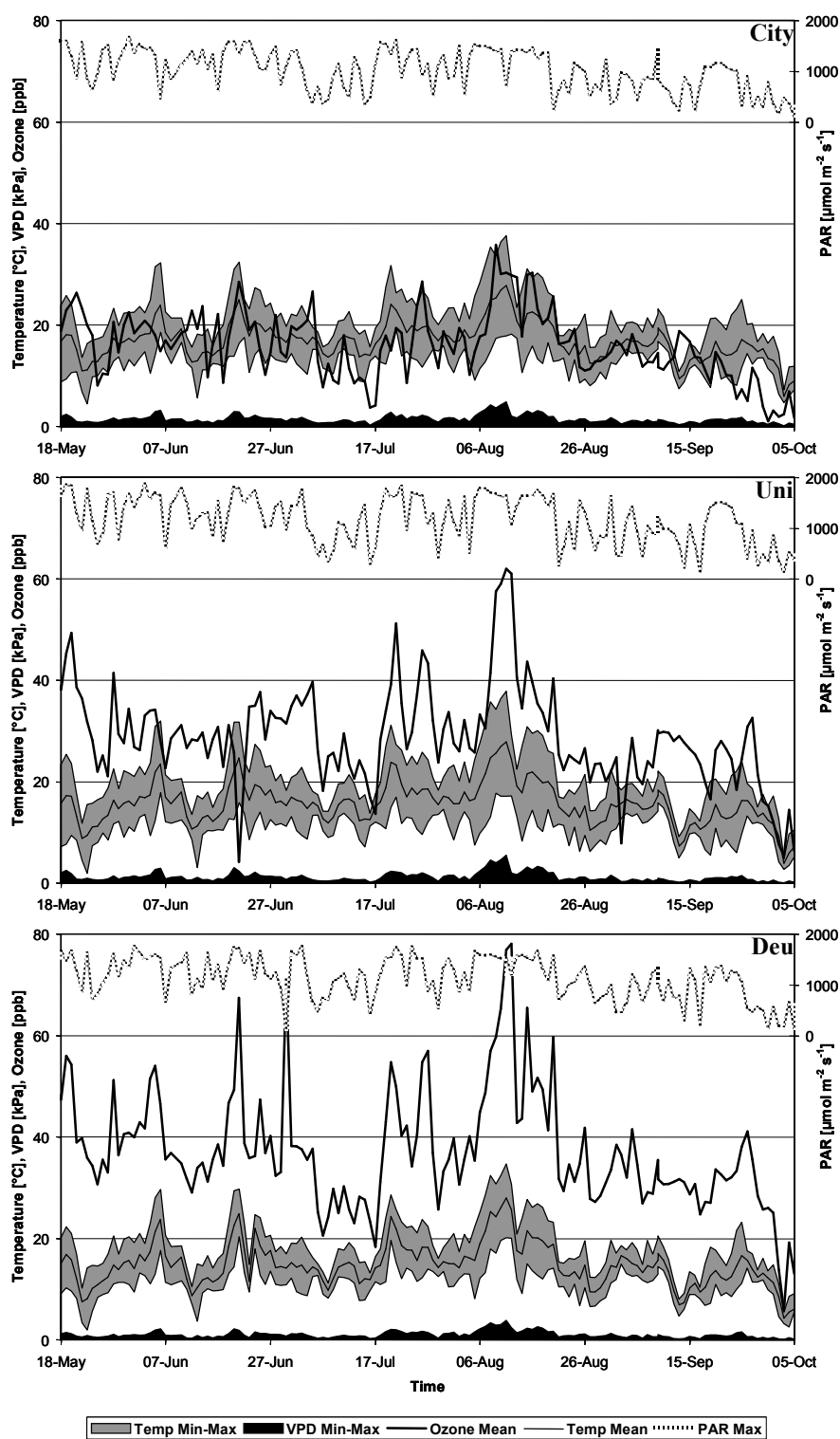
Figure 4.2   Time course of the climate and O_3 concentration at the sites Trier-City (top), Trier-University (middle) and Deuselbach (bottom) during the 1998 growing season, expressed as daily mean (air temperature, O_3 concentration), daily minimum (air temperature, VPD) and daily maximum (air temperature, VPD, PAR).
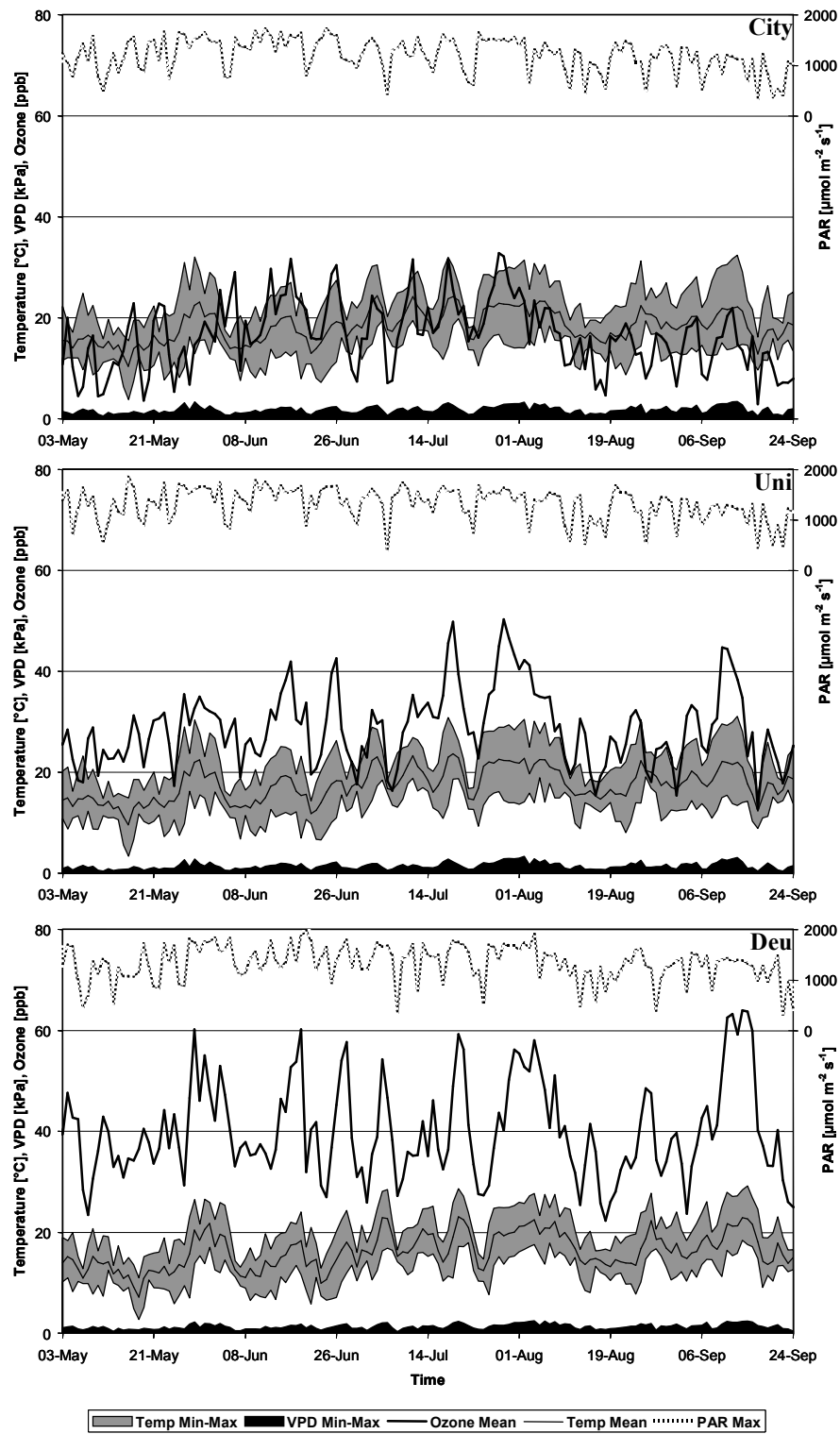
Figure 4.3   Time course of the climate and O_3 concentration at the sites Trier-City (top), Trier-University (middle) and Deuselbach (bottom) during the 1999 growing season, expressed as daily mean (air temperature, O_3 concentration), daily minimum (air temperature, VPD) and daily maximum (air temperature, VPD, PAR).
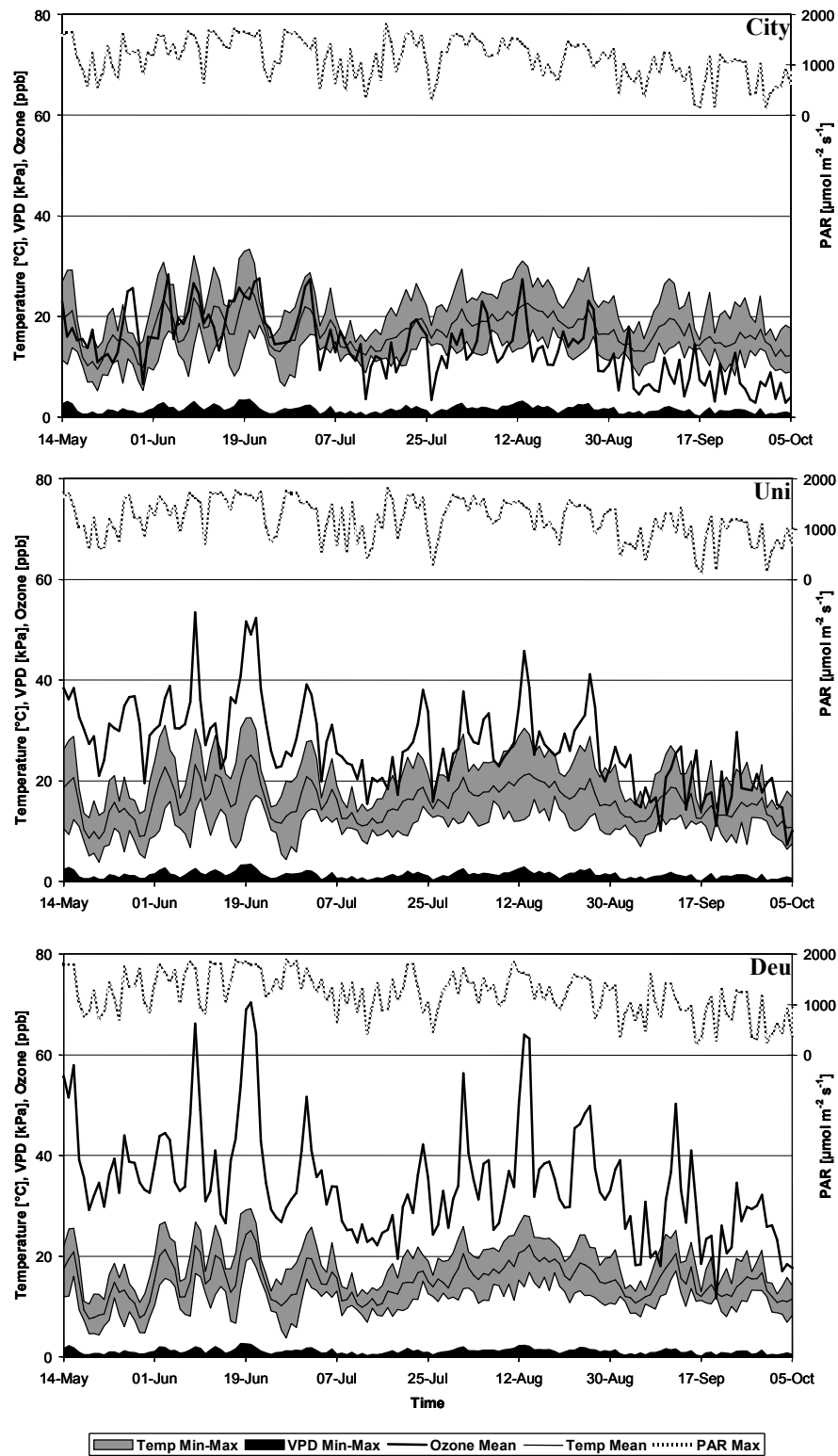
Figure 4.4   Time course of the climate and O$_3$ concentration at the sites Trier-City (top), Trier-University (middle) and Deuselbach (bottom) during the 2000 growing season, expressed as daily mean (air temperature, O$_3$ concentration), daily minimum (air temperature, VPD) and daily maximum (air temperature, VPD, PAR).
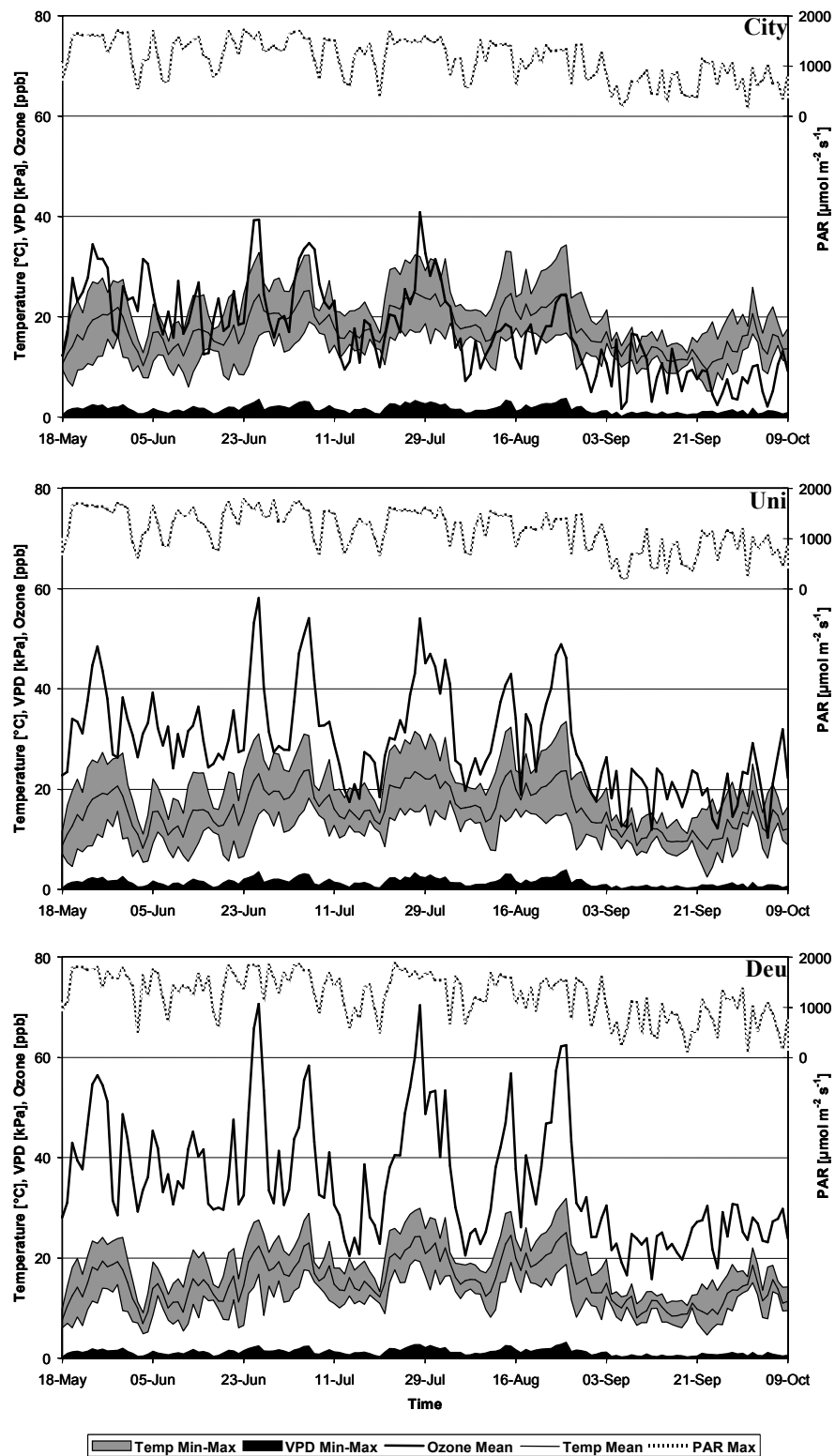
Figure 4.5   Time course of the climate and O₃ concentration at the sites Trier-City (top), Trier-University (middle) and Deuselbach (bottom) during the 2001 growing season, expressed as daily mean (air temperature, O₃ concentration), daily minimum (air temperature, VPD) and daily maximum (air temperature, VPD, PAR).

4.2   Spatial differences in physical and pollution climate

The results of the spatial analysis of the recorded climate and - to a lesser extent - pollution data basically reflect the geographical location of the three field sites, i.e. the altitude gradient between Trier-City (129 m a.s.l.), Trier-University (255 m a.s.l.) and Deuselbach (480 m a.s.l.) largely determines the site-to site climatic differences.

For all five GPs, the air temperature at the site Trier-City was always higher than at the site Trier-University, while it was always lowest in Deuselbach (only exception: GP 4 in 1998), the site with the highest altitude. However, the differences in mean air temperature between Deuselbach and Trier-University and Trier-University and Trier-City never exceeded 2 °C, in any year (Figure 4.6, Appendix A).

Due to its high dependence on air temperature, the VPD also tended to follow the ranking Trier-City > Trier-University > Deuselbach, with the highest values having been recorded in Trier-City (Figure 4.6, Appendix A). Some exceptions to this observation can however be found towards the end of the growing season of the years 1998 to 2001, when the average VPD value of Deuselbach is often slightly higher than that for the site Trier-University. The very high standard deviations indicate the high variability of the VPD data (Figure 4.6, Appendix A).

Similar magnitudes of variance can be found for PAR, indicating the large scatter of this parameter (Figure 4.6, Appendix A). There is however a general trend for the highest and lowest PAR values having been measured in Deuselbach and Trier-City, respectively, with the PAR values from the Trier-University site usually lying in between this range (Figure 4.6, Appendix A). Most exceptions from these results can be found in 1997, when the lowest PAR values were mostly recorded at the Trier-University site (Appendix A). This divergence from the general trend might be related to an inexact calibration of the measuring device at this site.

The lowest wind speed was always measured at the Trier-University site, closely followed by the measurements of the Trier-City site. In contrast, by far the highest wind speed – at least twice as high as that at the Trier-City site - was always recorded in Deuselbach (Figure 4.6, Appendix A). This ranking is likely to reflect the general wind accessibility conditions of the climate stations (for instance, Deuselbach is a very exposed site without any major vegetation in its vicinity).

The O$_3$ concentration data also showed a very distinct ranking with the highest and lowest concentrations always found in Deuselbach and Trier-City, respectively. The Trier-University site again represents intermediate conditions (Figure 4.6, Appendix A). These results clearly support the typical O$_3$ concentration pattern associated with distance from urban (pollution source) areas that are characteristic of this secondary pollutant and driven by the formation of O$_3$ downwind of precursor pollutant source, i.e. relatively low average (daily, weekly and monthly) O$_3$ concentrations in urban areas, followed by slightly higher O$_3$ concentrations in suburban areas and by far the highest concentrations in rural areas.

This distinct urban to rural gradient in O$_3$ concentration is also reflected in Figure 4.7, which shows the AOT40 values for all GPs of all growing seasons. Especially the bottom right figure clearly shows the much higher O$_3$ concentrations in Deuselbach. In fact, for most years the AOT40 for Deuselbach is higher than for the combined AOT40 of the two other sites.

4.3   Year-to-year variation of physical and pollution climate

Figure 4.6 gives an overview of the year-to-year differences of the measured air temperature, VPD, PAR, wind speed and O$_3$ concentration at all three sites by showing the growing season mean of these parameters. In general it appears that when averaged over the entire growing season, the differences of the measured data between the years become marginal.

However, the years 1997 and 1999 were on average warmer and drier than the years 1998, 2000 and 2001 at all sites, with particularly warm and dry periods in August 1997 (Figure 4.1, Appendix A) as well as in July and August 1999 (Figure 4.3, Appendix A). This finding is also reflected by higher average PAR values for 1997 and 1999 (Figure 4.6). In contrast, wind speed was lowest in 1997, especially during the warm and dry months July and August (Appendix A), and highest in year 1998 (Figure 4.6).

The year 2000 experienced the lowest mean O$_3$ concentrations at all sites, while the highest were recorded in 1997, except for Trier-City, where the highest average O$_3$

concentrations were measured in 2001. This trend is enhanced with AOT40 values (Figure 4.7), indicating the frequency of hourly O_3 concentrations that exceeded 40 ppb during the 1997 growing season. The year-to-year differences in O_3 concentration are in general more variable at the site Deuselbach compared to the other two sites.
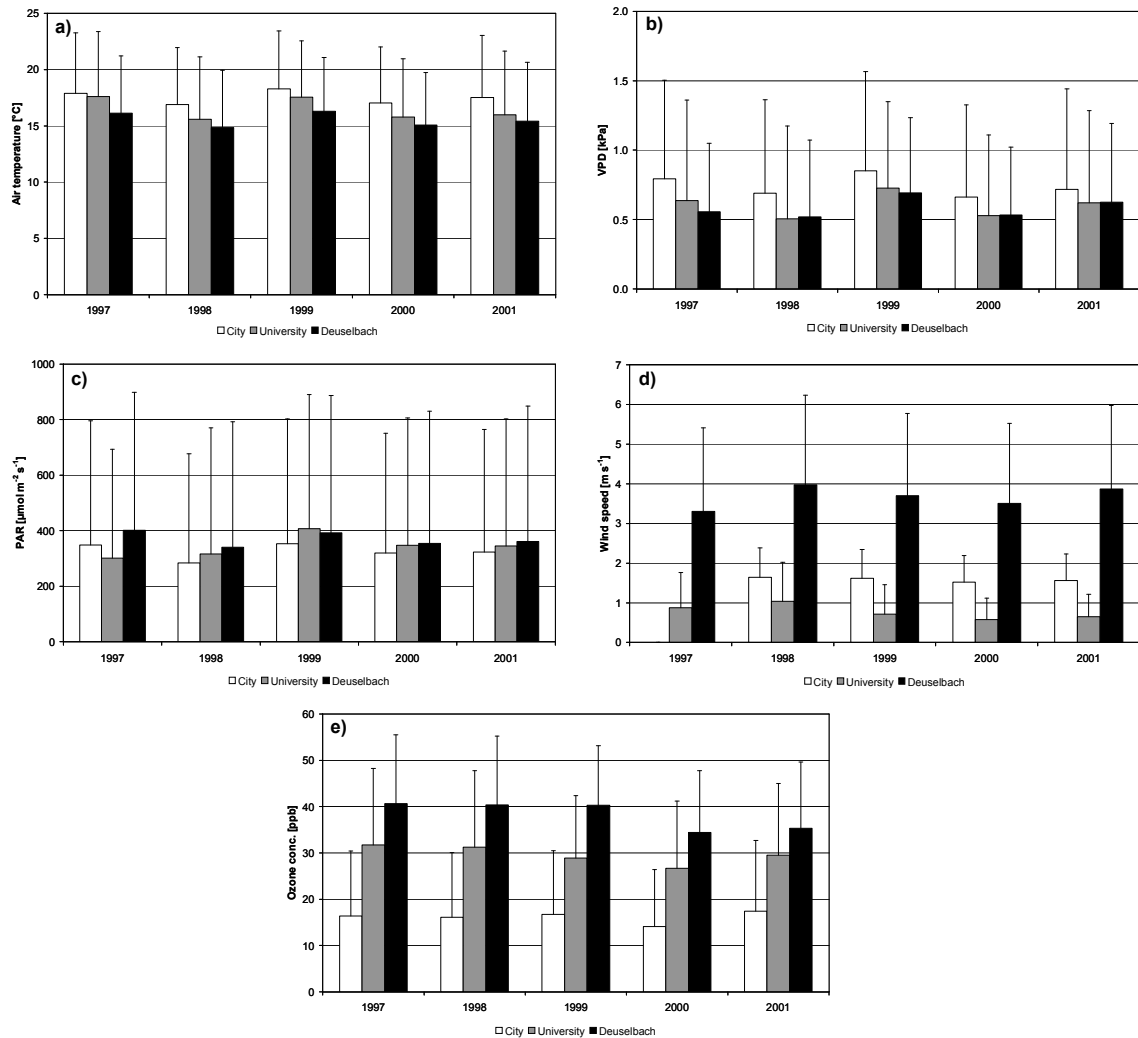
Figure 4.6   Mean (+ 1 S.D.) air temperature (a), VPD (b), PAR (c), wind speed (d) and O_3 concentration (e) of the growing seasons (5 GPs = 140 days) 1997 until 2001 at the sites Trier-City, Trier-University and Deuselbach. Wind speed data at the site Trier-University were not available for 1997.
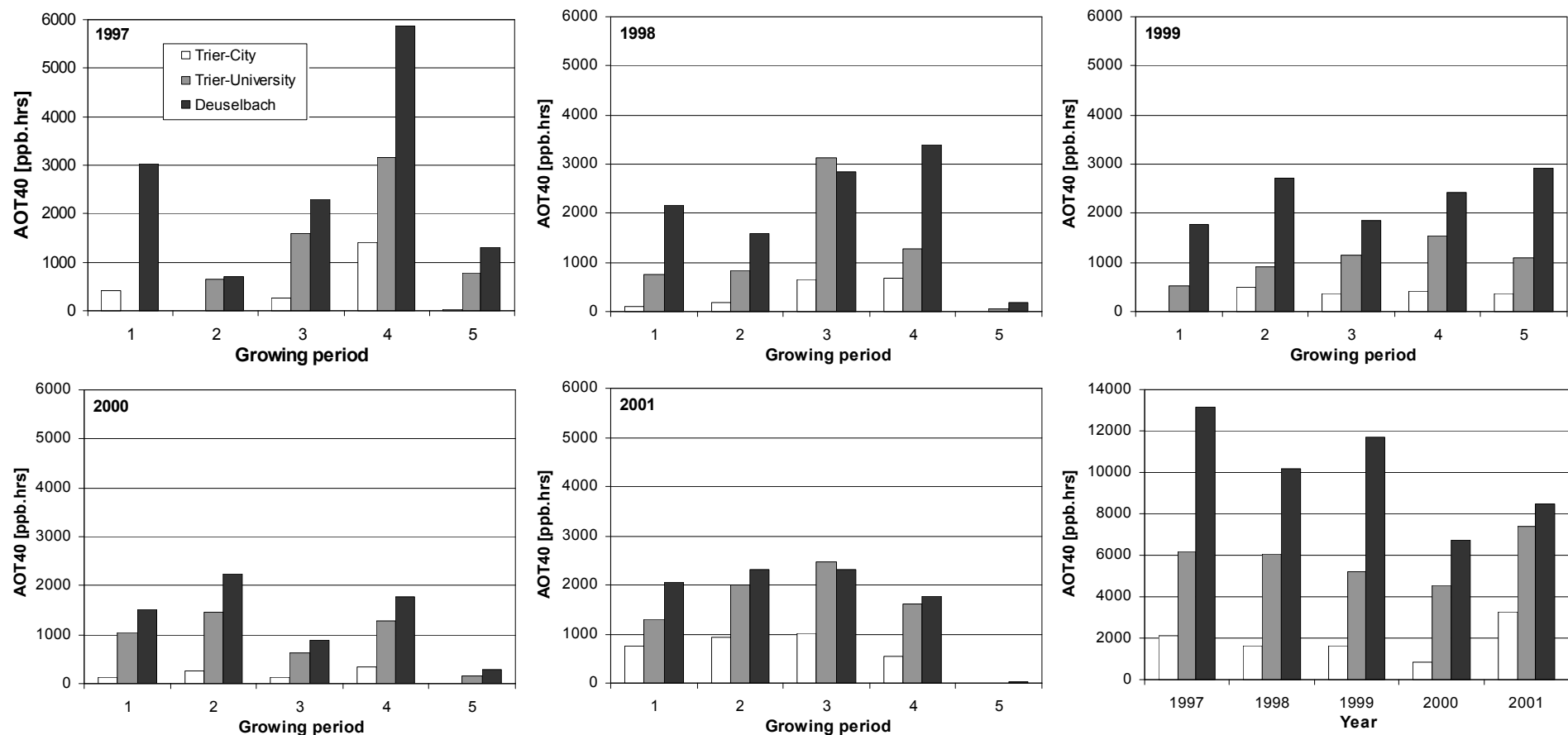
Figure 4.7   Calculated AOT40 values for growing periods 1 to 5 (GP = 28 days) at the sites Trier-City, Trier-University and Deuselbach for the study years 1997 until 2001. The bottom right figure represents the AOT40 of the entire growing season (i.e. sum of AOT40 of GP 1 to 5) at all threes sites for all five study years.

5   Description and analysis of model input data

In this chapter, observed g_s-data of both white clover clones recorded during the summer months of the years 1997 until 2001 and the co-occurring meteorological parameters are described and statistically analysed. Since ANNs are know for their limited ability to extrapolate outside the range of input data, it is extremely important in this study to ensure that the input dataset is truly representative of the entire range of meteorological conditions of a typical West European growing season in order to be able to develop a model that is capable of predicting O_3 fluxes for these conditions.

5.1   Descriptive statistics of model input data

The statistical interpretation of the observed g_s values for each of the two clones is described in relation to the meteorological parameters and O_3 concentrations in Table 5.1. In addition, statistics for two O_3 exposure indices and the exposure time are given. The NC-S and NC-R datasets comprise in total 9113 readings representing 23 days and 5224 readings representing 13 days, respectively. For the development of a combined g_s model, these two datasets were merged.

Both datasets comprise a similar range of PAR-data representing conditions of total darkness (PAR = 0 µmol m^{-2} s^{-1}) up to light saturation (PAR of approx. 1200 up to 2100 µmol m^{-2} s^{-1}) with an average PAR value for both datasets of approx. 1100 µmol m^{-2} s^{-1}. The average VPD value of 1.2 kPa is identical for both datasets as well as the minimum value of 0.1 kPa, but the amplitude of the VPD data is higher for the NC-R dataset due to its higher maximum value of VPD at 3.4 kPa as compared to a VPD of 2.9 kPa for the NC-S dataset. Analysis of the air temperature shows a very similar pattern with an identical mean and similar first and third quartile values, but a greater range of the temperature data for the NC-R dataset from 12.1 °C to 34.4 °C (amplitude: 22.3 °C) as compared to the NC-S dataset from 14.3 °C to 31.5 °C (amplitude: 17.2 °C). This indicates a higher number of outliers within the NC-R dataset in spite of the data quality control process.

Table 5.1   Descriptive statistics analysing g_s-, meteorological and O_3 concentration data recorded during the years 1997 until 2001 at the Trier-University site and corresponding exposure indices estimated for particular exposure periods. All parameters function as input for the ANN-model apart from g_s, which is the model output parameter (NC-S: $n = 9113$; NC-R: $n = 5224$).

NC-S	g_s [mmol H$_2$O m^{-2} s^{-1}]	Tcuv [°C]	PAR [μmol m^{-2} s^{-1}]	VPD [kPa]	Ozone [ppb]	AOT40 since exposure [ppb.h]	AOT40 of last 12 days [ppb.h]	Exposure time [days]
Maximum	841.1	31.5	2100.0	2.9	85.5	8429.5	2931.3	132.0
95%-Quantile	649.5	29.4	1868.0	2.3	75.0	8271.4	2805.6	130.0
3rd quartile	503.1	27.2	1630.0	1.5	58.3	5160.8	1740.2	87.0
Median	375.6	24.5	1229.0	1.1	47.1	3221.9	789.1	78.0
Mean	380.4	24.4	1102.8	1.2	48.3	3795.8	1112.4	75.5
1st quartile	269.5	21.9	585.0	0.8	37.8	2814.3	370.6	69.0
5%-Quantile	115.0	19.0	70.6	0.4	23.1	530.6	223.1	36.0
Minimum	0.4	14.3	0.0	0.1	9.3	530.6	129.4	29.0
S.D.	163.8	3.3	584.8	0.6	15.3	1881.2	840.3	24.7
S.E.	1.7	0.0	6.1	0.0	0.2	19.7	8.8	0.3

NC-R	g_s [mmol H$_2$O m^{-2} s^{-1}]	Tcuv [°C]	PAR [μmol m^{-2} s^{-1}]	VPD [kPa]	Ozone [ppb]	AOT40 since exposure [ppb.h]	AOT40 of last 12 days [ppb.h]	Exposure time [days]
Maximum	852.2	34.4	2288.0	3.4	83.1	8429.5	916.6	131.0
95%-quantile	583.1	31.4	1833.0	2.6	74.4	8106.8	804.5	127.0
3rd quartile	384.7	26.9	1661.0	1.6	58.6	3361.0	669.5	87.0
Median	288.2	24.6	1291.0	1.1	48.8	3055.8	428.2	79.0
Mean	299.6	24.4	1165.0	1.2	47.1	3485.7	480.9	85.8
1st quartile	205.4	22.3	704.0	0.6	36.4	2365.1	304.9	76.0
5%-quantile	64.5	18.1	109.0	0.4	17.6	952.0	210.5	43.0
Minimum	0.1	12.1	0.0	0.1	10.0	853.2	85.9	43.0
S.D.	148.0	3.8	553.9	0.7	16.2	1956.9	224.0	21.1
S.E.	2.0	0.1	7.7	0.0	0.2	27.1	3.1	0.3

There is little difference between the mean O_3 concentrations of 48.3 ppb and 47.1 ppb measured for the NC-S and the NC-R dataset respectively, and the range in concentration values is also similar at 9.3 ppb to 85.5 ppb and 10.0 ppb to 83.1 ppb for the NC-S and the NC-R datasets respectively. It can therefore be assumed that the datasets are representative of the range of meteorological and O_3 concentration conditions that would be typical during the growing season of grasslands and crops in the Trier region. Any data that might fall outside of these typical conditions are discussed below.

The mean of the exposure time (in days) representing the age of the test plants at the time of gas exchange measurements differ between 75 and 85 days for the sensitive and resistant clone respectively, indicating that the g_s measurements for the NC-R clone were taken on plants that had on average been exposed to ambient air for 10 days longer than their sensitive counter-parts. However, this difference is marginalized by the fact that the median value of the exposure time only slightly differs (i.e. by one day), as do the first and third quartiles.

A statistical analysis was also carried out for the calculated exposure indices "AOT40 since exposure", which represents the accumulated exposure at the time of each gas exchange measurement (i.e. O_3 concentrations above 40 ppb) the plant had been exposed to since its transfer to the ambient air field site, and "AOT40 of last 12 days", representing the accumulated exposure of the last 12 days. This is the average exposure time of the white clover cultivar prior to the incidence of the first visible foliar injury symptoms. No major differences were found in the "AOT40 since exposure" index between the datasets of the two clones, whereas the "AOT40 of last 12 days" index differed significantly between both datasets: the average value of the NC-S clone was more than two times higher than that of the NC-R clone, indicating that the g_s measurements were on average carried out on NC-S plants that had recently been exposed to more than double the AOT40 dose than NC-R plants.

5.2   Distribution of input data

The distribution of the g_s-data collected for both clones is further detailed in Figure 5.1 and Table 5.2. The high representation of more than 53 % of g_s values below 300 mmol H_2O m^{-2} s^{-1} PLA (projected leaf area) for the NC-R clone is noticeable, whereas only 30% of the NC-S g_s-data fall into this range.
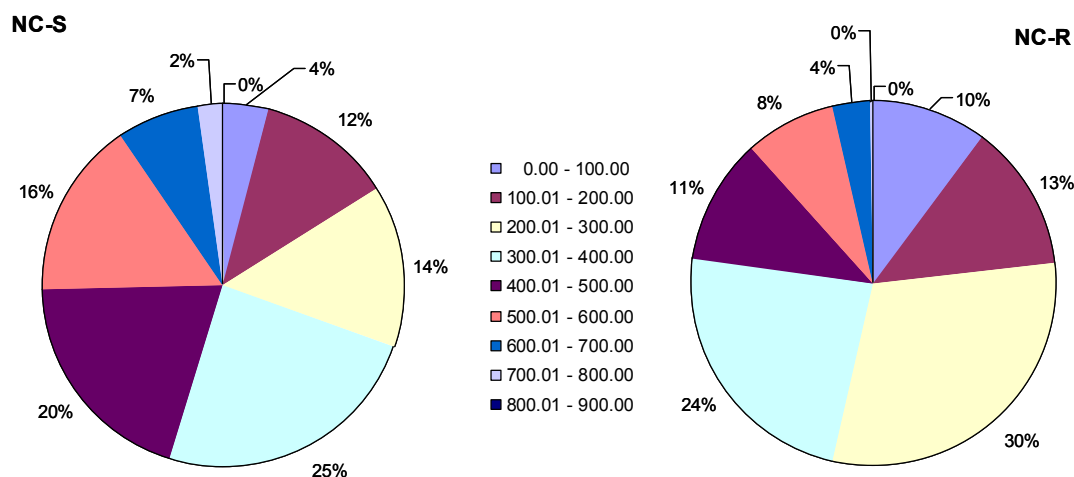
Figure 5.1   Distribution of g_s-data for the NC-S (left) and NC-R (right) clone.

Table 5.2   Absolute and relative distribution of g_s-data of both clover clones.

g_s [mmol H_2O m^{-2} s^{-1}]	NC-S	NC-S %	NC-R	NC-R %
0.00 - 100.00	379	4.2	542	10.4
100.01 - 200.00	1093	12.0	679	13.0
200.01 - 300.00	1318	14.5	1574	30.1
300.01 - 400.00	2194	24.1	1245	23.8
400.01 - 500.00	1799	19.7	575	11.0
500.01 - 600.00	1462	16.0	418	8.0
600.01 - 700.00	666	7.3	183	3.5
700.01 - 800.00	197	2.2	7	0.1
800.01 - 900.00	5	0.1	1	0.0

The distribution of the g_s datasets of both clones is shown in Table 5.3 in relation to selected classes of key meteorological parameters, O_3 concentrations, time and O_3 exposure indices. Note that the parameters "Year", "Month" and "Time of day" are only shown for analysis purposes and have not been included as inputs in the ANN models. This is because it is assumed the information given by the latter two is accounted for by the variation in the meteorological input parameters over the course of the growing season, whereas the parameter "Year" is not considered as being important given the type of model being developed.

Table 5.3   Relative distribution of g_s-datasets of both clover clones according to key meteorological parameters, O_3 concentration and time.

Year	NC-S	NC-R	Time of day	NC-S	NC-R
1997	8.0	12.7	0.01 – 1.00	0.0	0.0
1998	20.1	19.5	1.01 – 2.00	0.0	0.0
1999	18.9	27.8	2.01 – 3.00	0.0	0.0
2000	27.8	40.0	3.01 – 4.00	0.0	0.0
2001	10.0	0.0	4.01 – 5.00	0.0	0.0
2002	15.2	0.0	5.01 – 6.00	0.0	0.0
			6.01 – 7.00	0.0	0.6
Month	**NC-S**	**NC-R**	7.01 – 8.00	0.4	0.9
June	22.7	6.2	8.01 – 9.00	1.0	1.3
July	21.5	21.6	9.01 – 10.00	2.0	3.4
August	47.8	54.5	10.01 – 11.00	4.7	5.3
September	5.3	17.6	11.01 – 12.00	8.1	9.0
October	2.7	0.0	12.01 – 13.00	9.9	10.9
			13.01 – 14.00	10.4	10.9
Exposure Time (days)	**NC-S**	**NC-R**	14.01 – 15.00	11.1	10.2
21 - 40	14.0	0.0	15.01 – 16.00	11.3	10.3
41 - 60	8.7	6.2	16.01 – 17.00	11.3	10.4
61 - 80	27.8	56.4	17.01 – 18.00	9.6	9.3
81 - 100	41.5	19.7	18.01 – 19.00	8.3	8.3
101 - 120	0.0	4.9	19.01 – 20.00	5.7	6.0
121 - 140	8.0	12.7	20.01 – 21.00	3.1	2.9
			21.01 – 22.00	1.8	0.2
VPD [kPa]	**NC-S**	**NC-R**	22.01 – 23.00	0.8	0.0
0.00 – 0.50	9.4	12.7	23.01 – 0.00	0.5	0.0
0.51 – 1.00	35.8	32.5			
1.01 – 1.50	30.5	27.8	**PAR [μmol**		
1.51 – 2.00	11.8	15.7	**m⁻² s⁻¹]**	**NC-S**	**NC-R**
2.01 – 2.50	10.4	6.0	0	1.7	0.4
2.51 – 3.00	2.2	3.4	> 0 - 100	4.9	4.3
			101 - 200	3.4	1.7
Temperature [°C]	**NC-S**	**NC-R**	201 - 300	2.4	2.2
12.50 – 15.00	0.0	0.2	301 - 400	3.9	3.8
15.01 – 17.50	2.2	1.4	401 - 500	4.4	4.8
17.51 – 20.00	7.6	2.5	501 - 600	5.0	4.1
20.01 – 22.50	22.0	7.2	601 - 700	3.9	3.5
22.51 – 25.00	23.0	15.5	701 - 800	3.3	3.3
25.01 – 27.50	22.6	28.6	801 - 900	3.4	3.3
27.51 – 30.00	21.1	26.2	901 - 1000	4.0	3.9
30.01 – 32.50	1.5	11.4	1001 - 1100	3.8	4.6
32.51 – 35.00	0.0	4.0	1101 - 1200	4.4	5.5
			1201 - 1300	4.7	5.1
Ozone [ppb]	**NC-S**	**NC-R**	1301 - 1400	6.5	4.9
0.00 – 10.00	0.2	0.0	1401 - 1500	6.8	8.2
10.01 – 20.00	3.0	7.3	1501 - 1600	6.6	6.5
20.01 – 30.00	6.5	6.3	1601 - 1700	8.7	10.1
30.01 – 40.00	24.1	22.8	1701 - 1800	9.9	12.0
40.01 – 50.00	24.4	14.5	1801 - 1900	4.9	5.8
50.01 – 60.00	17.4	28.1	1901 - 2000	2.6	1.3
60.01 – 70.00	14.1	13.1	2001 - 2100	0.6	0.2
70.01 – 80.00	8.7	6.2	2101 - 2200	0.0	0.2
80.01 – 90.00	1.5	1.8	2201 - 2300	0.0	0.1

Table 5.3 (cont.)   Relative distribution of g_s-datasets of both clover clones according
to AOT40 exposure indices.

AOT40 since exposure (ppb.hrs)	NC-S	NC-R	AOT40 of last 12 days (ppb.hrs)	NC-S	NC-R
500-1000	7.5	6.2	0-250	14.0	19.2
1000-1500	0.0	0.0	250-500	21.3	39.5
1500-2000	2.2	11.2	500-750	7.2	22.9
2000-2500	5.5	10.4	750-1000	15.8	18.5
2500-3000	21.8	21.8	1000-1250	3.5	0.0
3000-3500	24.9	30.0	1250-1500	6.6	0.0
3500-4000	7.1	0.0	1500-1750	6.7	0.0
4000-4500	0.0	7.7	1750-2000	11.4	0.0
4500-5000	4.3	0.0	2000-2250	0.5	0.0
5000-5500	10.9	0.0	2250-2500	0.0	0.0
5500-6000	6.6	0.0	2500-2750	5.8	0.0
6000-6500	1.2	0.0	2750-3000	7.3	0.0
6500-7000	0.0	0.0			
7000-7500	0.0	0.0			
7500-8000	0.0	0.0			
8000-8500	8.0	12.7			

Table 5.3 clearly demonstrates that the input data of both clones are in general well distributed over a broad range, especially for the important meteorological input parameters air temperature, VPD and PAR. However, the frequency of data in different classes for the parameters "exposure time" (e.g. class "100-120 days" for NC-S), "AOT40 since exposure" and "AOT40 of last 12 days" show a higher variability, in particular for the NC-R dataset.

This variability is obvious in the scatter plots shown in Figure 5.2 and 5.4. In general, the data cloud is slightly denser and less patchy for the NC-S dataset, which can partly be explained by the higher number of data points of this dataset in comparison with the NC-R dataset. In addition, these scatter plots indicate that the parameters "ozone", "exposure time", "AOT40 since exposure" and "AOT40 of last 12 days" are available in hourly time steps, whereas the meteorological parameters had been recorded every minute.
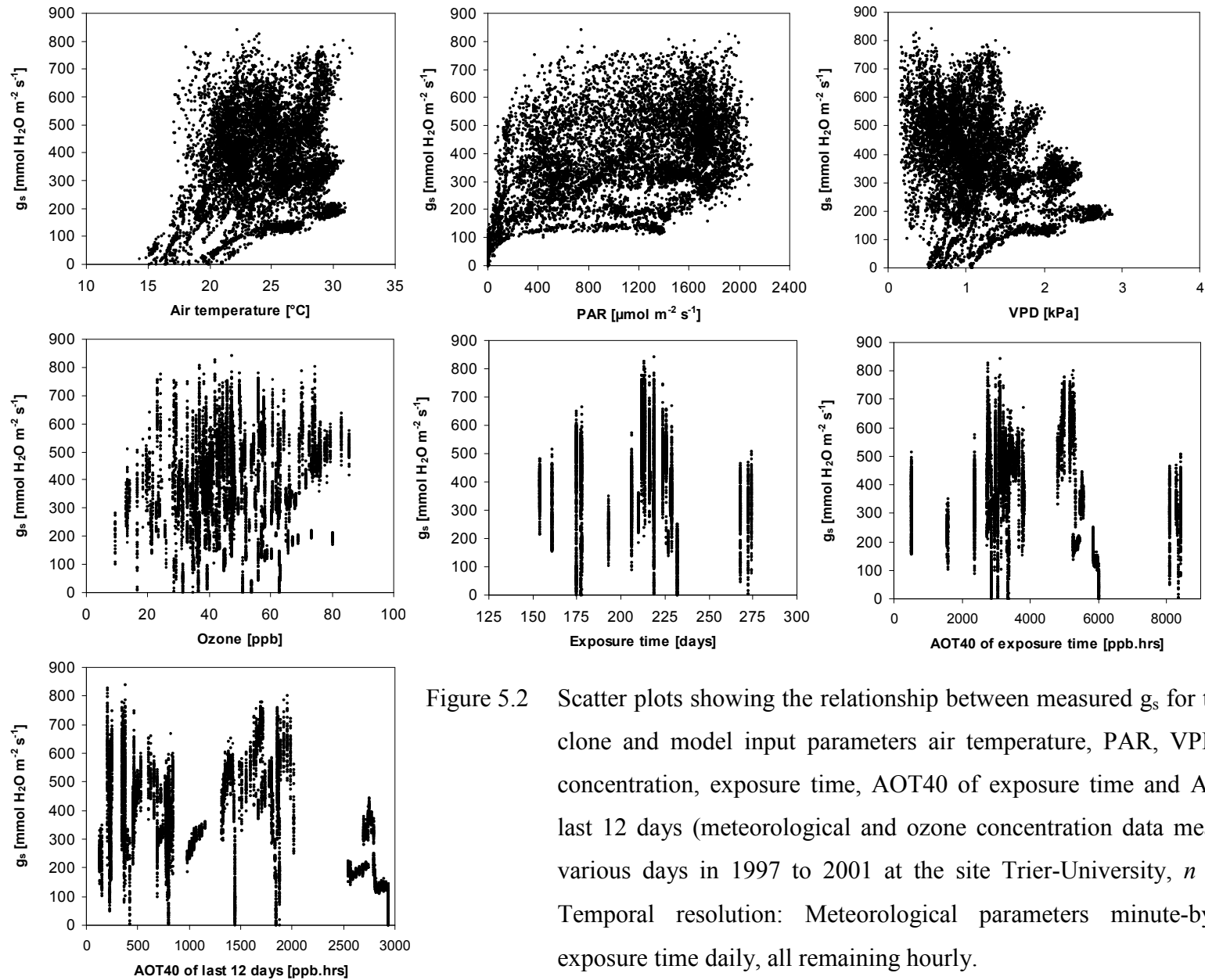
Figure 5.2   Scatter plots showing the relationship between measured g_s for the NC-S clone and model input parameters air temperature, PAR, VPD, ozone concentration, exposure time, AOT40 of exposure time and AOT40 of last 12 days (meteorological and ozone concentration data measured at various days in 1997 to 2001 at the site Trier-University, n = 9113). Temporal resolution: Meteorological parameters minute-by-minute, exposure time daily, all remaining hourly.
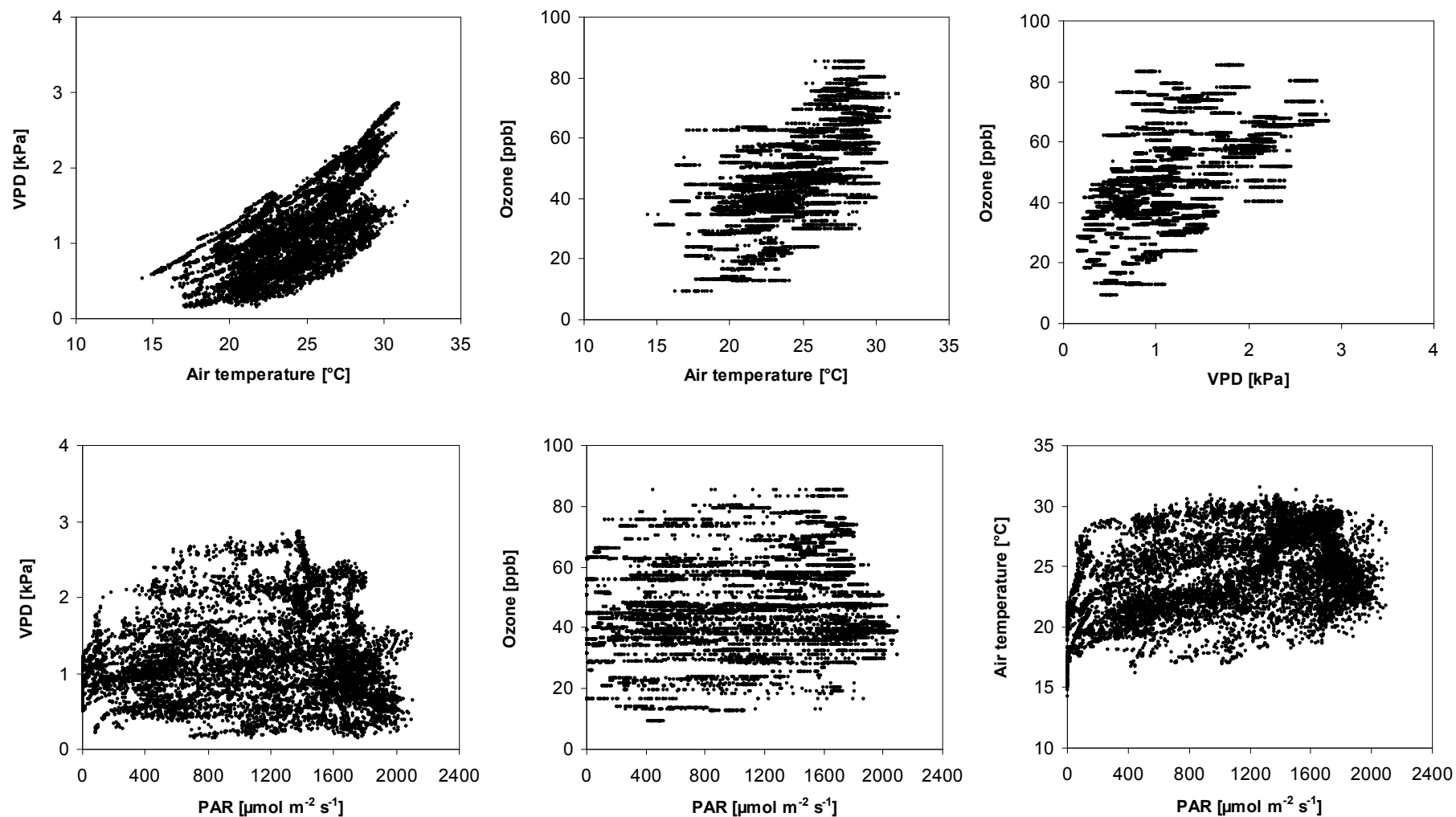
Figure 5.3   Scatter plots showing the relationship between meteorological parameters VPD, air temperature and PAR, as well as between O_3 concentration and these meteorological parameters of the NC-S dataset (measured data from various days in 1997 to 2001 at the site Trier-University, $n = 9113$). Temporal resolution: Meteorological parameters minute-by-minute, O_3 concentration hourly.
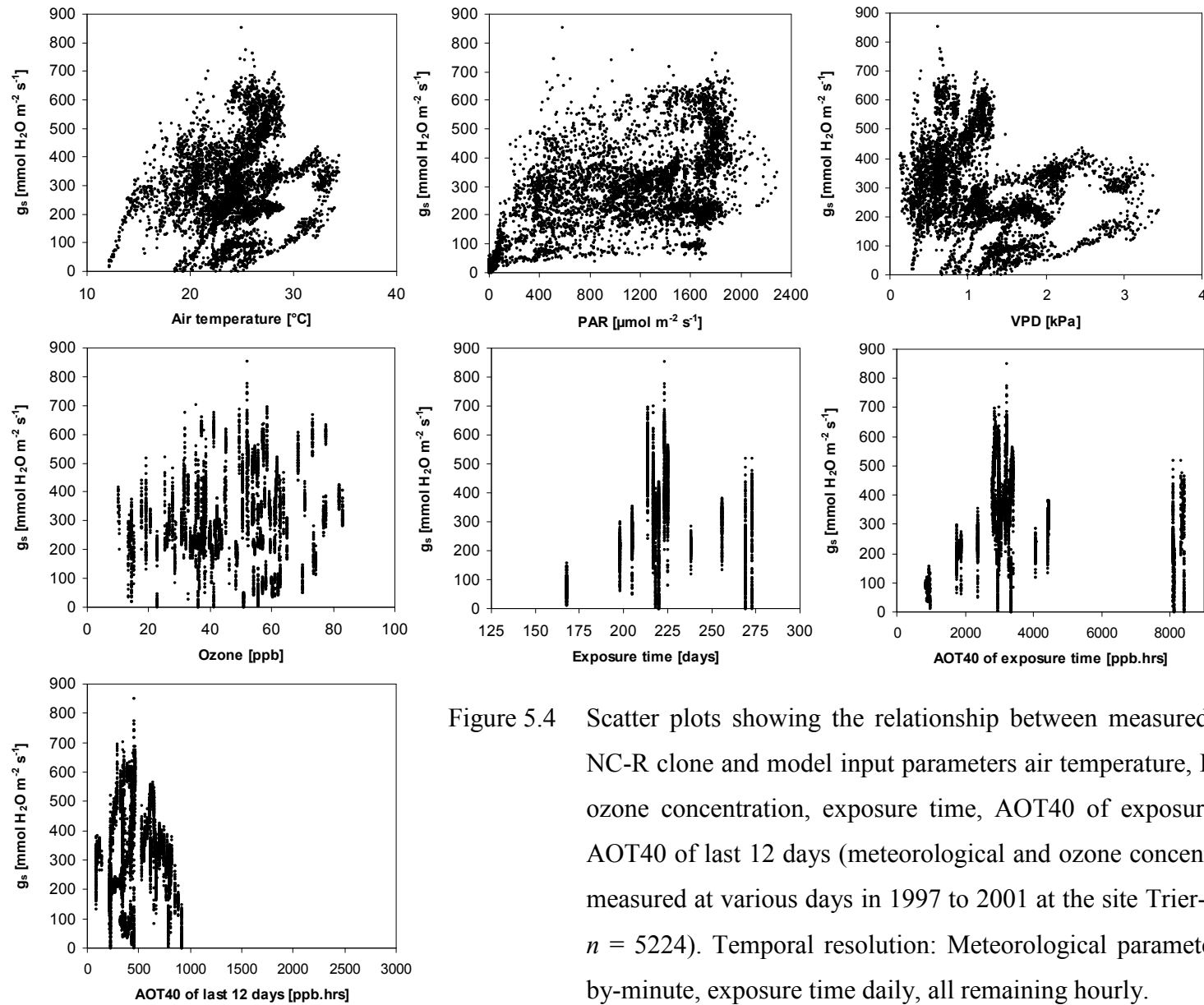
Figure 5.4   Scatter plots showing the relationship between measured g_s for the NC-R clone and model input parameters air temperature, PAR, VPD, ozone concentration, exposure time, AOT40 of exposure time and AOT40 of last 12 days (meteorological and ozone concentration data measured at various days in 1997 to 2001 at the site Trier-University, $n = 5224$). Temporal resolution: Meteorological parameters minute-by-minute, exposure time daily, all remaining hourly.
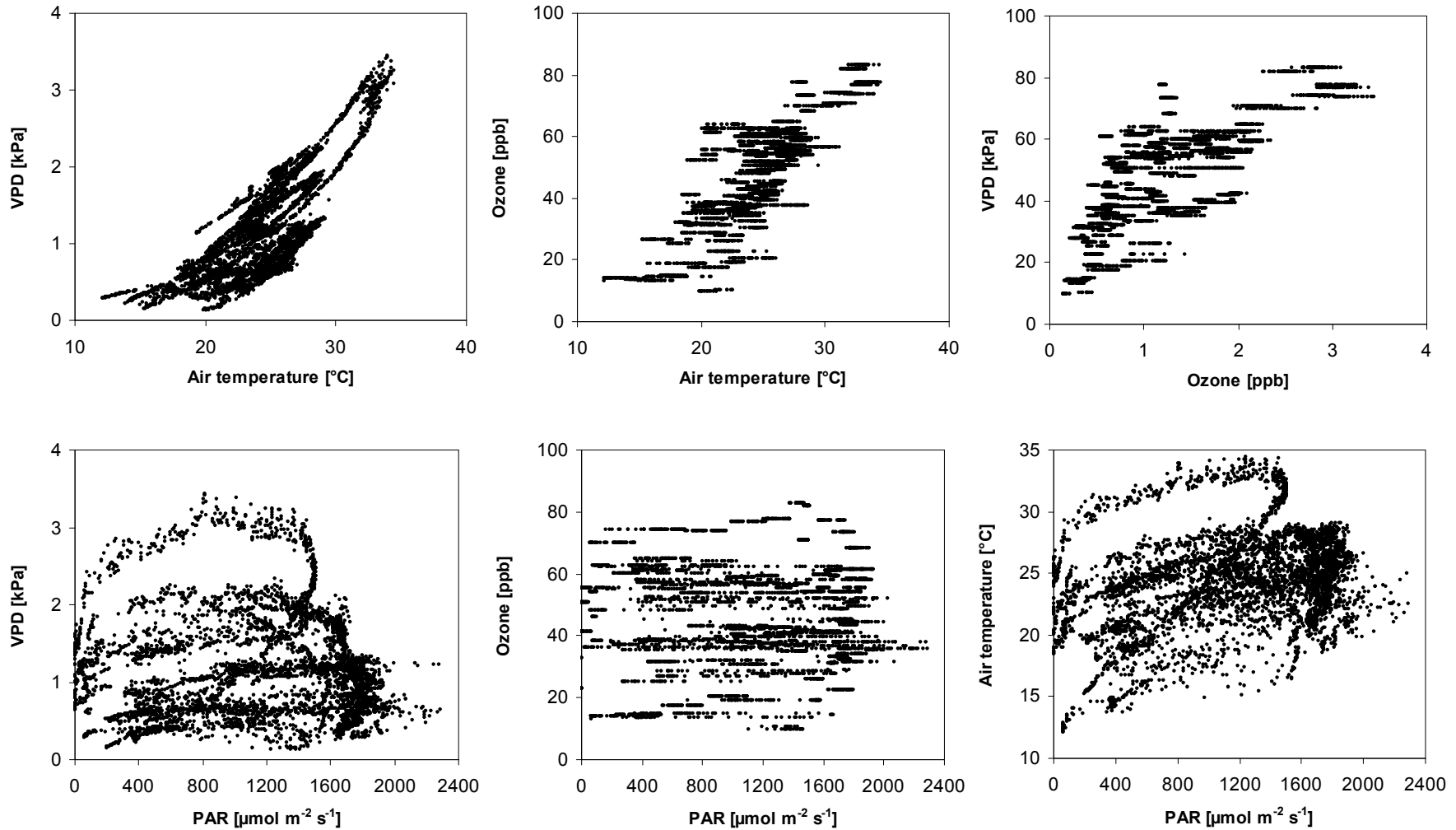
Figure 5.5   Scatter plots showing the relationship between meteorological parameters VPD, air temperature and PAR, as well as between O_3 concentration and these meteorological parameters of the NC-R dataset (measured data from various days in 1997 to 2001 at the site Trier-University, $n = 9113$). Temporal resolution: Meteorological parameters minute-by-minute, O_3 concentration hourly.

A first indication of the relationship between the parameters air temperature and PAR, VPD and O_3 concentration, between PAR and VPD and O_3 concentration as well as between VPD and O_3 concentration is given in Figure 5.3 and 5.5 for the NC-S and NC-R dataset, respectively. The scatter plots look rather similar for both datasets, with again a slightly higher patchiness for the NC-R dataset. Most evident is the strong dependency of VPD on air temperature (positive relationship), but also O_3 concentration shows a distinct positive correlation with air temperature. Similarly, the O_3 concentration is also positively correlated with VPD. The relationship between VPD as well as air temperature with PAR is slightly less obvious, though there is no doubt that both parameters are positively correlated with PAR. Only the correlation between O_3 and PAR is hard to define from the scatter plots of the present datasets.

These findings are also supported by the results of the Spearman's rank-order correlation test shown in Tables 5.4 and 5.5. It revealed, for both datasets, a significant positive association between air temperature and VPD with $r = 0.70$ and $r = 0.74$ for the NC-S and NC-R dataset, respectively. A similarly strong significant correlation was found between air temperature and O_3 concentration with correlation coefficients of $r = 0.68$ and $r = 0.76$ for the NC-S and NC-R dataset, respectively. This clearly indicates the strong dependence of tropospheric O_3 formation on air temperature, which can for instance often be experienced during hot summer periods in Germany.

Surprisingly, the association between air temperature and PAR is less strong, though also highly significant (it has to be pointed out that due to the large sample size, most correlations have been found to be highly significant).

Furthermore, there is a significant positive association between g_s and air temperature and PAR, whereas the correlation between g_s and VPD is significantly negative. The low correlation coefficients and contradictory (i.e. negative for NC-S but positive for NC-R dataset) associations between g_s and O_3 concentration, exposure time, "AOT40 of exposure" and "AOT40 of last 12 days" indicate the limited suitability of these parameters for predicting g_s.

Table 5.4 Results of the Spearman's rank-order correlation for NC-S clone dataset including g_s [mmol H_2O m_{-2} s^{-1}] and all 7 input variables used for the ANN g_s model, i.e. air temperature [°C], VPD [kPa], PAR [μmol m^{-2} s^{-1}], O_3 concentration [ppb], exposure time [days], "AOT40 of exposure time" [ppb.hrs] and "AOT40 of last 12 days" [ppb.hrs].

			g_s NC-S	exp. time	air temp.	PAR	VPD	ozone conc.	AOT40 exp.
Spearman's rho	exp. time	Correlation Coefficient	-.234**						
		Sig. (2-tailed)	.000						
		N	9113						
	air temp.	Correlation Coefficient	.135**	.149**					
		Sig. (2-tailed)	.000	.000					
		N	9113	9113					
	PAR	Correlation Coefficient	.425**	-.085**	.382**				
		Sig. (2-tailed)	.000	.000	.000				
		N	9113	9113	9113				
	VPD	Correlation Coefficient	-.352**	.118**	.698**	.009			
		Sig. (2-tailed)	.000	.000	.000	.397			
		N	9113	9113	9113	9113			
	ozone conc.	Correlation Coefficient	.115**	.012	.683**	.168**	.542**		
		Sig. (2-tailed)	.000	.248	.000	.000	.000		
		N	9113	9113	9113	9113	9113		
	AOT40 exp.	Correlation Coefficient	-.085**	.630**	.151**	-.245**	.146**	.245**	
		Sig. (2-tailed)	.000	.000	.000	.000	.000	.000	
		N	9113	9113	9113	9113	9113	9113	
	AOT40 12d.	Correlation Coefficient	-.181**	.030**	.419**	-.157**	.482**	.540**	.450**
		Sig. (2-tailed)	.000	.004	.000	.000	.000	.000	.000
		N	9113	9113	9113	9113	9113	9113	9113

**. Correlation is significant at the .01 level (2-tailed).

Table 5.5 Results of the Spearman's rank-order correlation for NC-R clone dataset including g_s [mmol H_2O m_{-2} s^{-1}] and all input variables used for the ANN g_s model, i.e. air temperature [°C], VPD [kPa], PAR [μmol m^{-2} s^{-1}], O_3 concentration [ppb], exposure time [days],"AOT40 of exposure time" [ppb.hrs] and "AOT40 of last 12 days" [ppb.hrs].

			g_s NC-R	exp. time	air temp.	PAR	VPD	ozone conc.	AOT40 exp.
Spearman's rho	exp. time	Correlation Coefficient	.169**						
		Sig. (2-tailed)	.000						
		N	5224						
	air temp.	Correlation Coefficient	.244**	-.314**					
		Sig. (2-tailed)	.000	.000					
		N	5224	5224					
	PAR	Correlation Coefficient	.411**	-.010	.311**				
		Sig. (2-tailed)	.000	.460	.000				
		N	5224	5224	5224				
	VPD	Correlation Coefficient	-.267**	-.349**	.743**	-.032*			
		Sig. (2-tailed)	.000	.000	.000	.020			
		N	5224	5224	5224	5224			
	ozone conc.	Correlation Coefficient	.078**	-.335**	.756**	.026	.695**		
		Sig. (2-tailed)	.000	.000	.000	.060	.000		
		N	5224	5224	5224	5224	5224		
	AOT40 exp.	Correlation Coefficient	.212**	.872**	-.080**	-.092**	-.174**	-.099**	
		Sig. (2-tailed)	.000	.000	.000	.000	.000	.000	
		N	5224	5224	5224	5224	5224	5224	
	AOT40 12d.	Correlation Coefficient	.038**	.014	.190**	-.092**	.242**	.203**	-.049**
		Sig. (2-tailed)	.005	.305	.000	.000	.000	.000	.000
		N	5224	5224	5224	5224	5224	5224	5224

**. Correlation is significant at the .01 level (2-tailed).

*. Correlation is significant at the .05 level (2-tailed).

5.3   Comparison of NC-S and NC-R stomatal conductance data

An important feature of this study was whether or not it would be necessary and desirable to develop separate ANN-based flux models for the NC-S and NC-R clover clones. This was assessed on the basis of results describing the statistical differences in g_s of both clones. In order to check the hypothesis that the mean g_s of both clover clones did not differ significantly, a statistical test of difference was carried out.

Due to the results of the Kolmogorov-Smirnov test (K-S test) for normal distribution, which confirmed that the distribution of both datasets differed significantly from normal (P = 0.000 for both datasets, see also Figure 5.6), the nonparametric Mann-Whitney U-test was used to test the statistical difference and revealed that the hypothesis that both g_s datasets are not significantly different from each other had to be rejected (P = 0.000). This result is supported by the box-plots presented in Figure 5.7, which show that the median values for g_s of the NC-S and the NC-R clone are 375.6 and 288.2, respectively (cf. Table 5.1). However, note that the absolute g_{max} is almost identical for both clones: NC-S = 841.1 mmol H_2O m^{-2} s^{-1}, NC-R = 852.2 mmol H_2O m^{-2} s^{-1} (cf. Table 5.1).
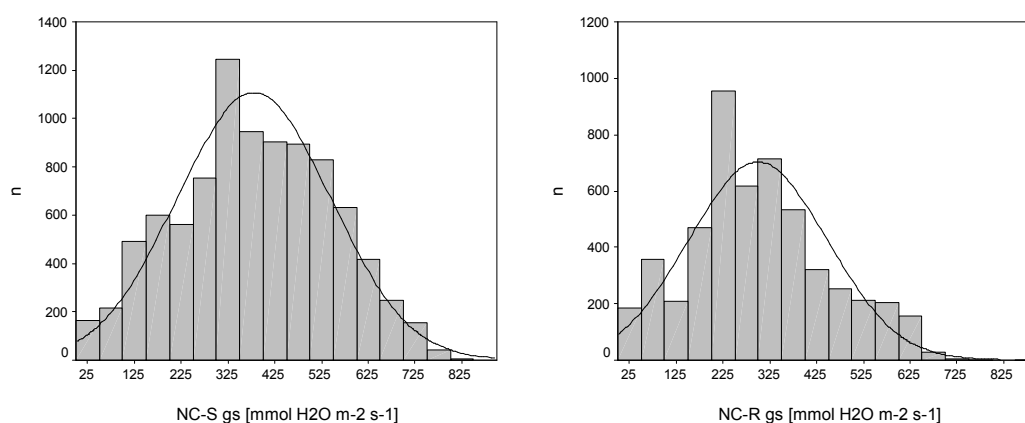
Figure 5.6   Histogram showing the distribution of the g_s datasets of the NC-S (left) and NC-R (right) clover clone (NC-S, $n = 9113$; NC-R, $n = 5224$).
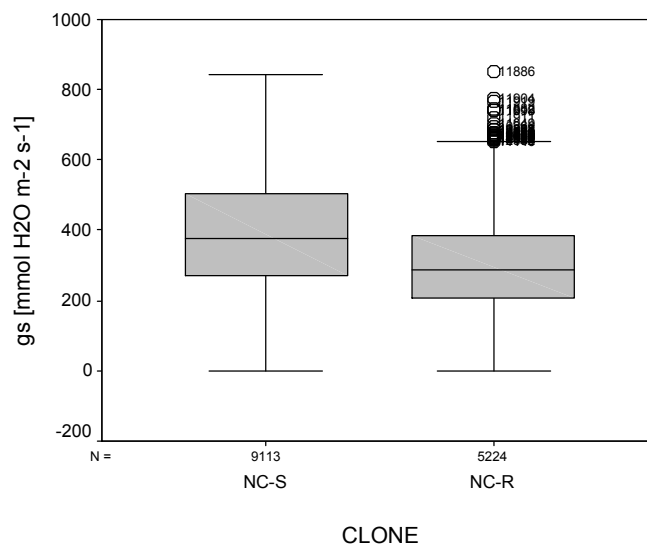
Figure 5.7   Box-plots showing the distribution of g_s-measurements of the NC-S
              (left) and NC-R (right) clover clone (NC-S, *n* = 9113; NC-R, *n* = 5224).
              Note the outliers for the NC-R clone.

To avoid any possible bias that may be introduced by the climatic conditions during
the experimental campaign, i.e. that particular climatic conditions may be more
favourable when measuring gas exchange of the NC-S plants leading to a higher g_s, it
was decided to create a subset of both g_s datasets representing non-limiting
meteorological conditions for white clover. Hence, these sub-datasets consist of
measurements carried out for the following meteorological conditions considered to
be optimum for g_s: air temperature between 22.5 and 25.0 °C, VPD between 0.75 and
1.25 kPa and PAR between 1200 and 1600 µmol m^{-2} s^{-1} (light saturation).

The derived g_s-subsets of data (NC-S: n = 186; NC-R: n = 197) were tested for normal
distribution (significantly different from normal distribution with P = 0.43 and P =
0.05 for NC-S and NC-R clone, respectively; also see Figure 5.8) and statistical
difference from each other using the Mann-Whitney U-test, which revealed – similar
to the test carried out for the entire dataset – a significantly higher g_s for the NC-S as
compared to the NC-R clone (P = 0.00). This result is again supported by the box-
plots presented in Figure 5.9, which show that the median g_s of the NC-S and the NC-
R clone is 464.45 and 254.60, respectively. It is obvious that here the difference

between the median g_s of both clones is even larger than found for the comparison of the entire datasets (see above).

These results showed that it was necessary to develop separate models for the NC-S and NC-R clones used in this study.
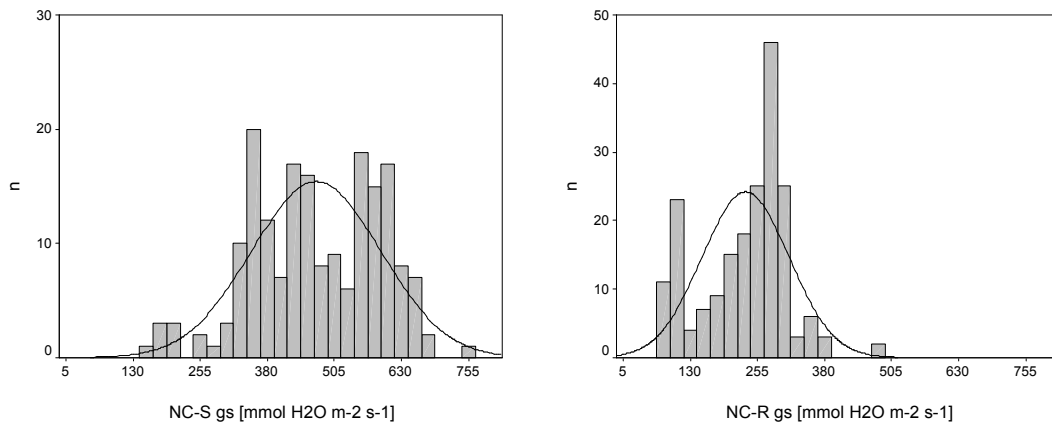
Figure 5.8   Histogram of distribution of g_s-data of the NC-S (left) and NC-R (right) clover clone measured under non-limiting meteorological conditions for g_s (NC-S, $n = 186$; NC-R, $n = 197$).
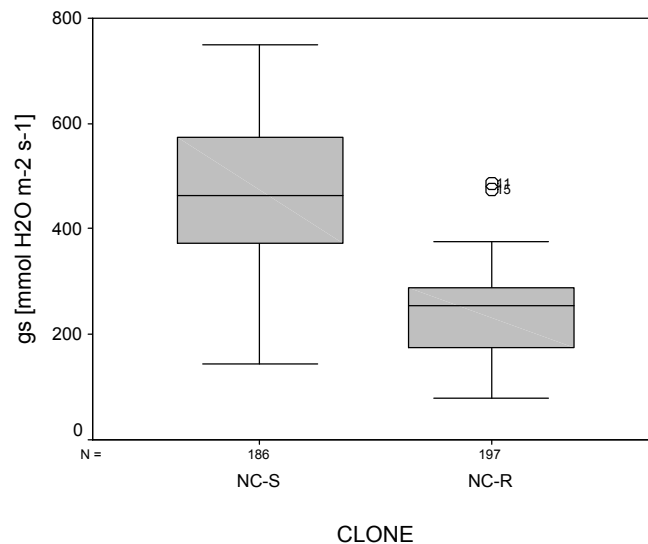
Figure 5.9   Box-plots showing the distribution of g_s-measurements of the NC-S (left) and NC-R (right) clover clone measured under non-limiting meteorological conditions for g_s (NC-S, $n = 186$; NC-R, $n = 197$).

5.4   Regression analysis of input data

Prior to the development of the ANN-based flux models for both clover clones, a stepwise (multiple) regression analysis of both g_s datasets was carried out to gain a first impression of the suitability of the seven input parameters in explaining the variation in the observations of the output parameter g_s. The results of this analysis are given in Table 5.6 and Table 5.7 for the NC-S and NC-R clover clone, respectively.

When all seven input parameters, i.e. air temperature [°C], VPD [kPa], PAR [μmol m$^-$^{2} s^{-1}], O_3 concentration [ppb], exposure time [days], "AOT40 of exposure time" [ppb.hrs] and "AOT40 of last 12 days" [ppb.hrs] are included as independent variables in the regression analysis (Model 7 in Tables 5.6 and 5.7), they are able to explain 62.8 % and 55.3 % of the variation in g_s of the NC-S and NC-R clover clone, respectively. Investigation of the component parts of the regression analysis suggests that for both datasets, PAR, VPD and air temperature - in that particular order – contributed the most to the explanation of the variation in g_s, i.e. 53.5 % and 48.4 % for the NC-S and NC-R dataset, respectively. The stepwise addition of the remaining four input parameters only slightly increased the regression coefficients and was not in the same order of importance for the NC-S and NC-R datasets (Tables 5.6 and 5.7).

Despite the fact that the multiple linear regression assumes not only a total independence of all independent variables but also a direct, combined linear effect of all independent variables on the dependent variable, it is very often used for describing complex biological cause-effect relationships like the one addressed in this study. Since both these assumptions are not valid for the two model input datasets used in this study (see for example results of the Spearman's rank-order correlation in Chapter 5.2.1), a multiple regression analysis seems to be less suitable for predicting g_s with the help of physical and pollution climate data using the NC-S and NC-R datasets available in this study.

It is expected that ANNs will perform better since they are capable of allowing for the highly complex, non-linear relationship between g_s and the prevailing physical- as well as pollution-climate conditions.

Table 5.6   Results of stepwise regression analysis for NC-S dataset.

Model	Predictor	Coefficient	P value	r²
1	Intercept	240.51	0.000	0.205
	PAR	0.13	0.000	
2	Intercept	361.16	0.000	0.351
	PAR	0.13	0.000	
	VPD	-109.82	0.000	
3	Intercept	-257.34	0.000	0.535
	PAR	0.05	0.000	
	VPD	-250.97	0.000	
	Air temperature	35.73	0.000	
4	Intercept	-220.21	0.000	0.553
	PAR	0.05	0.000	
	VPD	-255.87	0.000	
	Air temperature	37.55	0.000	
	Exposure time	-0.91	0.000	
5	Intercept	-224.57	0.000	0.578
	PAR	0.06	0.000	
	VPD	-267.58	0.000	
	Air temperature	38.20	0.000	
	Exposure time	-2.12	0.000	
	AOT40 exp. time	0.02	0.000	
6	Intercept	-222.29	0.000	0.628
	PAR	0.05	0.000	
	VPD	-239.96	0.000	
	Air temperature	42.15	0.000	
	Exposure time	-4.05	0.000	
	AOT40 exp. time	0.05	0.000	
	AOT40 12 days	-0.07	0.000	
7	Intercept	-214.24	0.000	0.628
	PAR	0.05	0.000	
	VPD	-239.80	0.000	
	Air temperature	40.80	0.000	
	Exposure time	-3.95	0.000	
	AOT40 exp. time	0.04	0.000	
	AOT40 12 days	-0.07	0.000	
	Ozone conc.	0.42	0.000	

Table 5.7   Results of stepwise regression analysis for NC-R dataset.

Model	Predictor	Coefficient	P value	r^2
1	Intercept	160.28	0.000	0.200
	PAR	0.12	0.000	
2	Intercept	220.90	0.000	0.251
	PAR	0.12	0.000	
	VPD	-50.47	0.000	
3	Intercept	-387.40	0.000	0.484
	PAR	0.03	0.000	
	VPD	-219.16	0.000	
	Air temperature	37.31	0.000	
4	Intercept	-494.24	0.000	0.510
	PAR	0.03	0.000	
	VPD	-230.28	0.000	
	Air temperature	40.38	0.000	
	AOT40 exp. time	0.01	0.000	
5	Intercept	-563.61	0.000	0.530
	PAR	0.03	0.000	
	VPD	-245.48	0.000	
	Air temperature	41.25	0.000	
	AOT40 exp. time	0.02	0.000	
	AOT40 12 days	0.10	0.000	
6	Intercept	-455.24	0.000	0.552
	PAR	0.03	0.000	
	VPD	-278.63	0.000	
	Air temperature	45.11	0.000	
	AOT40 exp. time	0.05	0.000	
	AOT40 12 days	0.11	0.000	
	Exposure time	-3.36	0.000	
7	Intercept	-443.84	0.000	0.553
	PAR	0.04	0.000	
	VPD	-277.36	0.000	
	Air temperature	42.63	0.000	
	AOT40 exp. time	0.05	0.000	
	AOT40 12 days	0.11	0.000	
	Exposure time	-3.12	0.000	
	Ozone conc.	0.62	0.000	

6   Development of the stomatal conductance models

6.1   General development of ANN-based stomatal conductance models

6.1.1   Architecture of network used in this thesis

Figure 6.1 shows the architecture of the backpropagation neural network used in this thesis when using all available input variables. Neurons from one layer feed-forward to all neurons of the next layer. There are no lateral connections within layers nor any feed-back connections between layers (feed-back connections are characteristic for recurrent ANNs used for time series modelling (cf. Pineda, 1987)).

| Input Layer | Hidden Layer | Output Layer |
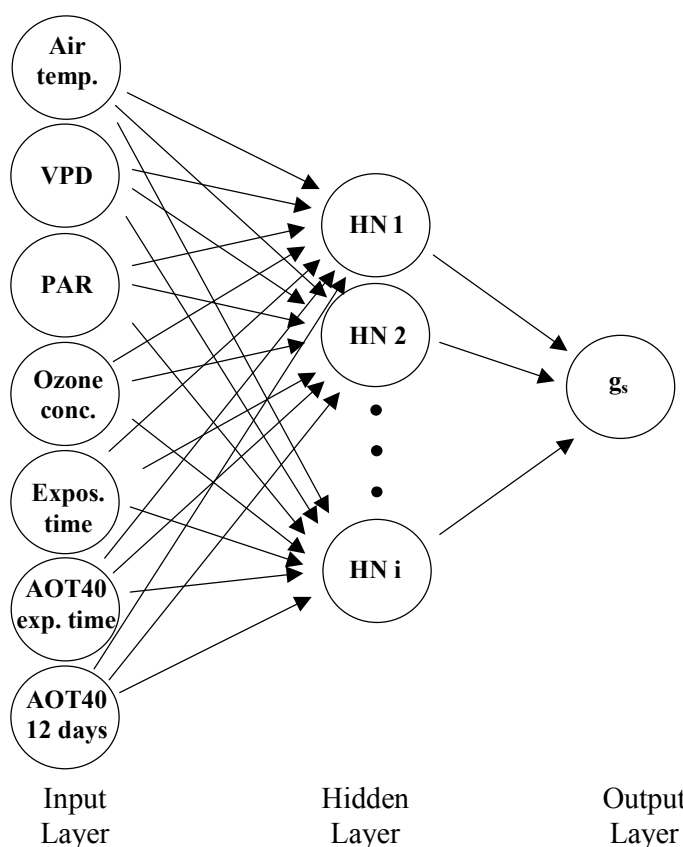
Figure 6.1   Architecture of the neural network used in this thesis, with air temperature [°C], VPD [kPa], PAR [μmol m^{-2} s^{-1}], O$_3$ concentration [ppb], exposure time [days], AOT40 of exposure time [ppb.hrs] and AOT40 of last 12 days [ppb.hrs] as input and g$_s$ [mmol H$_2$O m^{-2} s^{-1}] as output.

The input layer of the main initial ANN comprised seven neurons representing seven elements of information (variables) at the entry of the network: air temperature [°C], VPD [kPa], PAR [μmol m^{-2} s^{-1}], O_3 concentration [ppb], exposure time [days], AOT40 of exposure time [ppb.hrs] and AOT40 of last 12 days [ppb.hrs]. These elements of information are equivalent to independent variables in multiple regression analysis. The output layer of all neural networks (main and sub-networks) developed within this thesis consists of one neuron representing the stomatal conductance to water vapour (g_s) [mmol H_2O m^{-2} s^{-1}].

6.1.2   Data import and scaling

Typically for ANNs, the values of input and output neurons – here imported as Excel-spreadsheets by NeuroShell 2 - are scaled to the numeric range of 0 to 1 to ensure an identical range for all involved model variables which compensates effects of outliers in the dataset. Once the training is completed, the output values are re-scaled by reversing the action (e.g. Dimopoulos et al., 1999). NeuroShell 2 performs these two steps automatically, using a linear scaling function by default.

6.1.3   Division of input dataset into training, test and validation dataset

In order to prevent over-training of the network and to improve the generalisation and prediction ability of the final network, the two initial datasets of this thesis (i.e. measured g_s data for NC-S and NC-R clover clones with corresponding O_3 concentrations and meteorological variables) were randomly divided into a training, test and validation dataset in the relation of 60:20:20 using the NeuroShell 2 extraction command.

Prior to the main network training, this procedure was – as a pilot test - repeated three times which resulted in three different dataset divisions per clover clone dataset. The reason for this pilot test was to analyse whether or not different training, test and validation datasets (different in terms of the random selection rather number of data points, i.e. *n* and the relation 60:20:20 were always kept constant) might lead to different model results. This procedure was carried out for both the NC-R (*n* = 5224) and NC-S (*n* = 9113) dataset using all seven input parameters with 20 and 25 hidden

neurons (dataset size-related hidden neuron numbers suggested by NeuroShell 2), respectively. The variation of momentum and learning rate according to the ranges and steps described below led to 48 different sub-models for each dataset division. These sub-models were then applied to the previously extracted validation dataset with a subsequent comparison of predicted and measured g_s.

Table 6.1 shows the average predictive performance (expressed as coefficient of multiple determination (R^2) of predicted vs. measured values) for all three dataset divisions of both g_s-datasets (indicated as dataset 1 – 3 in Table 6.1). A varying random extraction of 60 % of the input data for training purposes of the model did result in slightly different predictive performances of the g_s model. However, the average R^2 - values differed to such a marginal extent that it was considered justifiable to stick to just **one** separation process of input data into training, test and validation data in the following training phase of the g_s models.

Table 6.1   Test of different separation of NC-S and NC-R datasets into training, test and validation datasets on predictive performance of models, expressed as average (*n* = 48 sub-models) R^2 value of predicted vs. measured g_s. Each dataset represents a different random division of input data into 60 % training, 20 % test and 20 % validation data (NC-S: *n* = 9113; NC-R: *n* = 5224).

	NC-S			NC-R		
	Dataset 1	Dataset 2	Dataset 3	Dataset 1	Dataset 2	Dataset 3
Mean of R^2	0.869	0.862	0.877	0.899	0.895	0.893
Stdev. (σ)	0.053	0.056	0.045	0.013	0.013	0.014

6.1.4   *Structure of hidden layer*

The number of neurons in the hidden layer was varied throughout the training phase of the neural networks. For the identification of the initial number of hidden neurons, NeuroShell 2 offers the computation of a default number according to the following formula:

Number of hidden neurons =   0.5 * (number of Inputs + Output) + Square Root of

number of patterns in training dataset   (6.1)

This led to an initial number of hidden neurons of 20 and 25 for the NC-R and NC-S dataset, respectively. These were considered the maximum numbers of hidden neurons and were subsequently reduced in steps of 1 down to 3 in order to find the minimum number of hidden neurons that could still reveal and hence predict the complex relationship between inputs and the output. The most commonly used method to identify the optimal number of hidden neurons ensuring the best prediction ability of the network is trial and error, which was as well used in this thesis. A further reason for varying the number of hidden neurons was the differing amount of input variables of sub-networks of the main network. These sub-networks were trained to test the importance of each variable for the predictive power of the network (see below). In other words, the performance of various sub-networks with different combinations of input variables were compared with the performance of the main network including all seven input variables.

A unique tool of NeuroShell 2 is the possibility to divide the hidden layer in three different slabs, i.e. groups of hidden neurons (not to be confused with multiple hidden layers working in serial rather than in parallel). This procedure provides the opportunity to select different activation functions for different slabs, so that the output layer will get "different views" of the data. In other words, different activation functions detect different features in a pattern processed through a network. For instance, one activation function applied to one slab might detect features in the mid-range, while a second slab with a different activation function may detect features from the upper or lower end of the dataset (Ward System Group Inc., 1996). In practice, this means that the total amount of hidden neurons is divided by three with each cluster of hidden neurons then being equipped with a different activation function.

Prior to the model development, the prediction ability of networks trained with this three-slab tool using different combinations of activation functions such as sigmoid logistic, hyperbolic tangent, Gaussian and/or Gaussian complement was compared with the predictive ability of a classic three-layer network. It was found that the three-

slab networks with a combination of the following three activation functions, where f (a_j) is the activation function of the jth neuron, always outperformed not only the classic three-layer network, but also three-slab networks with other combinations of activation functions:

i) Gaussian:

$$f(a_j) = \exp(-a_j{}^2) \tag{6.2}$$

ii) Gaussian complement:

$$f(a_j) = 1 - \exp(-a_j{}^2) \tag{6.3}$$

and

iii) hyperbolic tangent (tanh):

$$f(a_j) = \tanh(a_j{}^2) \tag{6.4}$$

In contrast, a non-linear sigmoidal (sigmoid logistic) activation function was used to calculate the output (g_s) based on the weighted and subsequently summed input signals coming from the hidden layer:

$$f(a_j) = \frac{1}{1 + \exp^{-aj}} \tag{6.5}$$

where $f(a_j)$ is the activation function of the jth neuron.

6.1.5 Setting of momentum and learning rate

The optimum configuration of the main model in terms of the settings of the learning rate and momentum – i.e. range and incremental steps – was identified via various tests prior to the main training phase of the networks. It appeared that for securing the best possible network training with the given noise in the input datasets, a range from 0.05 to 0.5 and 0.05 to 0.7 was most suitable for learning rate and momentum, respectively. The possible combinations (and incremental steps) of these weighting parameters are listed in Table 6.2. Accordingly, these 48 weighting parameter combinations were always applied during each training epoch (where an epoch represents one complete pass through the network without changing the number of

hidden neurons) resulting in 48 sub-models for model runs, with for example 25, 24, 23 etc. hidden neurons. As an example, this procedure resulted for the NC-S dataset using all seven input parameters in 1104 sub-models (48 model runs each for models with 25, 24, 23…. down to 3 hidden neurons → 48 (weighting parameter combinations) x 23 (hidden neuron classes) = 1104 (sub-models)). From these 1104 sub-models, the one with the best predicting ability of g_s was chosen as the final model for that particular combination of input parameters.

Table 6.2   Combinations of learning rate (η) and momentum (μ) used during training of ANNs.

μ \ η	0.05	0.1	0.2	0.3	0.4	0.5
0.05	✓	✓	✓	✓	✓	✓
0.1	✓	✓	✓	✓	✓	✓
0.2	✓	✓	✓	✓	✓	✓
0.3	✓	✓	✓	✓	✓	✓
0.4	✓	✓	✓	✓	✓	✓
0.5	✓	✓	✓	✓	✓	✓
0.6	✓	✓	✓	✓	✓	✓
0.7	✓	✓	✓	✓	✓	✓

6.1.6 Stopping criteria for network training

The training was stopped when the sum of squared errors between the predicted output value of the training and the output values of the test set was at its minimum (precisely, when the number of events – i.e. the presentation of a single training pattern to the network - since the internally calculated minimum last changed, exceeded 20,000) or the learning epochs reached a total number of 400. The resulting network was then applied to the validation dataset to test its general accuracy in predicting g_s.

6.2   General evaluation of models

6.2.1   Criteria for assessing predictive performance of models

The coefficient of determination (R^2) and the mean squared error (MSE) of the relationship between modelled and observed g_s were considered the main indicators for assessing the predictive performance of all models and sub-models. The higher the R^2 and the lower the MSE, the better the model. However, throughout the thesis in all tables and figures only the R^2 will be stated as the main indication for the performance of a network/model.

6.2.2   Sensitivity analysis

Furthermore, in order to evaluate this first judgement based on R^2 and MSE, as well as to test the performance of these models in terms of their predictive power over the entire range of all involved input parameters, a sensitivity analysis was carried out for each sub-model. This analysis gives a good visual indication of the relative importance of single variables on the dependent variable (g_s). This analysis involved the creation of effect-curves showing the dependence of g_s on each independent variable by varying the value of one independent parameter in constant steps across its entire range while keeping the value of all other independent variables constant at their mean.

Figure 6.2 gives an example for a sensitivity analysis carried out for two different sub-models for the NC-S dataset. These sub-models only varied in their learning rate and momentum (i.e. the number of inputs and hidden neurons was identical), but show different predictive performances: The relationship between g_s and PAR is less clear (small range of g_s, high g_s value for PAR = 0 μmol m^{-2} s^{-1}) for the sub-model with a learning rate of 0.3 and a momentum of 0.7 (graph g in figure 6.2) than for the sub-model with a learning rate of 0.2 and a momentum of 0.1 (graph c). Furthermore, the former shows an unexpected slight increase of g_s as VPD increases from 0 to 0.5 kPa (graph f), as well as a less clear influence of the exposure time on g_s (graph h).

In this case, the sub-model with a learning rate of 0.2 and a momentum of 0.1 (graphs a to d) would be considered the better choice due to its superior ability to predict g_s as a function of various meteorological parameters and time.
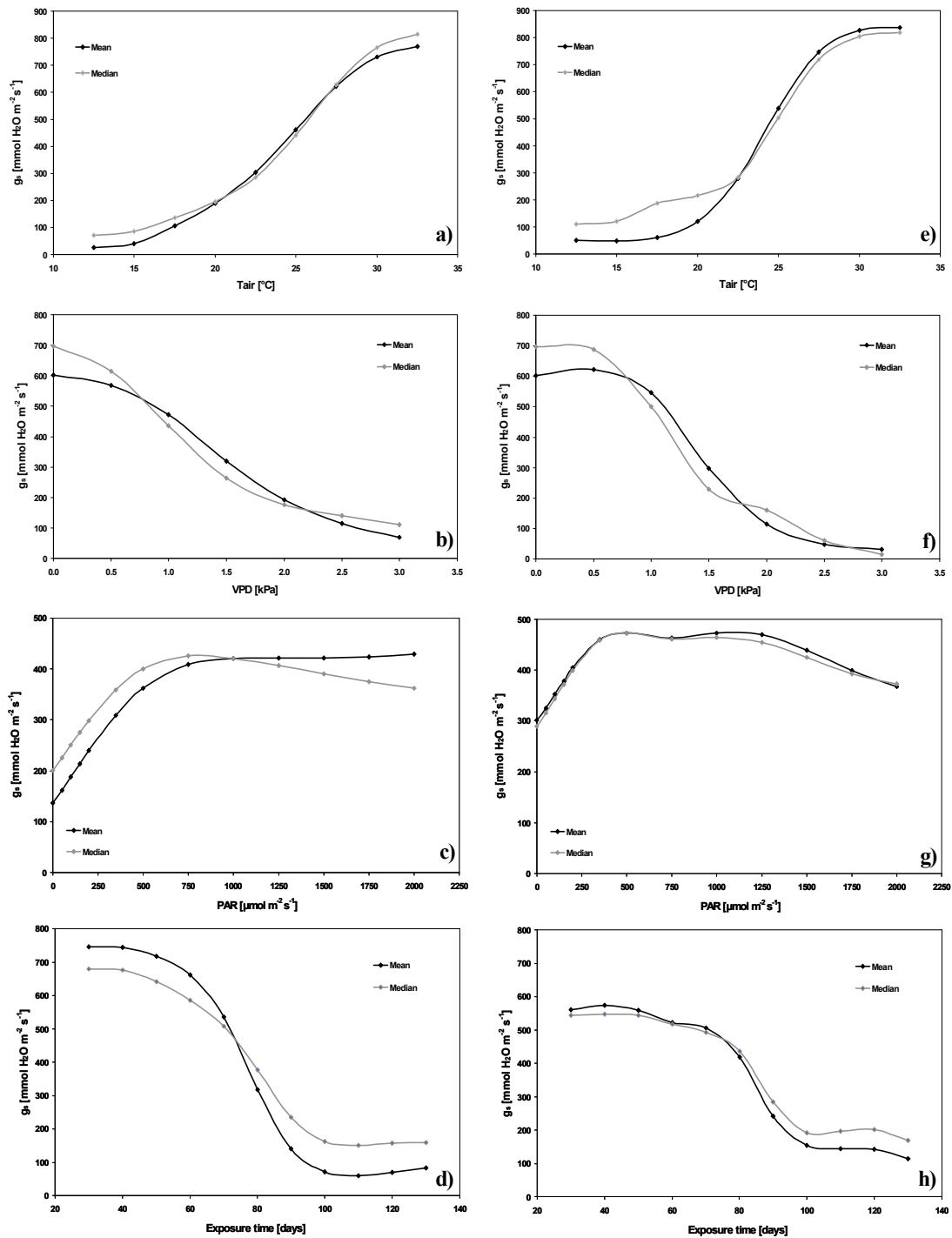
Figure 6.2   Sensitivity analysis of two NC-S g_s sub-models with identical number of inputs ($n = 7$) and hidden neurons ($n = 9$), but differing learning rates and momentums (0.2 and 0.1 (a - d) as opposed to 0.3 and 0.7 (e – h)). Shown are relationships between modelled g_s and the entire range of the parameters air temperature (a, e), VPD (b, f), PAR (c, g) and exposure time (d, h). For each graph, all other six input parameters were kept at their overall mean (black curve) and median (grey curve).
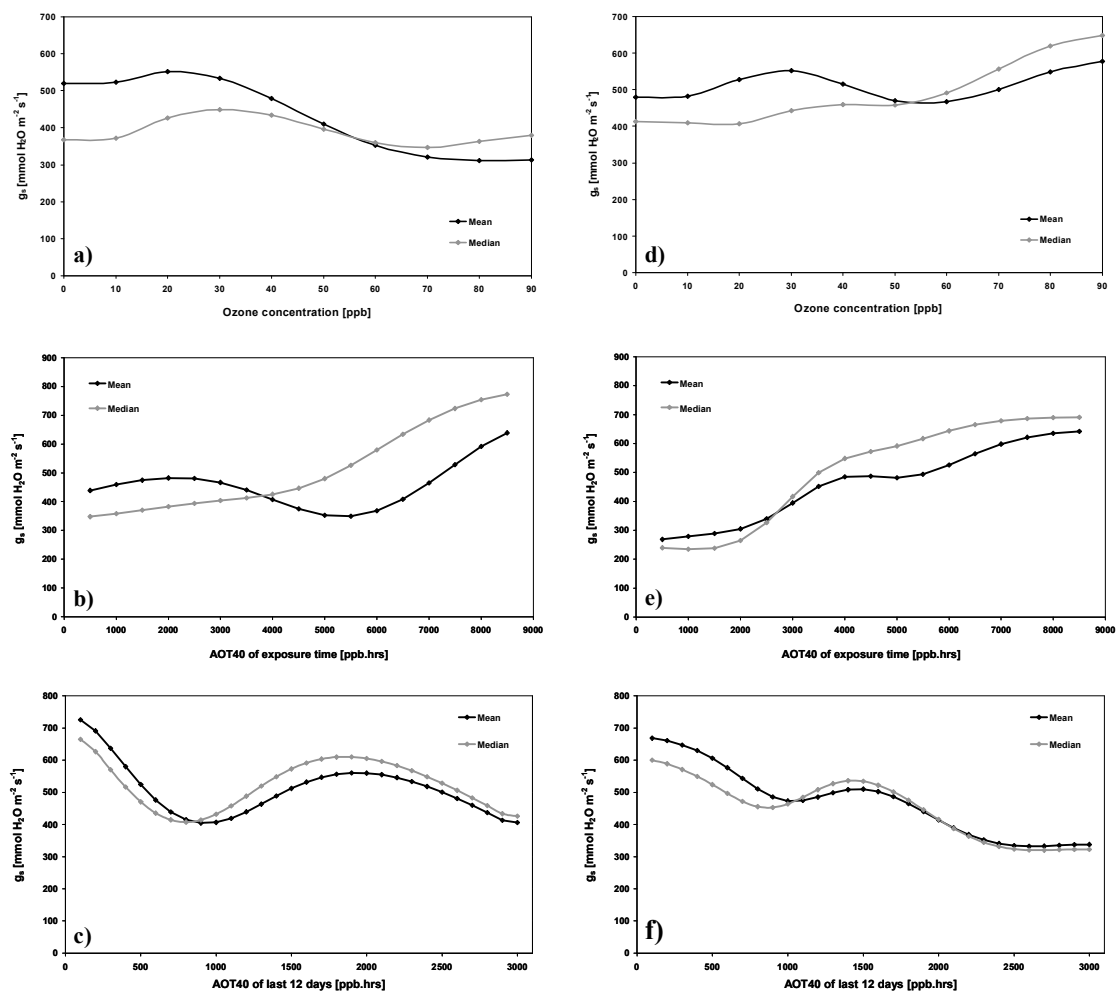
Figure 6.3   Sensitivity analysis of two NC-S g_s sub-models with identical number of inputs (n = 7) and hidden neurons (n = 9), but differing learning rates and momentums (0.2 and 0.1 (a - c) as opposed to 0.3 and 0.7 (d – f)). Shown are relationships between modelled g_s and the entire range of the parameters O_3 concentration (a, d), AOT40 of exposure time (b, e) and AOT40 of last 12 days (c, f). For each graph, all other six input parameters were kept at their overall mean (black curve) and median (grey curve).

A somewhat subjective scoring system was set up for the visual assessment of the performance of the sensitivity analysis, which was applied to all sub-models:

1 =   good performance (g_s shows "typical" - i.e. similar to what is reported in text books - dependence on meteorological variables and time);

2 =   mediocre performance (g_s shows an unexpected relationship to at least one meteorological variable or time);

3 =   bad performance (the relationship between g_s and a majority of meteorological variables and/or time is inconsistent).

The relationships between g_s and the O_3 concentration, "AOT40 since exposure" and "AOT40 of last 12 days" showed no clear trend for the same sub-models as described above, as can be seen in Figure 6.3.

6.2.3   *Diurnal time course test of model performance*

In addition, all sub-models were always applied to two different diurnal time courses of observed meteorological data to get a second visual indication of the networks' performance and to identify the ability of the network to cope with time series of data (e.g. from 7 a.m. till 9 p.m.). The two diurnal time courses used for this analysis were selected to represent a cloudless, warm summer day with a perfect parable-shaped PAR curve (Figure 6.4, graphs a and c), and a day with interrupted sunshine periods which resulted in distinct peaks of PAR, temperature and VPD (Figure 6.4, graphs b and d).

In this example, both sub-models predict obvious incremental steps of g_s (slightly larger for the 0.3/0.7 model, Figure 6.4 graph c) during the late morning hours of the cloudless summer day (graphs a and c), which when compared to the meteorological parameters can only be judged as a model artefact. At least, the 0.2/0.1 model is able to cope with the sudden, albeit brief drop in PAR at 18:20, which is not the case for the other model. For the cloudy day (Figure 6.4, graph b and d), the 0.2/0.1 model clearly reacts to the various drops in PAR when predicting g_s, i.e. g_s decreases when PAR decreases and vice versa, which is not the case for the 0.3/0.7 model.

Again, a somewhat subjective scoring system was set up for the visual assessment of the performance of the application of sub-models to diurnal time courses of measured meteorological data:

1 =   good performance (predicted diurnal time course of g_s shows good fit with measured diurnal time courses of PAR and air temperature);

2 =   mediocre performance (some divergence between predicted time course of g_s and time courses of meteorological parameters);

3 =   bad performance (no clear relationship between time course of g_s and time

         courses of meteorological parameters and/or clear artefacts in time course of

         g_s)
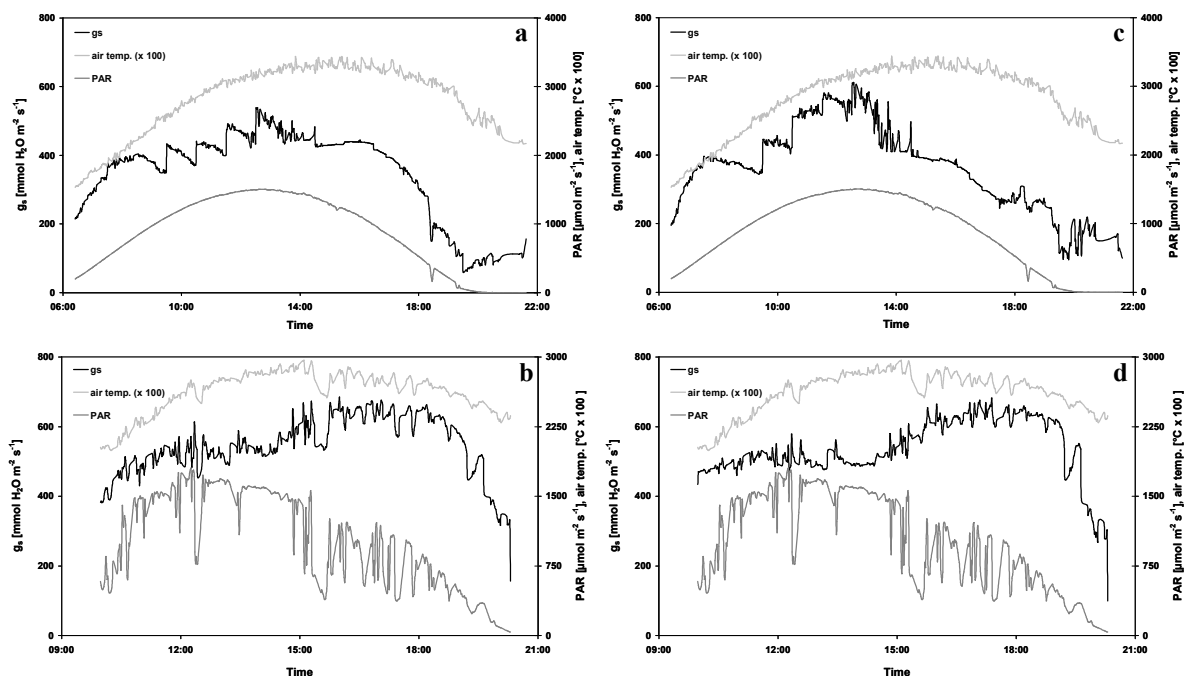
Figure 6.4   Application of two NC-S g_s sub-models only differing in their learning

               rate and momentum (0.2 and 0.1 (a, b) as opposed to 0.3 and 0.7 (c, d))

               to two diurnal time courses of measured meteorological data. Graph a

               and c: 08/08/98, graph b and d: 14/08/00. VPD (not shown) showed a

               very similar time course to air temperature.

It is important to bear in mind that the diurnal time courses used for this analysis
consisted of meteorological data (air temperature, VPD and PAR) that were
simultaneously measured alongside with g_s, i.e. these are meteorological data
measured with the gas exchange measuring system rather than at the nearby
meteorological station. This gave a clearer impression of how the clover clones
actually reacted to the prevailing meteorological conditions.

However, since modelled data would generally only be applied to data that are **not**
being used for the training of the model, which would have resulted in the exclusion
of entire measured diurnal datasets (consisting of approx. 600 single data points)
during the model development – a sacrifice thought to be too large here -, g_s sub-

models for the NC-S clone were always applied to diurnal time courses of meteorological data recorded during the measurements of g_s on the NC-R clover clone, and *vice versa*. The downside of this approach is that the modelled g_s data for one clone could only be compared with measured g_s data of the other clone. Given the significant difference in the average g_s (cf. Chapter 5.3) between the two clover clones, this comparison was judged to be of limited use for assessing the predictive performance of each developed sub-model. However, while the mean g_s differed significantly between clones, the general response of the g_s to PAR, air temperature and VPD was very similar for both clones. In other words the diurnal g_s profiles would be quite similar and hence could be used to indicate how the white clover responds to the prevailing meteorology over the course of a day.

6.2.4   *Assessment of parameter contribution*

In order to better understand the internal functioning of an ANN and to get an idea how to further develop the network - e.g. which input variable could be excluded without loosing too much information about the intrinsic, complex relationship between inputs and output -, it is of great help to determine the contribution of each input variable to the network's output.

The two most commonly used approaches for this parameter contribution analysis are the Garson's algorithm and the connection weight approach (cf. Chapter 2.4). Both require two matrices containing input-hidden and hidden-output weights. From these, the contribution of each input neuron to the output via the hidden neurons is calculated as the product of the input-hidden and hidden-output connection. While the Garson's algorithm then calculates the relative contribution of each input neuron to the outgoing signal of each hidden neuron and the sum of contributions of each input neuron to gain the relative importance of each input variable (%) by using **absolute** connection weights, the connection weight approach simply calculates the sum of the contributions of each input neuron using **relative** (or raw) connection weights (Table 6.3).

The main difference between these to methods is therefore the fact that the connection weight approach accounts for counteracting connection weights between input and

output variables, i.e. opposite directions ("+" and "–" or "–" and "+") for incoming and outgoing weights from the hidden neurons. It has to be stated that input variables with larger connection weights represent greater intensities of signal transfer and therefore are more important in the prediction process than variables with smaller weights. Furthermore, negative connection weights represent inhibitory effects on neurons (i.e. reducing the intensity of the incoming signal) and decrease the value of the predicted response, whereas positive connection weights represent excitatory effects on neurons (i.e. increasing the intensity of the incoming signal) and increase the value of the predicted response. Table 6.3 shows the results of the connection weight approach and the Garson's algorithm for the same NC-S sub-model as used as an example above (i.e. seven inputs, nine hidden neurons, learning rate of 0.2 and momentum of 0.1). When comparing the final rankings, there is clearly some agreement as well as some divergence between these two approaches.

After a thorough literature review (Chapter 2.4), it was decided to skip the Garson's algorithm in the following as it was generally outperformed in its ability to accurately quantify the importance of a variable in an ANN by the connection weight approach. In addition, NeuroShell 2 offers an internal option to predict the importance of each variable in the trained network. This internal ranking was always compared with the ranking derived from the connection weight approach. However, since NeuroShell 2 does not explain the mechanisms behind its variable ranking tool (the manual just states "The contribution factor is developed from an analysis of the weights of the trained neural network"; Ward Systems Group Inc., 1996), the results have been handled with great caution.

The connection weight approach, which has been proved to be very reliable, is basically a kind of very simple pruning tool as it clearly identifies those variables that only marginally contribute to the prediction of the output. In other words, when aiming for the reduction of inputs during the development process of the models in order to reduce their complexity, the input with the lowest contribution to the network as identified by the connection weight approach was always omitted first. Since this approach worked fine throughout the training of the models, no further specific pruning tools were applied.

Table 6.3   Comparison of the connection weight approach and the Garson's algorithm for a NC-S network with seven inputs, nine hidden neurons, a learning rate of 0.2 and a momentum of 0.1 (after Olden et al., 2004).

X ＼ Y	HN 1	HN 2	HN 3	HN 4	HN 5	HN 6	HN 7	HN 8	HN 9
Exposure time	1.43	-2.70	0.25	0.10	0.16	-0.36	-0.34	-0.26	-0.18
Air temper.	0.64	-0.40	0.20	0.06	-0.12	-0.38	-0.79	-0.34	0.36
PAR	-0.34	-0.02	-0.11	-0.01	0.06	0.05	-0.03	-0.13	-0.13
VPD	-0.93	0.56	-0.15	0.03	0.67	0.14	1.14	0.10	0.23
Ozone conc.	0.45	-0.04	0.07	0.24	-0.23	0.05	0.30	0.53	0.24
AOT40 expos.	1.15	-1.62	-0.83	-0.12	-0.01	-0.41	-1.47	-0.19	0.01
AOT40 12 d.	-1.79	-0.35	0.76	-0.01	-0.14	0.01	-0.60	-0.21	0.02

$$\times$$

	HN 1	HN 2	HN 3	HN 4	HN 5	HN 6	HN 7	HN 8	HN 9
g_s	-1.39	1.03	-0.62	-0.12	0.32	0.24	-0.67	0.27	-0.41

$$\downarrow$$

X ＼ Y	HN 1	HN 2	HN 3	HN 4	HN 5	HN 6	HN 7	HN 8	HN 9
Exposure time	-1.99	-2.79	-0.15	-0.01	0.05	-0.08	0.23	-0.07	0.07
Air temp.	-0.89	-0.41	-0.13	-0.01	-0.04	-0.09	0.52	-0.09	-0.15
PAR	0.48	-0.02	0.07	0.00	0.02	0.01	0.02	-0.04	0.05
VPD	1.29	0.58	0.09	0.00	0.21	0.03	-0.76	0.03	-0.10
Ozone conc.	-0.63	-0.04	-0.04	-0.03	-0.07	0.01	-0.20	0.15	-0.10
AOT40 expos.	-1.60	-1.67	0.51	0.01	0.00	-0.10	0.98	-0.05	0.00
AOT40 12 d.	2.49	-0.36	-0.47	0.00	-0.05	0.00	0.40	-0.06	-0.01

$$\text{Input}_X = \sum_{Y=A}^{E} \text{HN}_{XY} \qquad\qquad \text{Input}_X = \sum_{Y=A}^{E} \frac{\left|\text{HN}_{XY}\right|}{\sum_{Z=1}^{5}\left|\text{HN}_{ZY}\right|}$$

$$\downarrow \qquad\qquad\qquad\qquad\qquad\qquad \downarrow$$

	Importance	Rank			Importance	Rank
Exposure time	-4.74	1		**Exposure time**	1.71	2
Air temp.	-1.28	5		**Air temp.**	1.39	4
PAR	0.59	7		**PAR**	0.38	7
VPD	1.38	4		**VPD**	1.43	3
Ozone conc.	-0.97	6		**Ozone conc.**	1.31	5
AOT40 expos.	-1.92	3		**AOT40 expos.**	1.75	1
AOT40 12 days	1.95	2		**AOT40 12 days**	1.04	6

Connection Weight Approach   Garson's Algorithm

6.3   Development of final NC-S, NC-R and NC-SR g_s models

The Tables 6.4, 6.5 and 6.6 summarise the performance of the developed NC-S, NC-R and NC-SR g_s models with all seven input parameters, respectively. Presented are the results (mean and maximum criteria) for 48 sub-models each per hidden neuron class (from 25 or 20 down to 3), differing in their momentum and learning rate. In other words, each table row represents 48 sub-models. Listed criteria for the evaluation of the performance of models are i) the maximum R^2 value of the relationship between predicted and observed g_s (the latter representing a subset extracted from the input data), ii) the mean R^2 value ($n = 48$) of the relationship between predicted and observed g_s, iii) the median and mean scores ($n = 48$) of the sensitivity analysis, iv) the median and mean score ($n = 48$) of the application of the models to a diurnal time course representing a sunny day and vi) the median and mean score ($n = 48$) of the application of the models to a diurnal time course representing a cloudy day.

All models (NC-S, NC-R and NC-SR) performed very well in predicting g_s rates, with maximum R^2 values of 0.92 (25 HN), 0.93 (13 HN) and 0.88 (23 HN) for the NC-S, NC-R and NC-SR models, respectively. The mean R^2 values representing 48 sub-models of 0.89 (8 HN), 0.91 (9 HN) and 0.87 (9 HN) for the same NC-S, NC-R and NC-SR models, respectively were equally impressive. In general, the maximum and mean R^2 values did not differ substantially between different hidden neuron classes.

Table 6.4   Performance of ANN-based NC-S g_s sub-models with seven input parameters. Listed results showing maximum, median and mean (± 1 S.D.) values represent 48 sub-models - differing in momentum and learning rate - per hidden neuron class.

Inputs	HN	Max. R² modelled vs. observed g_s	Mean R² ± S.D. modelled vs. observed g_s	Median sensitivity analysis	Mean ± S.D. sensitivity analysis	Median diurnal time course, sunny	Mean ± S.D. diurnal time course, sunny	Median diurnal time course, cloudy	Mean ± S.D. diurnal time course, cloudy
7	25	0.9155	0.8771 ± 0.05	2.00	1.63 ± 0.53	2.00	2.00 ± 0.00	2.00	1.98 ± 0.14
7	24	0.9068	0.8640 ± 0.05	2.00	1.88 ± 0.33	2.00	1.98 ± 0.14	2.00	1.94 ± 0.24
7	23	0.9008	0.8662 ± 0.04	2.00	1.85 ± 0.36	2.00	2.00 ± 0.00	2.00	1.85 ± 0.36
7	22	0.9078	0.8695 ± 0.05	2.00	1.92 ± 0.28	2.00	2.00 ± 0.00	2.00	1.98 ± 0.14
7	21	0.9082	0.8794 ± 0.05	2.00	1.90 ± 0.31	2.00	1.96 ± 0.20	2.00	1.65 ± 0.48
7	20	0.9106	0.8775 ± 0.04	2.00	1.96 ± 0.20	2.00	1.98 ± 0.14	2.00	1.73 ± 0.45
7	19	0.9057	0.8813 ± 0.03	2.00	1.58 ± 0.50	2.00	2.00 ± 0.00	2.00	1.88 ± 0.33
7	18	0.9103	0.8828 ± 0.03	2.00	1.90 ± 0.31	2.00	1.96 ± 0.20	2.00	1.90 ± 0.31
7	17	0.9073	0.8843 ± 0.02	2.00	1.81 ± 0.39	2.00	1.96 ± 0.20	2.00	1.81 ± 0.39
7	16	0.9115	0.8874 ± 0.02	2.00	2.00 ± 0.00	2.00	1.88 ± 0.33	2.00	1.83 ± 0.38
7	15	0.9075	0.8899 ± 0.01	2.00	1.60 ± 0.49	2.00	1.98 ± 0.14	2.00	1.98 ± 0.14
7	14	0.9041	0.8899 ± 0.01	1.50	1.50 ± 0.51	2.00	2.00 ± 0.00	2.00	1.92 ± 0.28
7	13	0.9073	0.8876 ± 0.01	2.00	1.65 ± 0.48	2.00	1.98 ± 0.14	2.00	1.94 ± 0.24
7	12	0.9103	0.8929 ± 0.01	2.00	1.90 ± 0.31	2.00	1.98 ± 0.14	2.00	1.90 ± 0.31
7	11	0.9081	0.8924 ± 0.01	2.00	1.92 ± 0.28	2.00	1.83 ± 0.38	2.00	1.94 ± 0.24
7	10	0.9090	0.8887 ± 0.01	2.00	2.00 ± 0.00	2.00	1.94 ± 0.24	2.00	1.90 ± 0.31
7	9	0.9036	0.8907 ± 0.01	1.00	1.46 ± 0.50	2.00	2.00 ± 0.00	2.00	2.00 ± 0.00
7	8	0.9061	0.8913 ± 0.01	2.00	1.63 ± 0.49	2.00	2.00 ± 0.00	2.00	1.92 ± 0.28
7	7	0.9049	0.8897 ± 0.01	2.00	1.54 ± 0.50	2.00	1.98 ± 0.14	2.00	2.00 ± 0.00
7	6	0.9038	0.8884 ± 0.01	2.00	1.69 ± 0.47	2.00	2.00 ± 0.00	2.00	2.00 ± 0.00
7	5	0.9082	0.8885 ± 0.01	2.00	1.60 ± 0.49	2.00	1.96 ± 0.20	2.00	1.92 ± 0.28
7	4	0.9075	0.8844 ± 0.01	2.00	2.00 ± 0.00	2.00	2.00 ± 0.00	2.00	1.94 ± 0.24
7	3	0.8933	0.8611 ± 0.01	2.00	1.98 ± 0.14	2.00	1.94 ± 0.24	2.00	1.83 ± 0.38

Table 6.5 Performance of ANN-based NC-R g_s sub-models with seven input parameters. Listed results showing maximum, median and mean (± 1 S.D.) values represent 48 sub-models - differing in momentum and learning rate - per hidden neuron class.

Inputs	HN	Max. R² modelled vs. observed g_s	Mean R² ± S.D. modelled vs. observed g_s	Median sensitivity analysis	Mean ± S.D. sensitivity analysis	Median diurnal time course, sunny	Mean ± S.D. diurnal time course, sunny	Median diurnal time course, cloudy	Mean ± S.D. diurnal time course, cloudy
7	20	0.9278	0.8992 ± 0.01	1.00	1.17 ± 0.38	2.00	2.00 ± 0.00	1.00	1.33 ± 0.48
7	19	0.9218	0.9033 ± 0.01	1.00	1.04 ± 0.20	2.00	1.90 ± 0.31	2.00	1.56 ± 0.50
7	18	0.9135	0.9024 ± 0.01	1.00	1.06 ± 0.24	2.00	1.98 ± 0.14	2.00	1.54 ± 0.50
7	17	0.9315	0.9001 ± 0.01	1.00	1.15 ± 0.36	2.00	1.96 ± 0.20	1.00	1.19 ± 0.39
7	16	0.9288	0.9095 ± 0.01	1.00	1.15 ± 0.36	2.00	1.90 ± 0.31	1.50	1.50 ± 0.51
7	15	0.9239	0.9058 ± 0.01	1.00	1.29 ± 0.46	2.00	1.90 ± 0.31	2.00	1.52 ± 0.51
7	14	0.9172	0.9014 ± 0.01	1.00	1.25 ± 0.44	2.00	2.00 ± 0.00	1.00	1.21 ± 0.41
7	13	0.9340	0.9064 ± 0.01	1.00	1.15 ± 0.41	2.00	2.00 ± 0.00	1.00	1.13 ± 0.33
7	12	0.9250	0.9046 ± 0.01	1.00	1.08 ± 0.28	2.00	1.92 ± 0.28	1.00	1.42 ± 0.50
7	11	0.9156	0.9018 ± 0.01	1.00	1.04 ± 0.20	2.00	2.00 ± 0.00	1.00	1.02 ± 0.14
7	10	0.9096	0.9042 ± 0.00	1.00	1.06 ± 0.24	2.00	2.00 ± 0.00	1.00	1.08 ± 0.28
7	9	0.9277	0.9143 ± 0.01	1.00	1.06 ± 0.24	2.00	2.00 ± 0.00	1.00	1.13 ± 0.33
7	8	0.9213	0.9041± 0.01	2.00	1.52 ± 0.50	2.00	1.88 ± 0.33	1.00	1.27 ± 0.45
7	7	0.9301	0.9069 ± 0.01	1.00	1.02 ± 0.14	2.00	2.00 ± 0.00	1.00	1.46 ± 0.50
7	6	0.9158	0.9030 ± 0.01	1.00	1.19 ± 0.39	2.00	2.00 ± 0.00	1.00	1.02 ± 0.14
7	5	0.9261	0.9109 ± 0.01	1.00	1.35 ± 0.48	2.00	1.92 ± 0.28	2.00	1.58 ± 0.50
7	4	0.9203	0.9068 ± 0.00	2.00	1.75 ± 0.44	2.00	2.00 ± 0.00	2.00	1.75 ± 0.44
7	3	0.9190	0.9057 ± 0.01	1.00	1.38 ± 0.49	2.00	1.79 ± 0.41	2.00	1.56 ± 0.50

Table 6.6   Performance of ANN-based NC-SR g_s sub-models with seven input parameters. Listed results showing maximum, median and mean (± 1 S.D.) values represent 48 sub-models - differing in momentum and learning rate - per hidden neuron class.

Inputs	HN	Max. R² modelled vs. observed g_s	Mean R² ± S.D. modelled vs. observed g_s	Median sensitivity analysis	Mean ± S.D. sensitivity analysis	Median diurnal time course, sunny	Mean ± S.D. diurnal time course, sunny	Median diurnal time course, cloudy	Mean ± S.D. diurnal time course, cloudy
7	25	0.8714	0.8283 ± 0.05	2.00	1.96 ± 0.20	2.00	2.00 ± 0.00	2.00	1.96 ± 0.20
7	24	0.8724	0.8322 ± 0.05	2.00	1.71 ± 0.46	2.00	1.96 ± 0.20	2.00	1.88 ± 0.33
7	23	0.8751	0.8351 ± 0.05	2.00	1.65 ± 0.48	2.00	1.96 ± 0.20	2.00	1.83 ± 0.38
7	22	0.8658	0.8362 ± 0.03	2.00	1.81 ± 0.39	2.00	1.98 ± 0.14	2.00	1.98 ± 0.14
7	21	0.8715	0.8381 ± 0.04	2.00	1.96 ± 0.20	2.00	2.00 ± 0.00	2.00	1.96 ± 0.20
7	20	0.8720	0.8417 ± 0.03	2.00	1.79 ± 0.41	2.00	1.96 ± 0.20	2.00	1.96 ± 0.20
7	19	0.8722	0.8455 ± 0.03	2.00	1.52 ± 0.50	2.00	2.00 ± 0.00	2.00	2.00 ± 0.00
7	18	0.8642	0.8422 ± 0.03	2.00	1.63 ± 0.49	2.00	1.96 ± 0.20	2.00	1.83 ± 0.38
7	17	0.8681	0.8465 ± 0.02	2.00	1.92 ± 0.28	2.00	2.00 ± 0.00	2.00	1.79 ± 0.41
7	16	0.8709	0.8483 ± 0.02	2.00	1.96 ± 0.20	2.00	1.98 ± 0.14	2.00	1.96 ± 0.20
7	15	0.8676	0.8484 ± 0.02	2.00	1.94 ± 0.24	2.00	1.98 ± 0.14	2.00	1.90 ± 0.31
7	14	0.8710	0.8567 ± 0.01	2.00	1.65 ± 0.48	2.00	2.00 ± 0.00	2.00	1.98 ± 0.14
7	13	0.8697	0.8556 ± 0.01	2.00	1.75 ± 0.44	2.00	2.00 ± 0.00	2.00	1.94 ± 0.24
7	12	0.8700	0.8548 ± 0.01	2.00	1.71 ± 0.46	2.00	2.00 ± 0.00	2.00	1.88 ± 0.33
7	11	0.8729	0.8537 ± 0.01	2.00	1.54 ± 0.50	2.00	2.00 ± 0.00	2.00	1.81 ± 0.39
7	10	0.8692	0.8555 ± 0.01	2.00	1.98 ± 0.14	2.00	2.00 ± 0.00	2.00	1.98 ± 0.14
7	9	0.8707	0.8581 ± 0.01	2.00	1.94 ± 0.24	2.00	2.00 ± 0.00	2.00	1.96 ± 0.20
7	8	0.8701	0.8571 ± 0.01	2.00	1.98 ± 0.14	2.00	2.00 ± 0.00	2.00	1.98 ± 0.14
7	7	0.8709	0.8559 ± 0.01	1.00	1.46 ± 0.50	2.00	2.00 ± 0.00	2.00	1.98 ± 0.14
7	6	0.8654	0.8515 ± 0.01	2.00	1.60 ± 0.49	2.00	2.00 ± 0.00	2.00	1.98 ± 0.14
7	5	0.8640	0.8524 ± 0.01	2.00	2.00 ± 0.00	2.00	2.00 ± 0.00	2.00	1.92 ± 0.28
7	4	0.8621	0.8513 ± 0.01	2.00	1.90 ± 0.31	2.00	2.00 ± 0.00	2.00	1.85 ± 0.36
7	3	0.8602	0.8424 ± 0.01	2.00	1.92 ± 0.28	2.00	2.00 ± 0.00	2.00	1.52 ± 0.50

The sensitivity analysis and application of models to diurnal time-courses revealed however that high R^2 values of the comparison between predicted and observed g_s rates were not a guarantee for good results when applying the models to mean observed (sensitivity analysis) or external, previously unseen data (diurnal-time courses) – the latter as opposed to unseen data that had been prior to the training of the ANNs extracted from the input dataset and were used for the comparison between predicted and observed g_s data.

The results of the sensitivity analyses indicated the best performance with eight, seven and seven hidden neurons for the NC-S, NC-R and NC-SR sub-models, respectively. The application of the sub-models to diurnal time-courses of meteorological and O_3 data proved to be less successful, with most of the NC-S, NC-R and NC-SR sub-models struggling to predict realistic g_s rates for the sunny day. The cloudy day course was in particular a challenge for the NC-S and NC-SR sub-models, while most NC-R sub-models performed better here.

Interestingly, when considering the combined performance of all evaluation methods described above in order to select three sub-models that would function as the final NC-S, NC-R and NC-SR models, three sub-models with high numbers of hidden neurons performed best: 1) NC-S model with 20 hidden neurons, a learning rate of 0.4 and a momentum of 0.6, 2) NC-R model with 19 hidden neurons, a learning rate of 0.2 and a momentum of 0.6, and 3) NC-SR model with 24 HN hidden neurons, a learning rate of 0.5 and a momentum of 0.7.

The performance of these three models in terms of the direct comparison between predicted and observed g_s data, the diurnal time course test (sunny and cloudy day) and the sensitivity analysis are shown in Figures 6.5, 6.6 – 6.8 and 6.9, respectively.

The R^2 values of the comparison of predicted and observed g_s are equally high for all three models. All three models predict slightly lower g_s rates in direct comparison with observed g_s rates.
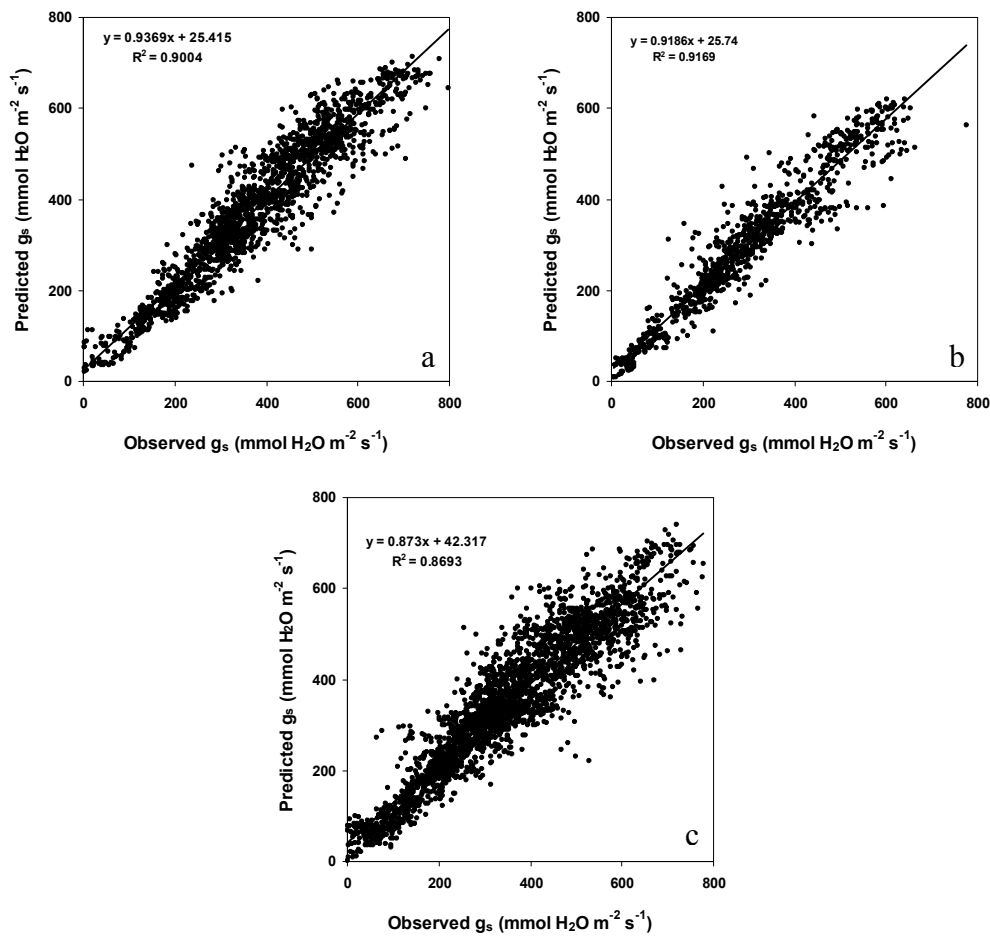
Figure 6.5   Predicted versus observed g_s for the NC-S (a), NC-R (b) and NC-SR (c) models with 7 input parameters and 20, 19 and 24 hidden neurons, respectively. The observed data represent 20 % of measured input dataset randomly extracted from input dataset prior to training of ANNs.

The application of the three models to diurnal time courses of a sunny and a cloudy day (Figures 6.6 – 6.8) reveal the general ability of all models to quickly react to a change in PAR and air temperature over the course of a day. The same was true for the relationship between g_s and VPD, which was closely correlated to the air temperature and is not shown here. In terms of the sunny day, all models however showed some scattering in the morning hours. In general, the NC-R model predicted the lowest, the NC-S model the highest rates of g_s.
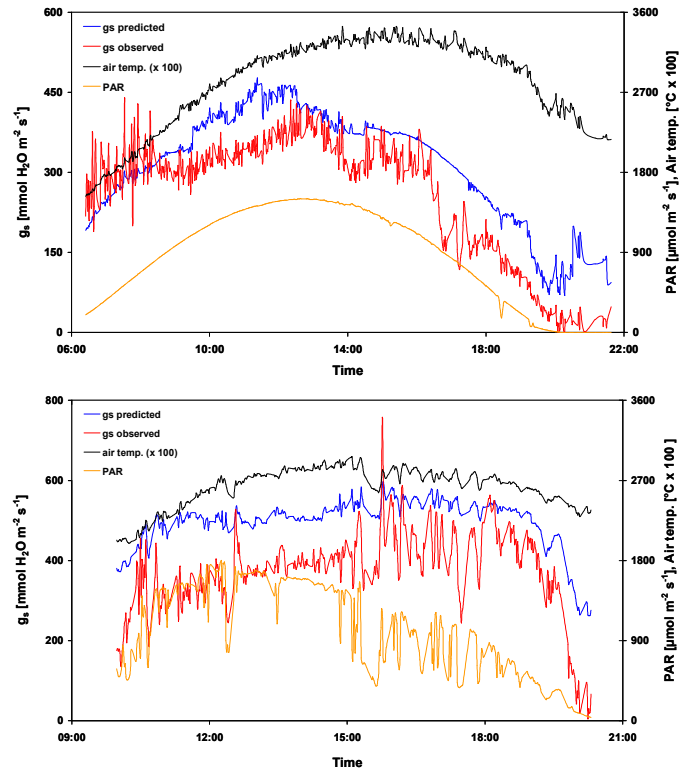
Figure 6.6   Diurnal time-course of modelled g_s using NC-S model with 7 inputs and 20 hidden neurons on a sunny (08.08.98, top) and cloudy day (14.08.00, bottom) in comparison with measured air temperature and PAR.
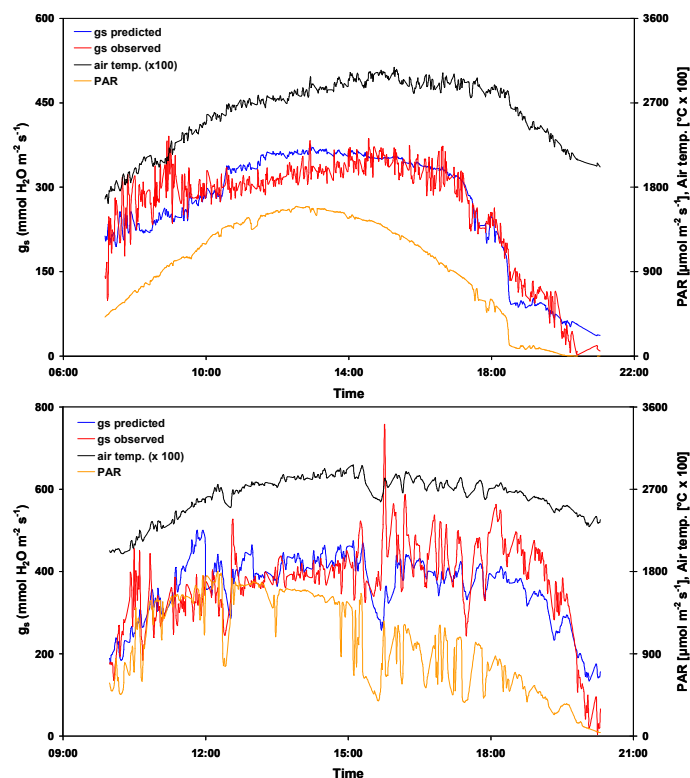
Figure 6.7   Diurnal time-course of modelled g_s using NC-R model with 7 inputs and 19 hidden neurons on a sunny (07.08.98, top) and cloudy day (14.08.00, bottom) in comparison with measured air temperature and PAR.
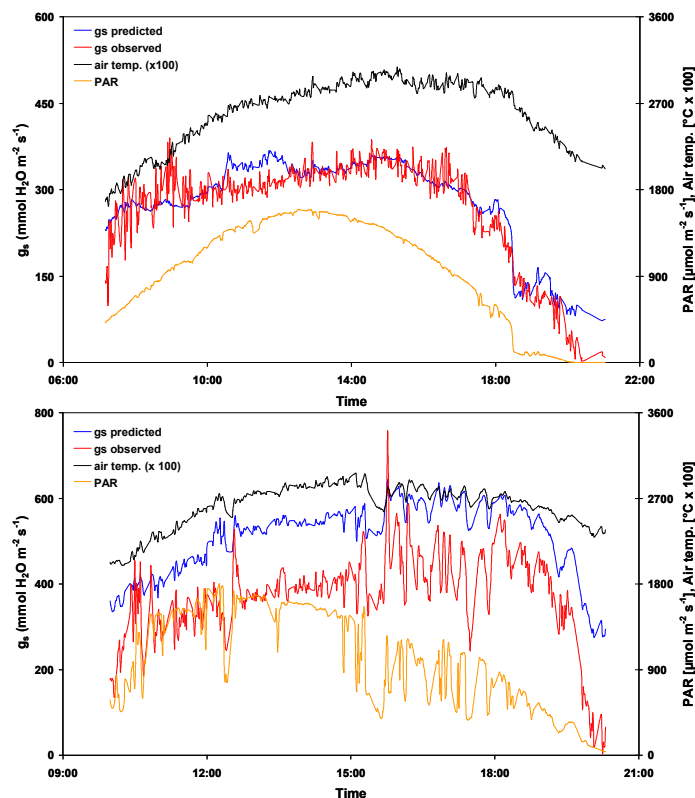
Figure 6.8   Diurnal timecourse of modelled g_s using NC-SR model with 7 inputs and 24 hidden neurons on a sunny (07.08.98, top) and cloudy day (14.08.00, bottom) in comparison with measured air temperature and PAR.

The sensitivity analyses revealed in general physiologically sensible and expected relationships between predicted g_s of all three models and air temperature, VPD and PAR (Figure 6.9 a - c). Precisely, g_s increases with increasing air temperature until approx. 30 °C, above which the curves shown in Figure 6.9 slowly reach a plateau, and decreases with increasing VPD from approximately 0.5 kPa upwards until reaching constant minimum conditions above approximately 2.5 kPa. The dependency of g_s on PAR is slightly unexpected, because it suggests an increase in g_s with increasing PAR until only approximately 500 to 750 µmol m^{-2} s^{-1}, where a low maximum of approx. 300 to 400 mmol H$_2$O m^{-2} s^{-1} is predicted with all models (lowest rate for NC-S model). This indicates that when keeping all other input parameters at their mean, no light-saturated rates for g_s could be predicted.

The exposure time effect curve (Figure 6.9 d) showed a decrease in g_s with increasing exposure time for the NC-S and NC-SR model, but failed to do so for the NC-R model. The relationship between O$_3$ concentration and g_s was meaningless (Figure 6.9 e), indicating that this parameter was not contributing to the prediction of g_s.
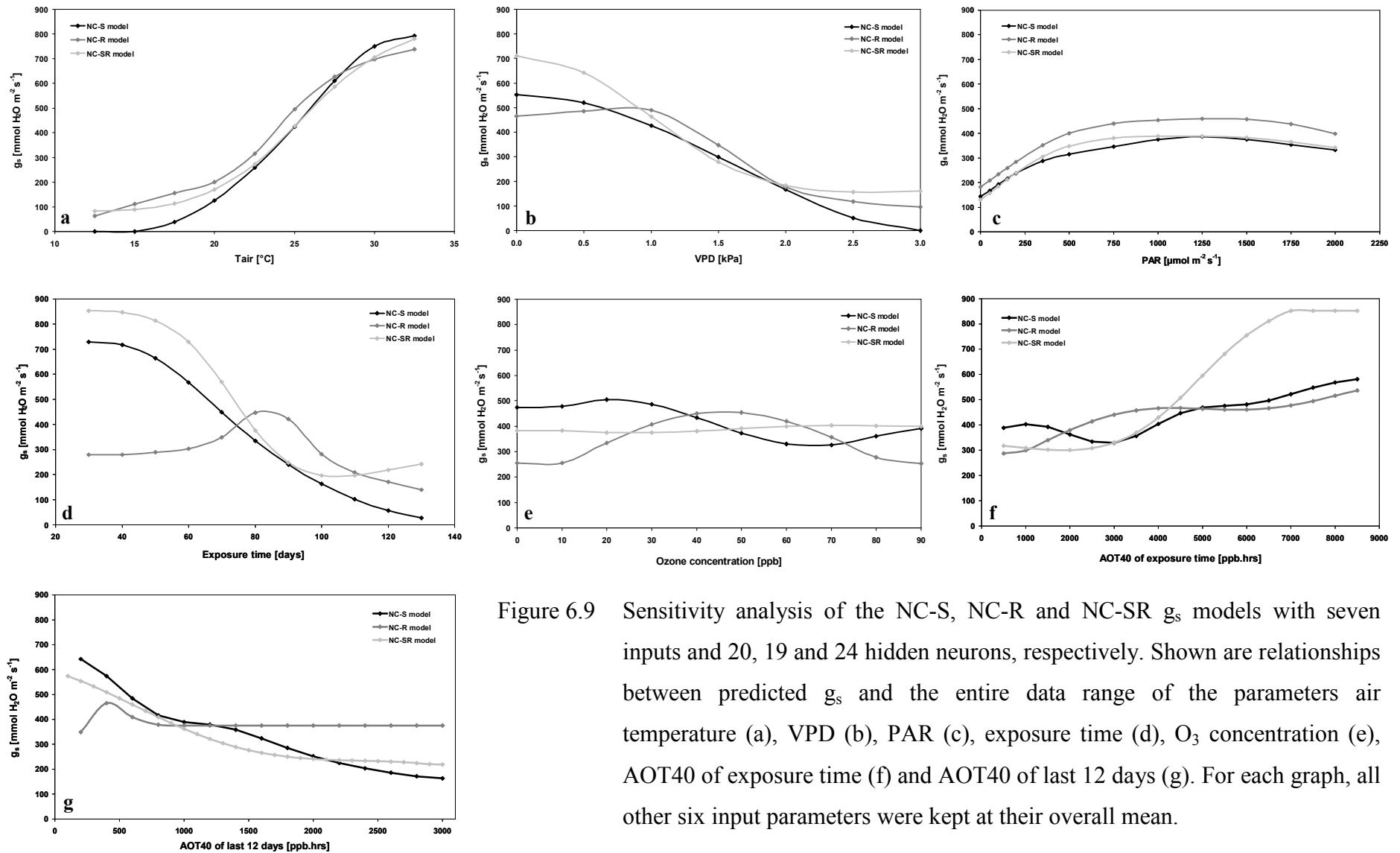
Figure 6.9   Sensitivity analysis of the NC-S, NC-R and NC-SR g_s models with seven inputs and 20, 19 and 24 hidden neurons, respectively. Shown are relationships between predicted g_s and the entire data range of the parameters air temperature (a), VPD (b), PAR (c), exposure time (d), O_3 concentration (e), AOT40 of exposure time (f) and AOT40 of last 12 days (g). For each graph, all other six input parameters were kept at their overall mean.

Unexpectedly, the NC-SR model predicted an increase in the g_s rate with increasing AOT40 of exposure time, while this effect was much less pronounced for the NC-S and NC-R models (Figure 6.9 f). The relationship between g_s and the AOT40 of the last 12 days was less clear, with a slight trend of a decreasing g_s with increasing AOT40 (Figure 6.9 g).

The analysis of the contribution of each input parameter in predicting g_s with the ANN-based NC-S, NC-R and NC-SR g_s models are shown in Table 6.7. This analysis gave varying results depending on which model was tested and whether the connection weights approach or the internal weighting tool of the ANN software NeuroShell was used. Since the former approach is well established and the NeuroShell manual does not explain how the latter approach actually works, it was decided to put more weight in the outcome of the connection weights approach. It showed in general a strong contribution of air temperature, as well as – to a slightly lesser extent - VPD and the AOT40 of the exposure time. In contrast and in agreement with the NeuroShell weighting tool, O_3 concentration was exposed as having in general little influence on the prediction of g_s, as well as the AOT40 of the last 12 days. This finding corresponded well with the results of the sensitivity analysis, which showed indifferent effect-curves for these two parameters.

Table 6.7   Ranking of input parameters describing their contribution to the prediction of g_s with the NC-S, NC-R and NC-SR model. Shown are the results of the connection weights approach and the internal weighting tool of the ANN software NeuroShell.

	Ranking connection weights			Ranking NeuroShell 2		
	NC-S	NC-R	NC-SR	NC-S	NC-R	NC-SR
Exposure time	4	3	2	5	6	2
Air temperature	1	1	3	1	2	3
PAR	6	6	7	4	4	5
VPD	3	4	1	3	1	7
O_3 concentration	5	7	4	7	7	6
AOT40 exp. time	2	2	5	2	5	1
AOT40 12 days	7	5	6	6	3	4

Based on these result, which were comparable to a simple pruning process, the parameters O_3 concentration and AOT40 of last 12 days were excluded and all three models were further developed with only five input parameters, since the main aim was to develop simple models, i.e. models with the lowest amount of hidden neurons and input parameters that could still predict the complex relationship between g_s and available input parameters. Although PAR did not contribute a lot to the prediction of g_s either, it was thought to be a key environmental variable driving g_s and was therefore not considered for exclusion.
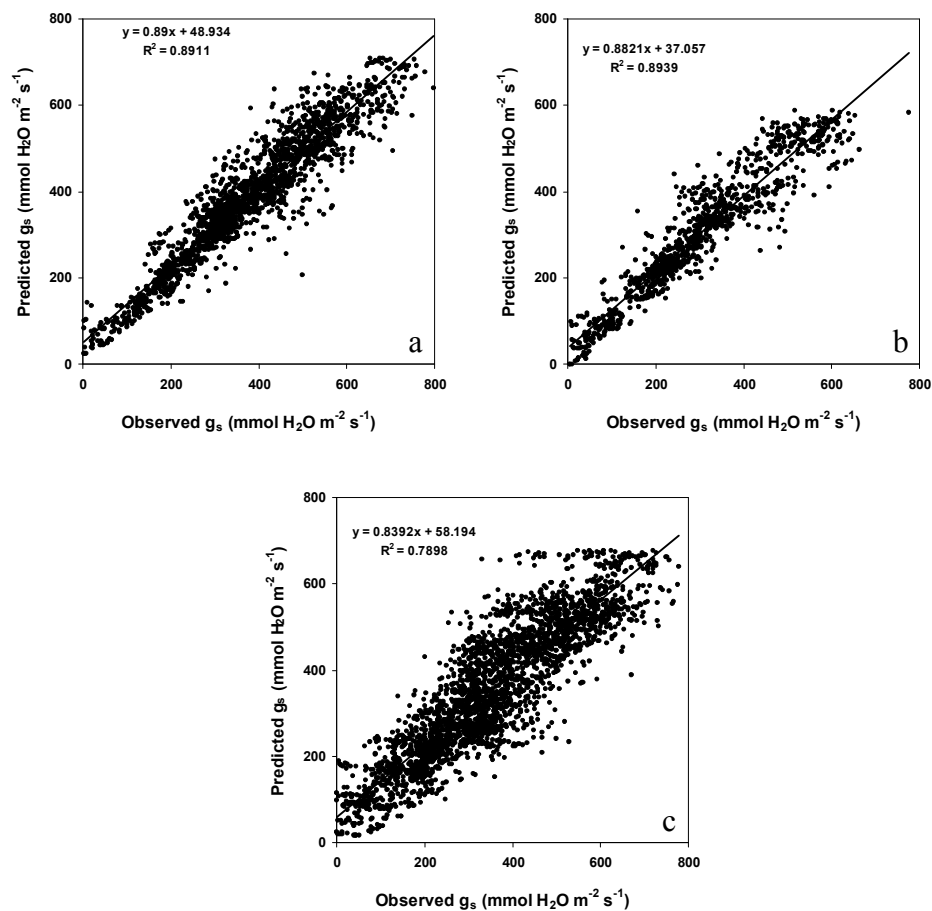
Figure 6.10   Predicted versus observed g_s for the NC-S (a), NC-R (b) and NC-SR (c) models with 5 input parameters and 18, 19 and 19 hidden neurons, respectively. The observed data represent 20 % of the measured data randomly extracted from the total dataset prior to the training of ANNs.

The same procedures as described above for the models with seven input parameters were applied in finding the best NC-S, NC-R and NC-SR models out of the vast pool

of available sub-models differing in number of hidden neurons, learning rate and momentum. This resulted in the final "five input models" with 18, 19 and 19 hidden neurons, learning rates of 0.2, 0.05 and 0.4 and momentums of 0.6, 0.7 and 0.5 for the NC-S, NC-R and NC-SR models, respectively.

The predictive performance of the final "five input models" did not drop substantially in comparison with the initial "seven input models" (from R^2 values of 0.90 to 0.89, 0.92 to 0.89 and 0.87 to 0.79 for the NC-S, NC-R and NC-SR model, respectively; Figures 6.5 and 6.10). The omission of the two parameters listed above was therefore believed to be justifiable and indeed desirable, since it led to simpler but equally meaningful models.
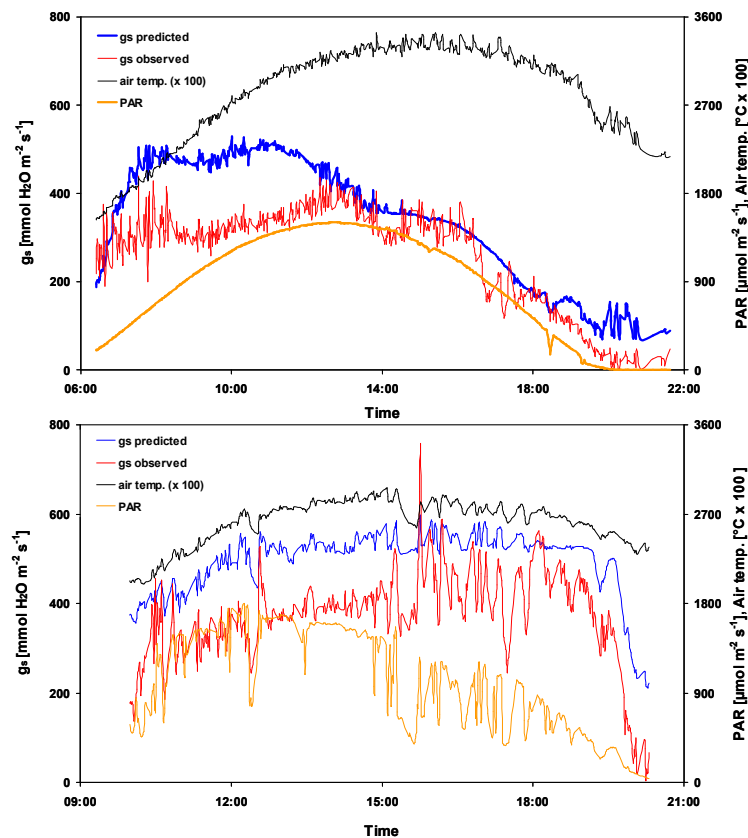
Figure 6.11   Diurnal time-course of modelled g_s using the NC-S model with five inputs and 18 hidden neurons on a sunny (08.08.98, top) and cloudy day (14.08.00, bottom) in comparison with measured air temperature and PAR. For reasons of comparison, the time curves of g_s of a NC-R clover clone measured on these days are also shown.

The application of the selected final models to diurnal time courses of a sunny and a cloudy day is depicted in Figures 6.11 to 6.13. All three models performed reasonably well in predicting the diurnal time course of the cloudy day, demonstrated by their ability to react to changes in PAR and temperature over the course of the day. Regarding the sunny day, all three models performed well in the afternoon, but showed in relation to the prevailing weather unexpected high rates of g_s in the morning hours. However, the also presented measured g_s rates (though from the contrasting clone – see Chapter 6.2.3) showed similar scatter in the morning hours, i.e. the models probably only reflected the unstable relationship between g_s and climate variables that is contained in the input dataset the ANNs were trained with.
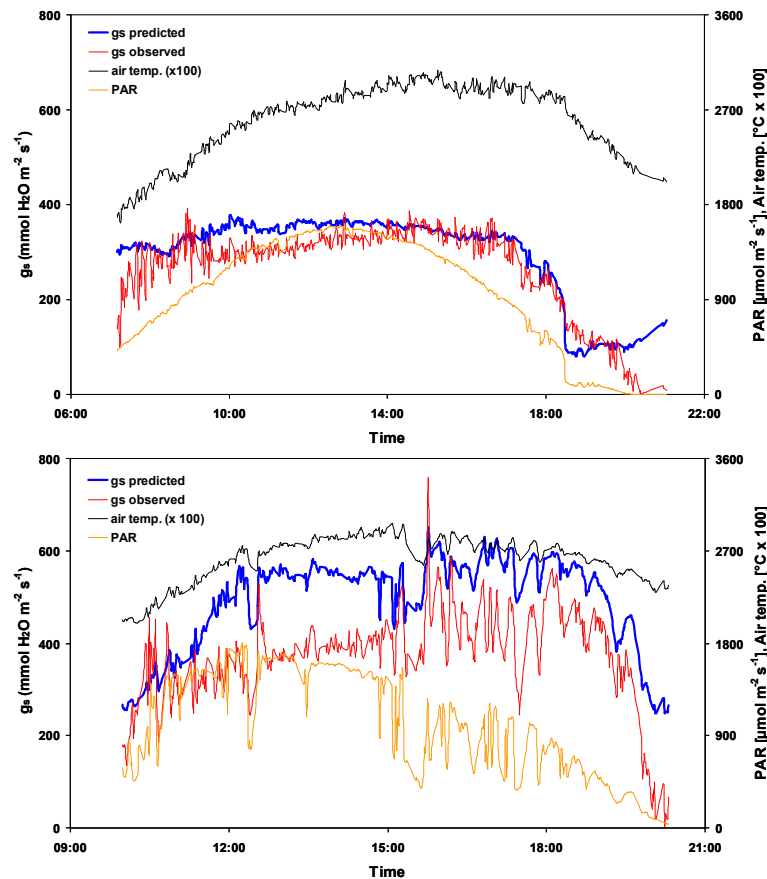
Figure 6.12   Diurnal time-course of modelled g_s using the NC-R model with five inputs and 19 hidden neurons on a sunny (07.08.98, top) and cloudy day (14.08.00, bottom) in comparison with measured air temperature and PAR. For reasons of comparison, a time curve of g_s of the NC-R clover clone measured on that day is also shown.
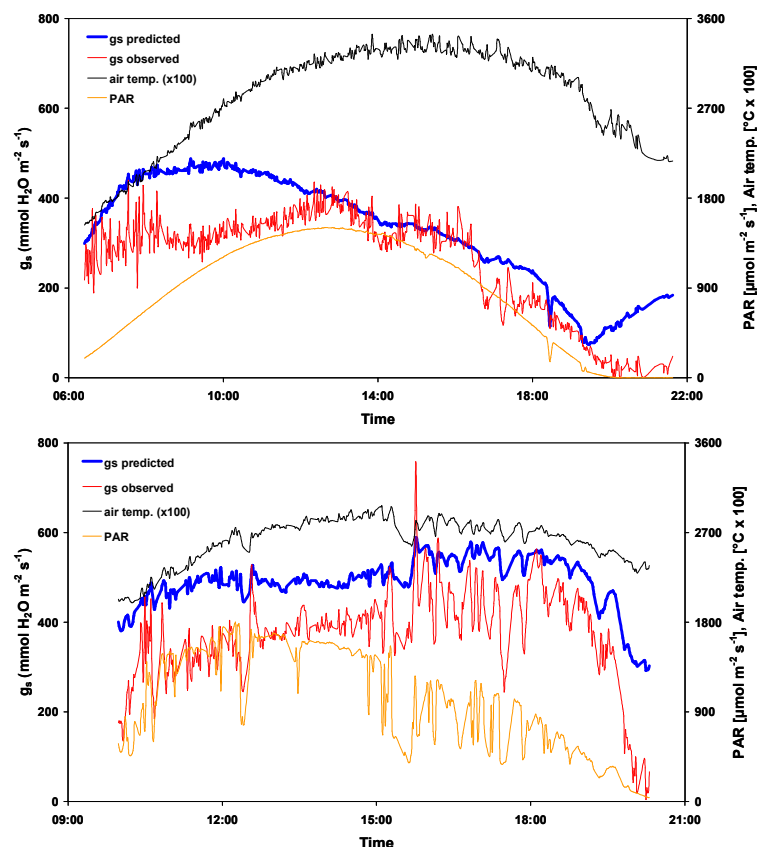
Figure 6.13 Diurnal time-course of modelled g_s using the NC-SR model with five
inputs and 19 hidden neurons on a sunny (08.08.98, top) and cloudy day
(14.08.00, bottom) in comparison with measured air temperature and
PAR. For reasons of comparison, a time curve of g_s of the NC-R clover
clone measured on that day is also shown.

Furthermore, the diurnal time courses of g_s indicate the general difficulties of the
models in predicting g_s for low light or indeed night-time conditions - all g_s curves for
instance show a substantial increase after the sunset on the sunny day. This is mainly
a problem linked with the limited ability of ANNs to extrapolate and the fact that the
input dataset only included very few low-light or night-time g_s measurements.

Since the night-time conditions have to be accounted for when calculating O_3 fluxes
for entire 28 day clover growing periods, an assumption for low light and night-time
g_s rates had to be made. It was therefore decided to presume a constant clone-specific
rate of g_s for PAR < 50 µmol m^{-2} s^{-1} and 50 µmol m^{-2} s^{-1} < PAR < 100 µmol m^{-2} s^{-1},
derived from the mean of the above mentioned measurements carried out in emerging

or full darkness (for the NC-SR model the mean of the combined measurements of both clones was calculated). These rates are listed in Table 6.8.

Table 6.8 Assumed constant low-light and night-time g_s rates (mmol H_2O m^{-2} s^{-1}) for the NC-S, NC-R and NC-SR models derived from g_s measurements on both clover clones for PAR < 50 µmol m^{-2} s^{-1} and 50 µmol m^{-2} s^{-1} < PAR < 100 µmol m^{-2} s^{-1}. The value for the NC-SR model is based on the pooled g_s measurements of both clones.

	g_{snight} (mmol H_2O m^{-2} s^{-1}) for PAR < 50 µmol m^{-2} s^{-1}	$g_{slowlight}$ (mmol H_2O m^{-2} s^{-1}) for 50 µmol m^{-2} s^{-1} < PAR < 100 µmol m^{-2} s^{-1}
NC-S model	110	39
NC-R model	52	17
NC-SR model	89	33

As for the "seven input models", the sensitivity analysis of the final three "five input models" revealed in general physiologically sensible and expected relationships between predicted g_s and air temperature and VPD (Figure 6.14 a - c). Again, the PAR effect curves reached their low maximum of 200 to 400 mmol H_2O m^{-2} s^{-1} early at 500 to 750 µmol m^{-2} s^{-1} PAR. The relationships between g_s and exposure time as well as AOT40 of the exposure time were less stable, but there was in general the trend that g_s decreased from approximately day 70 of exposure and increased with AOT40 of the exposure time until approximately 3500 ppb.hrs, after which this increase slowed down.
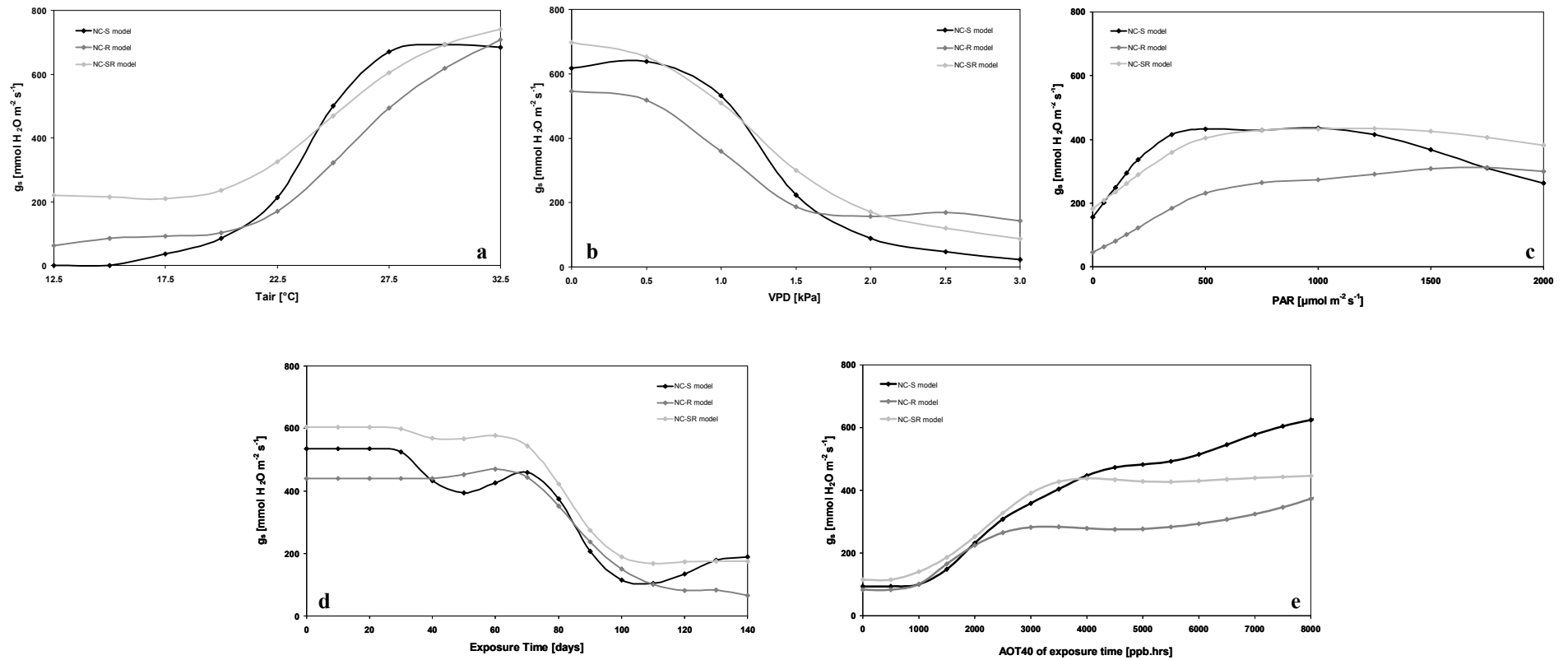
Figure 6.14 Sensitivity analysis of the NC-S, NC-R and NC-SR g_s models with five inputs and 18, 19 and 19 hidden neurons, respectively. Shown are relationships between predicted g_s and the entire data range of the parameters air temperature (a), VPD (b), PAR (c), exposure time (d) and AOT40 of exposure time (e). For each graph, all other four input parameters were kept at their overall mean.

The analysis of the contribution of each input parameter in predicting g_s with the ANN-based NC-S, NC-R and NC-SR g_s models are shown in Table 6.9. It gave again differing results depending on to the applied approach. The connection weights approach was believed to give the more reliable and realistic information (see above). It showed in general the strong contribution of air temperature and VPD as well as the low contribution of PAR in predicting g_s.

Table 6.9   Ranking of input parameters describing their contribution to the prediction of g_s with the NC-S, NC-R and NC-SR model. Shown are the results of the connection weights approach and the internal weighting tool of the ANN software NeuroShell.

	Ranking connection weights			Ranking NeuroShell 2		
	NC-S	NC-R	NC-SR	NC-S	NC-R	NC-SR
Exposure time	4	4	2	2	5	3
Air temperature	1	2	3	5	3	1
PAR	5	3	5	4	2	4
VPD	3	1	1	3	1	2
AOT40 exp. time	2	5	4	1	4	5

Based on the analysis of further exclusion of input parameters which all led to a substantially lower performance of the models in predicting g_s (data not shown), it was decided that the models with the five input parameters air temperature, VPD, PAR, exposure time and AOT40 of exposure time were the best choice for predicting O_3 fluxes to white clover. Accordingly, when in the following talking of the NC-S, NC-R or NC-SR model, this is always referring to the models with five input parameters described above.

7   Application of stomatal conductance and flux models

7.1   Application of g_s models to measured time-series data

The final three ANN-based g_s models were applied to datasets comprising of the main meteorological parameters and the O_3 concentration. These datasets covered five years of growing seasons of five months each at three experimental sites. Due to the vast amount of predicted g_s data, the following figures of seasonal courses of g_s rates are shown exemplary for all other growing seasons, years, sites and g_s models.

Figure 7.1 shows the time-courses of the air temperature, VPD, global radiation and predicted g_s of the sensitive clover clone using the NC-S model at the site Trier-University during growing periods 2 to 4 in 1997. Low g_s rates (here expressed as g_s to O_3) were predicted for hot and dry weather periods characterised by high VPD rates (e.g. 7th to 19th of August) despite the fact that these periods also showed the highest reported PAR values. The model predicted maximum rates of g_s of up to 420 mmol O_3 m^{-2} s^{-1} (i.e. approximately 690 mmol H_2O m^{-2} s^{-1}) for fairly hot but humid weather conditions, for example on August 2nd and 3rd. In contrast, the cold spell in late June with daily maximum temperatures of 15 to 17 °C led to relatively low g_s rates, indicating the overall strong dependence of the predicted g_s on air temperature.

When comparing the performance of the three different models applied to growing period 4 in 1997 at the site Trier-University (Figure 7.2), the differences in the range of predicted g_s become clear. While all three models react to the period of high VPD at the beginning of growing period 4 with reduced g_s - reflecting the closure of stomata to prevent excessive transpirational loss -, the predicted rates of g_s are always higher for the NC-S clone in relation to those of the NC-R clone. This is valid during dry and hot (beginning of August 1997) as well as during humid and cooler (end of August 1997) weather periods. The g_s rates predicted with the NC-SR model are in general closer to the rates predicted with the NC-S rather than the NC-R model.
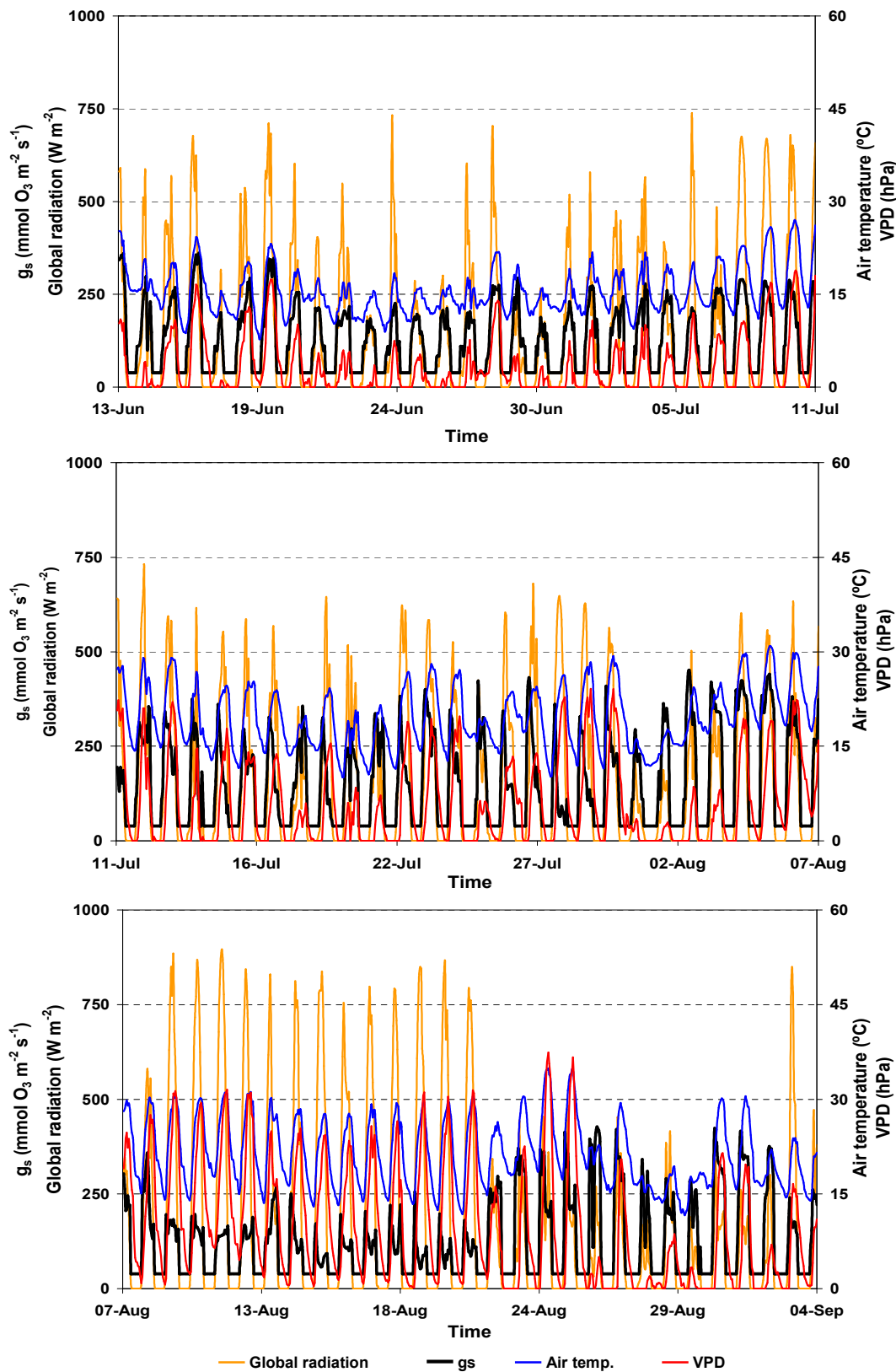
Figure 7.1   Seasonal time-courses (hourly means) of air temperature, VPD, global radiation and predicted g_s of the sensitive clover clone using the NC-S model. Shown are the central growing periods 2 to 4 at the site Trier-University in 1997.
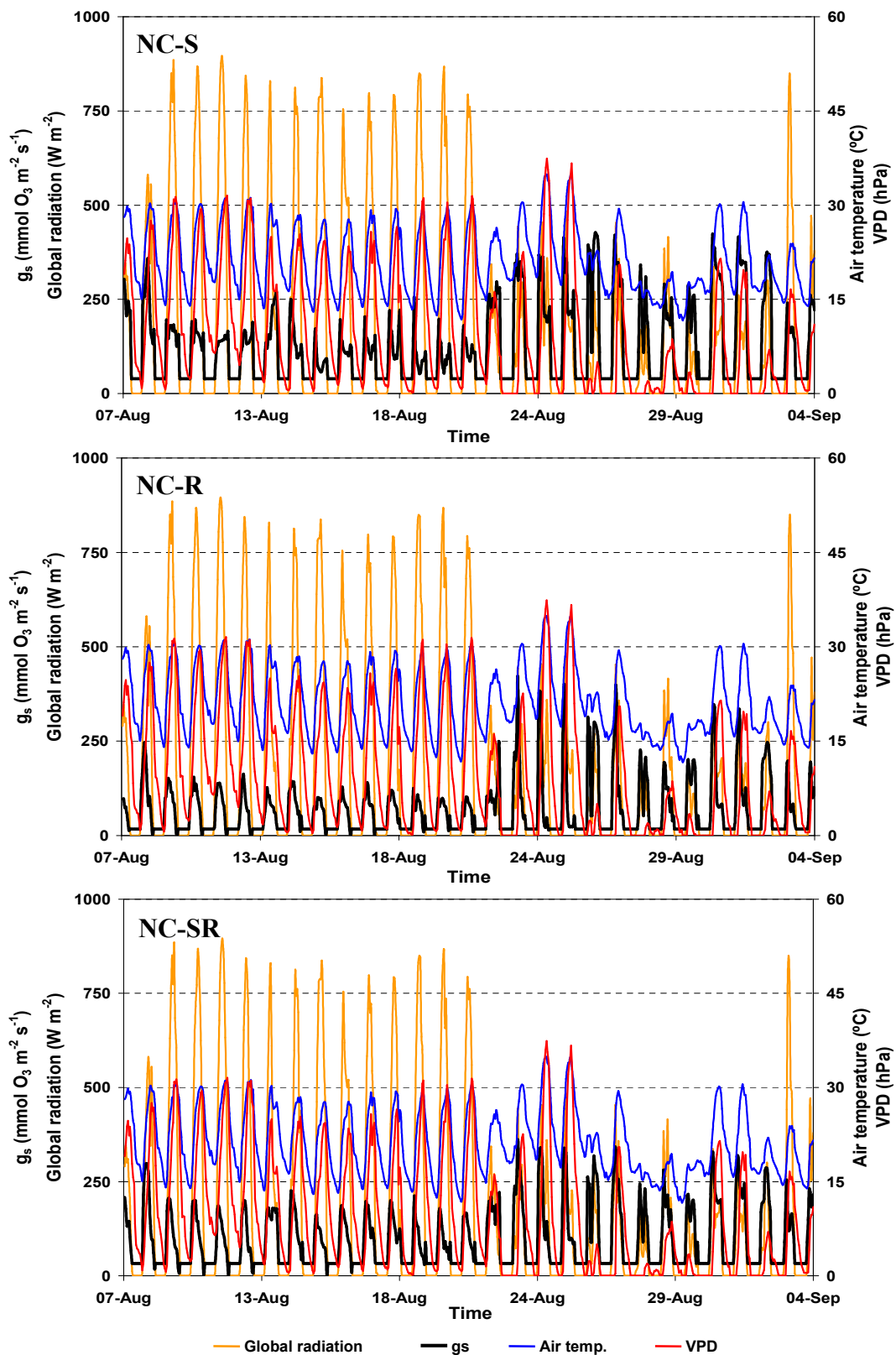
Figure 7.2 Seasonal time-courses (hourly means) of air temperature, VPD, global radiation and predicted g_s of the NC-S, NC-R and a hypothetical "intermediate" clover clone using the NC-S, NC-R and NC-SR model, respectively. Shown is growing period 4 at the site Trier-Univ. 1997.

All three models also proved to be able to account for various climate conditions, represented in Figure 7.3 by the three experimental sites. For instance, during the hot and dry weather period at the beginning of August, the VPD was much lower in Deuselbach as compared to the two other sites, resulting in higher g_s rates predicted for the NC-S clone in Deuselbach. The less extreme and lower range of climate conditions recorded in Deuselbach during growing period 4 in 1997 resulted in general in a more even curve of predicted g_s as compared to the other sites.

Figure 7.4 presents the 28-days average g_s rates for all growing periods of all years at each site, calculated with the NC-S, NC-R and NC-SR models. It is obvious that on average the NC-R model always predicted the lowest g_s rates, indicating that the ozone-resistant clover clone seems to have a lower gas exchange than the NC-S clone. In comparison with the two other sites, the highest g_s rates were in general predicted for Deuselbach, probably due to the usually more humid and therefore less g_s-limiting weather conditions there. 1997 was the year with the highest average g_s rates, probably due to long spells of warm **and** humid weather, while the analysis of seasonal variations in g_s rates does not reveal clear trends: In some years highest average g_s rates have been predicted for the beginning of the growing season, while in other years the middle or the end of the growing season showed the highest average g_s rates. This indicates that the prevailing climate clearly dominates the g_s rate, rather than the phenological stage (expressed in the model as exposure time) of the clover clone plants.
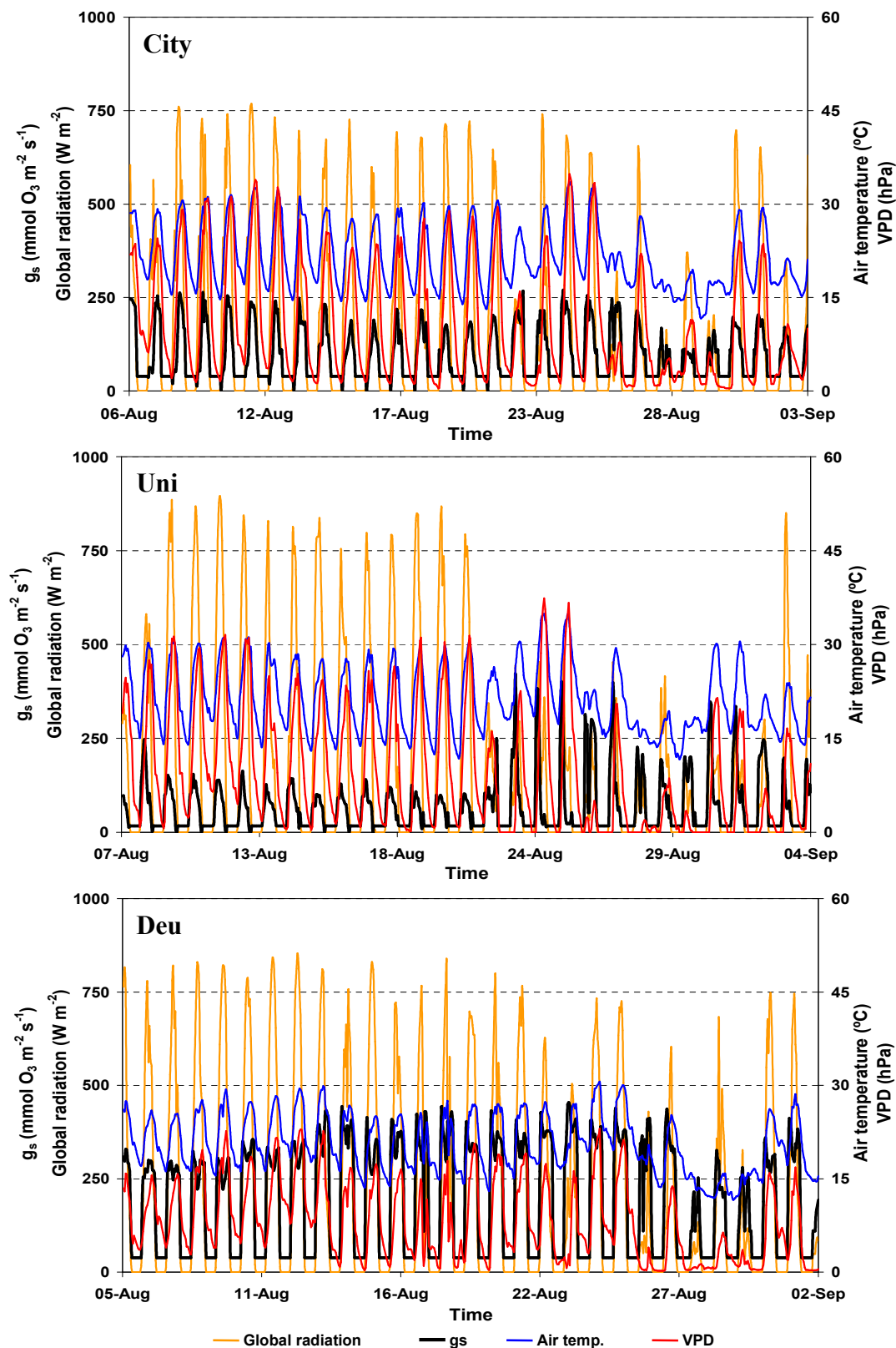
Figure 7.3   Seasonal time-courses (hourly means) of air temperature, VPD, global radiation and predicted g_s of the ozone-sensitive clover clone using the NC-S model at the sites Trier-City, Trier-University and Deuselbach. Shown is growing period 4 in 1997.
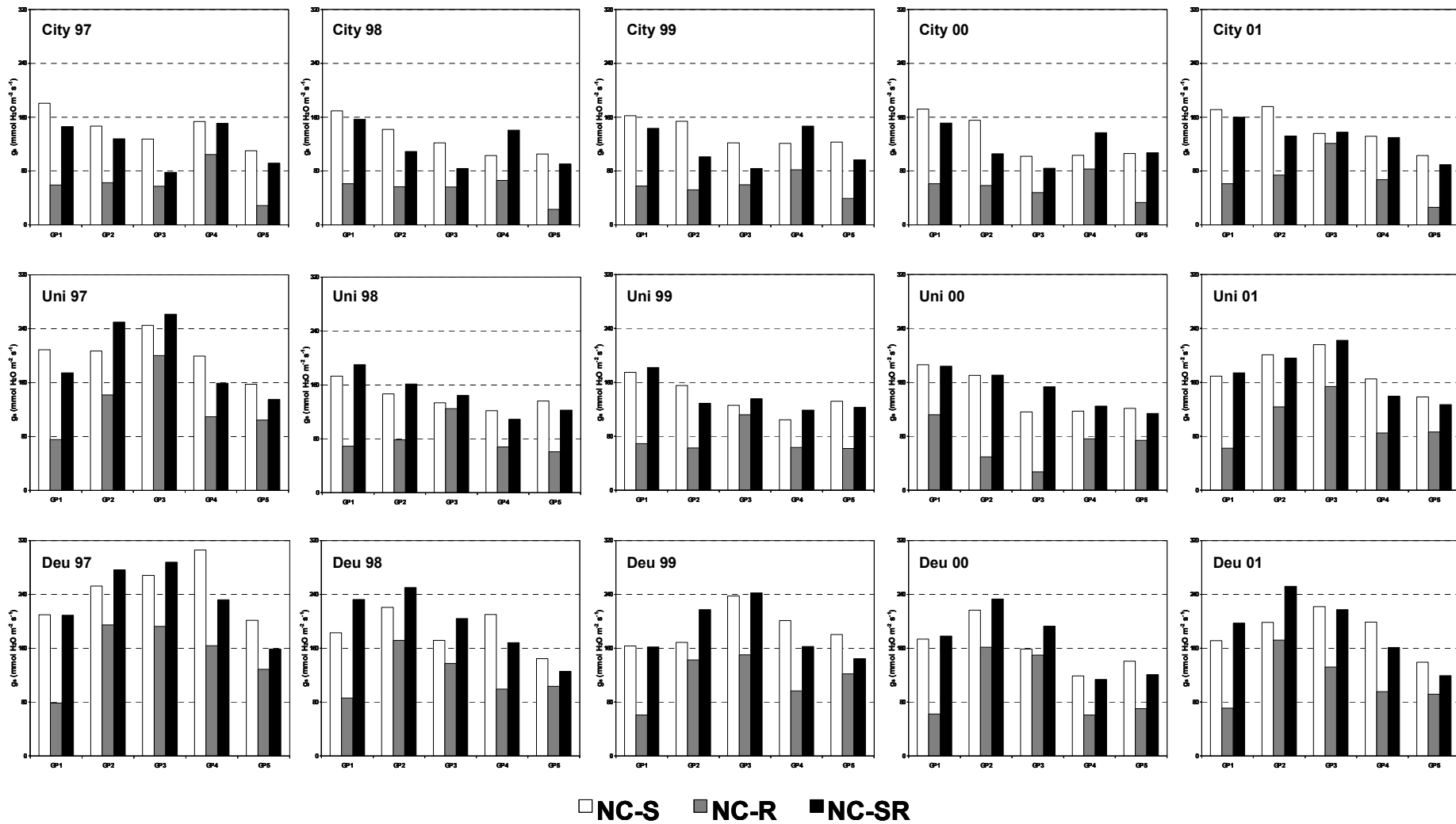
Figure 7.4   Average g_s rates predicted for the five growing periods of the years 1997 to 2001 at the sites Trier-City, Trier-University and Deuselbach with help of the ANN-based NC-S, NC-R and NC-SR g_s models.

7.2   Calculation of ozone fluxes

O_3 fluxes were calculated according to the methods described in Chapter 3.5. The main drivers of these calculations are the modelled g_s described in the previous chapter and the O_3 concentration at the canopy height. The flux calculations covered five years of growing seasons of five months each at the three experimental sites, using g_s rates modelled with the NC-S, NC-R or the NC-SR model. Similar to the presentation of the results in Chapter 7.1, the vast amount of calculated O_3 flux data made it necessary to show figures of time-series of calculated O_3 fluxes exemplary for all growing seasons, years, sites and g_s models.

Figure 7.5 presents the comparison of seasonal changes of O_3 fluxes calculated with the output of the NC-S, NC-R and NC-SR g_s models. Since all three graphs represent the same site (Trier-University, 1997), the recognisable differences in AFst0 are all based on the differences in g_s rates calculated with different g_s models. Accordingly, the accumulated O_3 fluxes based on NC-S model predictions are higher than fluxes calculated with the output of the NC-R g_s model, indicating higher O_3 fluxes into the NC-S than into the NC-R clover clone. There is no obvious relationship between the seasonal course of AOT40 and AFst0.

When comparing O_3 fluxes calculated with the NC-S g_s model for the three experimental sites (Figure 7.6), substantial differences in AFst0 can be found. These differences are based on the different modelled rates of g_s, as well as on the differing pollution climate of these three sites. Since Deuselbach in comparison with the two other sites not only recorded the highest average O_3 concentrations but also offered the best conditions for high g_s rates (see Chapter 7.1), the O_3 fluxes at this site outweigh the fluxes at the sites Trier-University and Trier-City considerably. This is in particular the case during growing period 4 in 1997, where the AFst0 in Deuselbach is higher than the combined AFst0 at the other two sites.
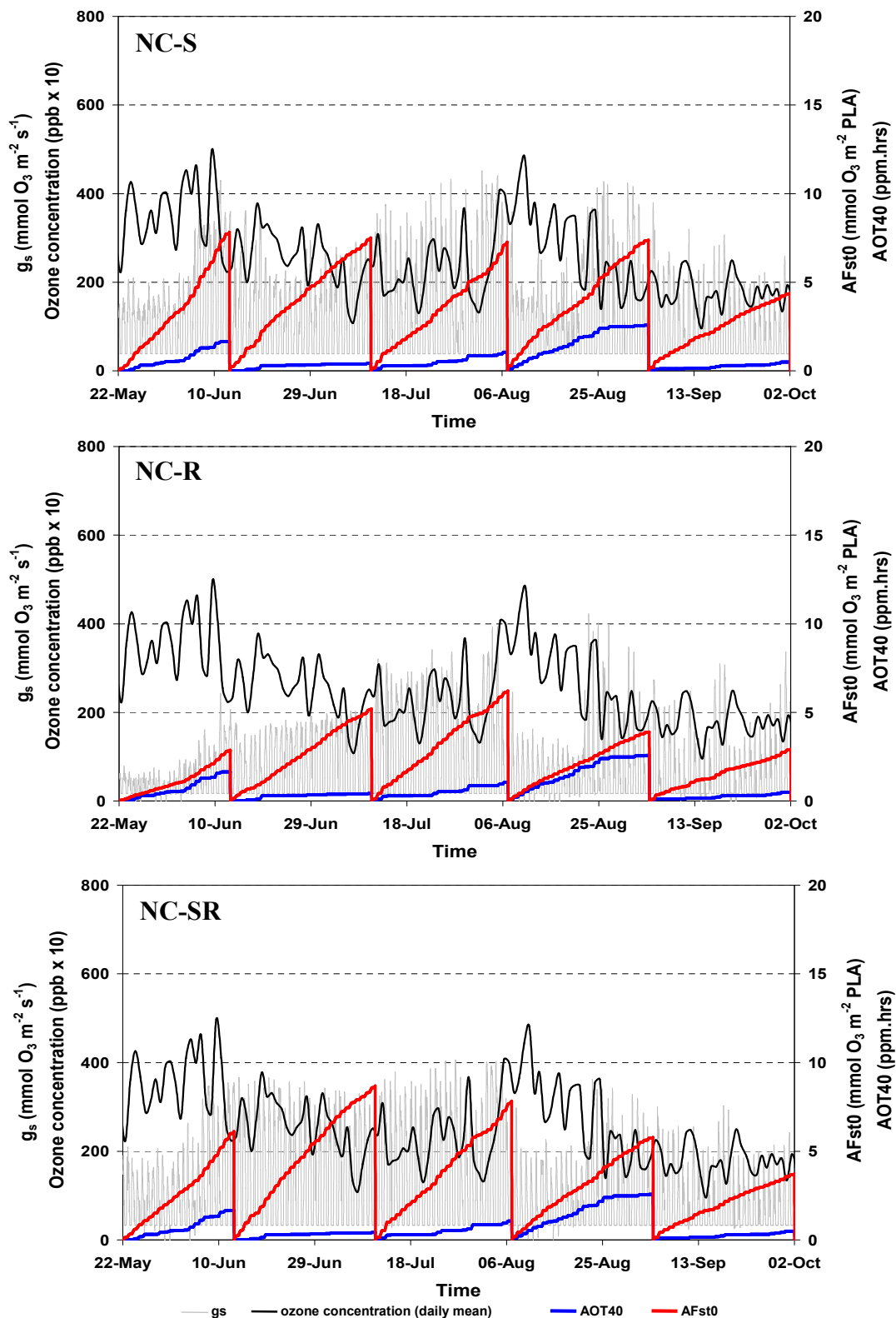
Figure 7.5   Seasonal time-courses of O_3 concentration (daily mean), AOT40, AFst0 and g_s (all hourly means), the latter predicted with the NC-S, NC-R and NC-SR model. Shown are five 28-days growing periods in 1997 at the site Trier-University.
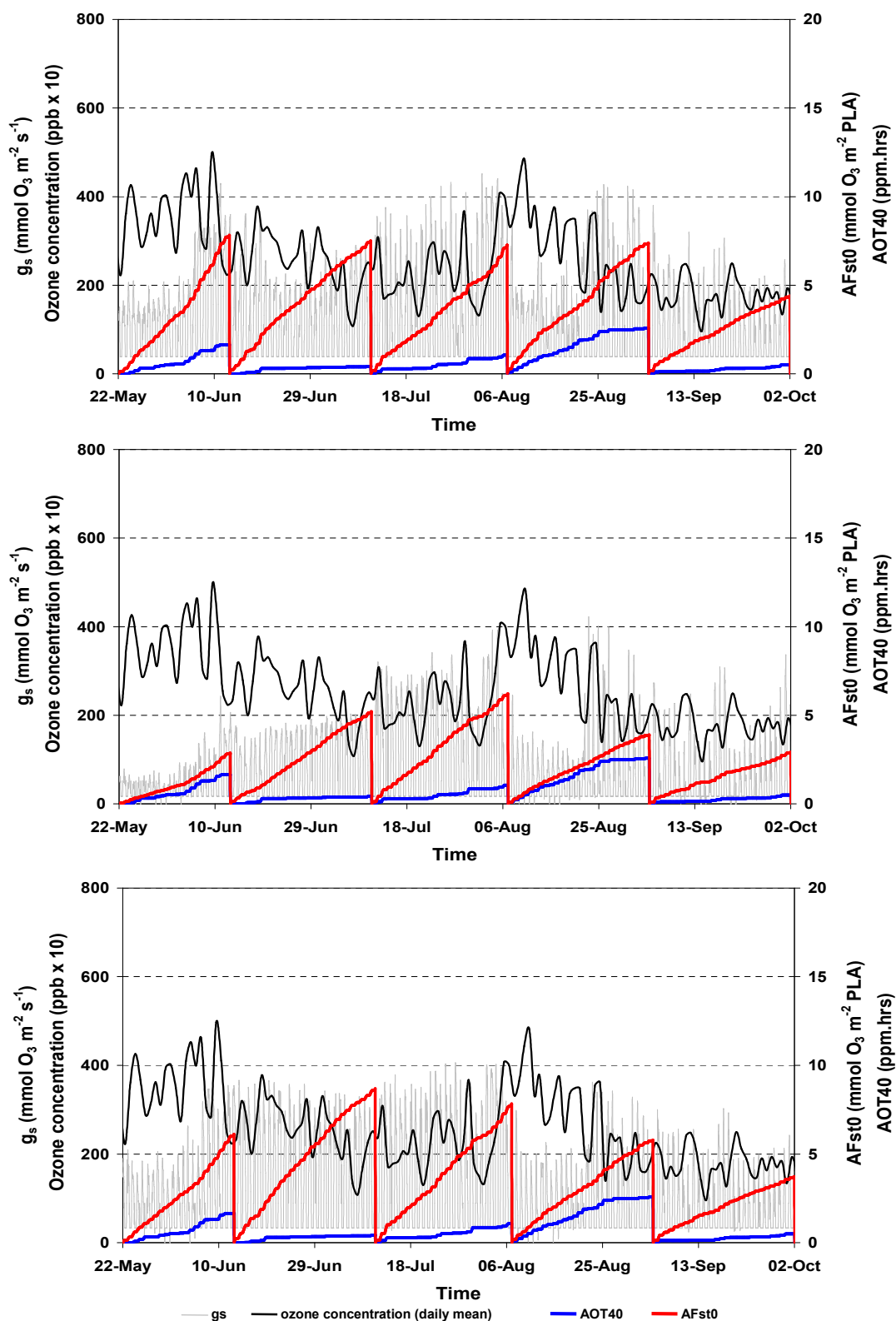
Figure 7.6   Seasonal time-courses of O_3 concentration (daily mean), AOT40, AFst0
and g_s predicted with the NC-S model (all hourly means). Shown are five
28-days growing periods in 1997 at the sites Trier-City, Trier-University
and Deuselbach.

Figure 7.7 summarizes the flux calculations based on the NC-S model results. Shown are the 28-day accumulated O_3 flux rates calculated with different uptake threshold (0 to 10 nmol m^{-2} s^{-1}), as well as the 28-day AOT40. As already indicated above, Deuselbach is the site with consistently higher O_3 flux rates than those calculated for the sites Trier-City and Trier-University. The lowest rates of g_s have been calculated for the Trier-City site. When comparing the AFst0 of different growing seasons, the highest flux rates have been predicted for the year 1997.

Since the AFst0 is hugely dependent on the O_3 concentration, Figure 7.7 indicates a positive relationship between AOT40 and AFst0.
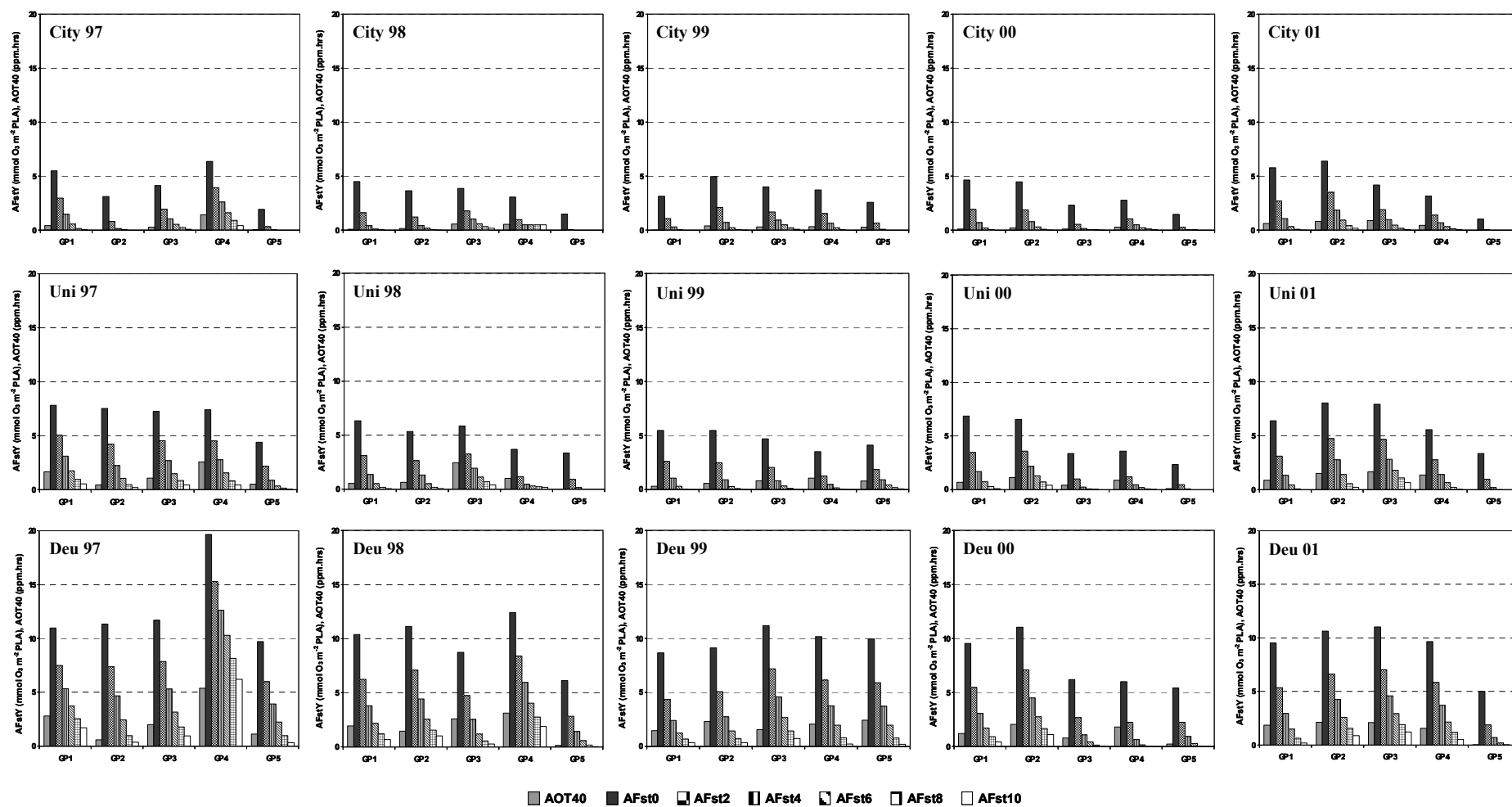
Figure 7.7   Comparison of 28-day accumulated O_3 flux rates calculated with different uptake threshold (0 to 10 nmol m^{-2} s^{-1}) and the 28-day AOT40. The flux rates are based on the NC-S g_s model. Shown are calculated values for five growing periods of the years 1997 to 2001 at the sites Trier-City, Trier-University and Deuselbach.

8 Description and analysis of response parameters

8.1 Description and analysis of visible foliar injury

At the end of each 28-day growth period (GP) prior to each harvest, a visible injury assessment was carried out on all 40 clover plants exposed at each site according to the standardised injury scoring system described in detail in Chapter 3.3.3. The results of these injury assessments are presented in Figures 8.1 to 8.5, separated according to genotype, growth period, site and year. Shown are the median injury score values, as well as the calculated AOT40 for the respective growth period.

It was decided to join the AOT40 values given in each graph of the Figures 8.1 to 8.5 with a line, thus indicating a **possible** gradient of the potentially phytotoxic O_3 concentration from Trier-City via Trier-University to Deuselbach. As described earlier (cf. Chapter 4.1), the AOT40 values were usually lowest in Trier-City and highest in Deuselbach.

The use of median rather than mean values, which was necessary due to the categorical nature of the variables, leads to somewhat similar results with often little difference in the median values for all three sites. The most frequent injury score for the sensitive genotype is 2 ("1 to 5 % of leaves with injury"), and for the resistant genotype 0 ("no symptoms, healthy").

In general, there were only very few GPs during the five experimental growing seasons where the ozone-sensitive clover clone was assessed to be healthy. This was the case for seven GPs at the site Trier-University, five GPs at the site Trier-City and three GPs in Deuselbach. The low median injury score of 0 for the sensitive clover clones always matched low AOT40 values of usually below 1000 ppb.hrs. In turn, high AOT40 values correlated well with high injury scores of up to 4 ("25 to 90 % of leaves with injury"). This was particularly the case in 1997 and 2001 (Figure 8.1 and 8.5, respectively), the two years with the highest O_3 concentrations of the entire study period. In fact, the O_3 concentrations were high enough in 1997 to also regularly affect the resistant clove clone with median injury scores of up to 3 ("5 to 25 % of leaves with injury"; Deuselbach GP 4).

However, there were, albeit very few, GPs with low median injury scores despite high AOT40 values, as shown for example for Deuselbach, for both clover clones in GP 2 during 1999 (Figure 8.3).

When comparing the median injury scores of the different field sites, it is surprising how uniform the results are. However, there is a general overall trend with higher injury scores at Trier-University and in Deuselbach in comparison to Trier-City. This again correlates well with the lowest AOT40 occurring at the site Trier-City.

In summary, the results clearly show the higher sensitivity of the NC-S genotype to O_3 in comparison to the NC-R genotype. Also, high AOT40 values are often associated with relatively high median injury score values for both genotypes, whereas the median values are only partly able to identify differences between the observed phyotoxic impacts at the three field sites.
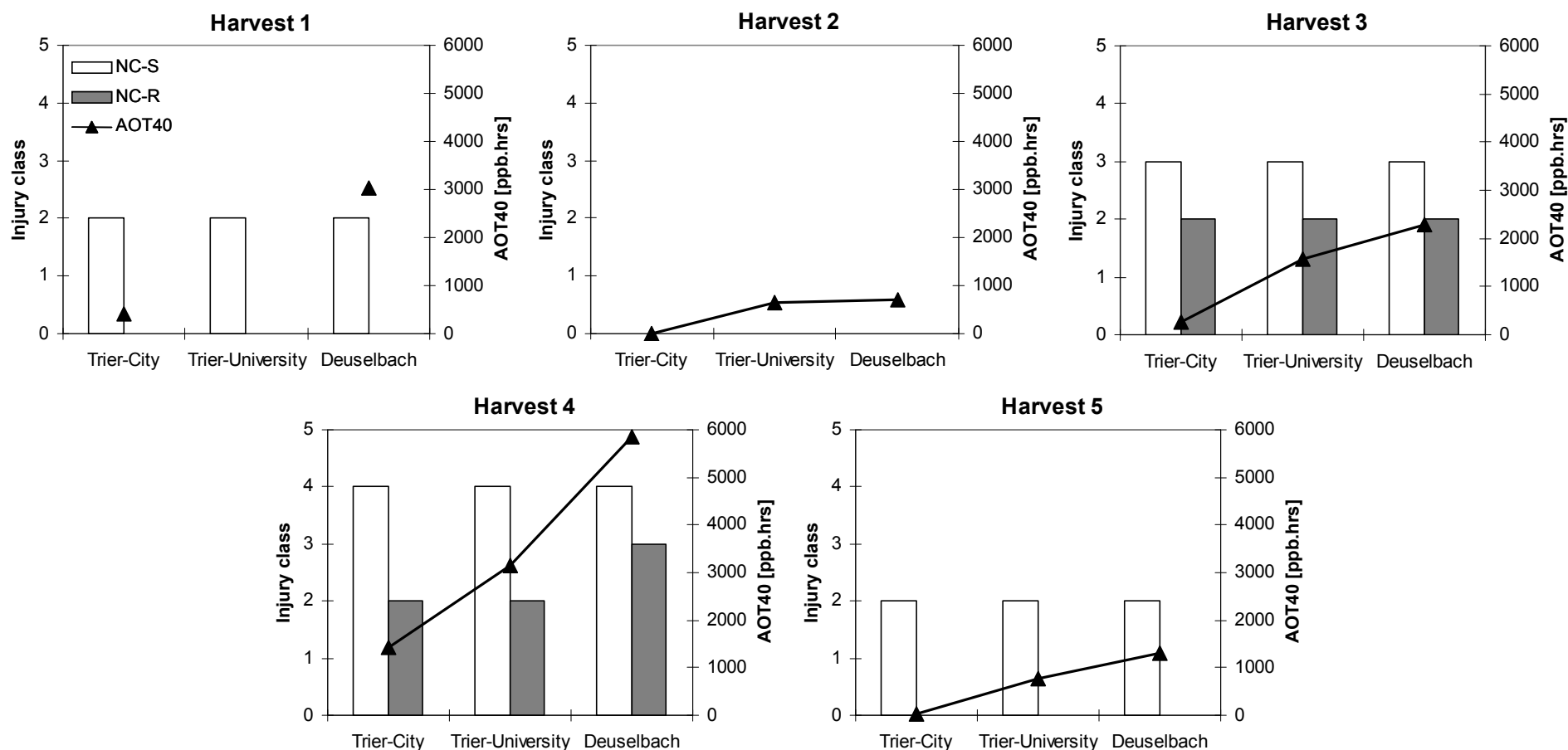
Figure 8.1   Ozone-induced visible foliar injury assessed on both clover clones (20 plants each) at every harvest in 1997 at the field sites Trier-City, Trier-University and Deuselbach, expressed as the median injury class, as well as the calculated AOT40 values for the respective 28-days growth period (N.B. there was no AOT40 value available for first growth period at Trier-University).
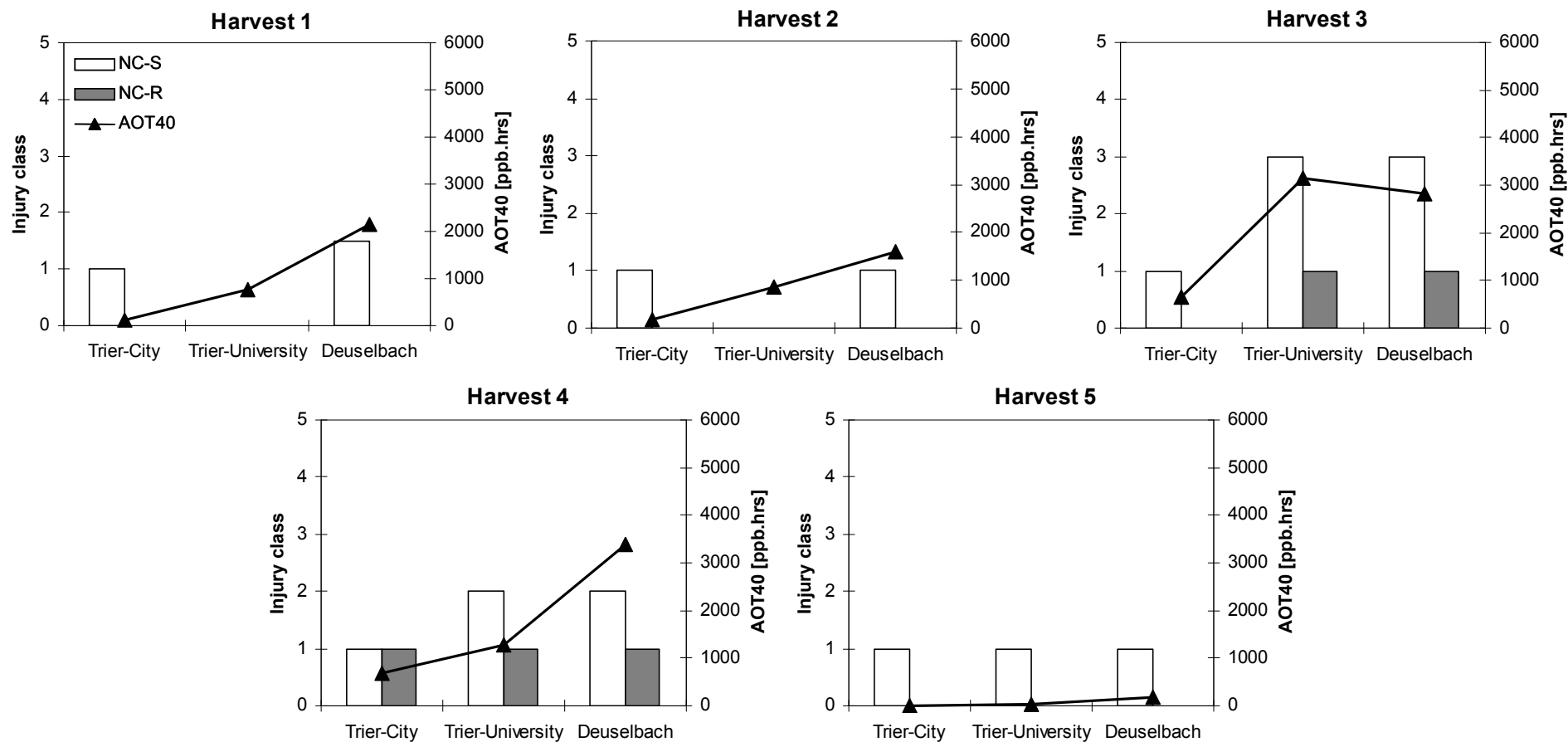
Figure 8.2   Ozone-induced visible foliar injury assessed on both clover clones (20 plants each) at every harvest in 1998 at the field sites Trier-City, Trier-University and Deuselbach, expressed as the median injury class, as well as the calculated AOT40 values for the respective 28-days growth period.
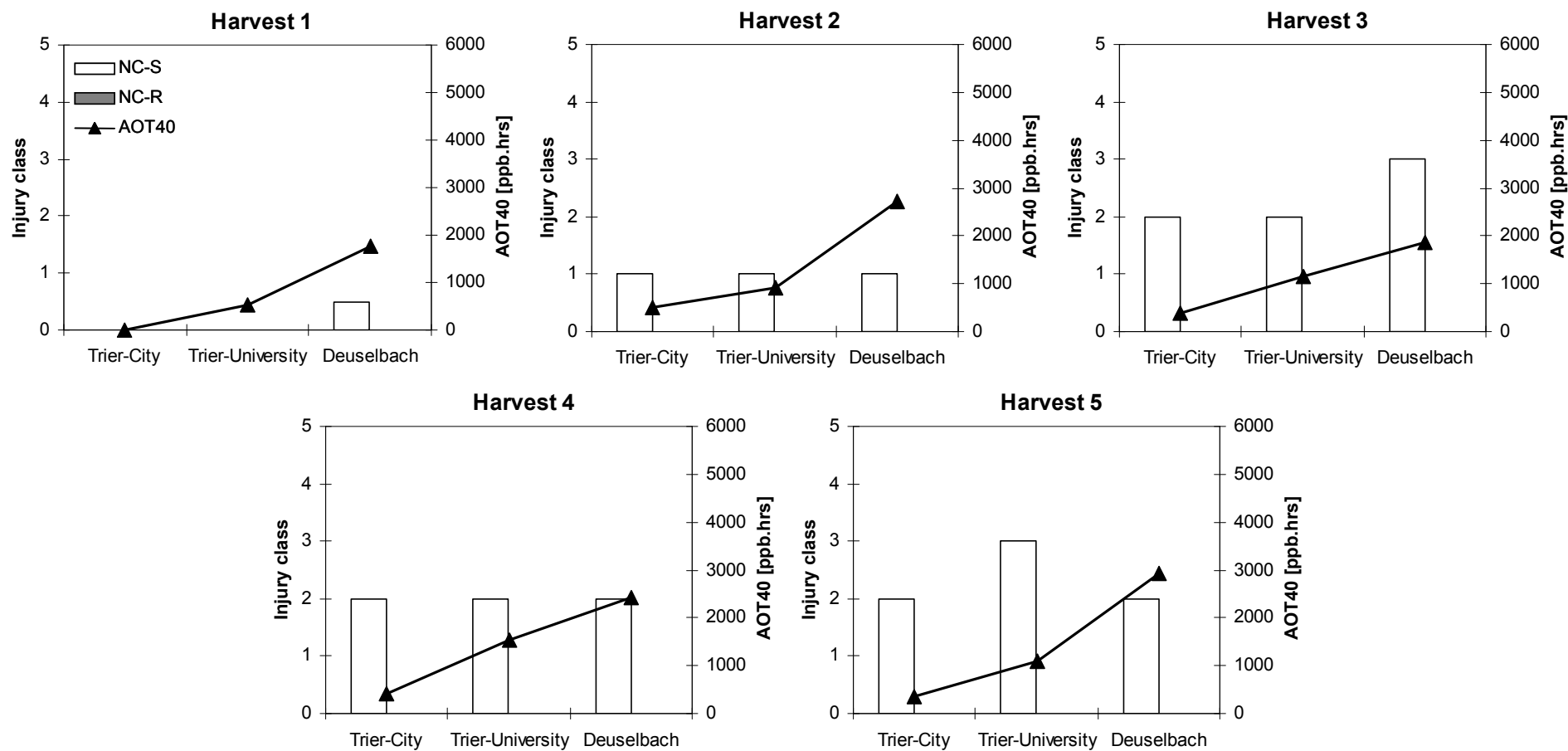
Figure 8.3   Ozone-induced visible foliar injury assessed on both clover clones (20 plants each) at every harvest in 1999 at the field sites Trier-City, Trier-University and Deuselbach, expressed as the median injury class, as well as the calculated AOT40 values for the respective 28-days growth period.
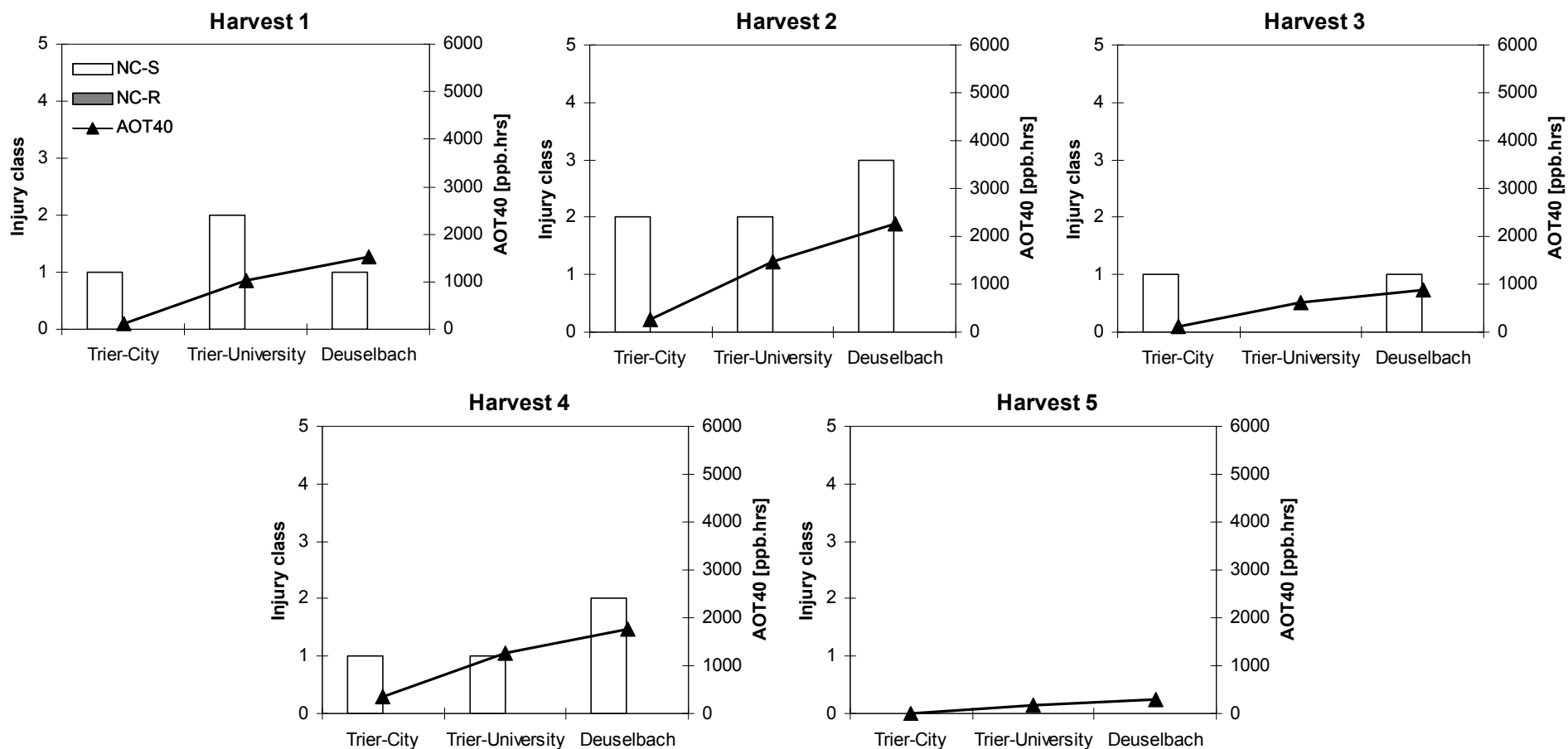
Figure 8.4   Ozone-induced visible foliar injury assessed on both clover clones (20 plants each at Trier-University; 10 plants each in Trier-City and Deuselbach) at every harvest in 2000 at three field sites, expressed as the median injury class, as well as the calculated AOT40 values for the respective 28-days growth period.
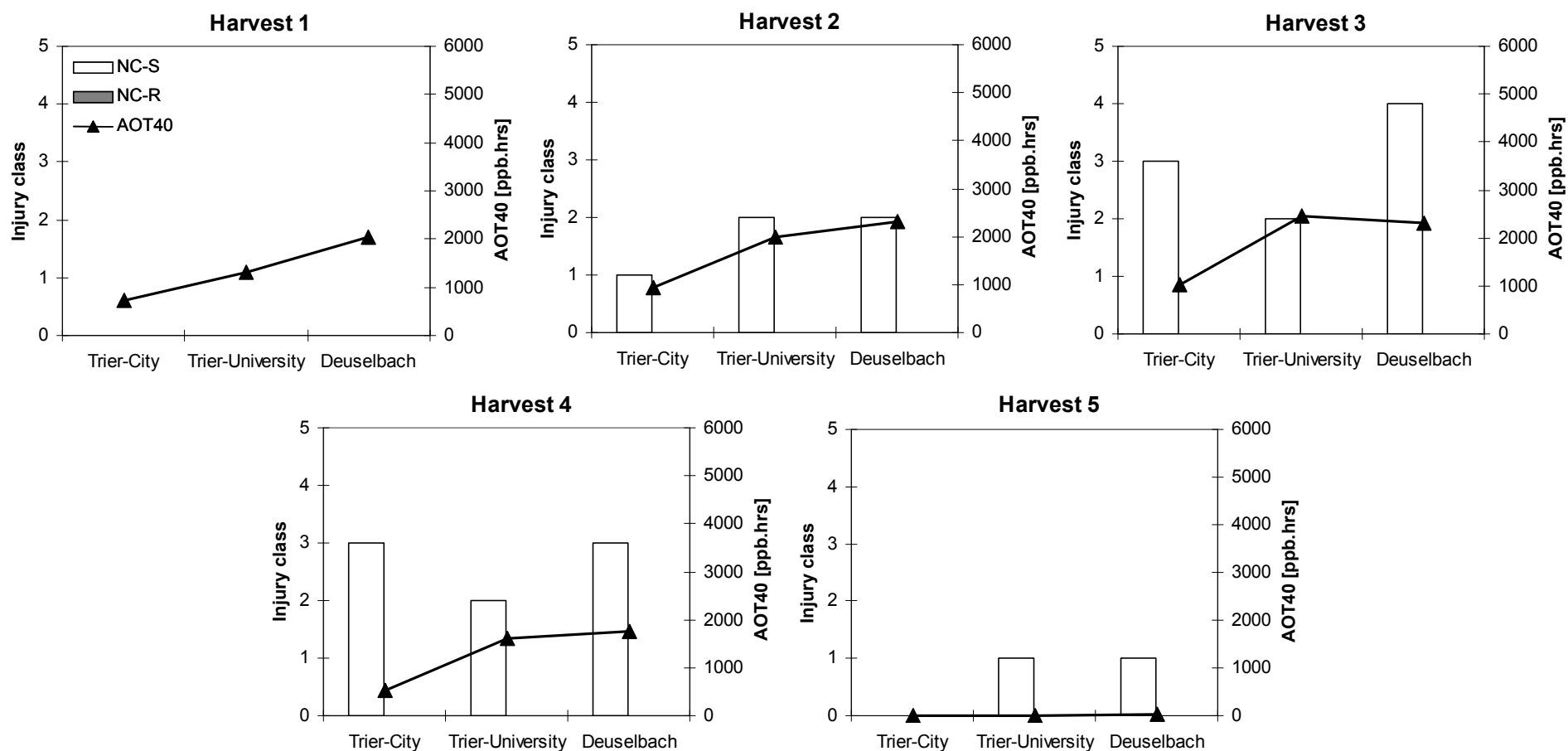
Figure 8.5   Ozone-induced visible foliar injury assessed on both clover clones (20 plants each at Trier-University; 10 plants of NC-S clone in Trier-City and Deuselbach, no NC-R clones were exposed at these two sites) at every harvest in 2001 at three field sites, expressed as the median injury class, as well as the calculated AOT40 values for the respective 28-days growth period.

8.2   Description and analysis of measured clover dry weight

At the end of each 28-days growth period, a destructive harvest of all 40 clover plants per site was carried out, taking away all forage material (including leaves and flowers) above 7cm plant height, plus stolons that had grown over the brim of the 15-litre pots. The harvested material (biomass) was dried and weighed (for details, see Chapter 3.3.3). The results of the dry weight (D.W.) analysis are presented in Figures 8.6 to 8.10, separated according to genotype, growth period, site and year. As an example, harvest 1 is representing the growth of the plants during the 28-day GP 1. Shown are the mean dry weights [g], the ratio between NC-S and NC-R dry weights (the equilibrium value of 1 is marked with a dotted line) as well as the AOT40 [ppb.hrs] and temperature sums [°C days x 10] for the respective growth period. While the AOT40 provides a means of characterising the pollution climate in terms of potential impact on the growth of the clover plants, the temperature sum is believed to be the main driver defining the impact of the prevailing climate on the growth of the plants.

For all years, sites and both genotypes the biomass increases from Harvest 1 to Harvest 3, with a maximum mean of between 80 to 110 g D.W. being reached depending on the year, before starting to decrease from Harvest 3 to Harvest 5. This decrease can be attributed primarily to the commencing senescence after three months of exposure (the plants are at this stage already four months old, if the first 28-day establishing period in the greenhouse is also taken into account), as well as to the changing weather, i.e. the approaching end of summer with associated reduction in sunshine hours. In fact, a clear drop in temperature sum from GP 4 to GP 5 was detected for all years at all sites (cf. Figure 8.6).

A less uniform picture can be seen when comparing the biomass harvested at the three different field sites. There is however a general trend that the biomass was usually lowest in Deuselbach at Harvest 1, while the plants seem to have been able to adapt to the colder, windier and wetter climate in Deuselbach from GP2 on, after which the biomass was often as high or even higher as the ones reported from Trier-City or/and Trier-University. This was the case despite the usually higher AOT40 values calculated for Deuselbach than for the two other sites, which gives an indication that the absolute biomass did not seem to have been influenced by the prevailing O_3 pollution climate.
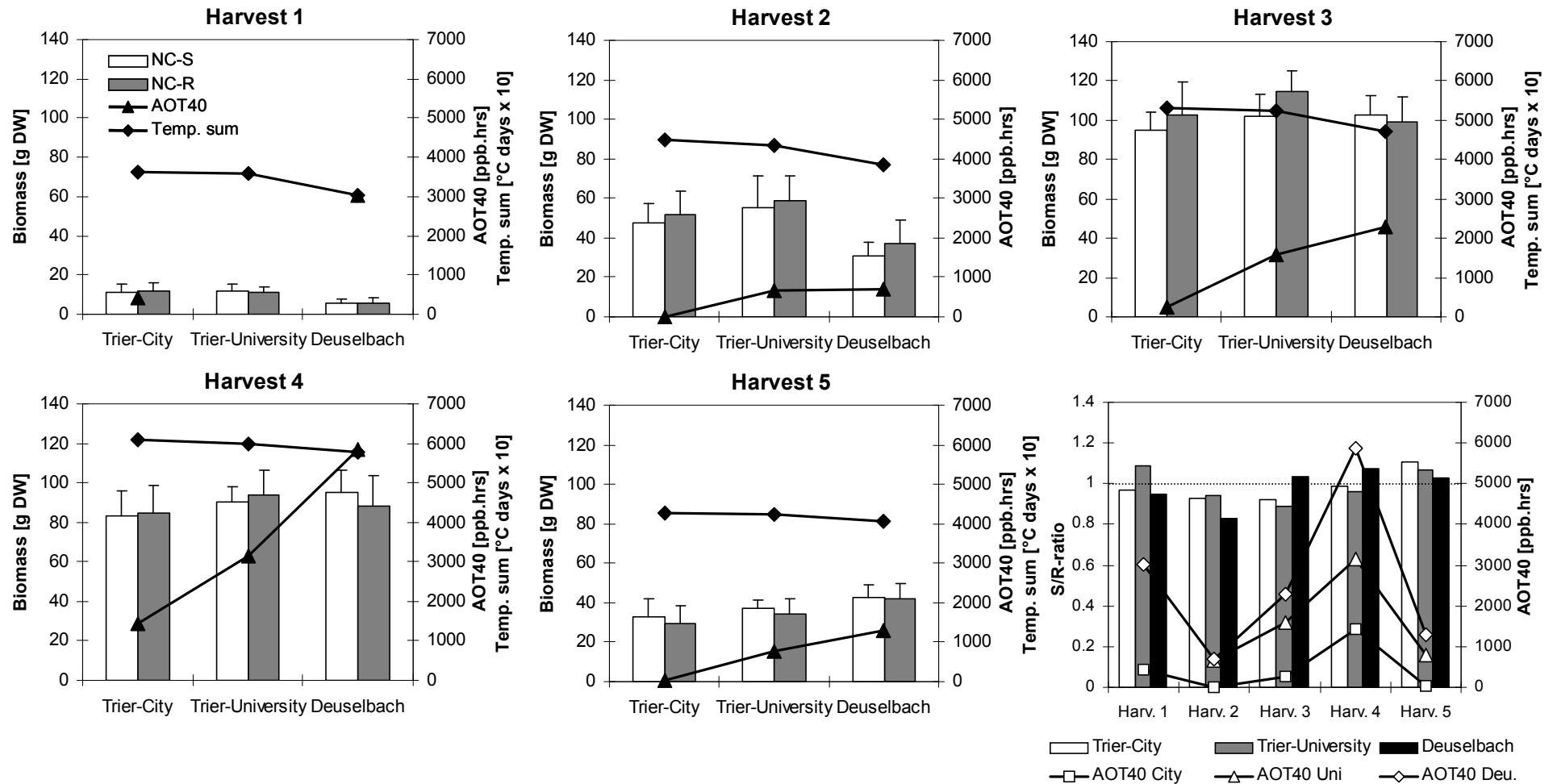
Figure 8.6   Mean biomass [g DW, + 1 S.D.] of NC-S and NC-R white clover clone plants ($n = 20$ for each clone) exposed to ambient air for 28-days. Shown are the results for Harvest 1 to 5 at the sites Trier-City, Trier-University and Deuselbach in 1997, as well as calculated AOT40 values (no AOT40 value available for first growth period at Trier-University) and temperature sums (baseline = 0°C) for the respective growth period. Bottom right graph: Ratio of biomass of NC-S and NC-R clone (S/R-ratio) of all five harvests at each site (dotted line = equilibrium value of 1).
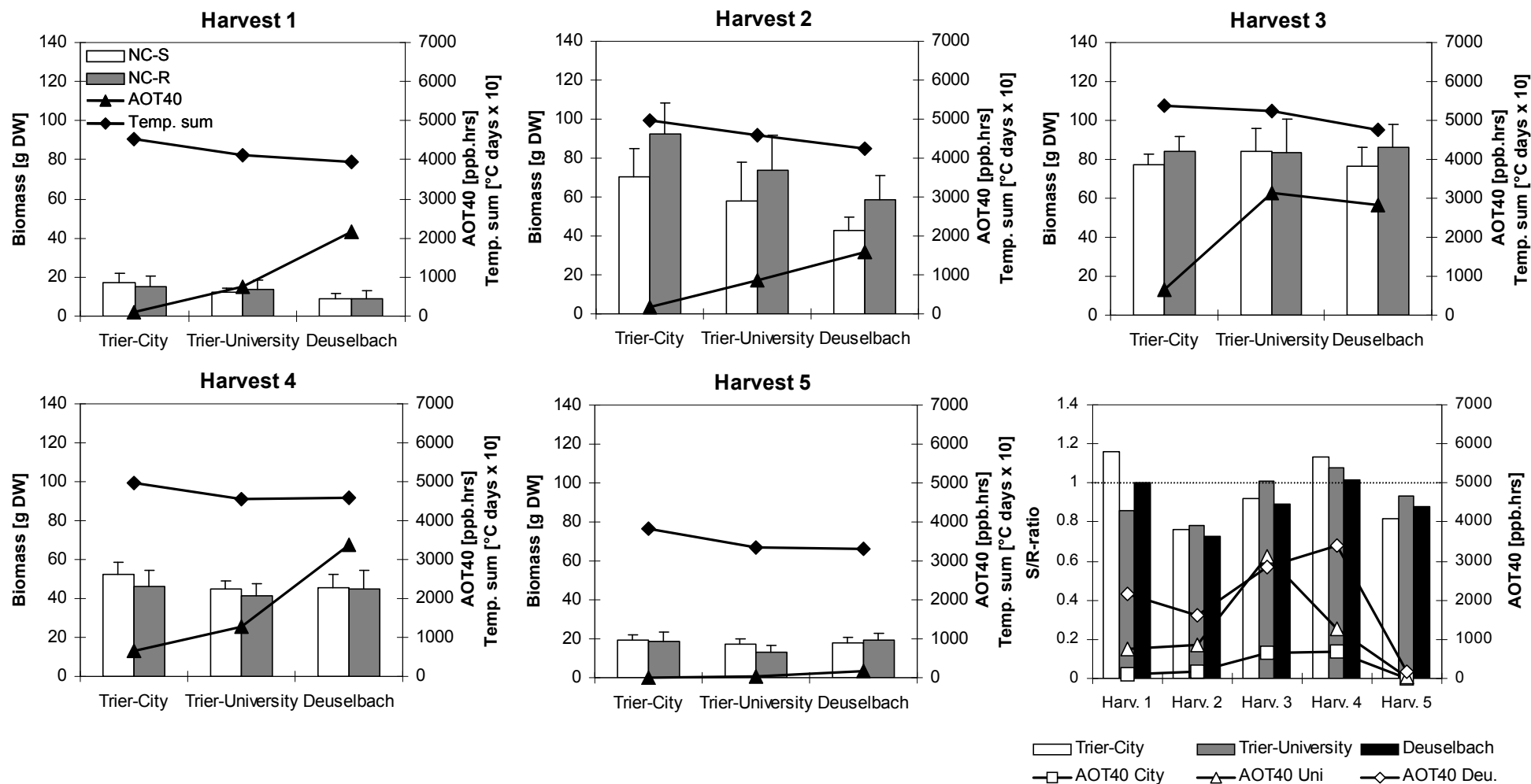
Figure 8.7   Mean biomass [g DW, + 1 S.D.] of NC-S and NC-R white clover clone plants (*n* = 20 for each clone) exposed to ambient air for 28-days. Shown are the results of Harvest 1 to 5 at the sites Trier-City, Trier-University and Deuselbach in 1998, as well as calculated AOT40 values and temperature sums (baseline = 0°C) for the respective growth period. Bottom right graph: Ratio of biomass of NC-S and NC-R clone (S/R-ratio) of all five harvests at each site (dotted line = equilibrium value of 1).
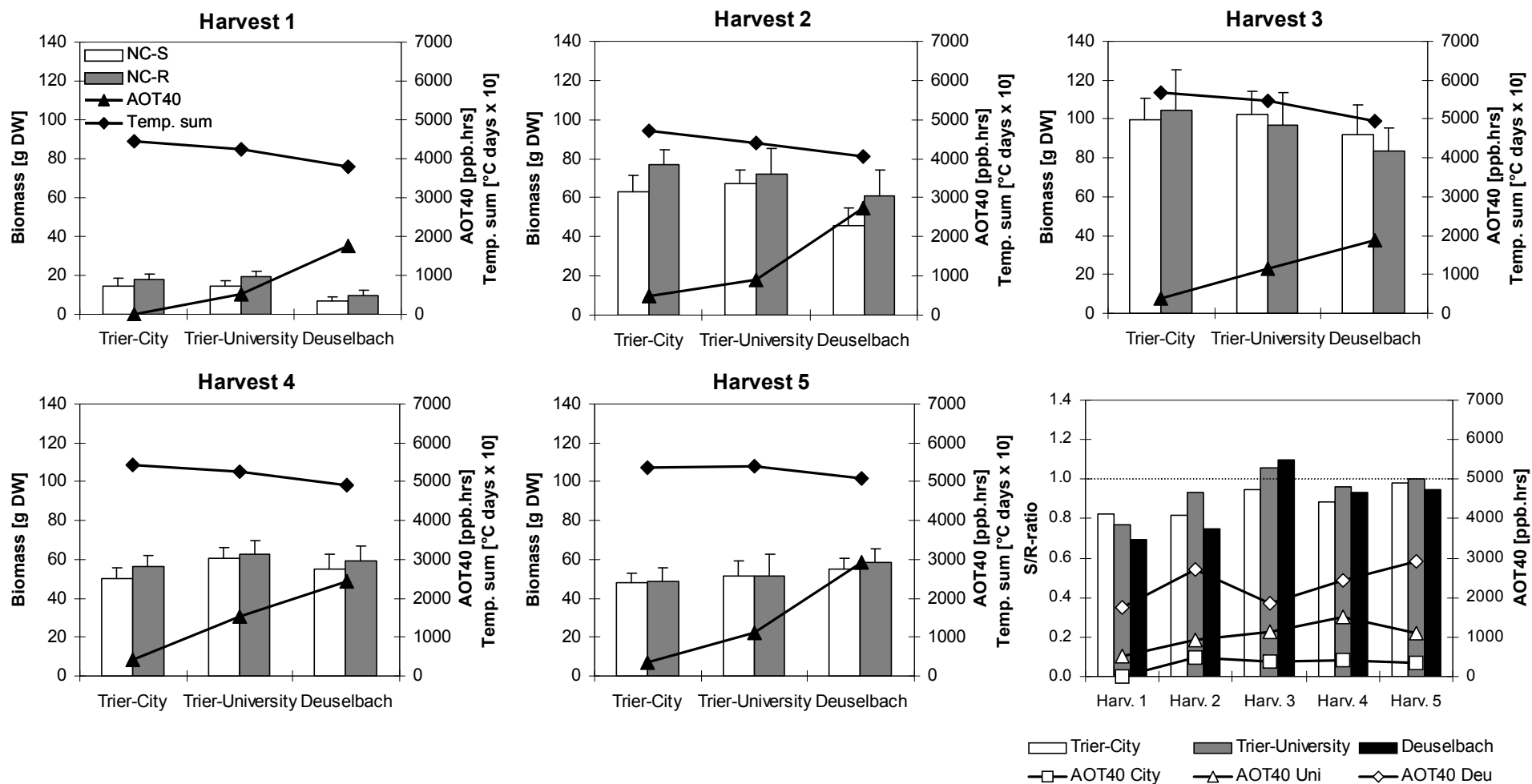
Figure 8.8   Mean biomass [g DW, + 1 S.D.] of NC-S and NC-R white clover clone plants (n = 20 for each clone) exposed to ambient air for 28-days. Shown are the results of Harvest 1 to 5 at the sites Trier-City, Trier-University and Deuselbach in 1999, as well as calculated AOT40 values and temperature sums (baseline = 0°C) for the respective growth period. Bottom right graph: Ratio of biomass of NC-S and NC-R clone (S/R-ratio) of all five harvests at each site (dotted line = equilibrium value of 1).
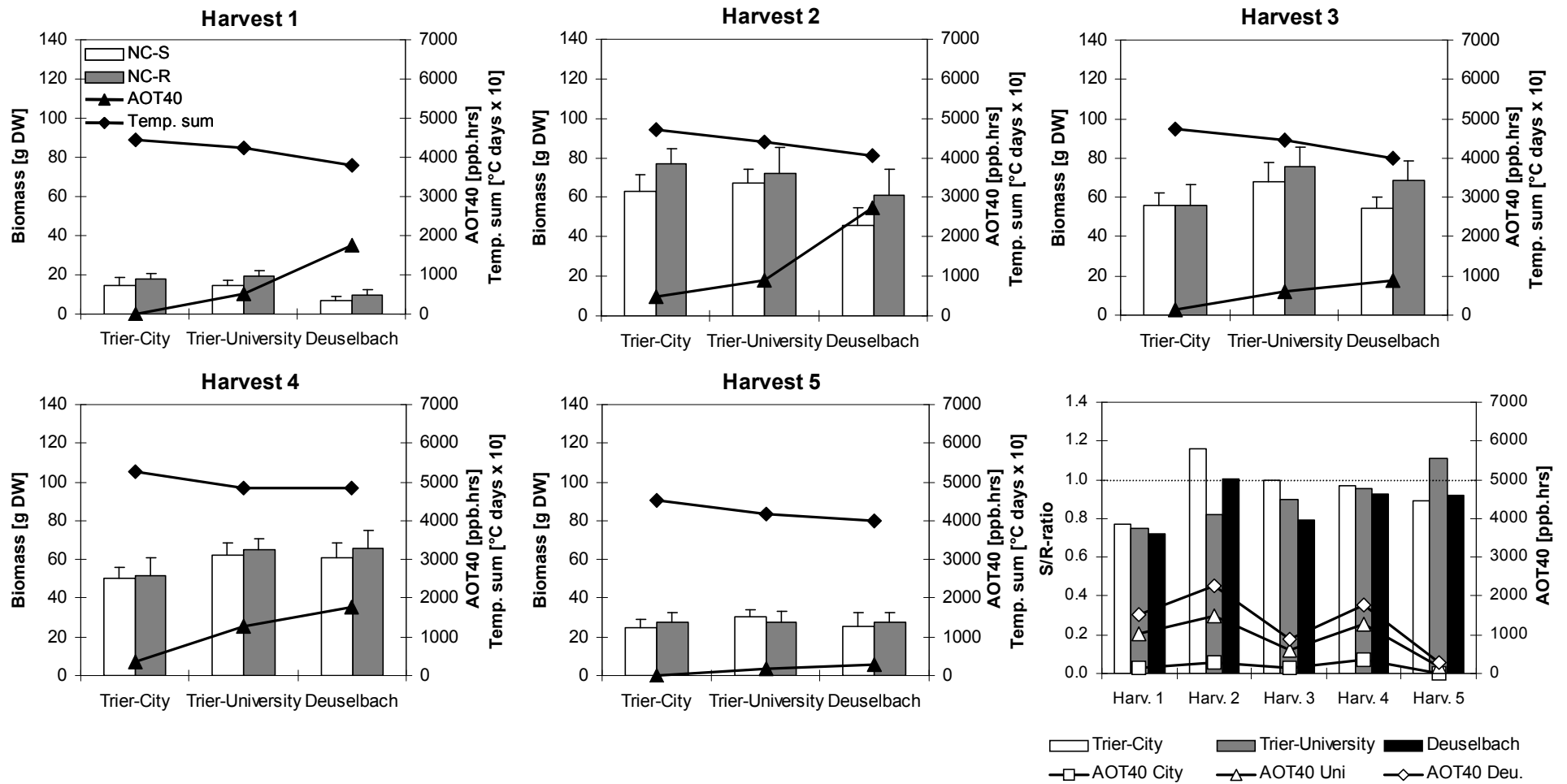
Figure 8.9   Mean biomass [g DW, + 1 S.D.] of NC-S and NC-R white clover clone plants (*n* = 20 for each clone at Trier-University; *n* = 10 for each clone in Trier-City and Deuselbach) exposed to ambient air for 28-days. Shown are the results of Harvest 1 to 5 at the sites Trier-City, Trier-University and Deuselbach in 2000, as well as calculated AOT40 values and temperature sums (baseline = 0°C) for the respective growth period. Bottom right graph: Ratio of biomass of NC-S and NC-R clone (S/R-ratio) of all five harvests at each site (dotted line = equilibrium value of 1).

142
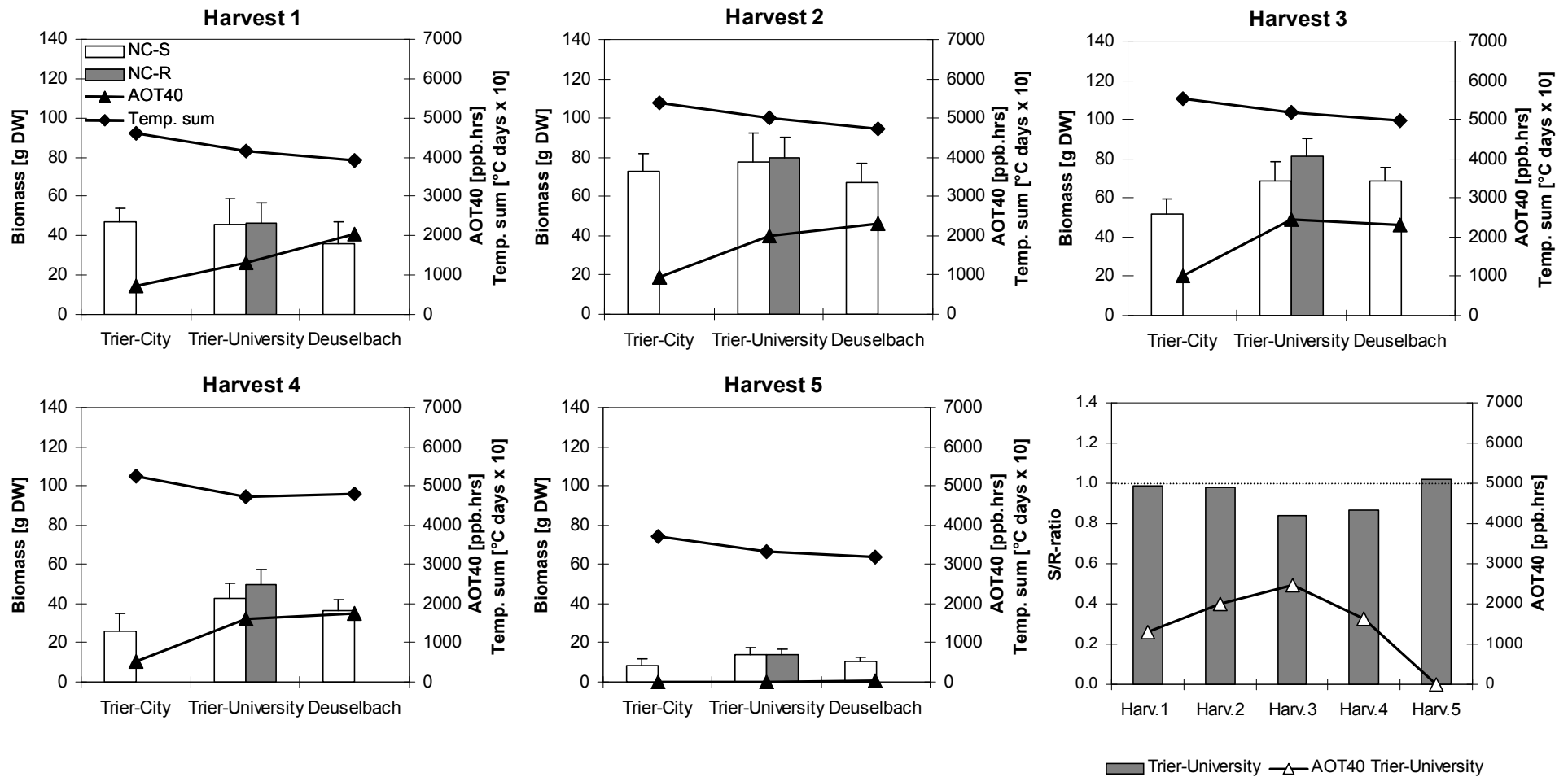
Figure 8.10   Mean biomass [g DW, + 1 S.D.] of NC-S and NC-R white clover clone plants ($n = 20$ for each clone at Trier-University; $n = 10$ for NC-S clone in Trier-City and Deuselbach, no NC-R clones were exposed at these two sites) exposed to ambient air for 28-days. Shown are the results of Harvest 1 to 5 at the sites Trier-City, Trier-University and Deuselbach in 2001, as well as calculated AOT40 values and temperature sums (baseline = 0°C) for the respective growth period. Bottom right graph: Ratio of biomass of NC-S and NC-R clone (S/R-ratio) of all five harvests at Trier-University (dotted line = equilibrium value of 1).

The ozone-sensitive NC-S clone would have been expected to grow less well in relation to the ozone-resistant NC-R clone in Deuselbach, the high O_3 pollution site, in comparison with the plants exposed to lower O_3 concentrations at the two remaining sites. However, while this effect, expressed in Figure 8.6 to 8.10 as the S/R-ratio (shown in the bottom right graphs), was detected at more than 50 % of the harvests, there were in each year at least two harvests where at one of the sites Trier-City or Trier-University the S/R-ratio was smaller than the one calculated for Deuselbach despite higher AOT40 values occurring at the latter site (e.g. Harvest 3 and 4 in 1997; Figure 8.6).

Also, the cases when the S/R-ratio was clearly below 1 did not necessarily match the higher AOT40 values and *vice versa*, as can be seen for example for Harvest 2 in 1998 (relatively low S/R-ratio despite relatively low AOT40; Figure 8.7) or Harvest 4 in 1997 (relatively high S/R-ratio despite relatively high AOT40; Figure 8.6). So while in general the NC-S clone did produce less biomass as can be proved by the S/R-ratio being mostly below 1, there is no obvious correlation with the AOT40 of the respective GPs.

In conclusion, when comparing the mean biomass of all harvests for all sites for different years (Figure 8.11), it is obvious that the NC-R clone always (apart from in Deuselbach in 1997) produced more biomass than the NC-S clone. However, the differences in biomass between the NC-S and the NC-R clone did not differ significantly between sites despite significant differences in AOT40 values accumulated over the entire time period of each years growing season (Figure 8.11).

When comparing the mean total dry weights of different years (Figure 8.12), it appears that the clover plants produced the most biomass in 1999, the year with the highest total temperature sum. In contrast, the year with the lowest temperature sums, 1998, showed the lowest total biomass at the sites Trier-University and Deuselbach.
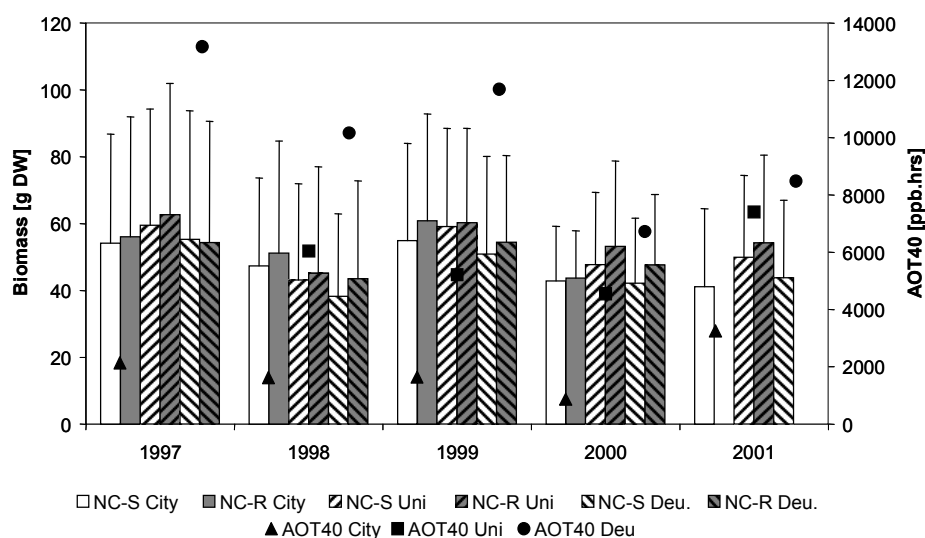
Figure 8.11   Mean biomass (g D.W., + 1 S.D.) of NC-S and NC-R clover plants of all five harvests and the corresponding AOT40 of the entire growing season of the years 1997 to 2001, presented for the sites Trier-City, Trier-Uni and Deuselbach (*n* = 100, apart from NC-S and NC-R in 2000 and NC-S 2001 at the sites Trier-City and Deuselbach with *n* = 50; no NC-R plants were exposed in Trier-City and Deuselbach in 2001). The AOT40 value for Trier-Uni in 1997 was omitted due to missing data for the first GP.
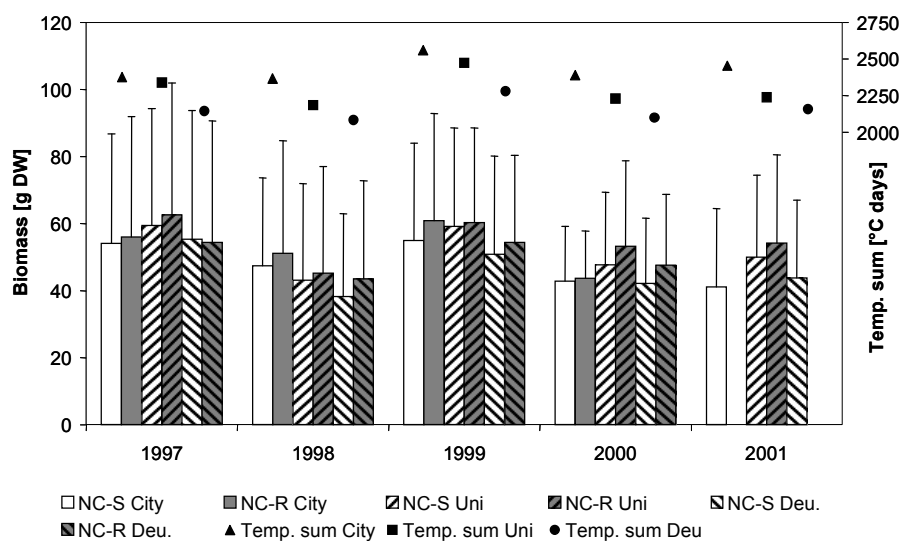
Figure 8.12   Mean biomass (g D.W., + 1 S.D.) of NC-S and NC-R clover plants of all five harvests and the corresponding temperature sums of the entire growing season of the years 1997 to 2001, presented for the sites Trier-City, Trier-Uni and Deuselbach (*n* = 100, apart from NC-S and NC-R in 2000 and NC-S in 2001 at the sites Trier-City and Deuselbach with *n* = 50; no NC-R plants were exposed in Trier-City and Deuselbach in 2001).

9   Dose-response relationships

The response parameters visible leaf injury and biomass reduction were related to uptake- (AFstX) and concentration-based (AOT40) O_3 indices in order to derive dose-response functions using linear regression analyses.

9.1   Response parameter visible leaf injury

Figure 9.1 shows various relationships between the assessed visible leaf injury on the NC-S clover clone, expressed as the median injury class, and the AFst4 based on g_s predictions using the NC-S g_s model as well as the AOT40. Presented are dose-response functions for single sites and combined sites.

For the flux-based O_3 index, a threshold of 4 nmol m^{-2} s^{-1} (AFst4) always resulted in the highest r² values for the relationship between foliar injury and O_3 dose. The best performance of the AFst4 was found when relating it to visible leaf injury recorded in Trier-City, the worst to injury recorded at the site Trier-University. When pooling all data, an unsatisfying r² value of 0.22 was yielded. In direct comparison, the concentration based O_3 index AOT40 outperformed the flux in explaining the variation in the observed foliar injury assessed in Deuselbach and at the site Trier-University. When pooling all data, the AOT40 also showed a better performance than the AFst4.

It has to be stressed that some of the shown dose-response functions are largely driven by one 1997 record of high O_3 concentration/flux and a related high score of visible leaf injury. When excluding this one data point, the r² values drop dramatically for both the AFst4 and AOT40 relationship with visible foliar injury recorded in Deuselbach and in Trier-City (data not shown).

The NC-R clone only showed significant visible leaf injury during some elevated O_3 concentration period, e.g. mainly in 1997. Because of the uniformity of the median injury score – usually 1 for the NC-R clone -, it was impossible to derive any sensible dose-response relationship between visible leaf injury on the NC-R clone and the AOT40 or the AFstX calculated with help of the NC-R g_s model (data not shown).
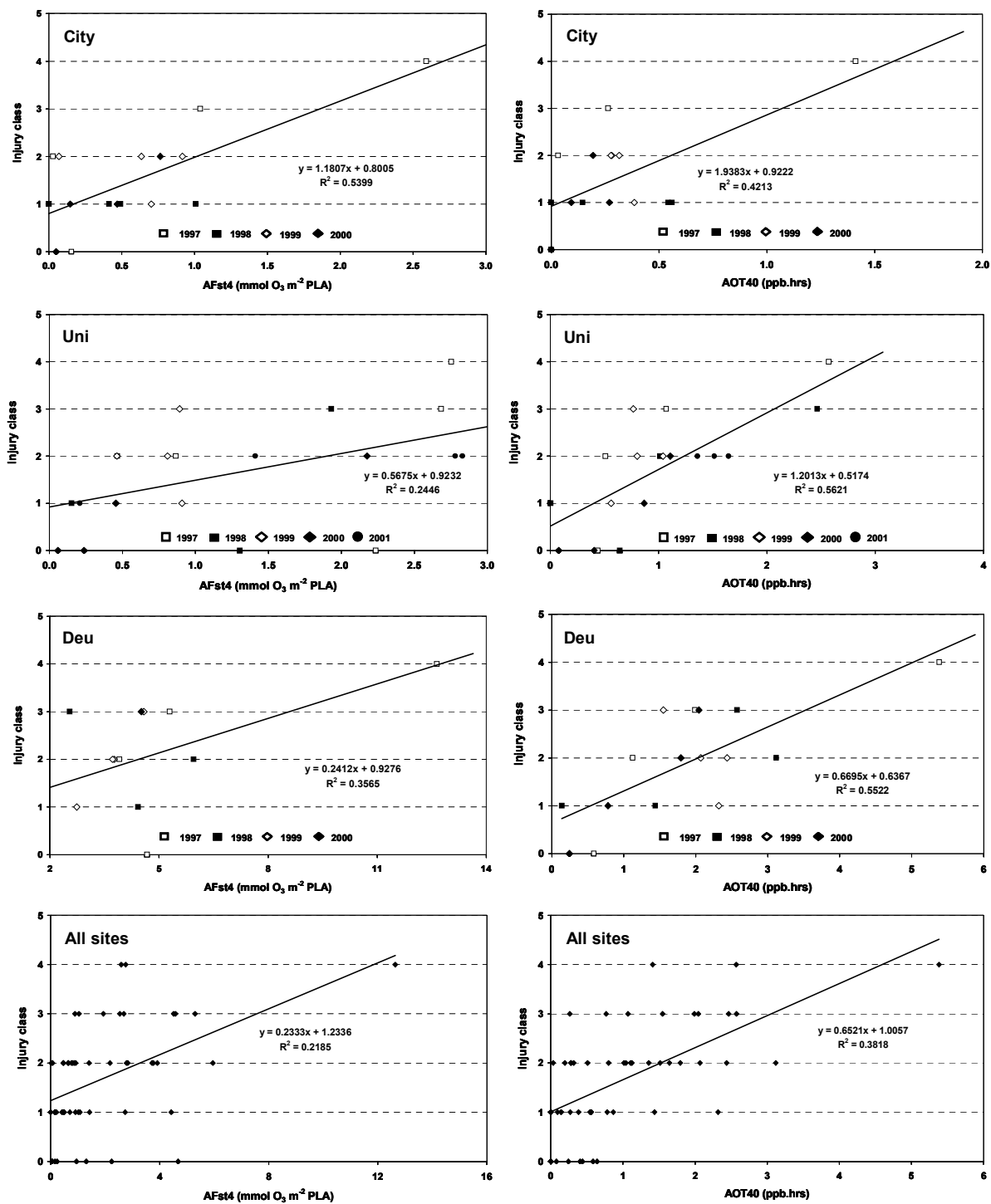
Figure 9.1   NC-S clone visible leaf injury expressed as median injury class assessed in 1997 to 2001 at the sites Trier-City, Trier-University and Deuselbach in relation to AFst4 (left column) and AOT40 (right column). Presented dose-response functions are based on linear regression analyses. The visible injury dataset consists of four assessments per site and year.

The same reason has to be mentioned for the failure of the attempt to relate the **first occurrence** of visible injury symptoms - usually reported towards the end of the second week after a harvest - to O_3 uptake or concentration indices. The uniformity of the median score values made it impossible to reveal clear dose-response functions.

9.2   Response parameter biomass
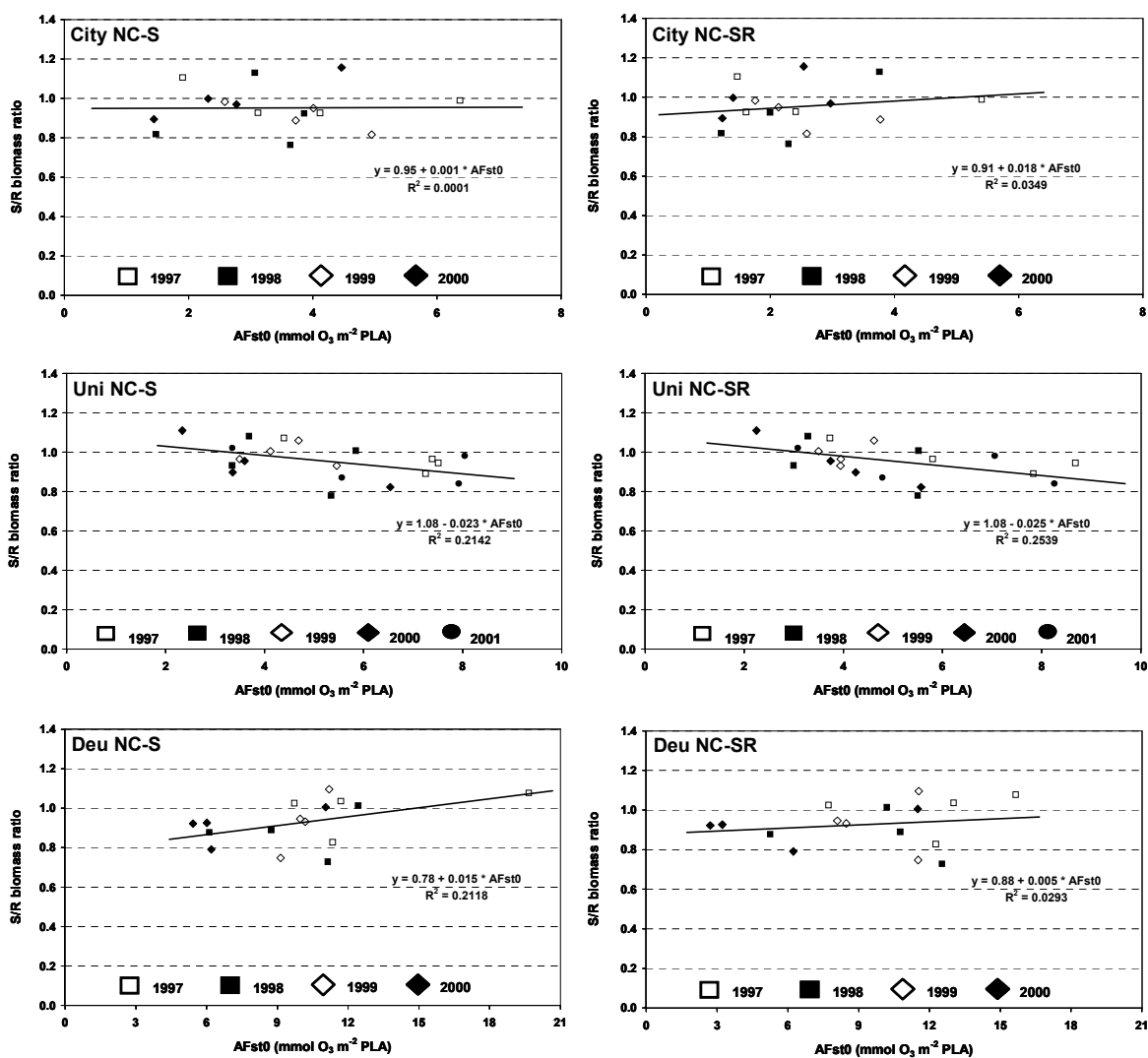
Figure 9.2   Relationship between NC-S/NC-R clone biomass ratio and predicted accumulated flux with the NC-S (left column) and the NC-SR (right column) g_s model using no flux threshold (AFst0) for all five exposure years 1997 to 2001 and all three sites Trier-City, Trier-University and Deuselbach. No NC-S/NC-R biomass ratios were available for the sites Trier-City and Deuselbach for 2001.

The derived dose-response relationships between NC-S/NC-R biomass ratio and AFstX are shown in Figure 9.2 and 9.3. Although for some sites and years satisfying dose-response relationships could be found (precisely Trier-University 1997 and 2000, see Figure 9.3), the general performance of relating AFstX to the NC-S/NC-R biomass ratio was bad (Figure 9.2).

Figure 9.3 also proves that for those sites and years for which sensible flux-based dose-response functions could be derived, the uptake rates using no uptake threshold (AFst0) always led to the highest r^2 values.
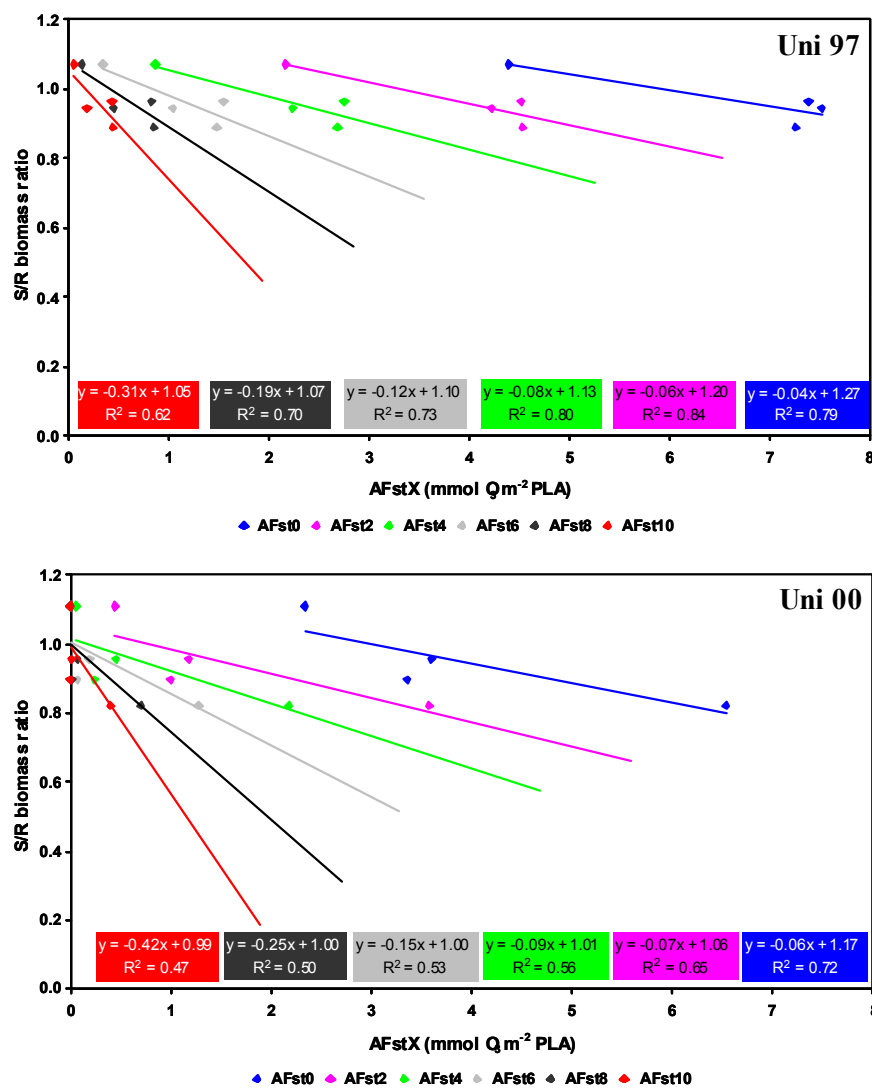
Figure 9.3   Performance of the NC-S flux model in describing relative NC-S clone biomass losses using different flux thresholds from 0 up to 10 nmol m^{-2} s^{-1} in the years 1997 and 2000 at the site Trier-University.

The use of the concentration based O_3 index AOT40 revealed similarly poor dose-response functions for single years and sites as can be seen in Figure 9.4, as well as for pooled data from all sites and years (data not shown). No clear relationships between AOT40 and the NC-S/NC-R biomass ratio could be revealed.
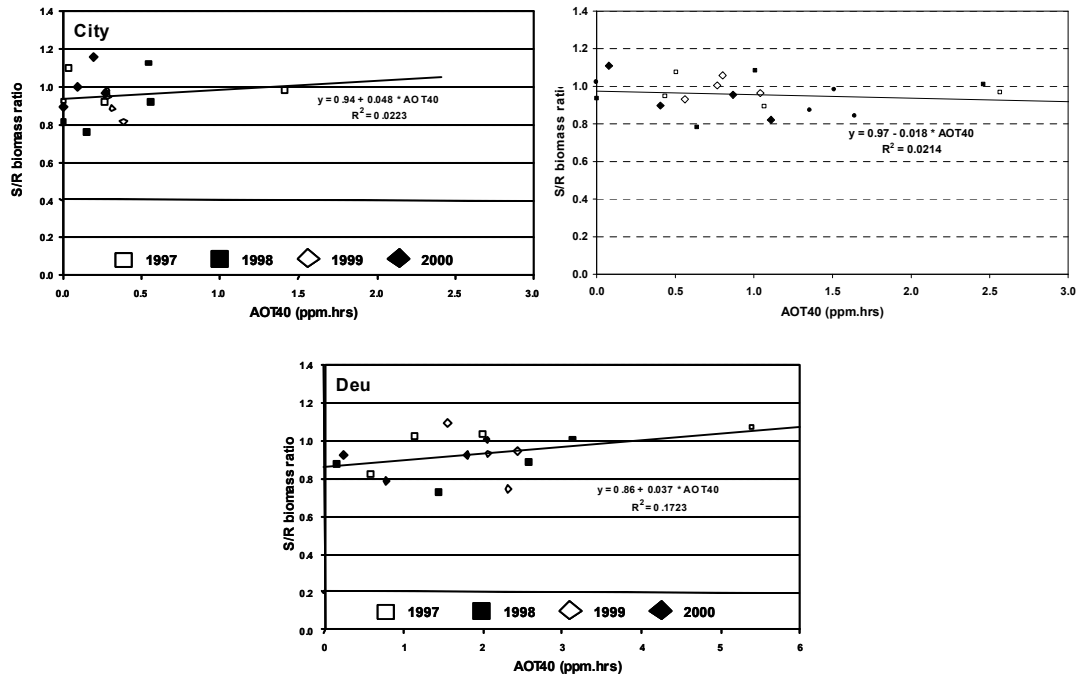
Figure 9.4   NC-S/NC-R clover clone biomass ratio in relation to AOT40 for all five exposure years 1997 to 2001 and all three sites Trier-City, Trier-University and Deuselbach. No NC-S/NC-R biomass ratios were available for the sites Trier-City and Deuselbach for 2001.
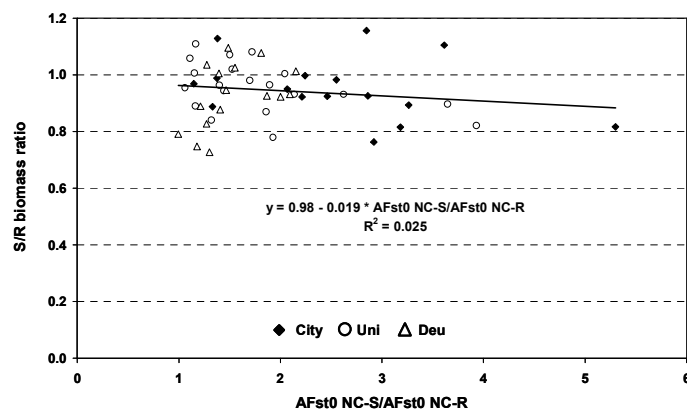
Figure 9.5   NC-S/NC-R clover clone biomass ratio in relation to ratio of accumulated fluxes without threshold predicted with the NC-S and NC-R model (NC-S AFst0/NC-R AFst0) for all five exposure years 1997 to 2001 and all three sites Trier-City, Trier-University and Deuselbach.

When relating the **ratio** between accumulated fluxes using the NC-S and NC-R model (AFstX NC-S/AFstX NC-R) to the NC-S/NC-R biomass ratio, no clear dose-response relationships could be derived either – neither for single sites nor for the pooled data (Figure 9.5).

In an attempt to overcome the dependence on the badly working NC-S/NC-R biomass ratio, the accumulated fluxes (AFst0) were linked to the **absolute** biomass of the clover clones separately. This would not allow any statements on the relative ozone-sensitivity of the NC-S clone because of the missing control, but could reveal if there was at all a relationship between the absolute biomass of the NC-S clone and the predicted flux using the NC-S g_s model and between the absolute biomass of the NC-R clone and the predicted flux using the NC-R g_s model. This analysis resulted in clear positive relationships between AFst0 and AOT40 and the biomass of both clones (Figure 9.6), i.e. the biomass of both clones increased with increasing O_3 flux and accumulated O_3 concentrations.
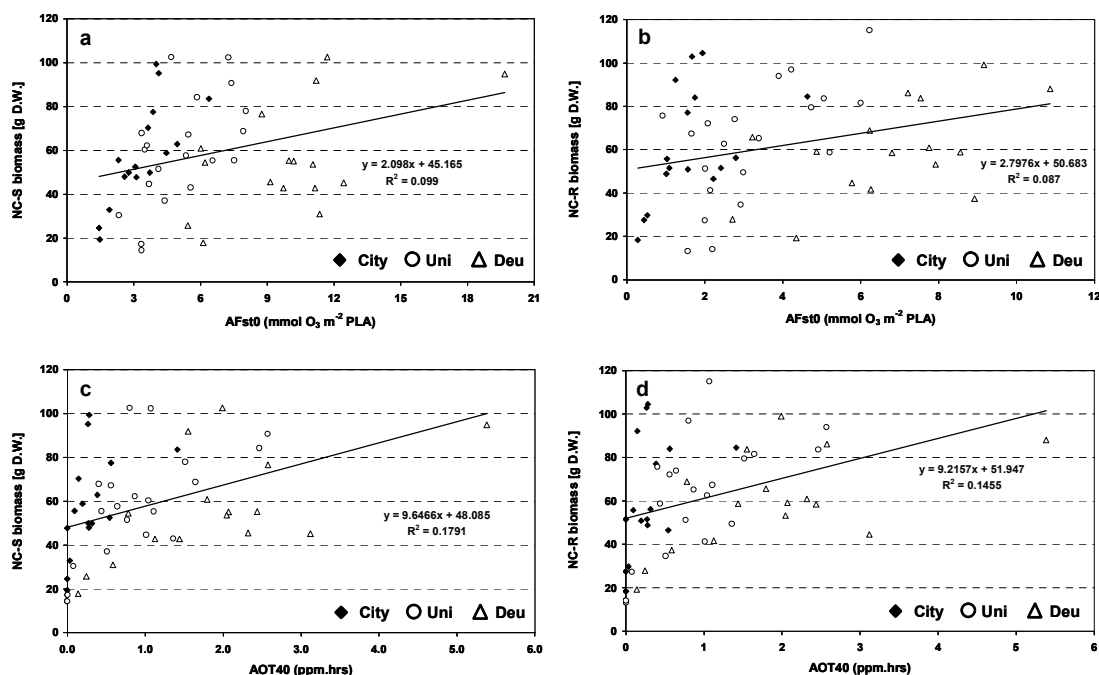
Figure 9.6   NC-S (a, c) and NC-R (b, d) clover clone biomass (g D.W.) in relation to predicted accumulated flux with the NC-S (a) and the NC-R (b) model using no threshold (AFst0), as well as in relation to AOT40 (c, d) for all five exposure years 1997 to 2001 and all three sites Trier-City, Trier-University and Deuselbach.

10   Discussion

10.1 Assessment of the ANN derived stomatal conductance models

In this thesis artificial neural networks have been used to develop stomatal conductance (g_s) models for white clover, which are driven by the meteorological parameters air temperature, photosynthetic active radiation and vapour pressure deficit, as well as the exposure time and the respective accumulated AOT40. Based on these models, O_3 fluxes to white clover were predicted for 28-day growing periods. The choice to use ANNs for this task was based on their reputation of being able to identify complex non-linear relationships between inter-correlated environmental variables, such as the dependence of g_s on key climatic parameters, and the variation of this relationship due to phenological changes and prevailing pollution climates (in this instance O_3) (Balls, 1996; Mills et al., 2000). Because of this ability, it was hypothesised that ANNs should produce more robust predictions of g_s in comparison to well-established conductance models of empirical or semi-mechanistic nature.

The ANNs were trained with recorded meteorological as well as O_3 concentration data, which were related to simultaneously occuring rates of g_s measured for potted plants of white clover clones exposed to ambient air.

Three separate models were developed, one for each clover clone (NC-S and NC-R) plus one combined model for both clones (NC-SR). Out of more than 15,000 sub-models differing in their amount and combination of inputs, number of hidden neurons, momentum as well as learning rate, three models that showed the best performance in predicting g_s were selected. The objective judgement of the performance of each sub-model was based on i) the comparison between modelled and previously extracted measured rates of g_s, ii) a sensitivity analysis to show the dependence of the output (g_s) on each input parameter, iii) the application of each model to datasets representing diurnal time courses of the prevailing climate on a sunny and a overcast day, and iv) the identification of the contribution of each input in predicting g_s using the connection weights approach.

Prior to the training process of the ANNs, it was shown that different random separations of the input data into training, test and validation datasets in the constant ratio 60:20:20 did not result in the development of principally differing g_s-models. The input dataset was therefore believed to be extensive enough to potentially lead to a satisfying prediction of g_s regardless of the extraction data chosen, which represented 20 % test and 20 % validation data.

In the following training process, trial and error methods were applied in order to identify the optimal number of hidden neurons. This number was varied between the maximum value as given per default by the ANN software (i.e. 25, 20 and 25 hidden neurons for the NC-S, NC-R and NC-SR model, respectively), down to a minimum of three. The aim was to identify the simplest model, i.e. the model with the lowest amount of hidden neurons that could still reveal and learn the complex relationship between g_s and the available input parameters. However, the models with the best performance never had fewer than 18 hidden neurons. This makes the interpretation of the models trickier, but was clearly necessary to optimise the predictive power of the networks/models. Furthermore, this is also an indication for the relative noisiness of the input datasets.

The ideal setting for learning rate and momentum - both important drivers for the direction and speed of the training – to ensure the development of models with a high predictive performance were identified by varying both parameters within a range of 0.05 to 0.7 also using trial and error. This proved to be time-consuming, but successful. While the learning rate tended to produce the best models with values at the lower end of the range mentioned (e.g. 0.1 or 0.2), the momentum showed best results with values at the higher end of the same range (e.g. 0.6 and 0.7). The latter is another clear sign of the relative noisiness of the input datasets.

The training of the network was initiated with all seven input parameters - i.e. air temperature, VPD, PAR, exposure time, O_3 concentration, AOT40 of last 12 days and AOT40 of the total exposure time up to that specific point of the growing period - that had initially been selected since they were expected to be able to contribute to the prediction of g_s. In fact, of all models, those with the maximum amount of seven input parameters always resulted in the highest R²-values between observed and predicted

g_s of up to 0.93. This does not come as a surprise, since – similar to a regression analysis – R^2-values usually increase with increasing number of independent variables. The question, however, is to what extent a particular variable can contribute to the explanation of the variation or the prediction of a dependent variable; if this contribution is marginal, then the inclusion of this variable only complicates and slows down the training process of an ANN.

Accordingly, when carrying out a sensitivity analysis for these models, it quickly became clear that the parameters O_3 concentration and AOT40 of last 12 days not only lacked any sensible relationship with g_s, but also seemed to negatively influence the relationship of some of the other inputs with g_s. In other words, although these two parameters did not really harm the network development, they contributed little to the models' ability to describe the relationship between model inputs and output.

This visual impression was supported by the results of the connection weights approach (for details, see below), which consistently indicated a low contribution of the parameters O_3 concentration and AOT40 of last 12 days in predicting g_s.

In fact, when excluding these two parameters from the input dataset due to the results of the sensitivity analysis and connection weights approach (an approach not hugely dissimilar to a simple pruning mechanism), the overall predictive performance of the final models did not substantially decrease (changes from R^2 0.90 to 0.89, 0.92 to 0.89 and 0.87 to 0.79 were found for the NC-S, NC-R and NC-SR model, respectively). This is a clear sign that neither the prevailing O_3 concentration nor the exposure to elevated O_3 concentrations over the course of the last 12 days substantially influenced (either negatively or positively) the gas exchange of both clover clones. The omission of these two parameters was therefore believed to be justifiable and indeed desirable.

The results of the sensitivity analysis of all sub-models - from which the final three models were selected - varied according to the number of hidden neurons, the learning rate and the momentum, but in general led to the expected dependence of g_s on air temperature, PAR and VPD. This was also the case for the three final NC-S, NC-R and NC-SR models with 18, 19 and 19 hidden neurons, learning rates of 0.2, 0.05 and 0.4 and momentums of 0.6, 0.7 and 0.5 for these models, respectively.

When keeping all other inputs constant at rates representing favourable (average) conditions for gas exchange of these clones, g_s increased with increasing air temperature until approx. 30 °C, above which the response functions indicated the onset of a more or less constant relationship between temperature and g_s. The sensitivity analysis suggested that this plateau was reached earlier for the NC-S clone. However, with the available input data, it was not possible to accurately predict above which air temperature g_s would start to be limited. Similarly, the models could not realistically predict g_s for temperatures below 12.5 °C, but the sensitivity analysis proposed that the g_s of the NC-S clone was more sensitive to decreases in temperature than the NC-R clone.

The sensitivity analysis also revealed that g_s decreased with increasing VPD from approximately 0.5 kPa until reaching constant minimum conditions as VPD exceeds approximately 2.5 kPa. The predicted amplitude between maximum and minimum VPD-driven g_s was much smaller for the NC-R than for the NC-S clone.

The dependency of g_s on PAR was somewhat more surprising. While there was a steady increase in g_s with increasing PAR until approximately 500 to 750 μmol m^{-2} s^{-1}, indicating early light-saturating conditions, the maximum predicted light-saturated g_s was with 400 and 200 mmol H$_2$O m^{-2} s^{-1} for the NC-S and NC-R clone respectively lower than expected. This unexpected result already indicated the limited contribution of PAR in predicting g_s for all three models, possibly caused by model input data only representing a limited range of this variable.

It has to be pointed out that at high light-saturated rates of PAR of above 1200 μmol m^{-2} s^{-1}, the NC-S model predicted a decrease in g_s. While this behaviour of the model can be attributed to light inhibitory processes, g_s rates of up to 150 mmol H$_2$O m^{-2} s^{-1} for PAR values of 50 μmol m^{-2} s^{-1} and lower (representing the time from dusk till dawn) suggest that the clover clones did not fully close their stomata during the night. Indeed, when looking at the input data used for training the models, there are various measurements with g_s values well above 0 mmol H$_2$O m^{-2} s^{-1} for dusk, dawn or conditions of complete darkness. The fact that the ANNs based models had problems in predicting g_s for night-time conditions - despite model input data clearly indicating night-time gas exchange - led to the decision to assume a constant clone-specific rate

of g_s for PAR < 100 μmol m^{-2} s^{-1}, derived from the mean of the above mentioned measurements carried out in very low light or full darkness.

The curves of the sensitivity analysis showing the relationship between g_s and exposure time are noisier, though all three models obviously show a trend towards decreasing g_s with increasing exposure time from approximately 40 to 60 days after the initial exposure date (transplantation day of plants from greenhouse into the field). In other words, the performance of the clover plants represented by a reduced gas exchange declined towards the end of the growing period, clearly indicating a senescence effect. This effect might have been caused by less favourable climatic conditions from growing period 4 or 5 on (with the onset of autumn), a general phenology-dependent change in the physiology of the clover clone plants, as well as ozone-induced sluggishness of the stomata. The latter is possible given that the plants have at that time already been exposed to ambient O_3 concentrations - sometimes well above 40 ppb - for more than three months. In this respect, exposure time acts rather as a surrogate parameter for phenology and the long-term effects of the pollution climate.

The relationship between the AOT40 of the respective exposure period and g_s was surprising as it indicated an increase in g_s with increasing AOT40 values between 1000 and 3000 ppb.hrs. This relationship was found for all three models and represented information given by the input data during the training of the ANNs. It may be explained by the fact that high AOT40 values usually co-occur with high temperature and PAR values, which – as described above – represent favourable gas exchange conditions for the clones used in this thesis.

Finally, it has to be stressed that the sensitivity analysis applied here always represented **average conditions** of all input parameters in respect to the input dataset apart from the one "target parameter" being investigated, which was varied across its entire measuring range. This means that this tool is in general able to reveal the relationship between various input parameters and g_s for average conditions, but might diverge from this relationship for non-average conditions, e.g. values representing the lower or upper end of the data range of the input parameters. Because of this, the outcome of the sensitivity analysis should be interpreted with great

caution, since it is unable to reveal the relationship between input and output for all possible data combinations, e.g. environmental conditions. Also, ANNs might have learned an inaccurate dependence of g_s on some of the input parameters for specific climate conditions (leading for example to local minima or maxima) as a result of an internal interpolation process, which may not have been disclosed by the sensitivity analysis carried out in this study.

For this reason, all models were also always applied to two measured diurnal time courses of air temperature, VPD and PAR (and their matching exposure time and its related AOT40 values), i.e. one sunny and one overcast day. As for the sensitivity analysis, this method only represents a certain combination of input parameters at certain points in time, which limits its general ability to present all conditions. However, since this step is seen as a time series test for the ability of the models to predict g_s for clover clones over the course of several hours, it was thought to be a good indication whether or not the models would be able to predict g_s and hence O_3 fluxes for entire growing seasons. It potentially would also disclose climatic conditions (combinations of air temperature, VPD and PAR values) the models had not be trained with, i.e. were not learnt from the input dataset.

Unfortunately, since it is not permitted to apply the models to data used for training and since it was necessary to have a complete diurnal dataset for this part of the investigation, the NC-S model had to be applied to a diurnal time course during which g_s on the NC-R clone was measured, and *vice versa*. Also, the selected overcast day - though not having been included in any model input dataset - only consisted of g_s data for the NC-R clone, which again complicated the direct comparison when applying the NC-S or NC-SR model. However, since both clones recorded rather similar g_s diurnal profiles, even if the absolute g_s values were variable, to changes in climatic conditions, this assessment was judged to be useful, i.e. the diurnal time course of measured g_s of a NC-R plant still provided valuable information as to the dependence of gas exchange on the prevailing climate when being compared with the modelled g_s for the same day using the NC-S model, and *vice versa*. More importantly, this method showed whether or not any of the selected models were capable of reproducing the g_s response to sudden changes in climate, such as an interspersed cloud-cover reducing the PAR.

The results showed that all three models were indeed able to cope with these sudden changes during the cloudy day, though to a lesser extent than experienced during the measuring campaigns, since the models seem to partly level out the distinctive peaks in PAR (as well as g_s) recorded at that day. Cloud-covered periods, well recognisable in terms of reduced PAR, are well correlated with reductions in g_s, which indicated that there was almost no time lag between decreasing PAR and decreasing g_s. However, in comparison to the measured g_s of a NC-R clover plant, all three models predicted higher g_s value.

Interestingly, all three models showed more problems in predicting a diurnal time course of a sunny day with a smooth bell-shaped air temperature and PAR curve throughout the day. All three models performed well during the afternoon of that day, but showed some unexpected over-prediction during the morning hours, which was in particular the case for the NC-S model. The over-prediction of this model before midday was experienced with all NC-S sub-models, indicating that either the respective input dataset contained a higher g_s for these climatic conditions (possibly due to high relative humidity rates in the early morning hours which interfered with the gas analyser of the measuring device – as can also be seen by the morning scatter of the measured g_s on that day) or – more realistically – that the model had to deal with climate conditions the ANN was not trained with and hence could not learn. This would be a typical example of an interpolation error.

However, is has to be pointed out that the selected sunny days only represented a certain point in time, i.e. no general conclusions stating that "the NC-S model is unable to cope with sunny conditions during the morning hours" are justified. Indeed, the over-prediction of g_s during the morning hours could only be found on very few days during the very hot first half of August in 1998, from which period the sunny day investigated here happens to be taken.

In order to shed more light on the black box of the ANNs, i.e. to better understand their internal functioning, the connection weights approach revealed the relative importance of each of the final five input parameters in predicting g_s. For all three models, the air temperature and VPD played an important role in this prediction, whereas PAR in general was of minor importance, in particular for the NC-S and NC-

SR model. The exposure time only played an important role for the combined model, whereas the AOT40 of the exposure time, rather surprisingly, contributed significantly to the NC-S model. These findings correspond well with the findings of the sensitivity analysis, i.e. the noisier the curve in the sensitivity analysis graphs, the minor the contribution of this particular parameter in predicting g_s.

The three models had R^2-values of 0.89 for both the NC-S and NC-R and 0.79 for the combined NC-SR model for the relationship between predicted and observed g_s. All models showed a slight under-prediction of g_s, indicated by intercept values of 49, 37 and 58 for the NC-S, NC-R and NC-SR model, respectively. This minor systematic error of all models is considered to only have a minimal impact on the prediction of g_s over the course of entire growing seasons. It does not influence the analysis of the gas exchange differences between the two clover clones, since all models showed similar slight under-predictions.

In agreement with the ANN input data, the predicted g_s values for the NC-S clone were in general significantly higher than those for the NC-R clone, highlighting the differences in gas exchange between these two clones. Surprisingly, the combined NC-SR model did not represent intermediate conditions but tended to predict rates of g_s similar to those calculated by the NC-S model.

10.2 Analysis of predicted seasonal ozone fluxes

For the prediction of O_3 fluxes to white clover at three sites in the Trier area, the ANN based g_s-models were applied to time series data covering 5-month growing seasons of five consecutive years.

The g_s-models proved to perform well in predicting g_s rates for daytime conditions over the time course of the 5-month growing seasons. For night time conditions, a clover clone specific constant g_s rate based on g_s measurements was assumed. The models were able to account for varying weather conditions during the course of the day and growing season. The time-courses of g_s revealed the importance of the air temperature and VPD in defining the g_s. For relatively cold weather periods – often encountered at the beginning or end of the 5-month growing seasons – and the

application of the NC-R model in particular, some surprisingly low g_s rates were predicted and therefore had to be interpreted with caution. This led to the decision to exclude any O_3 flux measurements during the **first** 28-day growing period of every growing season for the derivation of flux-response relationships.

The g_s-model application revealed in general most favourable climate conditions for g_s at the rural site Deuselbach as compared to the two other urban and sub-urban sites. There was no clear trend of a phenology-dependent seasonal variation in g_s, which indicates the overriding importance of the climate in defining the g_s.

Due to the consistently low g_s rates predicted for the NC-R clone, the average and accumulated 5-month g_s rates were always lower for this clone in comparison to the NC-S clone.

The application of the g_s-models for the prediction of O_3 fluxes disclosed by far highest seasonal O_3 flux rates - expressed as AFstX - at the site Deuselbach. This finding has to be attributed to the favourable climate conditions at this site, as well as to the higher O_3 concentrations measured there as compared to the sites Trier-City and Trier-University. Although the different models predicted different g_s rates, it was shown that the dominant cause for these site-dependent variable rates of AFstX was the O_3 concentration rather than the predicted g_s.

10.3 ANNs – a useful tool for developing stomatal conductance models?

The Chapter 10.1 already indicated some of the main strengths and weaknesses of the ANN based g_s-models. The results presented in Chapter 7 show that ANNs were in general capable of modelling g_s and hence pollutant fluxes for white clover, for typical climate conditions of the Trier region. In fact, high R^2-values of up to 0.93 for the relationship between predicted and observed g_s achieved for some sub-models are higher than those that tend to be achieved using empirical or semi-mechanistic models for the prediction of g_s (Emberson et al., 2000; Uddling, 2004; Büker et al., 2007). This would indicate that ANNs are indeed able to learn, interpret and apply knowledge related to g_s to predict the complex, non-linear relationship between g_s and micro-meteorological and phenological variables used as input in the models

presented here. It also demonstrates that ANNs are principally insensitive to inter-correlations between different input variables, a skill that was very beneficial for this study since the Spearman's rank-order correlation test (Chapter 5.2) proved strong correlations between some of the input parameters (e.g. VPD and air temperature).

However, these R^2-values should be interpreted with caution since the validation dataset – though randomly extracted from the input dataset – used for the comparison with the predicted data represents very similar conditions to those under which the models were trained. In other words, the ANNs identified the complex relationship between the five inputs and g_s based on the information they were provided with; this information comprised 9114 data points representing 23 days and 5224 data points representing 13 days for the NC-S and NC-R model, respectively.

Though the g_s measuring campaigns were planned according to the overall aim to achieve a dataset with good representation of typical growing conditions during the summer months in the Trier region, there will be climatic conditions the model was not trained for but will be forced to represent. This circumstance discloses one main weakness of ANNs: while they are able to interpolate to overcome small data gaps, ANNs are very sensitive to larger data gaps and have a very limited ability to extrapolate.

For example, in this thesis this necessitated the assumption of a constant night-time g_s (see Chapter 10.1) and might also have resulted in the slightly unrealistic predictions of g_s for particular day-time conditions – e.g. air temperatures below those included in the input data that occurred at the start of growing seasons (early May), low PAR values (induced by sudden cloud cover) despite hot and dry summer days etc. - during the growing seasons of the years 1997 to 2001. However, closer analysis of the diurnal time courses of predicted g_s did not reveal any major divergences from what would have been expected considering the prevailing climatic conditions, a result that is mainly attributed to the comprehensive input dataset (cf. Chapter 5). It is therefore fair to say that the statement "a model can only be as good as is its input" is possibly even more pertinent to ANNs than for any other type of model.

Another important characteristic for consideration when assessing the use of ANNs for model development is their sensibility to a change in the number of hidden neurons, as well as to a change in learning rate or momentum. Only a slight change in any of these three factors might lead to a different model in respect of its predictive ability. While this characteristic ensures that ANNs can reveal and learn even slight dependencies between any involved parameters, it also significantly complicates and slows down the network developing process. So far, time-consuming trial and error is still the best and most common method for the identification of the ideal model, a fact that often does not appeal to potential users of ANNs.

Another worrying feature of ANNs also found in this thesis is the variation of the contribution of input parameters to the prediction of the output. While VPD and air temperature were predominantly the main contributors to the prediction of g_s for all models developed within this study, all three remaining input parameters strongly varied in their importance during the model development process. This is on the one hand a sign for ANNs being able to trace similar information via different pathways during the training, but on the other hand also shows their susceptibility to follow wrong tracks that might be suggested by the input dataset.

Closely connected with this finding is the concern for a potential over-prediction of an ANN model leading to a bad generalisation, i.e. prediction ability. However, the intrinsic training procedure of the software largely prevents this error by constantly cross-checking the model output with test data that were extracted from the input dataset prior to the start of the training.

Last but not least, the criticism that ANNs are black box models that are difficult to interpret can nowadays partly be compensated via various ANN interpretation methods also used in this thesis. These methods help the user to get a better understanding of how the resulting network had been developed and how the training can be influenced by changing the combination of input parameters, adding or removing hidden neurons as well as varying the learning rate and momentum. Furthermore, there are now techniques available that reveal the impact of single input parameters on the dependent variable. However, in conclusion ANNs are still not as

easy to interpret as for instance empirical models, where an alteration of model inputs lead to an immediate, obvious and comprehensible change in the output.

As a consequence, ANNs are a good choice for developing site- and species-specific g_s-models provided that the input dataset is comprehensive and of high quality. The developed g_s-models can easily be applied to datasets representing similar climatic conditions to those the network was trained with. However, as soon as these specific condition boundaries and combinations are crossed, ANNs start to struggle to predict sensible rates of g_s. This for instance means that the g_s-model for potted clover clones developed in this thesis according to available physical and pollution climate data recorded in the Trier region may not be applicable in Southern or Northern Europe due to the different climates in these regions.

10.4 Comparison of different g_s models

The multiplicative Jarvis-type g_s-models (cf. Jarvis, 1976) that have been used in a number of O_3 flux models (perhaps best represented by the DO_3SE model developed by Emberson et al., 2000) is based on the presumption that an initially defined maximal g_s is potentially diminished by non-optimal meteorological conditions and phenological stage of the targeted plant. By doing so, this approach suggests that there is a multiplicative, linear and therefore one-dimensional relationship between the g_s and its driving variables. It has widely been recognised that this assumption is not always realistic but nevertheless provides a reasonably sound approach, especially when applied to large scale, i.e. regional, datasets (cf. Büker et al., 2007). However, from a purely plant physiological point of view, this approach will eventually have to be replaced by more sophisticated methods that take into account the complex dependence of g_s and gas exchange in general on a set of inter-correlated meteorological and phenological parameters.

Furthermore, one main criticism of this approach has always been the dependence of the predicted actual g_s on the correct initial definition of the maximum stomatal conductance (g_{max}). Since this definition is very difficult to make given the limited number of g_s datasets that are available for different cultivars, species and climate regions which meet the strict criteria that should be met to define this variable, there is

a danger that an unrepresentative maximum g_s would lead to a systematic over- or under-prediction of g_s and hence O_3 flux. In other words, the intrinsic problem of this multiplicative algorithm is the direct dependence of the actual g_s on this one key parameter.

In contrast, the Ball-Woodrow-Berry algorithm first developed in the late 1980's (Ball et al., 1987) and ever since extensively revised and applied (e.g. Leuning et al., 1995; Nikolov et al., 1995; Müller et al., 2005) assumes a direct and close relationship between net photosynthetic rate and g_s and as such has a more mechanistic approach to predict g_s. Specifically, it assumes that g_s is a function of net photosynthetic rate, relative humidity, CO_2-concentration at the leaf surface and a dimensionless factor m representing the species-specific composite sensitivity of g_s to net photosynthetic rate. In comparison with the multiplicative model, this approach is therefore able to account for plant-specific physiological processes by mechanistically coupling g_s and photosynthesis. The BWB-model is therefore often preferred by biologists/plant physiologists, although Büker et al. (2007) showed that the predictive performance of this model approach generally does not differ substantially from the multiplicative Jarvis-algorithm, at least when being applied to regional datasets, with R²-values for the relationship between measured and observed g_s of up to approximately 0.65 for both models.

One reason for the poorer than expected performance of the photosynthesis-based approach might be the assumption that the relationship between g_s and net photosynthetic rate is assumed to be of the same intensity throughout the growing season (constant factor m). However, several studies (Wohlfahrt et al., 1998; Kosugi et al., 2003; Müller et al., 2005) have shown that the parameter m might change with leaf age, which means that a decoupling of g_s and net photosynthetic rate is likely towards the end of the growing season. This phenomenon is rarely accounted for in the published literature.

Furthermore, the high input requirements have frequently been mentioned as an obvious limitation both in terms of input and parameterisation data of the BWB-algorithm (cf. Büker et al., 2007). The main reason for this is that the net photosynthetic rate, a parameter not always readily available, is required as an input

parameter. Accordingly, BWB-type models are often coupled with photosynthesis models (e.g. LEAFC3; Nikolov et al., 1997), which require detailed meteorological (e.g. ambient CO_2 concentration, dew-point temperature) and species-specific plant-physiological input parameters (e.g. V_{m25}, J_{m25}, K_{c25}, K_{o25}) often difficult to obtain.

These shortcomings of the multiplicative and photosynthesis-based models were the reason for considering ANNs as a tool for the prediction of g_s of white clover. However, as shown in the preceding Chapter 10.2, ANNs also have their distinctive disadvantages. Table 10.1 summarises the advantages and disadvantages of all three g_s modelling techniques.

Table 10.1   Overview of advantages and disadvantages of three main g_s-model approaches.

	Empirical algorithm (Jarvis approach)	Semi-mechanistic algorithm (BWB approach)	Artificial Neural Networks (approach used here)
Advantages	- flexibility to easily include and exclude factors in equation - well established - successfully applied to regional and local datasets	- relates g_s to eco-physiological (P_n) and biochemical factors - well established - successfully applied to regional and local datasets	- ability to reveal complex non-linear relationship between input and g_s - insensitivity to inter-correlation of input data - insensitivity to noisy input data
Disadvantages	- assumption of linear relationship between input and g_s - assumption of non-correlated input variables - strong dependence of predicted g_s on prescribed g_{max} - non-mechanistic nature of approach	- dependence on net photosynthesis (P_n) → must be observed or modelled - assumption that relationship between Pn and g_s stays constant throughout growing season - some required input parameters difficult to derive/obtain (e.g. *m*)	- limited extrapolation ability - time consuming training process - interpretation of ANNs difficult → black box model - limited acceptance among scientists and potential users

In conclusion, due to their strengths and weaknesses all three models have their own niche in which they perform best. While the empirical approach has been proved to

perform well on a regional level, both the semi-mechanistic approach and the ANNs are outperforming the empirical approach in predicting g_s on a site-specific level. ANNs are expected to better predict species- and site-specific g_s because they clearly outperform the other two approaches in revealing the complex relationship between available input parameters and g_s, however this comes at a price since the training process of the ANNs is time-consuming and their application is restricted to datasets that match more or less the range of the input data the ANNs were trained with.

10.5 Analysis of reported difference in sensitivity of NC-S and NC-R clones to ozone

The results presented in Chapter 8 clearly show the differing sensitivity of the NC-S and NC-R white clover clone to ambient O_3 exposure. In particular the ozone-induced foliar injury was much higher for the ozone-sensitive in comparison to the ozone-resistant clone. Furthermore, during reasonably warm and dry weather periods, the NC-S clone produced less biomass in relation to the NC-R clone, resulting in NC-S/NC-R ratios of below 1, with a minimum record of 0.73 for the second harvest in Deuselbach in 1998. Not surprisingly, the lowest NC-S/NC-R biomass ratio was reported from Deuselbach, since this is the site with the highest O_3 concentrations and indeed highest predicted g_s. However, some NC-S/NC-R biomass ratios of up to 1.1 were also recorded in Deuselbach, an elevated wind-exposed site in the Hunsrück mountains, especially during cooler and wetter growing periods, indicating the higher sensitivity of the NC-R clone to unfavourable growing conditions.

These findings indicate that the NC-S clover clone is not only more susceptible to acute visible foliar injury following short-term exposure to elevated O_3 concentrations, but also to long-term (here 28 day growing periods, followed by a harvest) O_3 exposure. This has also been reported from other research groups throughout Europe and North America (e.g. Heagle et al., 1995; Bermejo et al., 2002; Fagnano et al., 2004) and has led to mainly two theories being put forward to try to explain why the NC-S clone is more ozone-sensitive:

1) The on average higher g_s of the NC-S clone leads to higher O_3 fluxes into the plant interior as compared to the NC-R clone, causing more cell damage in the former. As an effect, acute visible injury is more pronounced on the NC-S

clone, while on a longer term its photosynthetic capacity is reduced, resulting in less biomass.

2) A lower detoxification potential, expressed for instance as lower concentration rates of antioxidants such as apoplastic ascorbate or glutathione, reduces the ability of the NC-S clone to cope with prevailing pollutant/ O_3 fluxes.

It might well be that there is no single explanation for the increased O_3 sensitivity of the NC-S clone, i.e. a mixture of physiological and biochemical processes may well govern the phytotoxicity of this clone to O_3.

The gas exchange measurements carried out for this thesis as well as the predictions of g_s for the course of entire growth periods using the developed ANN-based models indeed suggest that one of the main reasons for the higher susceptibility of the NC-S clone to O_3 might have been its higher g_s as compared to the NC-R clone: The predicted rate of g_s was in fact always, i.e. at all sites and for all growing periods during all five exposure years, significantly higher ($P = 0.000$) for the NC-S than for the NC-R clone. Logically, this resulted in significantly higher O_3 fluxes into the NC-S clover plants, which might explain the differences in foliar injury and biomass between the two clones.

Curves depicting the predicted g_s over the course of an entire growing season show that the NC-S clone is responding to dry weather conditions by limiting its gas exchange through a reduction in the width of the stomata, though to a lower extent than the NC-R clone. The strategy of the NC-S clone seems to be to sustain its photosynthetic activity as long as possible, rather than sufficiently closing the stomata to prevent the influx of pollutants. This behaviour, which probably would not have occurred in white clover growing under field conditions, can be partly explained by the experimental set-up of the clover clone bioindicator system used in this study. The well-maintained water supply of the clover plants (using constantly accessible water reservoirs) helped to minimise a decrease in the leaf water potential, which did not make a complete closure of the stomata necessary to stop water losses through transpiration for hot and dry weather conditions.

This is also a clear sign for the artificial nature of the bioindicator system used, which limits the application of the developed g_s-models to clover grown under field conditions. For field conditions, a soil water limitation parameter (e.g. soil water potential, soil moisture deficit, soil water content) would have had to be included as an input parameter for the training of the g_s-model.

Unfortunately, it was not possible (nor within the scope of this thesis) to analyse the concentration of (apoplastic) antioxidants known to be able to scavenge reactive oxygen species formed after an O_3 attack. These biochemicals that define the detoxification potential of plants have been shown to be able to react quickly to O_3 attacks, therefore (partly) compensating potentially harmful doses of pollutants such as O_3 (Castillo et al., 1987; Calzada et al., 2001; Van Hove et al., 2001). However, when directly comparing the levels of apoplastic ascorbate in both white clover clones used in this study, D'Haese et al. (2005) found that in comparison with the NC-R clone the NC-S clone always had higher levels of this antioxidant and concluded that high levels of apoplastic ascorbate do not necessarily induce a higher tolerance of plants to O_3. This is further support for the suggestion that physiological processes might primarily contribute to the relative ozone-sensitivity of the NC-S clone.

10.6 Concentration- vs. flux-based dose-response relationships

The O_3 exposure- and dose-response relationships developed in this thesis for the sensitive and resistant white clover clones are only partly satisfying. It proved to be very difficult to show sensible relationships between the exposure or the dose of O_3 - expressed either as AOT40 or accumulated modelled fluxes using various thresholds (AFstX), respectively - and the response parameter biomass, whereas the relationship of AOT40 and AFstX with the response parameter visible leaf injury yielded better results.

While a few significant relationships between biomass ratio and AFstX could be demonstrated for specific sites in specific years (e.g. AFst0 at Trier-University in 1997 and 2000), the overall performance was poor. In general, the dose-response relationships implied that the NC-S clone showed an increasingly reduced biomass in relation to the NC-R clone with increasing AFstX, whereas the results suggest the

opposite (increasing NC-S biomass in relation to NC-R biomass with increasing AFstX) for the Deuselbach site. For the Trier-City site, the clover showed no response to increasing AFstX whatsoever. These statements are true for the AFstX predicted with both the NC-S and the NC-SR model. When pooling all data, no clear relationship between dose and NC-S/NC-R biomass ratio could be determined.

Also, it was impossible to identify a general flux threshold that worked best for the derivation of dose-response relationships, there was however a trend that no threshold (AFst0) seemed to perform best.

Interestingly, the best (though usually mediocre or worse in absolute terms) dose-response relationships could in general be shown when relating the NC-S/NC-R biomass ratio to accumulated fluxes at the sub-urban site Trier-University. This might be explained by the fact that the models had also been trained with data recorded at this site, which in turn means that the application to more urban (Trier-City) and rural (Deuselbach) climate conditions has to be treated with caution. However, it might as well be an indication for the clover clone bioindicator system having worked best at this site.

Considering these poor results, other dose parameters were considered, such as the ratio between accumulated fluxes using the NC-S and NC-R model (AFstX NC-S/AFstX NC-R), which did not result in any improvement of the dose-response relationships. When relating the accumulated fluxes to the absolute biomass of the clover clones separately, positive relationships between AFstX and AOT40 and the biomass of both clones were detected. This shows that both clones benefited from the warmer climates experienced during growing periods with high O_3 concentrations rather than suffering from the higher pollutant doses at these times, which is another proof for the limited suitability of the clover clone bioindicator system in Central Europe.

The unsatisfying dose-response relationships using the NC-S/NC-R biomass ratio as response parameter are in agreement with reports from various other Central and Northern European members of the ICP Vegetation programme that have participated in the clover clone bioindicator campaign (personal communication). There is in fact

general agreement that the NC-R clone is less adapted to cold and moist climates than the NC-S clone, leading to lower biomass rates despite being more resistant to O_3. It therefore has to be judged as a weak if not unsuitable control for the evaluation of O_3 impacts on the NC-S clone. This theory is supported by the results of this thesis, showing that the relationships between flux and NC-S/NC-R biomass ratio are particularly bad for the site Deuselbach, the on average coolest and wettest site included in this study. In contrast, during hot and dry summer periods, the flux-response relationships improved, as can for instance be seen for the years 1997 and 1999 at the site Trier-University. Accordingly, Southern European researchers have shown that the clover bio-indicator system works well under Mediterranean climate conditions (e.g. Bermejo et al., 2002; Fagnano et al., 2004), which is not surprising considering the propagation and establishment of these white clover clones in the sub-tropical climates of North Carolina, U.S.A. (Heagle et al., 1995). The origin of these clones is hence an indication of their adaptation to hotter and drier climates. However, the usually higher O_3 contractions in Southern Europe might also contribute to the successful application of the clover bioindicator system there, which might in turn indicate that the Northern European O_3 concentrations are not high enough to cause substantial biomass reduction of the NC-S clone.

It was furthermore not possible to show whether the ozone-sensitivity of the NC-S clover clone differed over the course of the growing season, i.e. with phenological stage. The rates of the NC-S/NC-R biomass ratio varied throughout the entire growing season – quite possibly due to the enhanced climate induced variability in the growth of the NC-R clone - and did not allow any conclusions as to the temporal variation in the ozone-sensitivity of the sensitive clove clone.

One further reason for the difficulties in deriving strong relationships between O_3 flux and the NC-S/NC-R biomass ratio might be the fact that the g_s-models are based on leaf-level g_s measurements. Although the used leaves for gas exchange measurements (third or fourth from tip of the stolon) were believed to well represent the average gas exchange of the entire plant, a desirable up-scaling procedure from leaf to plant could not be derived due to the lack of LAI data. A first attempt to develop a canopy-flux model for white clover was presented by Harmens et al. (2006) but resulted in direct

comparison with the leaf-level flux model in a lower r^2 value for the dose-response function, which was the reason for turning down this approach here.

In comparison, the relationship of O_3 exposure and O_3 dose with the response parameter visible leaf injury was more satisfying. It could be shown that for all sites there is a positive relationship between 28-day AFstX – with best results for AFst4 – as well as 28-day AOT40 with visible leaf injury assessed at the end of 28-day growing periods. The AOT40 consistently outperformed the AFstX apart from the calculation for the site Trier-City, i.e. the exposure index usually explained more variation in the observed foliar injury than the uptake index. It has to be pointed out that the results of the linear regression (i.e. the r^2-values) shown in Figure 9.1 are very much driven by one 1997 data point representing very high O_3 concentrations and O_3 fluxes and related high injury scores. When excluding this data point, most regression results deteriorated.

Though the NC-R clone also showed some visible injury during high O_3 concentration periods, no sensible relationship between its median score (usually 0, sometimes 1) and O_3 exposure or dose indices could be developed. Furthermore, the relation between the **first occurrence** of visible injury on both clones – typically assessed during the second week (i.e. on average 12 days) after the last harvest – and O_3 exposure or dose indices did not deliver meaningful results (data not shown) because of the reported injury score, which when pooling the data was too even with median values of usually 1 for the NC-S and 0 for the NC-R clone.

This indicates the problems that occurred in using the response parameter visible leaf injury. First of all, despite working according to a standardised experimental protocol that precisely describes how to perform visible injury assessments, these assessments have to be considered as being somewhat subjective. These assessments were always carried out by the same person (the author of this thesis), which helped to minimise the variation in the recordings. However, some variation in the recorded assessments has to be attributed to the subjective judgement of the assessor, for example at the start of each growing season in May (which was another reason for always excluding the first 28-day growing period from any further analysis).

Another problem of the visible injury assessment is – as already mentioned above - the classification method: Though without doubt practical, its wide and varying range of injury within one class makes a proper analysis difficult. Rather than using a percentage of injured clover leaves, the median (the mean was not acceptable due to the ordinal nature of the data) injury class (from 0 to 5) had to be chosen in this thesis as the response parameter. Unfortunately, this led to very evenly distributed characterisations of the injury, with most injury on the NC-S clone either falling into class 2 (1 to 5 % of leaves injured) or class 3 (5 to 25 % of leaves injured).

In conclusion, these difficulties and shortcomings of the experiment strongly suggest that the reported poor dose-response relationships in respect to the response parameter biomass have to be mainly attributed to the failure of the bioindicator system under these particulate climate conditions rather than to a failure of the developed flux models. This statement is supported by the findings that no clear exposure-response relationship between relative biomass loss and AOT40 could be developed either, further indicating the limited suitability of the used bio-indicator system in quantifying O_3 effects on the growth of pot-grown clover clones or legumes and forbs in general.

However, the relationships between visible leaf injury and O_3 exposure or O_3 dose were more satisfying, which suggests that the clover clones are suitable as bio-indicators for the easy and inexpensive detection of effect of tropospheric O_3 on plants at a particular site.

With the results presented in this thesis, it is very difficult to give a sensible recommendation whether or not dose- rather than exposure-indices are more suitable to predict impacts of tropospheric O_3 on the NC-S and NC-R clones. In terms of biomass losses, a recommendation is indeed very difficult due to the poor results reported above. However, there is a slight trend for a better performance of the dose-rather than the exposure-index in predicting ozone-induced detrimental effects on the biomass production of clover clones; there is in other words certainly no reason why the flux approach should not be considered for this purpose. In contrast, the O_3 exposure index AOT40 seems to be the better choice in explaining and predicting leaf foliar injury of the (potted) white clover clones.

10.7 Conclusions and perspectives

The previous chapters showed in detail the advantages and disadvantages of the ANN-based g_s-models as well as the used clover clone bio-indication system. The overall representativeness and significance of the study has to be judged on these findings.

The scope of this study was to i) test ANNs for their suitability in developing g_s-models based on climatic, phenological and O_3 pollution data, ii) investigate whether the developed g_s-models for white clover clones are able to realistically predict O_3 fluxes to these plants, iii) compare the performance of O_3 dose- with O_3 exposure-indices in relation to recorded response parameters, iv) investigate whether or not the higher O_3 sensitivity of the NC-S clone might be related to higher rates of g_s as compared to the NC-R clone and v) evaluate the used bio-indicator system for its ability in quantifying ozone-induced impacts on two white clover clones and plants in general.

It has been shown that ANNs are indeed a useful tool for developing species-specific g_s-models for application on a site-specific scale. The application of the g_s-models specifically developed for an ozone-sensitive and ozone-resistant white clover clone grown under non-limiting water supply is therefore limited to these pot-grown clones and to West European climate conditions similar to those recorded in Trier. It is not possible – and indeed was not within the scope of this study - to apply the models and transfer the findings to field-grown plants, not even to field grown white clover, because of the species-specific nature of the models and the lack of any soil water model input parameters.

With the help of the developed ANN-based g_s-models, differences in O_3 fluxes between the two clones, different growth stages over the course of a 5-month growing season and different sites in the Trier area could be predicted.

When relating these O_3 flux rates to the response parameters NC-S/NC-R biomass ratio and visible leaf injury, reasonable dose-response functions (r^2 values of up to 0.54) could be developed for the latter, whereas the dose-response functions for the former were very weak (r^2 values of up to 0.21), possibly due to the leaf-level rather than canopy-level g_s-models developed here and the generally bad performance of the

white clover bioindicator system. The fact that exposure-response functions using AOT40 did not perform better stresses the limited suitability of the response parameter NC-S/NC-R biomass ratio in the Trier region.

A recommendation whether to use dose- or exposure-indices for quantifying O_3 impacts on the growth of clover is therefore difficult. However, the exposure index AOT40 outperformed the dose calculations in revealing and predicting the impact of O_3 on foliar leaf injury.

The g_s differed significantly between the two clones. The NC-S clone always showed higher rates and therefore higher O_3 fluxes, which might be one reason for its higher ozone-sensitivity as compared to the NC-R clone.

The white clover bio-monitoring system did not work well during relatively cool and wet growth periods, but performed better under warmer and drier weather conditions. The response parameter visible injury led to better dose-response relationships than the response parameter relative biomass loss.

One way how to overcome the reported difficulties in the two clones reacting differently to the prevailing climate would be to develop a clover growth model for each clone based on meteorological parameters. This would help to compensate the overlaying climate effect on the prediction of the NC-S/NC-R biomass ratio, which could then result in better dose-response relationships for the clover clones. Also, a further approach in up-scaling from leaf- to canopy-level fluxes using LAI data could potentially improve the dose-response functions.

Last but not least, repeating the experiment with field-grown clover clones and corresponding measurements of soil water parameters would enable the model to account for varying soil moisture conditions, which potentially would make it possible to transfer the dose-response functions to "naturally-grown" white clover in the field.

References

ACKLEY, D. H., HINTON, G. E. & T. J. SEJNOWSKI (1985). A learning algorithm for Boltzmann machines. Cognitive Science 9, 147-169.

ALEXANDER, J. & M. DRÜEKE (1992). Ozonimmissionen in Trier und Umgebung. In. MÜLLER, M. J. (Ed.). Beiträge zur Physischen Geographie und Landeskunde. Gerold Richter zum 60. Geburtstag gewidmet. Flensburger Regionale Studien, Flensburg, Sonderheft 2, 311-347.

ANDERSON, P. D., HOUPIS, J. L. J., HELMS, J. A. & B. MOMEN (1997). Seasonal variation of gas exchange and pigmentation in branches of three grafted clones of mature Ponderosa pine exposed to ozone and acid rain. Environmental Pollution 97(3), 253-263.

ANFOSSI, D., SANDRONI, S. & S. VIARENGO (1991). Tropospheric ozone in the nineteenth century. the Moncalieri series. Journal of Geophysical Research 96, 17349-17352.

ARNDT, U. (1992). Einführung in die Bioindikation. In. KOHLER, A. & U. ARNDT (Eds.). Bioindikatoren für Umweltbelastungen – Neue Aspekte und Entwicklungen. Margraf, Weikersheim, 13-18.

ARNDT, U., NOBEL, W. & B. SCHWEIZER (1987). Bioindikatoren. Möglichkeiten, Grenzen und neue Erkenntnisse. Ulmer, Stuttgart.

ASHENDEN, T. W., BELL, S. A. & C. R. RAFAREL (1995). Responses of white clover to gaseous pollutants and acid mist. implications for setting critical levels and loads. New Phytologist 130, 89-96.

ASHMORE, M. R. & J. N. B. BELL (1991). The role of ozone in global change. Annals of Botany 67, 39-48.

ASHMORE, M. R. (1984). Effects of ozone on vegetation in the United Kingdom. In. GRENNFELT, P. (Ed.). Proceedings International Workshop on the Evaluation of the Effects of Photochemical Oxidants on Human Health, Agricultural Crops, Forestry, Materials and Visibility. Swedish Environmental Research Institute, Göteborg, Sweden, 99-106.

ASHMORE, M. R., THWAITES, R. H., AINSWORTH, N., COUSINS, D. A., POWER, S. A. & A. J. MORTON (1995). Effects of ozone on calcareous grassland communities. Water, Air and Soil Pollution 85, 1527-1532.

ASHMORE, M., COYLE, M. & D. FOWLER (2002). Implications for increasing tropospheric background ozone concentrations for vegetation in the UK. A review for DEFRA under contract EPG 1/3/173.

ASHMORE, M., EMBERSON, L., KARLSSON, P.E. & H. PLEIJEL (2004a). Introduction for ozone deposition special issue. Atmospheric Environment 38, 2211-2212.

ASHMORE, M., EMBERSON, L., KARLSSON, P.E. & H. PLEIJEL (2004b). New directions: A new generation of ozone critical levels for the protection of vegetation in Europe. Atmospheric Environment 38, 2213-2214.

BALL, G. R., BENTON, J., PALMER-BROWN, D., FUHRER, J., SKÄRBY, L., GIMENO, B. S. & G. MILLS (1998). Identifying factors which modify the effects of ambient ozone on white clover (*Trifolium repens*) in Europe. Environmental Pollution 103, 7-16.

BALL, G. R., PALMER-BROWN, D., FUHRER, J., SKÄRBY, L., GIMENO, B. S. & G. MILLS (2000). Identification of non-linear influences on the seasonal ozone dose response of sensitive and resistant clover clones using artificial neural networks. Ecological Modelling 129, 153-168.

BALL, J. T., WOODROW, I. E. & J. A. BERRY (1987). A model predicting stomatal conductance and its contribution t the control of photosynthesis under different environmental conditions. In. BIGGINS, I. (Ed.). Progresses in photosynthesis research, Vol. IV. Martinus Nijhoff Publishers, Dordrecht, 221-224.

BALLS, G. R. (1996). Investigating the influences on plant ozone sensitivity using Artificial Neural networks. PhD thesis, Nottingham Trent University, Nottingham.

BALLS, G. R. (1996). Investigating influences on plant ozone sensitivity using Artificial Neural Networks. PhD Thesis, Nottingham Trent University.

BARAN, P., LEK, S., DELACOSTE, M. & A. BELAUD (1996). Stochastic models that predict trout population density or biomass on a mesohabitat scale. Hydrobiologia 337, 1-9.

BARCIELA, R. M., GARCÍA, E, & E. FERNANDEZ (1999). Modelling primary production in a coastal embayment affected by upwelling using dynamic ecosystem models and artificial neural networks. Ecological Modelling 120, 199-211.

BARNES, J. D., BENDER, J., LYONS, T. & A. BORLAND (1999). Natural and man-made selection for air pollution resistance. Journal of Experimental Biology 50, 1423-1435.

BAUMGARTEN, M., WERNER, H., HÄBERLE, K.-H., EMBERSON, L. D., FABIAN, P. & R. MATYSSEK (2000). Seasonal ozone response of mature beech trees (*Fagus sylvatica*) at high altitude in the Bavarian forest (Germany) in comparison with young beech grown in the filed and in phytotrons. Environmental Pollution 109, 431-442.

BAZOON, M., STACEY, D. A., CUI, C. & G. HARAUZ (1994). A hierarchical artificial neural network system for the classification of cortical cells. Proceedings of the IEEE International Conference on Neural Networks. Orlando, USA, 3521-3524.

BECK, J. & P. GRENNFELT (1994). Estimate of ozone production and destruction over north-western Europe. Atmospheric Environment 28, 129-140.

BECKER, K., SAURER, M., EGGER, A. & J. FUHRER (1989). Sensitivity of white clover to ambient ozone in Switzerland. New Phytologist 112, 235-243.

BENTON, J., FUHRER, J., GIMENO, B. S., SKÄRBY, L., PALMER-BROWN, D., BALL, G., ROADKNIGHT, C. & G. MILLS (2000). An international cooperative programme indicates the widespread occurrence of ozone injury on crops. Agriculture, Ecosystems and Environment 78, 19-30.

BENTON, J., FUHRER, J., GIMENO, B. S., SKÄRBY, L., PALMER-BROWN, D., BALL, G., ROADKNIGHT, C. & G. MILLS (2000). An international cooperative programme indicates the widespread occurrence of ozone injury on crops. Agriculture, Ecosystems and Environment 78, 19-30.

BERGMANN, E., BENDER, J. & H.-J. WEIGEL (1998). Zur Ozonempfindlichkeit von Wildpflanzenarten. Agrarökologie 30, Verlag Agrarökologie, Bern.

BERGMANN, E., BENDER, J. & H.-J. WEIGEL (1999). Ozone threshold doses and exposure-response relationships fort he development of ozone injury symptoms in wild plant species. New Phytologist 144, 423-435.

BERMEJO, V., GIMENO, B. S., GRANADOS, I., SANTAMARÍA, J., IRIGOYEN, J. J., BERMEJO, R., PORCUNA, J. L. & G. MILLS (2002). Investigating indices to explain the impacts of ozone on the biomass of white clover (*Trifolium repens* L. cv. Regal) at inland and coastal sites in Spain. New Phytologist 156, 43-55.

BISHOP, C. M. (1995). Neural networks for pattern recognition. Clarendon Press, Oxford.

BORRELL, P., BUILTJES, P. J. H., GRENNFELT, P. & Ö. HOV (Eds.) (1997). Photo-oxidants, acidification and tools. Policy applications of EUROTRAC results. Springer Verlag, Berlin.

BORRISS, H. & E. LIBBERT (1985). Wörterbuch der Biologie. Pflanzenphysiologie. Fischer, Stuttgart.

BORTIER, K., CEULEMANS, R. & L. DE TEMMERMAN (2000a). Effects of tropospheric ozone on woody plants. In. AGRAWAL, S. B. & M. AGRAWAL (Eds.). Environmental pollution and plant responses. Lewis Publishers, New York, 153-182.

BORTIER, K., DE TEMMERMAN, L. & R. CEULEMANS (2000b). Effects of ozone exposure in open-top chambers on poplar (*Populus nigra*) and beech (*Fagus sylvatica*). a comparison. Environmental Pollution 109, 509-516.

BRAUN, S. & W. FLÜCKIGER (1995). Effects of ambient ozone on seedlings of *Fagus sylvatica* L. and *Picea abies* (L.) Karst. New Phytologist 129, 33-44.

BREY, T., JARRE-TEICHMANN, A. & O. BORLICH (1996). Artificial neural network versus multiple linear regression. predicting P/B ratios from empirical data. Marine Ecology Progress Series 140, 251-256.

BREY, T., JARRE-TEICHMANN, A. & O. BORLICH (1996). Artificial neural network versus multiple linear regression. predicting P/B ratios from empirical data. Marine Ecology Progress Series 140, 251-256.

BROADMEADOW, M. (1998). Ozone and forest trees. New Phytologist 139, 123-125.

BÜKER, P. (1997). Einsatz der Bioindikatoren *Trifolium repens* und *Phaseolus vulgaris* zum Nachweis ozoninduzierter Blattschäden und Ernteverluste. Diploma thesis, Universität Trier, Trier.

BÜKER, P., EMBERSON, L.D., ASHMORE, M.R., CAMBRIDGE, H.M., JACOBS, C.M.J., MASSMANN, W.J., MÜLLER, J., NIKOLOV, N., NOVAK, K., OKSANEN, E., SCHAUB, M., DE LA TORRE, D.(2007). Comparison of different stomatal conductance algorithms for ozone flux modelling. Environmental Pollution, Vol. 146, 726-735.

BUNGENER, P., BALLS, G. R., NUSSBAUM, S., GEISSMANN, M., GRUB, A. & J. FUHRER (1999a). Leaf injury characteristics of grassland species exposed to ozone in relation to soil moisture condition and vapour pressure deficit. New Phytologist 142, 271-282.

BUNGENER, P., BALLS, G. R., NUSSBAUM, S., GEISSMANN, M., GRUB, A. & J. FUHRER (1999). Leaf injury characteristics of grassland species exposed to ozone in relation to soil moisture condition and vapour pressure deficit. New Phytologist 142, 271-282.

BUNGENER, P., NUSSBAUM, S., GRUB, A. & J. FUHRER (1999b). Growth response of grassland species to ozone in relation to soil moisture condition and plant strategy. New Phytologist 142, 283-293.

BURKE, H. B., HOANG, A. & D. B. ROSEN (1995). Survival function estimates in cancer using artificial neural networks. Proceedings of World Congress of Neural Networks, Vol. II, 748-749.

BURKE, H. B., HOANG, A. & D. B. ROSEN (1995). Survival function estimates in cancer using artificial neural networks. Proceedings of World Congress of Neural Networks, Vol. II, 748-749.

CAEMMERER, VON S. & G. D. FARQUHAR (1981). Some relationships between the biochemistry of photosynthesis and the gas exchange of leaves. Planta 153, 376-387.

CALZADA, I., MESANZA, J., CASADO, H. & F. J. CASTILLO (2001). Biochemical changes in needles of *Pinus radiata* D. Don trees in relationship to long-term ozone exposure indices. Environmental Pollution 114, 325-335.

CAMPBELL, G. S. & J. M. NORMAN (1998). An introduction to environmental physics (2nd edition). Springer Verlag, New York.

CASTILLO, F. J. & H. GREPPIN (1986). Balance between anionic and cationic extracellular peroxidase activities in *Sedum album* leaves after ozone exposure. Analysis of high-performance liquid chromatography. Physiologia Plantarum 68, 201-208.

CASTILLO, F. J. & H. GREPPIN (1988). Extracellular ascorbic acid and enzyme activities related to ascorbic acid metabolism in *Sedum album* L. leaves after ozone exposure. Environmental and Experimental Botany 28, 231-238.

CASTILLO, F. J., MILLER, P. R.. & H. GREPPIN (1987). Extracellular biochemical markers of photochemical oxidant air pollution damage to Norway spruce. Experientia 43, 111-115.

CASTILLO, F. J., PENEL, C. & H. GREPPIN (1984). Peroxidase release induced by ozone in *Sedum album* leaves. Involvement of Ca^{2+}. Plant Physiology 74, 846-851.

CHAKRABORTY, K., MEHROTRA, K., MOHAN, C. K. & S. RANKA (1992). Forecasting the behaviour of multivariate time series using neural network. Neural Networks 5, 961-970.

CHAPPELKA, A. H. & L. J. SAMUELSON (1998). Ambient ozone effects on forest trees of the eastern United States. a review. New Phytologist 139, 91-108.

CHEVONE, B., MANNING, W., VARBANOV, A. & S. KRUPA (1998). Relating ambient ozone concentrations to adverse biomass responses of white clover. A case study. Environmental Pollution 103, 103-108.

CHU, W. C. & N. K. BOSE (1998). Speech signal prediction using feedforward neural-network. Electronic Letters 34 (10), 999-1001.

CLARK, A. J., LANDOLT, W., BUCHER, J. B. & R. J. STRASSER (2000). Beech (*Fagus sylvatica*) response to ozone exposure assessed with a chlorophyll *a* fluorescence performance index. Environmental Pollution 109, 501-507.

CLOSS, H. (1979). Die Klimasituation im Regierungsbezirk Trier. In: Friedrich, L. (Ed.): Beiträge zur Trierischen Landeskunde, Trier.

COLASANTI, R. L. (1991). Discussions of the possible use of neural network algorithms in ecological modelling. Binary 3, 13-15.

COSATTO, E. & H. P. GRAF (1995). A neural-network accelerator for image-analysis. Micro, IEEE 15, 32-38.

COTTRELL, G. W. & M. FLEMING (1990). Face recognition using unsupervised feature extraction. Proceedings of the International Neural Networks Conference, vol. 1. Paris, France, 322-325.

COYLE, M., FOWLER, D. & M. ASHMORE (2003). New directions. Implications of increasing tropospheric background ozone concentrations for vegetation. Atmospheric Environment 37, 153-154.

CRAIGON, J., FANGMEIER, A., JONES, M. H., DONNELLY, A., BINDI, M., DE TEMMERMANN, L., PERSSON, K. & K. OJANPERÄ (2002). Growth and yield responses of potato to increasing CO_2 and ozone. European Journal of Agronomy 17, 273-290.

CRUTZEN, P. J. & P. H. ZIMMERMANN (1991). The changing photochemistry of the troposphere. Tellus 43A, 136-151.

CRUTZEN, P. J. (1973). The role of NO and NO2 in the chemistry of the troposphere and stratosphere. Annual Review of the Earth Planet Science 7, 443-472.

D'HAESE, D., VANDERMEIREN, K., ASARD, H. & N. HOREMANS (2005). Other factors than apoplastic ascorbate contribute to the differential ozone sensitivity of two clones of *Trifolium repens* L. Plant, Cell & Environment 28 (5), 623-632.

DAI, H. C. & C. MACBETH (1997). Effects of learning parameters on learning procedure and performance of a BPNN. Neural Networks 10 (8), 1505-1521.

DANIELL, T. M. & A. D. WUNDKE (1993). Neural networks – assisting in water quality modelling. Preprints, Watercomp, Melbourne, Australia, 51-57.

DANIELSEN, E. F. (1968). Stratospheric-tropospheric exchange based on radioactivity, ozone and potential vorticity. Journal of Atmospheric Science 25, 502-518.

DANIELSSON, H., GELANG, J. & H. PLEIJEL (1999). Ozone sensitivity, growth and flower development in *Phleum* genotypes of different geographic origin in the Nordic countries. Environmental and Experimental Botany 42, 41-49.

DARRALL, N. M. (1989). The effect of air pollutants on physiological processes in plants. Plant, Cell and Environment 12, 1-30.

DAVIES, T. D., KELLY, P. M., LOW, P. S. & C. E. PIERCE (1992). Surface ozone concentrations in Europe. Links with the regional-scale atmospheric circulation. Journal of Geophysical Research 97, 9819-9832.

DAVISON, A. W. & J. D. BARNES (1998). Effects of ozone on wild plants. New Phytologist 139, 135-151.

DE SILETS, L., GOLDEN, B., WANG, Q. & R. KUMAR (1992). Predicting salinity in the Chesapeake Bay using backpropagation. Computer and Operations Research 19 (3/4), 277-285.

DECOTEAU, D. R., SIMON, J. E., EASON, G. & R. A. REINERT (1986). Ozone-induced injury on field-grown watermelons. HortScience 21, 1369-1371.

DEKRUGER, D. & B. R. HUNT (1994). Image-processing and neural networks for recognition of cartographic area features. Pattern Recognition 27, 461-483.

DEUTSCH, J. C. (1998). Ascorbic acid oxidation by hydrogen peroxide. Analytical Biochemistry 255, 1-7.

DEVEAU, J. L., ORMROD, D. P., ALLEN, O. B. & D. W. BECKERSON (1987). Growth and foliar injury responses of maize, soybean and tomato seedlings exposed to mixtures of ozone and sulphur dioxide. Agriculture, Ecosystems and Environment 19, 223-240.

DIMOPOULOS, I., CHRONOPOULOS, J., CHRONOPOULOU-SERELI, A. & S. LEK (1999). Neural network models to study relationships between lead concentration in grasses and permanent urban descriptors in Athens city (Greece). Ecological Modelling 120, 157-165.

DIMOPOULOS, Y., BOURRET, P. & S. LEK (1995). Use of some sensitivity criteria fro choosing networks with good generalization. Neural Processing Letters 2, 1-4.

DONNELLY, A., CRAIGON, J., BLACK, C. R., COLLS, J. J. & G. LANDON (2001). Elevated CO_2 increases biomass and tuber yield in potato even at high ozone concentrations. New Phytologist 149, 265-274.

ECKEY-KALTENBACH, H. ERNST, D., HELLER, W. & H. SANDERMANN (1994). Biochemical plant response to ozone. IV. Cross-induction of defensive pathways in parsley plants. Plant Physiology 104, 67-74.

EDWARDS, M. & D. R. MORSE (1995). The potential for computer-aided identification in biodiversity research. Trends in Ecology and Evolution 10 (4), 153-158.

ELVIRA, S., ALONSO, R., CASTILLO, F. J. & B. S. GIMENO (1998). On the response of pigments and antioxidants of *Pinus halepensis* seedlings to Mediterranean climatic factors and long-term ozone exposure. New Phytologist 138, 419-432.

EMBERSON, L., ASHMORE, M. & F. MURRAY (Eds.) (2003). Air pollution impacts on crops and forests – A global assessment. Imperial College Press, London.

EMBERSON, L.D., SIMPSON, D., TUOVINEN, J.-P., ASHMORE, M.R., CAMBRIDGE, H.M. (2000). Towards a model of ozone deposition and stomatal uptake over Europe. Norwegian Meteorological Institute, Oslo, EMEP MSC-W Note X/00, pp.57.

ERBS, M. & A. FANGMEIER (2005). A chamberless field exposure system for ozone enrichment of short vegetation. Environmental Pollution 133, 91-102.

EVANS, C. G. (1972). The quantitative analysis of plant growth. University of California Press.

FAENSEN-THIEBES, A. (1983). Veränderungen im Gaswechsel, Chlorophyllgehalt und Zuwachs von *Nicotiana tabacum* L. und *Phaseolus vulgaris* L. durch Ozon und deren Beziehung zur Ausbildung von Blattnekrosen. Angewandte Botanik 57, 181-191.

FAGNANO, M., MEROLA, G., FORLANI, A., POSTIGLIONE, L & J. Fuhrer (2004). Monitoring yield losses from ozone pollution in a Mediterranean environment. A comparison of methods. Water, Air and Soil Pollution 155, 383-398.

FARAGE, P. K. & S. P. LONG (1995). An *in vivo* analysis of photosynthesis during short-term O_3 exposure in three contrasting species. Photosynthesis Research 43, 11-18.

FARAGE, P. K. & S. P. LONG (1999). The effects of O_3 fumigation during leaf development on photosynthesis of wheat and pea. An *in vivo* analysis. Photosynthesis Research 59, 1-7.

FARAGE, P., LONG, S., LECHNER, E. & N. BAKER (1991). The sequence of change within the photosynthetic apparatus of wheat following short-term exposure to ozone. Plant Physiology 95, 529-535.

FARAGGI, D. & R. SIMON (1995). A neural network model for survival data. Statistics in Medicine 14, 73-82.

FARQUHAR, G. D. & T. D. SHARKEY (1982). Stomatal conductance and photosynthesis. Annual Review of Plant Physiology 33, 317-345.

FELLENBERG, G. (1990). Chemie der Umweltbelastung. Teubner, Stuttgart.

FINLAYSON-PITTS, B. J. & J. N. PITTS (2000). Chemistry of the upper and lower atmosphere. Academic Press, San Diego, California.

FISCUS, E. L., REID, C. D., MILLER, J. E. & A. S. HEAGLE (1997). Elevated CO_2 reduces O_3 flux and O_3-induced yield losses in soybeans. Possible implications for elevated CO_2 studies. Journal of Experimental Botany 48(307), 307-313.

FISHMAN, J., SOLOMON, S. & P. J. CRUTZEN (1979). Observational and theoretical evidence in support of a significant in-situ photochemical source of tropospheric ozone. Tellus 31, 432-446.

FLAGLER, R. B. (Ed.) (1998). Recognition of air pollution injury to vegetation. A pictorial atlas. 2nd edition. Air and Waste Management Association, Pittsburgh, USA.

FOOT, J. P., CAPORN, S. J. M., LEE, J. A. & T. W. ASHENDEN (1996). The effect of long-term ozone fumigation on the growth, physiology and frost sensitivity of *Calluna vulgaris*. New Phytologist 133, 503-511.

FOWLER, D., CAPE, J. N., COYLE, M., FLECHARD, C., KUYLENSTIERNA, J., HICKS, K., DERWENT, D., JOHNSON, C. & D. STEVENSON (1999a). The global exposure of forests to air pollutants. Water, Air and Soil Pollution 116, 5-32.

FOWLER, D., CAPE, J. N., COYLE, M., SMITH, R. I., HJELLBREKKE, A.-G., SIMPSON, D., DERWENT, R. G. & C. E. JOHNSON (1999b). Modelling photochemical oxidant formation, transport, deposition and exposure of terrestrial ecosystems. Environmental Pollution 100, 43-55.

FOWLER, D., FLECHARD, C., SKIBA, U., COYLE, M. & J. N. CAPE (1998). The atmospheric budget of oxidized nitrogen and its role in ozone formation and deposition. New Phytologist 139, 11-23.

FOYER, C. H. & P. M. MULLINEAUX (Eds.) (1994). Causes of photooxidative stress and amelioration of defence systems in plants. CRC Press, Boca Raton.

FUCHS, F. (1994). Modellierung der Ozon-Immissionsbelastung in Rheinland-Pfalz - Studien zur physikochemischen Entwicklung von Oxidantien in anthropogen kontaminierten Luftmassen. Mainzer Geographische Studien 38, Mainz.

FUHRER, J. (2003). Agroecosystem responses to combinations of elevated CO_2, ozone, and global climate change. Agriculture, Ecosystems and Environment 97, 1-20.

FUHRER, J., GRANDJEAN GRIMM A., TSCHANNEN, W. & H. SHARIAT-MADARI (1992). The response of spring wheat (*Triticum aestivum* L.) to ozone at higher elevations. II. Changes in yield, yield components and grain quality in response to ozone flux. New Phytologist 121, 211-219.

FUHRER, J., PERLER, R. & H. SHARIAT-MADARI (1993). Growth and gas exchange characteristics of two clones of white clover *Trifolium repens* L. differing in ozone sensitivity. Angewandte Botanik 67, 163-167.

FUHRER, J., SHARIAT-MADARI, H., PERLER, R., TSCHANNEN, W. & A. GRUB (1994). Effects of ozone on managed pasture. II. Yield, species composition, canopy structure, and forage quality. Environmental Pollution 86, 307-314.

GARSON, G. D. (1991). Interpreting neural network connection weights. Artificial Intelligence Expert 6, 47-51.

GEVREY, M., DIMOPOULOS, I. & S. LEK (2003). Review and comparison of methods to study the contribution of variables in artificial neural networks. Ecological Modelling 160, 249-264.

GILLET, J. M. (1985). Taxonomy and morphology. In: TAYLOR, N. L. (Ed.). Clover science and technology. Agronomy Monograph 25, American Society of Agronomy (ASA), Madison, U.S.A., 21 – 28.

GIMENO, B. S., BERMEJO, V., REINERT, R. A., ZHENG, Y. & J. BARNES (1999). Adverse effects of ambient ozone on watermelon yield and physiology at a rural site in Eastern Spain. New Phytologist 144, 245-260.

GIMENO, B. S., BERMEJO, V., SANZ, J., DE LA TORRE, D. & J. M. GIL (2004). Assessment of the effects of ozone exposure and plant competition on the reproductive ability of three therophytic clover species from Iberian pastures. Atmospheric Environment 38(15), 2295-2303.

GOH, A. T. C. (1995). Back-propagation neural networks for modelling complex systems. Artificial Intelligence in Engineering 9, 143-151.

GOSWAMI, P. & SRIVIDYA (1996). A novel neural network design for long-range prediction of rainfall pattern. Current Science 70 (6), 447-457.

GRAEDEL, T. E. & P. J. CRUTZEN (1993). Atmospheric change – an earth system perspective. Freeman and Company, New York.

GRANDJEAN GRIMM, A. & J. FUHRER (1992). The response of spring wheat (*Triticum aestivum* L.) to ozone at higher elevations. III. Responses of leaf and canopy gas exchange, and chlorophyll fluorescence to ozone flux. New Phytologist 122, 321-328.

GRANDJEAN, A. & J. FUHRER (1989). Growth and leaf senescence in spring wheat (*Triticum aestivum*) grown at different ozone concentrations in open-top field chambers. Physiologia Plantarum 77, 389-394.

GRIMES, H. D., PERKINS, K. K. & W. F. BOSS (1983). Ozone degrades into hydroxyl radicals under physiological conditions. Plant Physiology 72, 1016-1020.

GUDERIAN, R., TINGEY, D. T. & R. RABE (1985). Effects of photochemical oxidants on plants. In: GUDERIAN, R. (Ed). Air pollution by photochemical oxidants. Springer, Berlin, 129-333.

GÜNTHARDT-GOERG, M. S. (1996). Different responses to ozone of tobacco, poplar, birch, and alder. Journal of Plant Physiology 148, 207-214.

GÜNTHARDT-GOERG, M. S., McQUATTIE, C. J., MAURER, S. & B. FREY (2000). Visible and microscopic injury in leaves of five deciduous tree species related to current critical ozone levels. Environmental Pollution 109, 489-500.

GUZY, M. R. & R. L. HEATH (1993). Response to ozone of varieties of common bean (*Phaseolus vulgaris* L.). New Phytologist 124, 617-625.

HARMENS, H., MILLS, G., HAYES, F., JONES, L., WILLIAMS, P. & the participants of the ICP Vegetation (2006). Air pollution and vegetation. Annual report 2005/06. ICP Vegetation Coordination Centre, Centre for Ecology and Hydrology, Bangor, UK. http://icpvegetation.ceh.ac.uk

HASSAN, I. A., BENDER, J. & H. J. WEIGEL (1999). Effects of ozone and drought stress on growth, yield and physiology of tomatoes (*Lycopersicon esculentum* Mill. cv. Baladey). Gartenbauwissenschaft 64(4), 152-157.

HEAGLE, A. S. & J. E. MILLER (1996). Effects of rooting medium and fertilizer rate on response of white clover to tropospheric ozone. Environmental Pollution 91(1), 113-119.

HEAGLE, A. S. & L. A. STEFANSKI (2000). Relationship between ambient ozone regimes and white clover forage production using different ozone exposure indexes. Atmospheric Environment 34, 735-744.

HEAGLE, A. S. (1989). Ozone and crop yield. Annual Review of Phytopathology 27, 397-423.

HEAGLE, A. S., BODY, D. & W. HECK (1973). An open-top field chamber to assess the impact of air pollution on plants. Journal of Environmental Quality 2, 365-368.

HEAGLE, A. S., McLAUGHLIN, M. R., MILLER, J. E., JOYNER, R. L. & S. E. SPRUILL (1991). Adaptation of a white clover population to ozone stress. New Phytologist 119, 61-68.

HEAGLE, A. S., MILLER, J. E. & D. E. SHERRILL (1994). A white clover system to estimate effects of tropospheric ozone on plants. Journal of Environmental Quality 23, 613-621.

HEAGLE, A. S., MILLER, J. E., CHEVONE, B. I., DRESCHEL, T. W., MANNING, W. J., Mc COOL, P. M., MORRISON, C. L., NEELY, G. E. & J. REBBECK (1995). Response of a white clover indicator system to tropospheric ozone at eight locations in the United States. Water, Air and Soil Pollution 85, 1373-1378.

HEAGLE, A. S., MILLER, J. E., SHERRILL, D. E. & J. O. RAWLINGS (1993). Effects of ozone and carbon dioxide mixtures on two clones of white clover. New Phytologist 123, 751-762.

HEAGLE, A. S., REINERT, R. A. & J. E. MILLER (1996). Response of white clover to ozone in different environments. Journal of Environmental Quality 25, 273-278.

HEATH, R. L. & G. E. TAYLOR JR. (1997). Physiological processes and plant responses to ozone exposure. In. SANDERMANN, H., WELLBURN, A. R. & R. L. HEATH (Eds.). Forest decline and ozone. Ecological Studies 127. Springer, Berlin, 317-368.

HEATH, R. L. (1980). Initial events in injury to plants by air pollutants. Annual Review of Plant Physiology 31, 395-431.

HEATH, R. L. (1987). The biochemistry of ozone attack on the plasma membrane of plant cells. In. SAUNDERS, J. A., KOSAK-CHANNING, L. & E. E. CONN (Eds.). Recent Advances in Phytochemistry 21. Plenum Press, New York, 29-54.

HEATH, R. L. (1994). Alterations of plant metabolism by ozone exposure. In. ALSCHER, R. G. & A. R. WELLBURN (Eds.). Plant responses to gaseous environment. Chapman & Hall, London, 121-146.

HECHT-NIELSEN, R. (1990). Neurocomputing. Addison-Wesely, Massachusetts.

HEGGESTAD, H. E. (1991). Origin of Bel-W3, Bel-C and Bel-B tobacco varieties and their use as indicators of ozone. Environmental Pollution 74, 264-291.

HILL, A. C. & N. LITTLEFIELD (1969). Ozone. Effect on apparent photosynthesis, rate of transpiration, and stomatal closure. Environmental Science & Technology 3(1), 52-56.

HIRAFUJI, M. & T. KUBOTA (1994). Chaos of plant growth under changing environment. Environmental control in biology 32, 31-39.

HOPFIELD, J. J. (1982). Neural networks and physical systems with emergent collective computational abilities. Proceedings of the National Academy of Sciences of the United States of America 79, 2554-2558.

HOPTROFF, R. G. (1993). The principles and practice of time series forecasting and business modelling using neural nets. Neural Computing and Applications 1, 59-66.

HOPTROFF, R. G. (1993). The principles and practice of time series forecasting and business modelling using neural nets. Neural Computing and Applications 1, 59-66.

HUBICK, K. T. (1992). Artificial Neural Networks in Australia. Department of Industry, Technology and Commerce, Commonwealth of Australia, Canberra.

ICP VEGETATION (1998). Experimental protocol for the 1998 season. ICP Coordination Centre, Bangor, UK.

ICP VEGETATION (2004). Air pollution and vegetation. UNECE ICP Vegetation Annual Report 2003/2004. ICP Vegetation Centre, Bangor. UK.

IPCC (2001). A report of working group I of the Intergovernmental Panel on Climate Change. http.//www.ipcc.ch/.

JARVIS, P.G. (1976). The interpretation of the variation in leaf water potential and stomatal conductance found in canopies in the field. Philosophical Transactions of the Royal Society of London, B 273, 593-610.

JACOBSEN, J. S. & A. C. HILL (1970). Recognition of air pollution injury to vegetation. A pictorial atlas. Air Pollution Control Association, Pittsburgh.

JAMAÏ, A., TOMMASINI, R., MARTINOIA, E. & S. DELROT (1996). Characterization of glutathione uptake in broad bean leaf protoplasts. Plant Physiology 111, 1145-1152.

JETTER, R., RIEDERER, M. & K. J. LENDZIAN (1996). The effect of dry O_3, SO_2 and NO_2 on reconstituted epicuticular wax tubules. New Phytologist 133, 207-216.

JOHNSON, C. E., STEVENSON, D. S., COLLINS, W. J. & R. G. DERWENT (2001). Role of climate feedback on methane and ozone studied with a coupled Ocean-Atmosphere-Chemistry model. Geophysical Research Letters 28, 1723-1726.

JONES, H. G. (1992). Plants and microclimate (2nd edition) Cambridge University Press, Cambridge.

KANGASJÄRVI, J., TALVINEN, J., UITRAINEN, M. & R. KARJALAINEN (1994). Plant defence systems induced by ozone. Plant Cell and Environment 17, 783-794.

KARLSSON, P. E., MEDIN, E. L., SELLDÉN, G., WALLIN, G., OTTOSSON, S., PLEIJEL, H. & L. SKÄRBY (2002). Impact of ozone and reduced water supply on the biomass accumulation of Norway spruce saplings. Environmental Pollution 119, 237-244.

KARLSSON, P. E., MEDIN, E. L., WALLIN, G., SELLDÉN, G. & L. SKÄRBY (1997). Effects of ozone and drought stress on the physiology and growth of two clones of Norway spruce (*Picea abies*). New Phytologist 136, 265-275.

KARNOSKY, D. F., ZAK, D. R., PREGITZER, K. S., AWMACK, C. S., BOCKHEIM, J. G., DICKSON, R. E., HENDREY, G. R., HOST, G. E., KING, J. S., KOPPER, B. J., KRUGER, E. L., KUBISKE, M. E., LINDROTH, R. L., MATTSON, W. J., McDONALD, E. P., NOORMETZ, A., OKSANEN, E., PARSONS, W. F. J., PERCY, K, E., PODILA, G. K., RIEMENSCHNEIDER, D. E., SHARMA, P., THAKUR, R., SÔBER, A., SÔBER, J., JONES, W. S., ANTTONEN, S., VAPAAVUORI, E., MANKOVSKA, B., HEILMAN, W. & J. G. ISEBRANDS (2003). Tropospheric O_3 moderates responses to temperate hardwood forests to elevated CO_2. A synthesis of molecular to ecosystem results from the Aspen FACE project. Functional Ecology 17, 289-304.

KARUL, C., SOYUPAK, S., ÇILESIZ, A. F., AKBAY, N. & E. GERMEN (2000). Case studies on the use of neural networks in eutrophication modelling. Ecological Modelling 134, 145-152.

KASIBHATLA, P. S., LEVY II, H. & W. J. MOXIM (1993). Global NO_x, HNO_3, PAN and NO_y distributions from fossil fuel combustion emissions. A model study. Journal of Geophysical Research 98, 7165-7180.

KELLOMÄKI, S. & K.-Y. WANG (1997a). Effects of elevated O_3 and CO_2 on chlorophyll fluorescence and gas exchange in Scots pine during the third growing season. Environmental Pollution 97(1-2), 17-27.

KELLOMÄKI, S. & K.-Y. WANG (1997b). Effects of elevated O_3 and CO_2 concentrations on photosynthesis and stomatal conductance in Scots pine. Plant, Cell and Environment 20, 995-1006.

KELLOMÄKI, S., ROUVINEN, I., PELTOLA, H., STRANDMAN, H. & R. STEINBRECHER (2001). Impact of global warming on the tree species composition of boreal forests in Finland and effects on emissions of isoprenoids. Global Change Biology 7, 531-544.

KERSTIENS, G. & K. J. LENDZIAN (1989). Interaction between ozone and plant cuticles. I. Ozone deposition and permeability. New Phytologist 112, 13-19.

KHOTANZAD, A. & J.-H. LU (1991). Shape and texture recognition by a neural network. In. SETHI, I. K. & A. K. JAIN (Eds.), Artificial Neural Networks and Statistical Pattern Recognition – Old and New Connections. Elsevier Science Publishers B.V., Amsterdam.

KLUMPP, A., ANSEL, W., KLUMPP, G., BELLUZZO, N., CALATAYUD, V., CHAPLIN, N., GARREC, J. P., GUTSCHE, H.-J-, HAYES, M., HENTZE, H.-W., KAMBEZIDIS, H., LAURENT, O., PEÑUELAS, J., RASMUSSEN, S., RIBAS, A., RO-POULSEN, H., ROSSI, S., SANZ, M. J., SHANG, H., SIFAKIS, N. & P. VERGNE (2002). EuroBionet. A Pan-European Biomonitoring Network for Urban Air Quality Assessment. Environmental Science & Pollution Research 9 (3), 199-203.

KOHONEN, T. (1982). Self-organized formation of topologically correct feature maps. Biological Cybernetics 43, 59-69.

KOHONEN, T. (1984). Self-organization and associative memory. Springer Verlag, Berlin.

KOSUGI, Y., SHIBATA, S., KOBASHI, S. (2003). Parameterization of the CO_2 and H_2O gas exchange of several temperate deciduous broad-leaved trees at the leaf scale considering seasonal changes. Plant, Cell and Environement 26, 285-301.

KOUKOL, J. & W. M. DUGGER JR. (1967). Anthocyanin formation as a response to ozone and smog treatment in *Rumex crispus* L. Plant Physiology 42, 1023-1024.

KRUPA, S. V. & W. J. MANNING (1988). Atmospheric ozone. Formation and effects on vegetation. Environmental Pollution 50, 101-137.

KRUPA, S., McGRATH, M. T., ANDERSEN, C. P., BOOKER, F. L., BURKEY, K. O., CHAPPELKA, A. H., CHEVONE, B. I., PELL, E. J. & B. A. ZILINSKAS (2001). Ambient ozone and plant health. Plant Disease 85, 4-12.

KUNG, S. Y. & J. S. TAUR (1995). Decision-based neural networks with signal image classification analysis. IEEE Transactions on Neural Networks 6, 170-181.

LAISK, A., KULL, O. & H. MOLDAU (1989). Ozone concentration in leaf intercellular air spaces is close to zero. Plant Physiology 90, 1163-1167.

LANDESAMT FÜR UMWELTSCHUTZ UND GEWERBEAUFSICHT (1978-2001). Monatsberichte über die Messergebnisse des Zentralen Immissionsmessnetzes ZIMEN für Rheinland-Pfalz. Mainz.

LANDOLT, W., BÜHLMANN, U., BLEULER, P. & J. B. BUCHER (2000). Ozone exposure-response relationships for biomass and root/shoot ratio of beech (*Fagus sylvatica*), ash (*Fraxinus excelsior*), Norway spruce (*Picea abies*) and Scots pine (*Pinus sylvestris*). Environmental Pollution 109, 473-478.

LANGEBARTELS, C., KERNER, K., LEONARDI, S., SCHRAUDNER, M., TROST, M. HELLER, W. & H. SANDERMANN (1991). Biochemical plant response and ozone. I. Differential induction of polyamine and ethylene biosynthesis in tobacco. Plant Physiology 95, 882-889.

LARCHER, W. (1994). Ökophysiologie der Pflanzen. Ulmer, Stuttgart.

LARSON, R. A. (1988). The antioxidants of higher plants. Phytochemistry 27, 969-978.

LAWSON, T., CRAIGON, J., BLACK, C. R., COLLS, J. J., TULLOCH, A.-M. & G. LANDON (2001). Effects of elevated carbon dioxide and ozone on the growth and yield of potatoes (*Solanum tuberosum*) grown in open-top chambers. Environmental Pollution 111, 479-491.

LEK, S. & J. F. GUÉGAN (1999). Artificial neural networks as a tool in ecological modelling, an introduction. Ecological Modelling 120, 65-73.

LEK, S., BELAUD, A., BARAN, P., DIMOPOULOS, I. & M. DELACOSTE (1996a). Role of some environmental variables in trout abundance models using neural networks. Aquatic Living Research 9, 23-29.

LEK, S., DELACOSTE, M., BARAN, P., DIMOPOULOS, I., LAUGA, J. & S. AULAGNIER (1996b). Application of neural networks to modelling nonlinear relationships in ecology. Ecological Modelling 90, 39-52.

LERNER, B. (1994). Feature selection and chromosome classification using a multilayer perceptron neural network. Proceedings of the IEEE International Conference on Neural Networks. Orlando, USA, 3540-3545.

LEUNING, R. (1995). A critical appraisal of a combined stomatal-photosynthesis model for C_3 plants. Plant, Cell and Environment 18, 339-355.

LEVITT, J. (1980). Responses of plants to environmental stress. Academic Press, New York.

LOGAN, J. A. (1985). Tropospheric ozone. Seasonal behaviour, trends, and anthropogenic influence. Journal of Geophysical Research 90, 10463-10482.

LONG, S. P. & S. L. NAIDU (2002). Effects of oxidants at the biochemical, cell and physiological levels, with particular reference to ozone. In. BELL, J. N. B. & M. TRESHOW (Eds.). Air pollution and plant life. Wiley & Sons, Chichester, 69-88.

LÜTHY-KRAUSE, B., BLEULER, P. & W. LANDOLT (1989). Black poplar and red clover as bioindicators for ozone at a forest site. Angewandte Botanik 63, 111-118.

LUWE, M., TAKAHAMA, U. & U. HEBER (1993). Role of ascorbate in detoxifying ozone in the apoplast of spinach (*Spinacia oleracea* L.) leaves. Plant Physiology 101, 969-976.

LYONS, T. M. & J. D. BARNES (1998). Influence of plant age on ozone resistance in *Plantago major*. New Phytologist 138, 83-89.

LYONS, T. M., BARNES, J. D. & A. W. DAVISON (1997). Relationships between ozone resistance and climate in European populations of *Plantago major*. New Phytologist 136, 503-510.

LYONS, T. M., OLLERENSHAW, J. H. & J. D. BARNES (1999). Impacts of ozone on *Plantago major*. Apoplastic and symplastic antioxidant status. New Phytologist 141, 253-263.

MADAMANCHI, N. R., HAUSLADEN, A., ALSCHER, R. G., AMUNDSON, R. G. & S. FELLOWS (1991). Seasonal changes in antioxidants in red spruce (*Picea rubens* Sarg.) from three field sites in the northeastern United States. New Phytologist 118, 331-338.

MAIER, H. R. & G. C. DANDY (1997). Modelling cyanobacteria (blue-green bacteria) in the river Murray using artificial neural networks. Mathematics and Computers in Simulation 43, 377-386.

MAIER, H. R. & G. C. DANDY (1998). The effect of internal parameters and geometry on the performance of back-propagation neural networks: an empirical study. Environmental Modelling & Software 13, 193-209.

MAIER, H. R., DANDY, G. C. & M. D. BURCH (1998). Use of artificial neural networks for modelling Cyanobacteria anabaena spp. in the river Murray, South Australia. Ecological Modelling 105, 257-272.

MANEL, S., DIAS, J. M. & S. J. OMEROD (1999). Comparing discriminant analysis, neural networks and logistic regression for predicting species distribution. A case study with a Himalayan river bird. Ecological Modelling 120, 337-347.

MARENCO, A., GOUGET, H., NÉDÉLEC, P., PAGÉS, J.-P. & F. KARCHER (1994). Evidence of a long-term increase in tropospheric ozone from Pic Du Midi data series. Consequences. Positive radiative forcing. Journal of Geophysical Research 99, 16617-16632.

MARTIN, M. J., FARAGE, P. K., HUMPHRIES, S. W. & S. P. LONG (2000). Can the stomatal changes caused by acute ozone exposure be predicted by changes occurring in the mesophyll? A simplification for models of vegetation response to the global increase in tropospheric elevated ozone episodes. Australian Journal of Plant Physiology 27, 211-219.

MATTERS, G. L. & J. G. SCANDALIOS (1987). Synthesis of isozymes of superoxide dismutase in maize leaves in response to O_3, SO_2, and elevated O_2. Journal of Experimental Botany 38, 842-852.

MATYSSEK, R. & J. L. INNES (1999). Ozone – a risk factor for trees and forests in Europe? Water, Air and Soil Pollution 116, 199-226.

MATYSSEK, R., GÜNTHARDT-GOERG, M. S., LANDOLT, W. & T. KELLER (1993). Whole-plant growth and leaf formation in ozonated hybrid poplar (*Populus x euamericana*). Environmental Pollution 81, 207-212.

MATYSSEK, R., GÜNTHARDT-GOERG, M. S., SAURER, M. & T. KELLER (1992). Seasonal growth, $\delta^{13}C$ in leaves and stem, and phloem structure of birch (*Betula pendula*) under low ozone concentrations. Trees 6, 69-76.

McCULLOCH, W. S. & W. Pitts (1943). A logical calculus of the ideas immanent in nervous activity. Bulletins of Mathematics and Biophysics 5, 461-482.

McKEE, I. F., FARAGE, P. K. & S. P. LONG (1995). The interactive effects of elevated CO_2 and O_3 concentrations on photosynthesis in spring wheat. Photosynthesis Research 45, 111-119.

MEHLHORN, H., O'SHEA, J. M. & A. R. WELLBURN (1990). Electron spin resonance evidence for the formation of free radicals in plants exposed to ozone. Physiologia Plantarum 82, 336-338.

MEHLHORN, H., O'SHEA, J. M. & A. R. WELLBURN (1991). Atmospheric ozone interacts with stress ethylene formation by plants to cause visible plant injury. Journal of Experimental Botany 42(234), 17-24.

MEYER, U., KÖLLNER, B., WILLENBRINK, J. & G. H. M. KRAUSE (2000). Effects of different ozone regimes on photosynthesis, assimilates and thousand grain weight in spring wheat. Agriculture, Ecosystems and Environment 78, 49-55.

MIDDLETON, J. T., KENDRICK, J. B. Jr. & H. W. SCHWALM (1950). Injury to herbaceous plants by smog or air pollution. Plant Disease Reporter 34, 245-252.

MIKKELSEN, T. N. (1995). Physiological responses of *Fagus sylvatica* L. exposed to low levels of ozone in open-top chambers. Trees 9, 355-361.

MILLER, C. A. & D. D. DAVIS (1981). Effect of temperature on stomatal conductance and ozone injury of pinto bean leaves. Plant Disease 65 (9), 750-751.

MILLER, J. D., ARTECA, R. N. & E. J. PELL (1999). Senescence-associated gene expression during ozone-induced leaf senescence in Arabidopsis. Plant Physiology 120, 1015-1023.

MILLS, G., BALL, G., HAYES, F., FUHRER, J., SKÄRBY, L., GIMENO, B., DE TEMMERMAN, L., HEAGLE, A. & MEMBERS OF THE ICP VEGETATION PROGRAMME (2000). Development of a multi-factor model for predicting the effects of ambient ozone on the biomass of white clover. Environmental Pollution 109, 533-542.

MILLS, G., BALL, G., HAYES, F., FUHRER, J., SKÄRBY, L., GIMENO, B., DE TEMMERMAN, L., HEAGLE, A. & MEMBERS OF THE ICP VEGETATION PROGRAMME (2000). Development of a multi-factor model for predicting the effects of ambient ozone on the biomass of white clover. Environmental Pollution 109 (3), 533-542.

MINSKY, M. & S. PAPERT (1969). Perceptrons. MIT Press, Cambridge.

MOLDAU, H. (1998). Hierarchy of ozone scavenging reactions in the plant cell wall. Physiologia Plantarum 104, 617-622.

MOLDAU, H., SÕBER, J. & A. SÕBER (1990). Differential sensitivity of stomata and mesophyll to sudden exposure of bean shoots to ozone. Photosynthetica 24(3), 446-458.

MONTEITH J. L. & M. H. UNSWORTH (1990). Principles of environmental physics. 2nd edition, Edward Arnold Publishers, London.

MÜLLER, J. F. & G. BRASSEUR (1995). IMAGES. A three-dimensional chemical transport model of the global troposphere. Journal of Geophysical Research 100, 16445-16490.

MÜLLER, J., WERNECKE, P. & W. DIEPENBROCK (2005). LEAFC3-N: a nitrogen-sensitive extension of the CO_2 and H_2O gas exchange model LEAFC3 parameterised and tested for winter wheat (*Triticum aestivum* L.). Ecological Modelling 183, 183-210.

MUSSELMAN, R. C. & W. J. MASSMAN (1999). Ozone flux to vegetation and its relationship to plant response and ambient air quality standards. Atmospheric Environment 33, 65-73.

NIKOLOV, N. T., MASSMAN, W. J. & A. W. SCHOETTLE (1995). Coupling biochemcial and biophysical processes at the leaf level: an equilibrium photosynthesis model for leaves of C3-plants. Ecological Modelling 80, 205-235.

NOVAK, K., SCHAUB, M., FUHRER, J., SKELLY, J. M., HUG, C., LANDOLT, W., BLEULER, P. & N. KRÄUCHI (2005). Seasonal trends in reduced leaf gas exchange and ozone-induced foliar injury in three ozone sensitive woody plant species. Environmental Pollution 136, 33-45.

NOVAK, K., SKELLY, J. M., SCHAUB, M., KRÄUCHI, N., HUG, C., LANDOLT, W. & P. BLEULER (2003). Ozone air pollution and foliar injury development on native plants of Switzerland. Environmental Pollution 125, 41-52.

OGAWA, K., KANEMATSU, S. & K. ASADA (1996). Intra- and extracellular localisation of 'cytosolic' CuZn-superoxide disumutase in spinach leaf and hypocotyl. Plant and Cell Physiology 37, 790-799.

OJANPERÄ, K., PÄTSIKKÄ, E. & T. YLÄRANTA (1998). Effects of low ozone exposure of spring wheat on net CO_2 uptake, Rubisco, leaf senescence and grain filling. New Phytologist 138, 451-460.

OLDEN, J. A. & D. A. JACKSON (2002). Illuminating the "black box". A randomization approach for understanding variable contributions in artificial neural networks. Ecological Modelling 154, 135-150.

OLDEN, J. A., JOY, M. K. & R. G. DEATH (2004). An accurate comparison of methods for quantifying variable importance in artificial neural networks using simulated data. Ecological Modelling 178, 389-397.

OLLERENSHAW, J. H. & T. LYONS (1999a). Impacts of ozone on the growth and yield of field-grown winter wheat. Environmental Pollution 106, 67-72.

OLLERENSHAW, J. H., LYONS, T. & J. D. BARNES (1999b). Impacts of ozone on the growth and yield of field-grown winter oilseed rape. Environmental Pollution 104, 53-59.

OLTMANS, S. J. & H. LEVY (1994). Surface ozone measurements from a global network. Atmospheric Environment 28, 9-24.

ORR, R. K. (1995). Use of probabilistic neural networks to predict mortality following cardiac surgery. Proceedings of World Congress of Neural Networks, Vol. II, 754-757.

OTTOSSON, S., WALLIN, G., SKÄRBY, L., KARLSSON, P. E., MEDIN, E. L., RÄNTFORS, M., PLEIJEL, H. & G. SELLDÉN (2003). Four years of ozone exposure in OTCs combined with high or low supply of phosphorus reduced biomass production in Norway spruce (*Picea abies*). Trees 17, 299-307.

ÖZESMI, S. L. & U. ÖZESMI (1999). An artificial neural network approach to spatial habitat modelling with interspecific interaction. Ecological Modelling 116, 15-31.

PÄÄKKÖNEN, E., METSÄRINNE, S., HOLOPAINEN, T. & L. KÄRENLAMPI (1995). The ozone sensitivity of birch (*Betula pendula*) in relation to the developmental stage of leaves. New Phytologist 132, 145-154.

PÄÄKKÖNEN, E., SEPPÄNEN, S., HOLOPAINEN, T., KOKKO, H., KÄRENLAMPI, S., KÄRENLAMPI, L. & J. KANGASJÄRVI (1998). Induction of genes for the stress proteins PR-10 and PAL in relation to growth, visible injuries and stomatal conductance in birch (*Betula pendula*) clones exposed to ozone and/or drought. New Phytologist 138, 295-305.

PALUDAN-MÜLLER, G., SAXE, H. & J. W. LEVERENZ (1999). Responses to ozone in 12 provenances of European beech (*Fagus sylvatica*). genotypic variation and chamber effects on photosynthesis and dry-matter partitioning. New Phytologist 144, 261-273.

PARUELO, J. M. & F. TOMASEL (1997). Prediction of functional characteristics of ecosystems. A comparison of artificial neural networks and regression models. Ecological Modelling 98, 173-186.

PASTOR-BÁRCENAS, O., SORIA-OLIVAS, E., MARTÍN-GUERRERO, J. D., CAMPS-VALLS, G., CARRASCO-RODRÍGUEZ, J. L. & S. del VALLE-TASCÓN (2005). Unbiased sensitivity analysis and pruning techniques in neural networks for surface ozone modelling. Ecological Modelling 182, 149-158.

PEARSON, M. & T. A. MANSFIELD (1994). Effects of exposure to ozone and water stress on the following season's growth of beech (*Fagus sylvatica*). New Phytologist 126, 511-515.

PEARSON, S., DAVISON, A. W., REILING, K., ASHENDEN, T. & J. H. OLLERENSHAW (1996). The effects of different ozone exposures on three contrasting populations of *Plantago major*. New Phytologist 132, 493-502.

PENKETT, S. A. & K. A. BRICE (1986). The spring maximum in photo-oxidants in the northern hemisphere troposphere. Nature 319, 655-657.

PERCY, K. E., AWMACK, C. S., LINDROTH, R. L., KUBISKE, M. E., KOPPER, B. J., ISEBRANDS, J. G., PREGITZER, K. S., HENDREY, G. R., DICKSON, R. E., ZAK, D. R., OKSANEN, E., SOBER, J., HARRINGTON, R. & D. F. KARNOSKY (2002). Altered performance of forest pests under atmospheres enriched by CO_2 and O_3. Nature 420, 403-407.

PIHL KARLSSON, G. (2003). Clover as a bioindicator for phytotoxic ozone. PhD thesis, Göteborg University, Göteborg.

PIHL KARLSSON, G., KARLSSON, P. E. & H. PLEIJEL (submitted). Can stomatal conductance and leaf thickness explain the difference in ozone sensitivity between three different clover species?

PIHL KARLSSON, G., KARLSSON, P. E., DANIELSSON, H. & H. PLEIJEL (2003). Clover as a tool for bioindication of phytotoxic ozone – 5 years of experience from southern Sweden – consequences for the short-term critical levels. The Science of the Total Environment 301, 205-213.

PIHL KARLSSON, G., PLEIJEL, H., SILD, E., DANIELSSON, H., SELLDÉN, G., ERICSON, L. & L. SKÄRBY (1995b). Clover Sweden – a national three-year study of the effects of tropospheric ozone on *Trifolium subterraneum* L. Water, Air and Soil Pollution 85, 1503-1508.

PIHL KARLSSON, G., SELLDÉN, G., SKÄRBY, L. & H. PLEIJEL (1995a). Clover as an indicator plant for phytotoxic ozone concentrations. Visible injury in relation to species, leaf age and exposure dynamics. New Phytologist 129, 355-365.

PINEDA, F. (1987). Generalization of backpropagation to recurrent neural networks. Physical Review Letter 19 (59), 2229-2232.

PLEIJEL, H. & H. DANIELSSON (1997). Growth of 27 herbs and grasses in relation to ozone exposure and plant strategy. New Phytologist 135, 361-367.

PLEIJEL, H. (Ed.) (1999). Ground-level ozone – a threat to vegetation. Swedish Environmental Protection Agency, Report 4970, Stockholm.

PLEIJEL, H., DANIELSSON, H., KARLSSON, G. P., GELANG, J., KARLSSON, P. E. & G. SELLDÉN (2000). An ozone – flux relationship for wheat. Environmental Pollution 109, 453-462.

PLEIJEL, H., DANIELSSON, H., VANDERMEIREN, K., BLUM, C., COLLS, J. & K. OJANPERÄ (2002). Stomatal conductance and ozone exposure in relation to potato tuber yield – results from the European CHIP programme. European Journal of Agronomy 17, 303-317.

PLEIJEL, H., OJANPERÄ, K. & L. MORTENSEN (1997). Effects of tropospheric ozone on the yield and grain protein content of spring wheat (*Triticum aestivum* L.) in the Nordic countries. Acta Agriculturae Scandinavica. Section B, Soil & Plant Science 47, 20-25.

POFF, N. L., TOKAR, S. & P. Johnson (1996). Stream hydrological and ecological responses to climate change assessed with an artificial neural network. Limnology and Oceanography 41 (5), 857-863.

POLLE, A., CHAKRABARTI, K., SCHURMANN, W. & H. RENNENBERG (1990). Composition and properties of hydrogen peroxide decomposing systems in extracellular and total extracts from needles of Norway spruce (*Picea abies* L. Karst.). Plant Physiology 94, 312-319.

POLLE, A., OTTER, T. & F. SEIFERT (1994). Apoplastic peroxidases and lignification in needles of Norway spruce (*Picea abies* L.). Plant Physiology 106, 53-60.

POLLE, A., PFIRRMANN, T., CHAKRABARTI, K. & H. RENNENBERG (1993). The effects of enhanced ozone and enhanced carbon dioxide concentrations on biomass, pigments and antioxidative enzymes in spruce needles (*Picea abies* L.). Plant, Cell and Environment 16, 311-316.

PORG (1993). Third report of the United Kingdom Photochemicals Oxidants Review Group. UK Department of Environment, London.

PORG (1997). Ozone in the United Kingdom. Fourth report of the United Kingdom Photochemicals Oxidants Review Group. Department of the Environment, Transport and the Regions, London.

POSTIGLIONE, L., FAGNANO, M. & G. MEROLA (2000). Response to ambient ozone of two white clover (*Trifolium repens* L. cv. "Regal") clones, one resistant and one sensitive, grown in a Mediterranean environment. Environmental Pollution 109, 525-531.

PRATHER, M., EHHALT, D., DENTENER, F., DERWENT, R., DLUGOKENCKY, E., HOLLAND, E., ISAKSEN, I., KATIMA, J., KIRCHHOFF, V., MATSON, P., MIDGLEY, P. & M. WANG (2001). Atmospheric chemistry and greenhouse gases. In. HOUGHTON, J. T., DING, Y., GRIGGS, D. J., NOGUER, M., VAN DER LINDEN, P. J., DAI, X., MASKELL, K. & C. A. JOHNSON (Eds.). Climate change 2001. The scientific basis. Contribution of working group I to the Third Assessment Report of the International Panel on Climate Change. Cambridge University Press, Cambridge, 239-287.

RAHIM, M. G., GOODYEAR, C. C., KLEIJN, W. B., SCHROETER, J. & M. M. SONDHI (1993). On the use of neural networks in articulatory speech synthesis. Journal of Acoustical Society of America 93, 1109-1121.

RAMOS-NINO, M. E., RAMIREZ-RODRIGUEZ, C. A., CLIFFORD, M. N. & M. R. ADAMS (1997). A comparison of quantitative structure-activity relationships for the effect of benzoic and cinnamic acids on *Listera monocytogenes* using multiple linear regression, artificial neural networks and fuzzy systems. Journal of Applied Microbiology 82, 168-176.

RANGARAJAN, A., CHELLAPPA, R. & B. S. MANJUNATH (1991). Markov random fields and neural networks with applications to early vision problems. In. SETHI, I. K. & A. K. JAIN (Eds.). Artificial Neural Networks and Statistical Pattern Recognition – Old and New Connections. Elsevier Science Publishers B.V., Amsterdam.

RANIERI, A., D'URSO, G., NALI, C., LORENZINI, G. & G. F. SOLDATINI (1996). Ozone stimulates apoplastic antioxidant systems in pumpkin leaves. Physiologia Plantarum 97, 381-387.

RECKNAGEL, F., FRENCH, M., HARKONEN, P. & K. I. YABUNAKA (1997). Artificial neural network approach for modelling and prediction of algal blooms. Ecological Modelling 96, 11-28.

REFENES, A. N., AZEMA-BARAC, M., CHEN, W. & S. A. KAROUSSOS (1993). Currency exchange rate prediction and neural network design strategies. Neural Computing and Applications 1, 46-58.

REICH, P. B. & R. G. AMUNDSON (1985). Ambient levels of ozone reduce net photosynthesis in tree and crop species. Science 230, 566-570.

REILING, K. & A. W. DAVISON (1992). The response of native, herbaceous species to ozone. Growth and fluorescence screening. New Phytologist 120, 29-37.

REINER, S., WILTSHIRE, J. J. J., WRIGHT, C. J. & J. J. COLLS (1996). The impact of ozone and drought on the water relations of ash trees (*Fraxinus excelsior* L.). Journal of Plant Physiology 148, 166-171.

REINERT, R. A., EASON, G. & J. BARTON (1997). Growth and fruiting of tomato as influenced by elevated carbon dioxide and ozone. New Phytologist 137, 411-420.

REITER, E. R. (1975). Stratospheric-tropospheric exchange processes. Reviews of Geophysics and Space Physics 13, 459-474.

RICH, S., WAGGONER, P. E. & H. TOMLINSON (1970). Ozone uptake by bean leaves. Science 169, 79-80.

RICHARDS, B. L., MIDDLETON, J. T. & W. B. HEWITT (1958). Air pollution with relation to agronomic crops. V. Oxidant stipple on grape. Agronomy Journal 50, 559-561.

RITTER, G. (1996). Einwirkungen von Luftschadstoffen unter besonderer Berücksichtigung von Ozon auf Pflanzen im Stadtgebiet Trier. Diplomarbeit Universität Trier, Trier.

ROADKNIGHT, C. M., BALLS, G. R., MILLS, G. E. & D. PALMER-BROWN (1997). Modeling complex environmental data. IEEE Transactions on Neural Networks 8 (4), 852-862.

ROSENBLATT, F. (1962). Principles of neurodynamics. Spartan Books, New York.

ROSENDAHL, K. E. & A. C. HANSEN (2000). Valuation of crop damage due to air pollution. In. GEORGANTZÍS, N. & I. J. BARREDA TARRAZONA (Eds.). Spatial economics and ecosystems – The interaction between economics and the natural environment. WIT Press, Southampton, 237-256.

RUMELHART, D. E. & J. L. McCLELLAND (1986). Parallel distribution processing: Exploration in the microstructure of cognition, Volume 1: Foundations. MIT Press, Cambridge, Massachusetts.

RUMELHART, D. E., HINTON, G. E. & R. J. WILLIAMS (1986). Learning representations by back-propagating error. Nature 323, 533-536.

RYAN, M., MüLLER, C., DI, H. J. & K. C. CAMERON (2004). The use of artificial neural networks (ANNs) to simulate N_2O emissions from a temperate grassland ecosystem. Ecological Modelling 175, 189-194.

SAMUELSON, L. J., KELLY, J. M., MAYS, P. A. & G. S. EDWARDS (1996). Growth and nutrition of *Quercus rubra* L. seedlings and mature trees after three seasons of ozone exposure. Environmental Pollution 91(3), 317-323.

SANDERMANN, H. JR., ERNST, D., HELLER, W. & C. LANGEBARTELS (1998). Ozone. An abiotic elicitor of plant defence reactions. Trends in Plant Science 3, 47-50.

SANDERS, G. E. & J. BENTON (1995). Ozone pollution and plant responses in Europe – An illustrated guide. The Nottingham Trent University, Department of Life Sciences, Nottingham, UK.

SANDERS, G. E., COLLS, J. J., CLARK, A. G., GALAUP, S., BONTE, J. & J. CANTUEL (1992a). *Phaseolus vulgaris* and ozone. Results from open-top chamber experiments in France and England. Agriculture, Ecosystems and Environment 38, 31-40.

SANDERS, G. E., ROBINSON, A. D., GEISSLER, P. A. & J. J. COLLS (1992b). Yield stimulation of a commonly grown cultivar of *Phaseolus vulgaris* L. at near-ambient ozone concentrations. New Phytologist 122, 63-70.

SAXE, H. (1991). Photosynthesis and stomatal response to polluted air and the use of physiological and biochemical response for early detection and diagnostic tools. Advanced Botanical Research 18, 1-128.

SCARDI, M. (1996). Artificial neural networks as empirical models for estimating phytoplankton production. Marine Ecology Progress Series 139, 289-299.

SCHENONE, G., BOTTESCHI, G., FUMAGALLI, I. & F. MONTINARO (1992). Effects of ambient air pollution in open-top chambers on bean (*Phaseolus vulgaris* L.). New Phytologist 122, 689-697.

SCHÖNEBURG, E. (1990). Stock price prediction using neural networks. A project report. Neurocomputing 2, 17-27.

SCHRAUDNER, M., LANGEBARTELS, C. & H. SANDERMANN (1997). Changes in biochemical status of plant cells induced by the environmental pollutant ozone. Physiologia Plantarum 100, 274-280.

SCHRÖTER, W., LAUTENSCHLÄGER, K.-H. & H. BIBRACK (1991). Taschenbuch der Chemie. Fachbuchverlag Leipzig, Leipzig.

SCHULZE, E. (1999). Ozon-Biomonitoring mit unterschiedlich sensitiven Weißklee-Genotypen entlang eines Höhengradienten in der Region Trier. Diploma thesis, Universität Trier, Trier.

SEGINER, I., BOULARD, T. & B. J. BAILEY (1994). Neural network models of the greenhouse climate. Journal of Agricultural Engineering Research 59, 203-216.

SILD, E., PLEIJEL, H. & G. SELLDÉN (1999). Response of subterranean clover (*Trifolium subterraneum*) to ozone in relation to plant age and light conditions during exposure. New Phytologist 143, 315-321.

SIMINI, M., SKELLY, J. M., DAVIS, D. D., SAVAGE, J. E. & A. C. COMRIE (1992). Sensitivity of four hardwood species to ambient ozone in north central Pennsylvania. Canadian Journal of Forest Research 22, 1789-1799.

SIMPSON, D., GUENTHER, A., NICHOLAS HEWITT, C. & R. STEINBRECHER (1995). Biogenic emissions in Europe. 1. Estimates and uncertainties. Journal of Geophysical Research 100, 22875-22890.

SKÄRBY, L. (1984). Studies of ozone effects on crops and forest trees in Sweden. In. GRENNFELT, P. (Ed.). Proceedings International Workshop on the Evaluation of the Effects of Photochemical Oxidants on Human Health, Agricultural Crops, Forestry, Materials and Visibility. Swedish Environmental Research Institute, Göteborg, Sweden, 113-117.

SKÄRBY, L., RO-POULSEN, H., WELLBURN, F. A. M. & L. J. SHEPPARD (1998). Impacts of ozone on forests. A European perspective. New Phytologist 139, 109-122.

SMITH, J. & R. N. ELI (1995). Neural-network models of rainfall-runoff processes. Journal of Water Resources Planning and Management 121 (6), 499-508.

SNYDER, K. A., RICHARDS, J. H. & L. A. DONOVAN (2003). Night-time conductance in C_3 and C_4 species: do plants lose water at night? Journal of Experimental Botany 54, 861-865.

SOJA, G., REICHENAUER, T. G., EID, M., SOJA, A.-M., SCHABER, R. & H. GANGL (2004). Long-term ozone exposure and ozone uptake of grapevines in open-top chambers. Atmospheric Environment 38, 2313-2321.

STAEHELIN, J., THUDIUM, J., BUEHLER, R., VOLZ-THOMAS, A. & W. GRABER (1994). Trends in surface ozone concentrations in Arosa (Switzerland). Atmospheric Environment 28, 75-88.

STARRETT, S. K. & G. L. ADAMS (1997). Using artificial neural networks and regression to predict percentage of applied nitrogen leached under turfgrass. Communications in Soil Science Plant Analytical 28, 497-507.

STOCKWELL, W. R., KRAMM, G., SCHEEL, H.-E., MOHNEN, V. A. & W. SEILER (1997). Ozone formation, destruction and exposure in Europe and the United States. In: SANDERMANN, H., WELLBURN, A. R. & R. L. HEATH (Eds.). Forest decline and ozone. Ecological Studies 127. Springer, Berlin, 1-38.

STRELLER, S. & G. WINGSLE (1994). *Pinus sylvestris* L. needles contain extracellular CuZn superoxide dismutase. Planta 192, 195-201.

TAKAHAMA, U. & T. ONIKI (1992). Regulation of peroxidase-dependant oxidation of phenolics in the apoplast of spinach leaves by ascorbate. Plant and Cell Physiology 33, 379-387.

TAN, H., PROKHOROV, D. V. & D. C. WUNSCH (1995). Probabilistic and time-delay neural network techniques for conservative short-term stock trend prediction. Proceedings of World Congress of Neural Networks, Vol. II, 44-47.

TANG, Y., CHEVONE, B. I. & J. L. HESS (1999). Ozone-responsive proteins in a tolerant and sensitive clone of white clover (*Trifolium repens*). Environmental Pollution 104, 89-98.

TANGANG, F. T., HSIEH, W. W. & B. TANG (1997). Forecasting the equatorial pacific sea surface temperatures by neural network models. Climate Dynamics 13 (2), 135-147.

TEMPLE, P. J. (1990). Growth and yield responses of processing tomato (*Lycopersicon esculentum* Mill.) cultivars to ozone. Environmental and Experimental Botany 30(3), 283-291.

TINGEY, D. T. & G. E. JR. TAYLOR (1981). Variation in plant response to ozone. A conceptual model of physiological events. In. UNSWORTH, M. & D. ORMROD (Eds). Effects of gaseous air pollutants in agriculture and horticulture. Butterwort, London, 113-138.

TINGEY, D. T., STANDLEY, C. & R. W. FIELD (1976). Stress ethylene evolution. A measure of ozone effects on plants. Atmospheric Environment 10, 969-974.

TIRAKIS, A., SUKISSIAN, L. & S. KOLLIAS (1990). An adaptive technique for segmentation and classification of textured images. Proceedings of the International Neural Networks Conference, vol. 1. Paris, France, 31-34.

TJOELKER, M. G., VOLIN, J. C., OLEKSYN, J. & P. B. REICH (1993). Light environment alters response to ozone stress in seedlings of *Acer saccharum* Marsh. and hybrid *Populus* L. - I. *In situ* net photosynthesis, dark respiration and growth. New Phytologist 124, 627-636.

TONNEIJCK, A. E. G. & C. J. VAN DIJK (1997a). Effects of ambient ozone on injury and yield of *Phaesolus vulgaris* at four rural sites in the Netherlands as assessed by using ehtylenediurea (EDU). New Phytologist 135, 93-100.

TONNEIJCK, A. E. G. & C. J. VAN DIJK (1997b). Assessing effects of ambient ozone on injury and growth of *Trifolium subterraneum* at four rural sites in the Netherlands with ehtylenediurea (EDU). Agriculture, Ecosystems and Environment 65, 79-88.

TONNEIJCK, A. E. G. & C. J. VAN DIJK (1998). Responses of bean (*Phaseolus vulgaris* L. cv. Pros) to chronic ozone exposure at two levels of atmospheric ammonia. Environmental Pollution 99, 45-51.

TONNEIJCK, A. E. G. (1983). Foliar responses of 24 bean cultivars (*Phaseolus vulgaris* L.) to various concentrations of ozone. Netherlands Journal of Plant Physiology 89, 99-104.

TORSETHAUGEN, G., PITCHER, L. H., ZILINSKAS, B. A. & E. J. PELL (1997). Overproduction of ascorbate perioxidase in the tobacco chloroplast does not provide protection against ozone. Plant Physiology 114, 529-537.

TOUPANCE, G. & F. ARANDA (1993). Spatial evolution of annual ozone profiles over France and western Europe. In. BORRELL, P. M., BORRELL, P., CVITAS, T. & W. SEILER (Eds.). Proceedings of the EUROTRAC symposium 1992, SPB, The Hague, 133-139.

TURCSÁNYI, E., CARDOSO-VILHENA, J., DAYMOND, J., GILLESPIE, C., BALAGUER, L., OLLERENSHAW, J. & J. BARNES (1999). Impacts of tropospheric ozone. Past, present and likely future. In. SINGH, S. N. (Ed.). Climate change and plants. Springer, Berlin.

TURCSÁNYI, E., LYONS, T., PLÖCHL, M. & J. BARNES (2000). Does ascorbate in the mesophyll cell walls form the first lines of defence against ozone? Testing the concept using broad bean (*Vicia fabia* L.). Journal of Experimental Botany 51(346), 901-910.

UBA (1994). Daten zur Umwelt 1992/93. Schriftreihe des Umweltbundesamtes. Schmidt, Berlin.

UBA (2002). Daten zur Umwelt 2000. Schriftreihe des Umweltbundesamtes. Schmidt, Berlin.

UDDLING, J. (2004). Uptake of ozone and its impact on silver birch. Ph.D. thesis, Department of Botany, Göteborg University, Sweden.

UNECE (2004). Revised manual on methodologies and criteria for mapping critical levels/loads and geographical areas where they are exceeded. Umweltbundesamt, Berlin, Germany. www.icpmapping.org

UTRIAINEN, J. & T. HOLOPAINEN (2000). Impact of increased springtime O_3 exposure on Scots pine (*Pinus sylvestris*) seedlings in central Finland. Environmental Pollution 109, 479-487.

v. CAEMMERER, S. & G. D. FARQUHAR (1981). Some relationships between the biochemistry of photosynthesis and the gas exchange of leaves. Planta 153, 376-387.

v. WILLERT, D. J., MATYSSEK, R. & W. HERPPICH (1995). Experimentelle Pflanzenökologie. Thieme Verlag, Stuttgart.

VAN HOVE, L. W. A. & M. E. BOSSEN (1994). Physiological effects of five months exposure to low concentrations of O_3 and NH_3 on Douglas fir (*Pseudotsuga menziesii*). Physiologia Plantarum 92, 140-148.

VAN HOVE, L. W. A., BOSSEN, M. E., SAN GABINO, B. G. & C. SGREVA (2001). The ability of apoplastic ascorbate to protect poplar leaves against ambient ozone concentrations. A quantitative approach. Environmental Pollution 114, 371-382.

VAN WIJK, M. T. & W. BOUTEN (1999). Water and carbon fluxes above European coniferous forests modelled with artificial neural networks. Ecological Modelling 120, 181-197.

VANDERHEYDEN, D., SKELLY, J., INNES, J., HUG, C., ZHANG, J., LANDOLT, W. & P. BLEULER (2001). Ozone exposure thresholds and foliar injury on forest plants in Switzerland. Environmental Pollution 111, 321-331.

VANDERMEIREN, K., DE TEMMERMAN, L. & N. HOOKHAM (1995). Ozone sensitivity of *Phaeolus vulgaris* in relation to cultivar differences, growth stage and growing conditions. Water, Air and Soil Pollution 85, 1455-1460.

VINGARZAN, R. (2004). A review of surface O_3 background levels and trends. Atmospheric Environment 38, 3431-3442.

VIOTTI, P., LIUTI, G. & P. DI GENOVA (2002). Atmospheric urban pollution: applications of an artificial neural network (ANN) to the city of Perugia. Ecological Modelling 148, 27-46.

VOLIN, J. C., REICH, P. B. & T. J. GIVNISH (1998). Elevated carbon dioxide ameliorates the effects of ozone on photosynthesis and growth. Species respond similarly regardless of photosynthetic pathway of plant functional group. New Phytologist 138, 315-325.

VOLK, M., GEISSMANN, M., BLATTER, A., CONTAT, F. & J. FUHRER (2003). Design and performance of a free-air exposure system to study long-term effects of ozone on grasslands. Atmospheric Environment 37, 1341-1350.

VOLZ, A. & D. KLEY (1988). Evaluation of the Montsouris series of ozone measurements made in the nineteenth century. Nature 332, 240-242.

WALLIN, G., SKÄRBY, L. & G. SELLDÉN (1990). Long-term exposure of Norway spruce, *Picea abies* (L.) Karst., to ozone in open-top chambers. I. Effects on the capacity of the net

photosynthesis, dark respiration and leaf conductance of shoots of different ages. New Phytologist 115, 335-344.

WALZ, H. GmBH (1996). Portable Photosynthesis System HCM-1000. User manual, Effeltrich, Germany.

WANG, X. & D. L. MAUZERALL (2004). Characterizing distributions of surface ozone and its impact on grain production in China, Japan and South Korea. 1990 and 2020. Atmospheric Environment 38, 4383-4402.

WARD SYSTEMS GROUP INC. (1996). NeuroShell® 2. Frederick, Maryland.

WARNECK, P. (1988). The chemistry of the natural atmosphere. Academic Press, New York.

WGE (Working Group on Effects of the UNECE Convention on Long-Range Transboundary Air Pollution) (2004). Review and assessment of air pollution effects and their recorded trends. NERC (National Environment Research Council), UK.

WHITEHEAD, P. G., HOWARD, A. & C. ARULMANI (1997). Modelling algal growth and transport in rivers – a comparison of time series analysis, dynamic mass balance and neural network techniques. Hydrobiologia 349, 39-46.

WILBOURN, S., DAVISON, A. W. & J. H. OLLERENSHAW (1995). The use of an unenclosed field fumigation system to determine the effects of elevated ozone on a grass-clover mixture. New Phytologist 129, 23-32.

WYTHOFF, B. J., LEVINE, S. P. & S. A. TOMELLINI (1990). Spectral peak verification and recognition using a multilayered neural network. Analytical Chemistry 62 (24), 2702-2709.

YEUNG, D. S. & H. S. FONG (1994). Handwritten Chinese character recognition by rule-embedded neocognitron. Neural Computing and Applications 2 (4), 216-226.

YUN, S.-C. & J. A. LAURENCE (1999a). The response of clones of *Populus tremuloides* differing in sensitivity to ozone in the field. New Phytologist 141, 411-421.

YUN, S.-C. & J. A. LAURENCE (1999b). The response of sensitive and tolerant clones of *Populus tremuloides* to dynamic exposure under controlled environmental conditions. New Phytologist 143, 305-313.

ZELITCH, I. (1982). The close relationship between net photosynthesis and crop yield. Bioscience 32(10), 796-802.

ZHANG, J., FERDINAND, J. A., VANDERHEYDEN, D. J., SKELLY, J. M. & J. L. INNES (2001). Variation of gas exchange within native plant species of Switzerland and relationships with ozone injury. An open-top experiment. Environmental Pollution 113, 177-185.

ZHANG, M., FULCHER, J. & R. A. SCOFIELD (1997). Rainfall estimation using artificial neural network group. Neurocomputing 16, 97-115.

ZHENG, Y., LYONS, T. & J. BARNES (2000). Effects of ozone on the production and utilization of assimilates of *Plantago major*. Environmental and Experimental Botany 43, 171-180.

APPENDIX A

Descriptive statistics of climate data

Figure A.1 Mean (+ 1 S.D.) air temperature (a), VPD (b), PAR (c), wind speed (d) and O_3 concentration (e) of all growth periods (GP = 28 days) at the sites Trier-City, Trier-University and Deuselbach in 1997. In each sub-figure, the far right set of bars represents the mean of all five GPs, i.e. the growing season mean. Wind speed data at the site Trier-University were not available for 1997.

Figure A.2   Mean (+ 1 S.D.) air temperature (a), VPD (b), PAR (c), wind speed (d) and O_3 concentration (e) of all growth periods (GP = 28 days) at the sites Trier-City, Trier-University and Deuselbach in 1998. In each sub-figure, the far right set of bars represents the mean of all five GPs, i.e. the growing season mean.
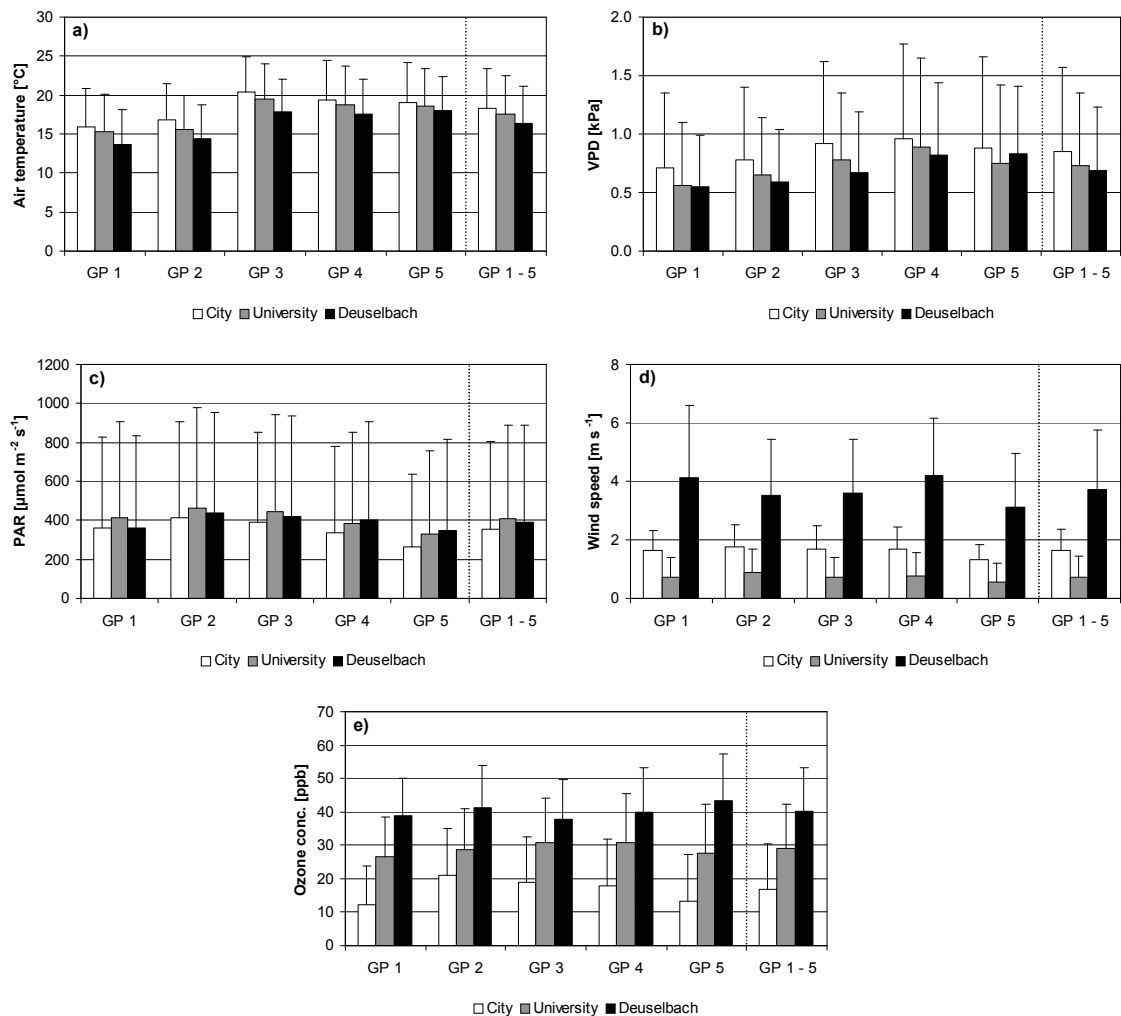
Figure A.3   Mean (+ 1 S.D.) air temperature (a), VPD (b), PAR (c), wind speed (d)
and O₃ concentration (e) of all growth periods (GP = 28 days) at the sites
Trier-City, Trier-University and Deuselbach in 1999. In each sub-figure,
the far right set of bars represents the mean of all five GPs, i.e. the
growing season mean.
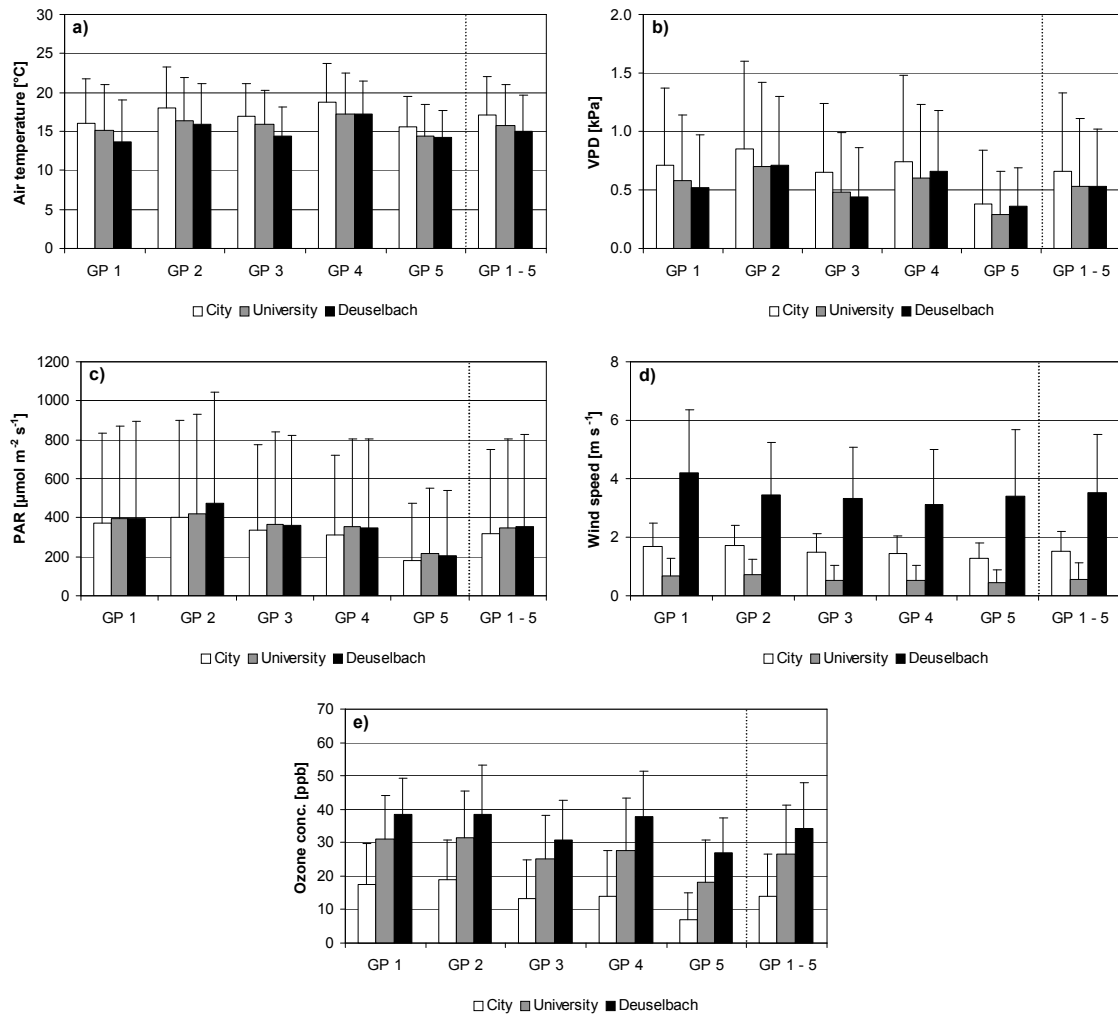
Figure A.4   Mean (+ 1 S.D.) air temperature (a), VPD (b), PAR (c), wind speed (d) and O_3 concentration (e) of all growth periods (GP = 28 days) at the sites Trier-City, Trier-University and Deuselbach in 2000. In each sub-figure, the far right set of bars represents the mean of all five GPs, i.e. the growing season mean.
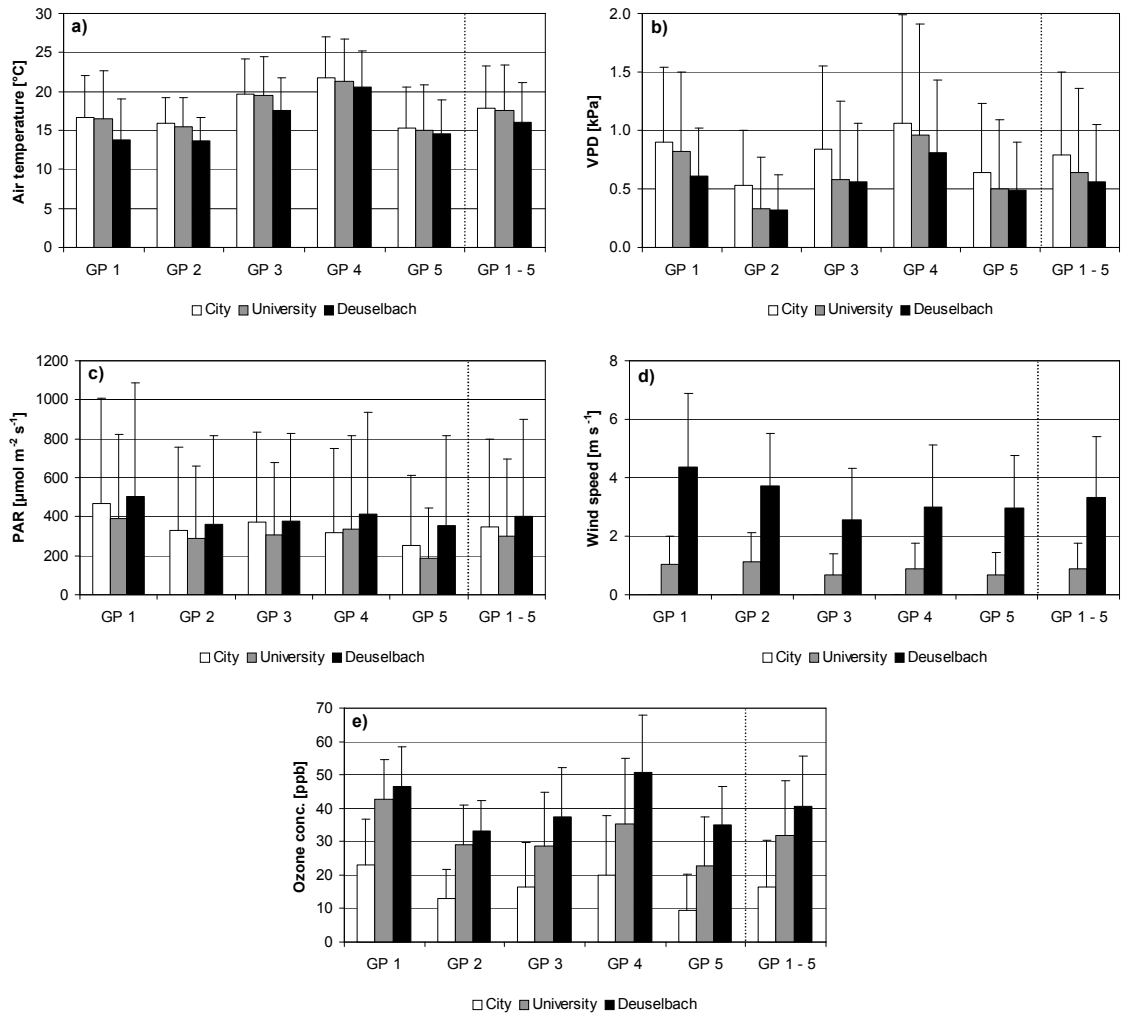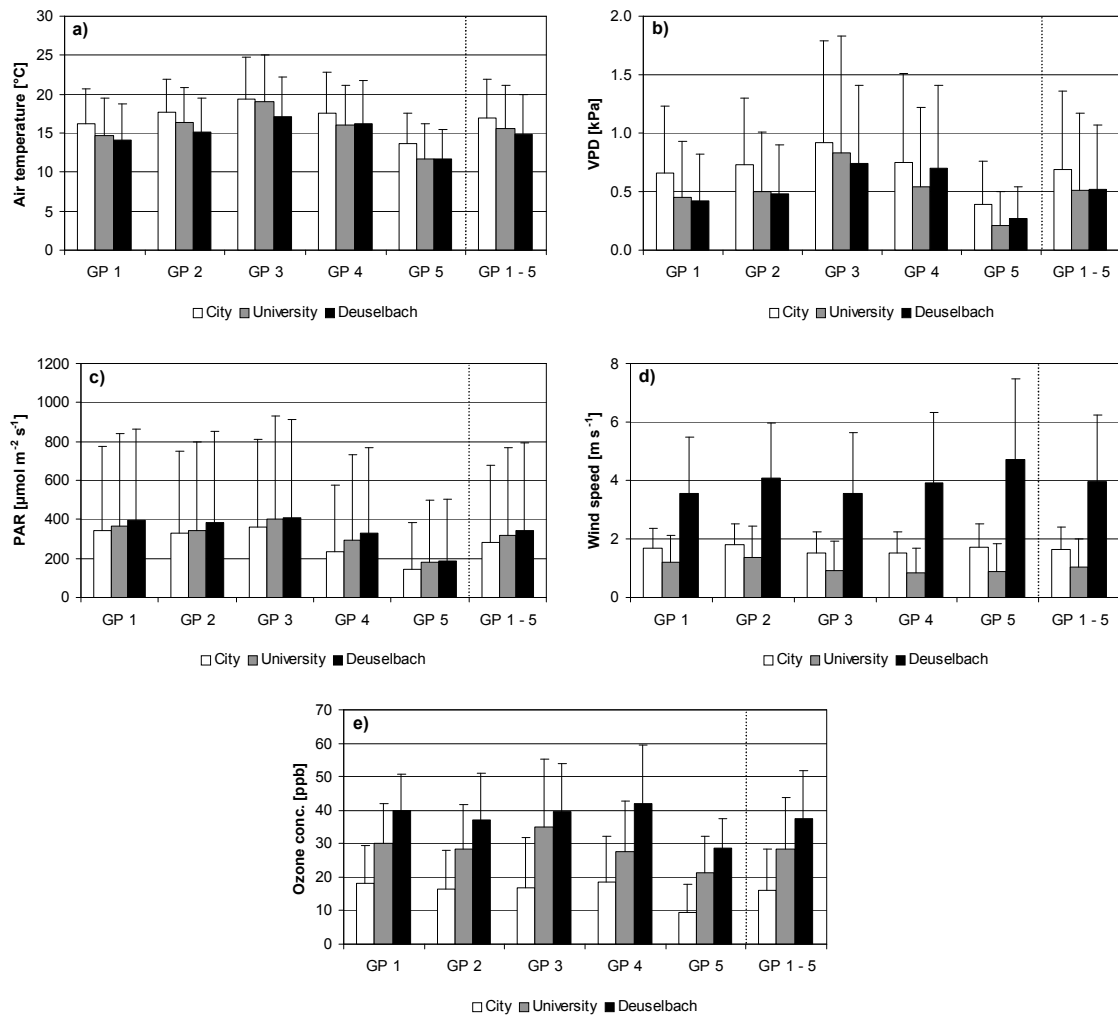
Figure A.5   Mean (+ 1 S.D.) air temperature (a), VPD (b), PAR (c), wind speed (d)
and O_3 concentration (e) of all growth periods (GP = 28 days) at the sites
Trier-City, Trier-University and Deuselbach in 2001. In each sub-figure,
the far right set of bars represents the mean of all five GPs, i.e. the
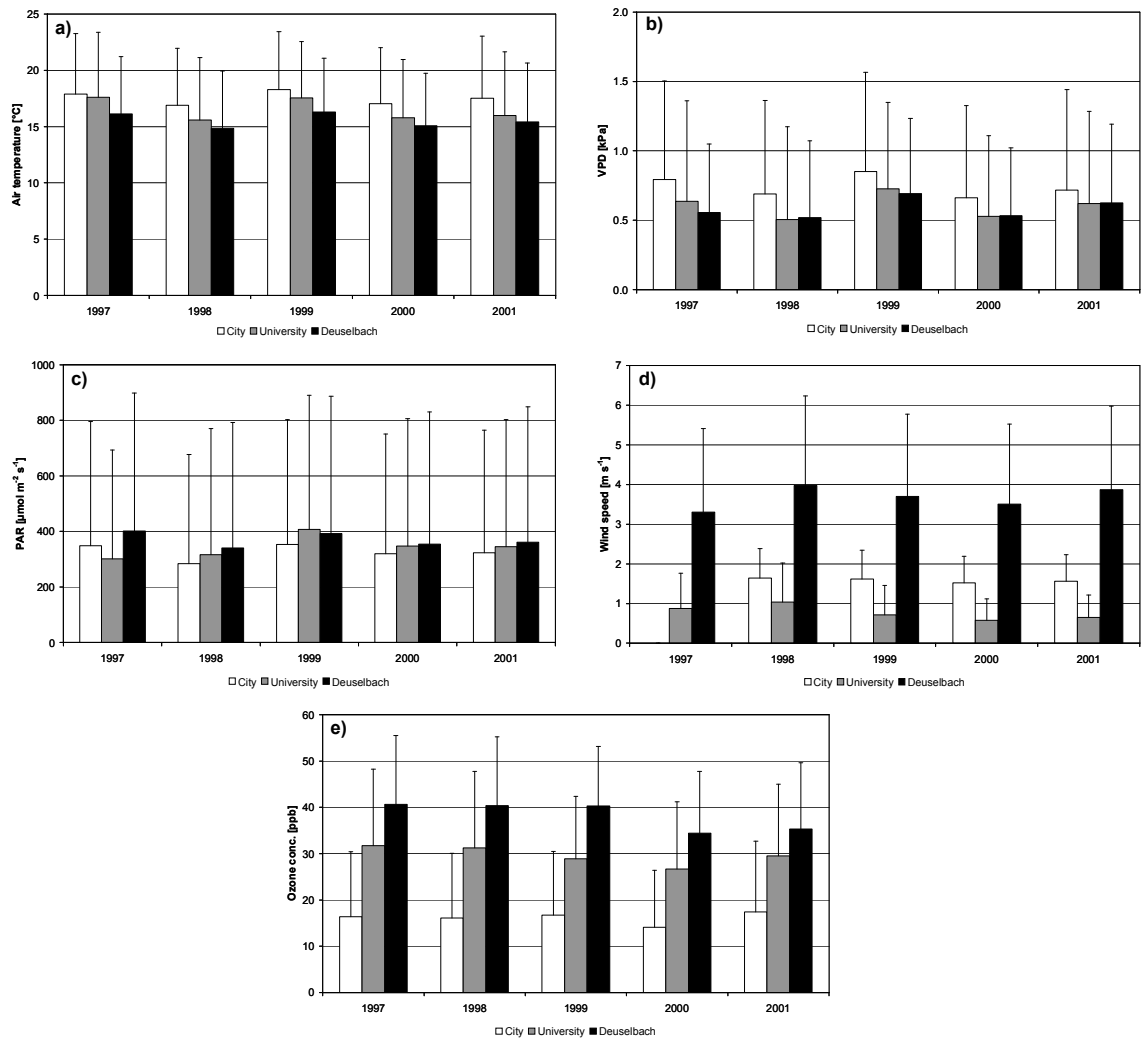growing season mean.

Table A.1   Mean (± S.E.) and range (maximum and minimum) of air temperature, VPD, PAR, wind speed and O_3 concentration of 1997 growth periods (GP = 28 days) 1 to 5 at the three experimental sites Trier-City, Trier-University and Deuselbach.

City	Temperature [°C]	VPD [kPa]	PAR [µmol m^{-2} s^{-1}]	Wind speed [m/s]	Ozone [ppb]
Mean (± S.E.)					
GP 1	16.59 ± 0.24	0.90 ± 0.03	470.06 ± 23.35	*	23.13 ± 0.59
GP 2	15.94 ± 0.12	0.53 ± 0.02	330.38 ± 16.40	*	12.80 ± 0.35
GP 3	19.70 ± 017	0.84 ± 0.03	371.57 ± 18.13	*	16.35 ± 0.52
GP 4	21.71 ± 0.20	1.06 ± 0.04	320.84 ± 16.49	*	20.06 ± 0.69
GP 5	15.24 ± 0.20	0.64 ± 0.02	251.32 ± 13.92	*	9.60 ± 0.41
Range					
GP 1	5.50 - 30.70	0.05 - 2.86	0.00 - 1727.49	*	0.47 - 67.48
GP 2	8.65 - 25.40	0.03 - 1.93	0.00 - 1694.49	*	0.47 - 39.23
GP 3	11.05 - 30.05	0.03 - 2.49	0.00 - 1751.75	*	0.47 - 55.34
GP 4	11.65 - 33.55	0.04 - 3.48	0.00 - 1491.66	*	0.47 - 66.55
GP 5	4.80 - 26.00	0.01 - 2.26	0.00 - 1309.20	*	0.47 - 51.14

University	Temperature [°C]	VPD [kPa]	PAR [µmol m^{-2} s^{-1}]	Wind speed [m/s]	Ozone [ppb]
Mean (± S.E.)					
GP 1	16.53 ± 0.27	0.82 ± 0.03	387.25 ± 18.89	1.03 ± 0.04	42.69 ± 0.51
GP 2	15.48 ± 0.14	0.33 ± 0.02	290.64 ± 14.19	1.14 ± 0.04	29.04 ± 0.46
GP 3	19.49 ± 0.19	0.58 ± 0.03	303.12 ± 14.68	0.67 ± 0.03	28.77 ± 0.63
GP 4	21.33 ± 0.21	0.96 ± 0.04	335.91 ± 18.47	0.87 ± 0.03	35.20 ± 0.76
GP 5	15.07 ± 0.22	0.50 ± 0.02	187.36 ± 9.83	0.66 ± 0.03	22.83 ± 0.56
Range					
GP 1	3.57 - 32.07	0.00 - 3.20	0.00 - 1444.75	0.00 - 4.60	14.56 - 82.97
GP 2	7.75 - 27.00	0.00 - 1.88	0.00 - 1431.16	0.00 - 5.00	1.20 - 68.94
GP 3	10.07 - 30.88	0.00 - 2.41	0.00 - 1405.93	0.00 - 4.93	2.85 - 77.92
GP 4	11.65 - 34.88	0.00 - 3.74	0.00 - 1739.04	0.00 - 4.37	1.03 - 89.55
GP 5	2.08 - 27.15	0.00 - 2.38	0.00 - 1227.68	0.00 - 3.57	0.79 - 66.64

Deuselbach	Temperature [°C]	VPD [kPa]	PAR [µmol m^{-2} s^{-1}]	Wind speed [m/s]	Ozone [ppb]
Mean (± S.E.)					
GP 1	13.86 ± 0.23	0.61 ± 0.02	506.07 ± 25.20	4.35 ± 0.11	46.58 ± 0.51
GP 2	13.68 ± 0.11	0.32 ± 0.01	361.64 ± 17.63	3.70 ± 0.07	33.36 ± 0.35
GP 3	17.52 ± 0.17	0.56 ± 0.02	379.45 ± 17.71	2.56 ± 0.07	37.35 ± 0.58
GP 4	20.57 ± 0.18	0.81 ± 0.02	412.35 ± 20.23	2.98 ± 0.08	50.78 ± 0.66
GP 5	14.52 ± 0.17	0.49 ± 0.02	351.09 ± 17.84	2.94 ± 0.07	35.12 ± 0.44
Range					
GP 1	4.31 - 26.44	0.04 - 1.75	0.00 - 1938.09	0.00 - 10.84	17.24 - 88.85
GP 2	7.68 - 24.57	0.03 - 1.20	0.00 - 1913.83	0.38 - 8.51	9.54 - 64.36
GP 3	9.25 - 27.83	0.01 - 1.84	0.00 - 1636.26	0.00 - 9.94	9.41 - 80.44
GP 4	11.59 - 30.60	0.02 - 2.31	0.00 - 1656.64	0.16 - 11.99	15.81 - 85.49
GP 5	4.81 - 24.66	0.01 - 1.69	0.00 - 1554.74	0.00 - 8.39	5.57 - 66.72

Table A.2   Mean (± S.E.) and range (maximum and minimum) of air temperature, VPD, PAR, wind speed and O_3 concentration of 1998 growth periods (GP = 28 days) 1 to 5 at the three experimental sites Trier-City, Trier-University and Deuselbach.

City	Temperature [°C]	VPD [kPa]	PAR [µmol m^{-2} s^{-1}]	Wind speed [m/s]	Ozone [ppb]
Mean (± S.E.)					
GP 1	16.21 ± 0.18	0.66 ± 0.02	344.57 ± 16.57	1.66 ± 0.03	18.35 ± 0.43
GP 2	17.67 ± 0.16	0.73 ± 0.02	329.89 ± 16.22	1.78 ± 0.03	16.40 ± 0.45
GP 3	19.41 ± 0.21	0.92 ± 0.03	361.77 ± 17.35	1.52 ± 0.03	16.91 ± 0.58
GP 4	17.57 ± 0.20	0.75 ± 0.03	236.43 ± 13.21	1.54 ± 0.03	18.53 ± 0.52
GP 5	13.59 ± 0.15	0.39 ± 0.01	143.31 ± 9.39	1.72 ± 0.03	9.49 ± 0.32
Range					
GP 1	4.40 - 32.25	0.02 - 3.10	0.00 - 1673.14	0.60 - 3.95	0.47 - 49.93
GP 2	8.95 - 32.35	0.05 - 2.89	0.00 - 1589.68	0.60 - 4.50	0.47 - 56.46
GP 3	8.70 - 36.35	0.02 - 4.18	0.00 - 1612.00	0.60 - 4.65	0.47 - 72.10
GP 4	8.00 - 37.60	0.00 - 4.82	0.00 - 1466.43	0.35 - 4.15	0.47 - 81.19
GP 5	4.65 - 25.00	0.03 - 1.81	0.00 - 1168.48	0.60 - 4.30	0.47 - 37.10

University	Temperature [°C]	VPD [kPa]	PAR [µmol m^{-2} s^{-1}]	Wind speed [m/s]	Ozone [ppb]
Mean (± S.E.)					
GP 1	14.69 ± 0.19	0.45 ± 0.02	366.92 ± 18.16	1.20 ± 0.04	30.03 ± 0.47
GP 2	16.35 ± 0.17	0.50 ± 0.02	342.94 ± 17.55	1.37 ± 0.04	28.30 ± 0.51
GP 3	19.02 ± 0.23	0.83 ± 0.04	403.54 ± 20.28	0.91 ± 0.04	35.04 ± 0.78
GP 4	16.09 ± 0.19	0.54 ± 0.03	291.09 ± 16.95	0.82 ± 0.03	27.58 ± 0.59
GP 5	11.72 ± 0.17	0.21 ± 0.01	178.48 ± 12.23	0.90 ± 0.04	21.26 ± 0.42
Range					
GP 1	1.93 - 31.95	0.00 - 2.93	0.00 - 1873.07	0.00 - 4.23	1.28 - 109.93
GP 2	7.17 - 31.75	0.00 - 3.09	0.00 - 1809.98	0.00 - 4.70	1.69 - 70.56
GP 3	7.50 - 37.85	0.00 - 5.49	0.00 - 1831.01	0.00 - 4.88	1.32 - 118.49
GP 4	6.22 - 30.87	0.00 - 3.34	0.00 - 1742.05	0.00 - 3.32	2.89 - 93.56
GP 5	2.72 - 24.10	0.00 - 1.47	0.00 - 1512.36	0.00 - 3.98	2.77 - 50.70

Deuselbach	Temperature [°C]	VPD [kPa]	PAR [µmol m^{-2} s^{-1}]	Wind speed [m/s]	Ozone [ppb]
Mean (± S.E.)					
GP 1	14.03 ± 0.18	0.42 ± 0.02	393.67 ± 18.20	3.57 ± 0.07	39.87 ± 0.41
GP 2	15.22 ± 0.6	0.48 ± 0.02	381.98 ± 18.06	4.08 ± 0.07	37.10 ± 0.53
GP 3	17.15 ± 0.19	0.74 ± 0.03	410.96 ± 19.22	3.56 ± 0.08	39.51 ± 0.56
GP 4	16.16 ± 0.22	0.70 ± 0.03	327.83 ± 17.09	3.94 ± 0.09	41.95 ± 0.67
GP 5	11.67 ± 0.15	0.27 ± 0.01	188.60 ± 12.24	4.71 ± 0.11	28.53 ± 0.35
Range					
GP 1	1.92 - 29.60	0.01 - 2.17	0.00 - 1761.46	0.01 - 2.17	14.80 - 71.28
GP 2	8.26 - 29.67	0.02 - 2.20	0.00 - 1756.61	0.02 - 2.20	13.08 - 85.71
GP 3	7.76 - 32.40	0.03 - 3.39	0.00 - 1748.84	0.03 - 3.39	5.78 - 80.05
GP 4	6.56 - 34.65	0.01 - 3.86	0.00 - 1668.29	0.01 - 3.86	8.92 - 96.90
GP 5	2.54 - 23.15	0.01 - 1.60	0.00 - 1369.38	0.01 - 1.60	1.45 - 55.69

Table A.3   Mean (± S.E.) and range (maximum and minimum) of air temperature, VPD, PAR, wind speed and O$_3$ concentration of 1999 growth periods (GP = 28 days) 1 to 5 at the three experimental sites Trier-City, Trier-University and Deuselbach.

City	Temperature [°C]	VPD [kPa]	PAR [µmol m^{-2} s^{-1}]	Wind speed [m/s]	Ozone [ppb]
Mean (± S.E.)					
GP 1	15.91 ± 0.19	0.71 ± 0.02	361.69 ± 17.90	1.64 ± 0.03	12.36 ± 0.44
GP 2	16.77 ± 0.18	0.78 ± 0.02	415.44 ± 18.90	1.76 ± 0.03	21.04 ± 0.53
GP 3	20.35 ± 0.17	0.92 ± 0.03	388.49 ± 17.87	1.70 ± 0.03	19.04 ± 0.52
GP 4	19.29 ± 0.20	0.96 ± 0.03	338.40 ± 17.02	1.70 ± 0.03	17.74 ± 0.55
GP 5	19.12 ± 0.19	0.88 ± 0.03	263.45 ± 14.02	1.30 ± 0.02	13.47 ± 0.53
Range					
GP 1	3.75 - 32.00	0.03 - 3.30	0.00 - 1661.50	0.60 - 4.40	0.47 - 46.47
GP 2	7.20 - 28.95	0.04 - 2.49	0.00 - 1726.52	0.60 - 4.60	0.47 - 64.91
GP 3	10.45 - 31.95	0.05 - 3.10	0.00 - 1647.91	0.60 - 4.05	0.47 - 61.41
GP 4	8.65 - 31.40	0.04 - 3.22	0.00 - 1556.68	0.60 - 4.20	0.47 - 56.51
GP 5	9.60 - 32.35	0.05 - 3.37	0.00 - 1419.84	0.60 - 3.15	0.47 - 59.08

University	Temperature [°C]	VPD [kPa]	PAR [µmol m^{-2} s^{-1}]	Wind speed [m/s]	Ozone [ppb]
Mean (± S.E.)					
GP 1	15.24 ± 0.19	0.56 ± 0.02	412.80 ± 18.92	0.71 ± 0.03	26.56 ± 0.45
GP 2	15.67 ± 0.17	0.65 ± 0.02	464.89 ± 19.83	0.87 ± 0.03	28.80 ± 0.47
GP 3	19.55 ± 0.17	0.78 ± 0.02	444.17 ± 19.25	0.71 ± 0.03	30.65 ± 0.52
GP 4	18.69 ± 0.19	0.89 ± 0.03	385.11 ± 18.04	0.74 ± 0.03	30.73 ± 0.57
GP 5	18.61 ± 0.18	0.75 ± 0.03	332.00 ± 16.10	0.55 ± 0.03	27.79 ± 0.56
Range					
GP 1	3.32 - 30.38	0.00 - 2.78	1.00 - 1850.74	0.00 - 3.40	4.11 - 58.60
GP 2	6.60 - 26.72	0.05 - 2.20	1.94 - 1778.60	0.00 - 3.55	5.95 - 69.63
GP 3	9.27 - 30.87	0.03 - 2.80	1.94 - 1730.40	0.00 - 3.08	3.93 - 76.88
GP 4	8.07 - 30.53	0.01 - 3.29	1.94 - 1676.38	0.00 - 3.20	3.47 - 68.16
GP 5	8.82 - 31.07	0.01 - 3.02	1.94 - 1451.87	0.00 - 3.73	3.19 - 70.36

Deuselbach	Temperature [°C]	VPD [kPa]	PAR [µmol m^{-2} s^{-1}]	Wind speed [m/s]	Ozone [ppb]
Mean (± S.E.)					
GP 1	13.59 ± 0.17	0.55 ± 0.02	362.89 ± 18.20	4.10 ± 0.10	38.81 ± 0.43
GP 2	14.46 ± 0.17	0.59 ± 0.02	436.86 ± 20.02	3.52 ± 0.07	41.31 ± 0.49
GP 3	17.83 ± 0.16	0.67 ± 0.02	422.01 ± 19.73	3.58 ± 0.07	37.85 ± 0.46
GP 4	17.48 ± 0.18	0.82 ± 0.02	399.32 ± 19.52	4.20 ± 0.08	39.99 ± 0.51
GP 5	18.05 ± 0.16	0.83 ± 0.02	347.44 ± 17.65	3.12 ± 0.07	43.28 ± 0.53
Range					
GP 1	2.71 - 26.55	0.01 - 2.23	0.00 - 1836.19	0.33 - 16.30	10.95 - 72.85
GP 2	5.71 - 25.85	0.01 - 1.96	0.00 - 1965.26	0.35 - 8.63	14.38 - 76.59
GP 3	7.60 - 28.60	0.04 - 2.36	0.00 - 1768.25	0.27 - 9.07	14.10 - 81.49
GP 4	7.74 - 27.65	0.05 - 2.48	0.00 - 1906.06	0.51 - 9.47	15.95 - 71.92
GP 5	9.07 - 29.15	0.05 - 2.45	0.00 - 1618.79	0.00 - 10.70	43.28 - 10.44

Table A.4　Mean (± S.E.) and range (maximum and minimum) of air temperature, VPD, PAR, wind speed and O_3 concentration of 2000 growth periods (GP = 28 days) 1 to 5 at the three experimental sites Trier-City, Trier-University and Deuselbach.

City	Temperature [°C]	VPD [kPa]	PAR [μmol m^{-2} s^{-1}]	Wind speed [m/s]	Ozone [ppb]
Mean (± S.E.)					
GP 1	16.05 ± 0.22	0.71 ± 0.03	374.11 ± 17.79	1.70 ± 0.03	17.66 ± 0.47
GP 2	18.11 ± 0.21	0.87 ± 0.03	410.42 ± 19.29	1.72 ± 0.03	18.79 ± 0.47
GP 3	17.01 ± 0.16	0.65 ± 0.02	333.44 ± 17.08	1.48 ± 0.02	13.17 ± 0.45
GP 4	18.68 ± 0.19	0.74 ± 0.03	311.10 ± 15.89	1.44 ± 0.02	13.97 ± 0.53
GP 5	15.69 ± 0.15	0.38 ± 0.02	183.02 ± 11.42	1.30 ± 0.02	7.18 ± 0.31
Range					
GP 1	5.20 - 32.10	0.02 - 3.05	0.00 - 1670.23	0.45 - 4.95	0.47 - 53.71
GP 2	6.10 - 33.40	0.02 - 3.49	0.00 - 1712.93	0.60 - 3.95	0.47 - 57.21
GP 3	8.80 - 29.45	0.04 - 2.72	0.00 - 1804.16	0.60 - 3.60	0.47 - 55.34
GP 4	9.20 - 31.05	0.00 - 3.13	0.00 - 1521.74	0.60 - 3.85	0.47 - 67.72
GP 5	8.20 - 27.50	0.00 - 2.05	0.00 - 1237.39	0.60 - 3.35	0.47 - 41.10

University	Temperature [°C]	VPD [kPa]	PAR [μmol m^{-2} s^{-1}]	Wind speed [m/s]	Ozone [ppb]
Mean (± S.E.)					
GP 1	15.23 ± 0.23	0.58 ± 0.02	399.10 ± 18.57	0.68 ± 0.02	31.09 ± 0.50
GP 2	16.42 ± 0.22	0.70 ± 0.03	419.29 ± 19.60	0.71 ± 0.02	31.14 ± 0.54
GP 3	15.94 ± 0.17	0.48 ± 0.02	364.26 ± 18.27	0.54 ± 0.02	25.30 ± 0.50
GP 4	17.27 ± 0.20	0.60 ± 0.02	351.09 ± 17.50	0.54 ± 0.02	27.62 ± 0.61
GP 5	14.46 ± 0.16	0.30 ± 0.01	216.02 ± 13.16	0.42 ± 0.02	18.03 ± 0.49
Range					
GP 1	3.83 - 30.97	0.01 - 2.68	0.00 - 1721.67	0.00 - 4.08	2.80 - 76.59
GP 2	4.37 - 32.55	0.02 - 3.40	0.00 - 1761.13	0.00 - 2.77	2.57 - 77.76
GP 3	7.45 - 29.25	0.00 - 2.53	0.00 - 1799.31	0.00 - 2.30	2.57 - 77.52
GP 4	6.90 - 30.43	0.00 - 2.87	0.00 - 1559.92	0.00 - 2.57	0.47 - 79.39
GP 5	6.37 - 26.98	0.00 - 1.79	0.00 - 1412.40	0.00 - 2.15	0.47 - 60.94

Deuselbach	Temperature [°C]	VPD [kPa]	PAR [μmol m^{-2} s^{-1}]	Wind speed [m/s]	Ozone [ppb]
Mean (± S.E.)					
GP 1	13.67 ± 0.20	0.52 ± 0.02	396.53 ± 19.10	4.19 ± 0.08	38.37 ± 0.42
GP 2	15.95 ± 0.20	0.71 ± 0.02	476.49 ± 21.98	3.45 ± 0.07	38.43 ± 0.57
GP 3	14.37 ± 0.14	0.44 ± 0.02	362.40 ± 17.76	3.34 ± 0.07	30.65 ± 0.46
GP 4	17.19 ± 0.16	0.66 ± 0.02	347.67 ± 17.69	3.12 ± 0.07	37.67 ± 0.53
GP 5	14.29 ± 0.13	0.36 ± 0.01	202.84 ± 12.94	3.40 ± 0.09	27.10 ± 0.41
Range					
GP 1	4.35 - 26.80	0.03 - 1.98	0.00 - 1841.04	0.00 - 11.85	17.07 - 89.69
GP 2	3.75 - 29.41	0.03 - 2.65	0.00 - 1880.83	0.25 - 9.90	16.06 - 108.72
GP 3	6.85 - 25.90	0.04 - 1.99	0.00 - 1792.51	0.00 - 9.20	8.71 - 82.28
GP 4	8.60 - 28.10	0.05 - 2.27	0.00 - 1833.27	0.00 - 10.85	11.93 - 79.77
GP 5	7.90 - 25.10	0.04 - 1.60	0.00 - 1597.44	0.00 - 13.65	4.74 - 60.78

Table A.5   Mean (± S.E.) and range (maximum and minimum) of air temperature, VPD, PAR, wind speed and O$_3$ concentration of 2001 growth periods (GP = 28 days) 1 to 5 at the three experimental sites Trier-City, Trier-University and Deuselbach.

City	Temperature [°C]	VPD [kPa]	PAR [µmol m^{-2} s^{-1}]	Wind speed [m/s]	Ozone [ppb]
Mean (± S.E.)					
GP 1	16.49 ± 0.19	0.76 ± 0.02	410.05 ± 19.05	1.73 ± 0.03	23.28 ± 0.55
GP 2	19.33 ± 0.20	0.94 ± 0.03	435.98 ± 19.77	1.65 ± 0.03	22.89 ± 0.62
GP 3	19.87 ± 0.20	0.82 ± 0.03	367.25 ± 17.95	1.57 ± 0.03	19.35 ± 0.63
GP 4	18.63 ± 0.22	0.76 ± 0.03	252.21 ± 14.06	1.43 ± 0.02	14.01 ± 0.56
GP 5	13.33 ± 0.14	0.30 ± 0.01	151.28 ± 9.50	1.43 ± 0.02	7.54 ± 0.28
Range					
GP 1	5.95 - 27.75	0.00 - 2.47	0.00 - 1705.17	0.60 - 4.20	0.47 - 66.55
GP 2	7.35 - 32.85	0.01 - 3.51	0.00 - 1720.70	0.60 - 4.85	0.47 - 75.19
GP 3	9.30 - 32.35	0.00 - 3.30	0.00 - 1675.08	0.60 - 4.10	0.47 - 81.96
GP 4	8.55 - 34.35	0.00 - 3.71	0.00 - 1434.40	0.60 - 3.55	0.47 - 73.09
GP 5	5.15 - 25.85	0.00 - 1.67	0.00 - 1146.16	0.60 - 3.40	0.47 - 33.16

University	Temperature [°C]	VPD [kPa]	PAR [µmol m^{-2} s^{-1}]	Wind speed [m/s]	Ozone [ppb]
Mean (± S.E.)					
GP 1	14.80 ± 0.20	0.67 ± 0.02	411.42 ± 19.07	0.69 ± 0.02	32.42 ± 0.47
GP 2	17.91 ± 0.20	0.85 ± 0.03	454.76 ± 20.35	0.72 ± 0.02	33.51 ± 0.63
GP 3	18.58 ± 0.20	0.71 ± 0.03	400.88 ± 18.83	0.69 ± 0.02	32.79 ± 0.63
GP 4	16.74 ± 0.24	0.65 ± 0.03	285.63 ± 15.47	0.57 ± 0.02	28.71 ± 0.67
GP 5	11.90 ± 0.15	0.23 ± 0.01	173.48 ± 10.67	0.58 ± 0.02	20.30 ± 0.37
Range					
GP 1	5.42 - 27.27	0.02 - 2.55	0.00 - 1704.20	0.00 - 2.60	4.20 - 66.78
GP 2	5.65 - 31.03	0.00 - 3.50	0.00 - 1773.75	0.00 - 3.07	0.93 - 81.73
GP 3	7.73 - 31.50	0.00 - 3.20	0.00 - 1612.32	0.00 - 2.82	4.90 - 83.13
GP 4	6.82 - 33.45	0.00 - 3.83	0.00 - 1499.42	0.00 - 2.52	1.87 - 84.76
GP 5	2.48 - 24.95	0.00 - 1.38	0.00 - 1178.51	0.00 - 3.40	0.47 - 43.43

Deuselbach	Temperature [°C]	VPD [kPa]	PAR [µmol m^{-2} s^{-1}]	Wind speed [m/s]	Ozone [ppb]
Mean (± S.E.)					
GP 1	14.00 ± 0.18	0.62 ± 0.02	442.52 ± 20.25	3.87 ± 0.08	39.63 ± 0.44
GP 2	16.87 ± 0.17	0.77 ± 0.02	467.39 ± 21.58	3.83 ± 0.09	38.81 ± 0.60
GP 3	17.81 ± 0.18	0.74 ± 0.02	400.29 ± 19.55	3.60 ± 0.08	37.99 ± 0.58
GP 4	16.90 ± 0.22	0.73 ± 0.03	321.98 ± 17.50	3.70 ± 0.08	35.42 ± 0.59
GP 5	11.47 ± 0.13	0.27 ± 0.01	174.85 ± 11.15	4.32 ± 0.08	24.86 ± 0.24
Range					
GP 1	4.89 - 24.10	0.03 - 1.99	0.00 - 1809.01	0.00 - 9.16	12.66 - 74.02
GP 2	6.02 - 28.90	0.04 - 2.45	0.00 - 1859.48	0.28 - 12.85	7.59 - 89.90
GP 3	8.16 - 29.90	0.03 - 2.71	0.00 - 1874.04	0.00 - 10.10	12.47 - 84.53
GP 4	6.51 - 31.90	0.05 - 3.16	0.00 - 1608.12	0.00 - 11.55	10.23 - 75.65
GP 5	4.67 - 22.05	0.04 - 1.12	0.00 - 1368.41	0.00 - 10.40	6.72 - 44.44

Zusammenfassung

Troposphärisches Ozon (O_3) kann zahlreiche negative Effekte bei Pflanzen hervorrufen, wie z.B. sichtbare Blattschäden, Biomass-Einbußen oder verfrühte Seneszens. Die Hintergrundkonzentrationen dieses sekundären Luftschadstoff sind im Laufe der letzten Jahrzehnte stetig gestiegen und eine Umkehr dieses Trends ist vorläufig nicht abzusehen. Aus diesem Grund sind Strategien zur Reduktion der Ozon-Vorläufersubstanzen notwendig, die sich auf den Nachweis von phytotoxischen Wirkungen Ozons stützen können müssen. Aus diesem Grund ist der Einsatz von Bioindikations-Verfahren sehr populär, da er auf einfache, kostengünstige Weise den Einfluss on Luftschadstoffen auf Pflanzen nachweisen kann und damit eine Beurteilung der Luftqualität zulässt.

Während traditionell konzentrationsbasierte Verfahren, wie z.B. der AOT40 (Summe der Ozonkonzentrationen über 40 ppb), mit oben genannten Wirkungsparametern in Beziehung gesetzt wurde, weiß man heute, dass die stomatär aufgenommene Dosis von Luftschadstoffen besser mit den auftretenden Wirkungen in Beziehung gebracht werden kann. Das hat dazu geführt, dass die Nachfrage von Fluss-Modellen, speziell Ozonfluss-Modellen, stetig gestiegen ist. Diese Modelle sind alle von der möglichst exakten Bestimmung bzw. Modellierung der stomatären Leitfähigkeit (g_s) abhängig.

In der vorliegenden Arbeit wurde mit Hilfe künstlicher neuronaler Netze (ANNs) ein Modell der stomatären Leitfähigkeit für zwei Weiß-Klee-Klone mit unterschiedlicher Ozon-Sensivität (*Trifolium repens* L. cv Regal; NC-S (Ozon-sensitiv) und NC-R (Ozon-resistent)) entwickelt. Zuvor wurden die beiden Klee-Klone für ein Ozonwirkungs-Monitoring im Freiland ausgewählt, da sie im Rahmen von Bioindikations-Verfahren erfolgreich in Europa zum Nachweis von Ozon-Schäden an Pflanzen eingesetzt worden waren.

Das Biomonitoring wurde während der Vegetationsperioden der Jahre 1997 bis 2001 an drei Standorten in der Region Trier durchgeführt, die sich durch eine unterschiedliche Verteilung der Ozonkonzentration im Tages- wie auch im Jahresverlauf auszeichnen. Als Wirkungsparameter wurden sichtbare Blattschäden und das Verhältnis der Biomasse zwischen NC-S und NC-R Klon aufgenommen. An beiden Klonen wurden ferner Gaswechselmessungen durchgeführt, die im Folgenden als Output eines ANN-basierten Models der stomatären Leitfähigkeit fungierten. Als Input dienten die zeitgleich gemessenen meteorologischen Parameter Lufttemperatur,

Wasserdampfdruck-Defizit (VPD) und photosynthetisch aktive Strahlung (PAR), sowie die Ozonkonzentration. Die Wahl des Modell-Typs fiel auf ANNs, weil sie dafür bekannt sind, komplexe nicht-lineare Zusammenhänge zwischen Eingangs- und Ausgangsparametern aufdecken zu können.

Die Entwicklung und Evaluation des Modells wurde detailliert beschrieben. Das resultierende stomatäre Leitfähigkeitsmodell wurde dann zur Berechnung von Ozonflüssen eingesetzt, die im Anschluss mit den nachgewiesenen Ozon-Wirkungen (Blattschäden, relativer Biomasseverlust) in Verbindung gesetzt wurden.

Das Modell war in der Lage, ein enges Verhältnis zwischen stomatärer Leitfähigkeit und den meteorologischen Eingangsparametern aufzudecken und zu erlernen, anhand dessen im Folgenden Zeitreihen von Klee-Ozonflüsse für alle drei Standorte berechnet wurden. Der Versuch, gute Dosis-Wirkungsbeziehungen zwischen diesen Flüssen und den aufgenommenen Wirkungsparametern zu erzielen, wurde nur zum Teil erreicht. Während die sichtbaren Blattschäden positiv mit den ermittelten Ozonflüssen korrelierten, konnten keine eindeutigen Beziehungen zwischen dem NC-S/NC-R Biomasse-Verhältnis und der modellierten aufgenommenen Ozonflussmenge gefunden werden.

Ein Grund für dieses Ergebnis war u.U. der schlechte Wuchs des NC-R Klons bei kühlen und feuchten Witterungen. Ausserdem könnten die ermittelten Blatt-bezogenen Ozonflussraten nicht repräsentativ für Ozonflüsse in die **ganze** Pflanze gewesen sein.

Ein Nachteil der ANNs ist zudem ihr weitgehendes Unvermögen, extrapolieren zu können, das heisst sie treffen nur gute Vorhersagen für Klimabedingungen, die auch im Trainingsdatensatz enthalten waren. Dementsprechend könnten für einige (extreme) Wetterbedingungen fehlerhafte Ozonflussraten vorhergesagt worden sein, wobei darauf hingewiesen werden muss, dass der Trainingsdatensatz der ANNs ausgesprochen umfangreich war und dieses Problem daher nur selten auftraf.

Der NC-S Klon zeigte eine durchgehend höhere stomatäre Leitfähigkeit, was ein Grund für seine höhere Ozon-Sensitivität sein könnte.

Es muss abschließend darauf hingewesen werden, dass das Modell mit Daten immer wassergesättigter Kleepflanzen trainiert wurde, d.h. eine Anwendung auf Freiland-bedingungen ist nicht möglich.

Summary

Tropospheric ozone (O_3) is known to have various detrimental effects on plants, such as visible leaf injury, reduced growth and premature senescence. Since the background concentrations of this air pollutant are increasing and are expected to further increase in the near future, strategies for the abatement of O_3 are required. These strategies have to be based on evidence of impacts, a fact that has made the use of bio-monitoring methods increasingly popular. While the impacts of O_3 on plants were traditionally related to O_3 exposure metrics, such as the AOT40 index (accumulated exposure over a threshold of 40 ppb), there is now general agreement that these impacts are more closely related to the O_3 dose absorbed through the stomata. This led to an increasing interest in the development of appropriate O_3 flux models, all of which are strongly dependant on the correct estimation of stomatal conductance (g_s).

This thesis aimed at developing an artificial neural network (ANN) based O_3 flux model for two white clover clones (*Trifolium repens* L. cv Regal; NC-S (sensitive) and NC-R (resistant)) differing in their sensitivity to O_3. These clones were selected for this study since they have successfully been used in European bio-monitoring campaigns for the detection of phytotoxic O_3 effects and are well represented in various European grassland communities.

The approach of this study was twofold: Firstly, a bio-monitoring experiment exposing the clover clones to ambient air was carried out during five consecutive growing seasons (1997 to 2001) at three sites in the city centre of Trier, on the premises of the University of Trier and in Deuselbach (Hunsrück), representing urban, suburban and rural climate and pollution conditions, respectively. The response parameters visible leaf injury and biomass ratio between NC-S and NC-R clone were regularly assessed. Furthermore, gas exchange measurements were carried out on both clones in order to obtain information on their rate of g_s and its dependence on the prevailing climate. Secondly, a g_s model was developed using the measured g_s data as output and the corresponding climate and O_3 data as input. ANNs were used for this task because of their ability to reveal, learn and predict highly complex non-linear

relationships between two or more variables, such as the dependence of g_s on air temperature, vapour pressure deficit (VPD) and photosynthetic active radiation (PAR), as well as on prevailing pollutant concentrations (here: O_3). These parameters functioned as input of the ANN-based model, whereas the g_s was the output. The development of the model was documented in detail and various model evaluation tools were applied. The resulting g_s model was used as basis for O_3 flux calculations, which were then related to the response parameters visible injury and relative biomass loss assessed at the experimental sites.

The results showed that the ANNs were indeed capable of revealing and learning the complex relationship between g_s and key meteorological parameters and O_3 concentration indices, with resulting r² values for the relationship between measured and modelled g_s of up to 0.93. The model was able to predict realistic rates of g_s and hence O_3 fluxes for entire growing seasons provided that the data the model was applied to were within the range of data it was trained with, but when relating these fluxes to the response parameters described above, only weak dose-response relationships could be obtained. This might be an indication for the limited suitability of the white clover bio-monitoring system for Central European climate conditions due to the fact that the NC-R clone proved to be sensitive to cold and wet weather conditions. Furthermore, the leaf level O_3 flux predictions might not be representative for the O_3 uptake of entire plants. Last but not least, it has to be stressed that ANNs have a very limited ability to extrapolate, leading in this case to potentially questionable O_3 flux rates for weather conditions the model was not trained with. However, due to the very comprehensive input dataset, these problems have been restricted to relatively extreme weather conditions (e.g. cold periods at the beginning or end of growing seasons). The ANN approach to develop g_s models was discussed in relation to multiplicative and net-photosynthesis based g_s models.

The study also revealed significantly higher g_s-rates for the NC-S clone, which might be an explanation for its higher ozone-sensitivity as compared to the NC-R clone.

Last but not least, it has to be pointed out that the model was trained with g_s data of potted, well-watered clover plants and is therefore not applicable to clover growing in the field due to the missing link to soil water conditions.

Lebenslauf

Name	Patrick Büker
Adresse	45 Scott Street York YO23 1NR England
Staatsangehörigkeit	Deutsch
Geburtsdatum	24.06.1969
Geburtsort	Herford

Schulbildung

1975-1979 Grundschule Quernheim
1979-1989 Freiherr-vom-Stein Gymnasium Bünde

Studium:

1991-1997 Angewandte Physische Geographie/ Geowissenschaften (Abschluss Diplom-Geograph, Universität Trier)
Thema der Diplomarbeit:
Einsatz der Bioindikatoren *Trifolium repens* und *Phaseolus vulgaris* zum Nachweis ozon-induzierter Blattschäden und Ernteverluste
2001-2003 Promotionsstudium Geographie/ Geowissenschaften, Universität Trier

Beruflicher Werdegang

1997-2002 Wissenschaftlicher Mitarbeiter im FB VI Geographie/Geowissenschaften der Universität Trier, Abteilung Geobotanik
2003 Research Associate, Centre for Ecology and Hydrology (CEH), Bangor, Wales, UK
2003-heute Research Associate, Stockholm Environment Institute (SEI), University of York, York, UK